D/1996/5769/2
ISBN 90-73802-50-4

KATHOLIEKE UNIVERSITEIT LEUVEN
FACULTEIT DER TOEGEPASTE WETENSCHAPPEN
DEPARTEMENT WERKTUIGKUNDE
AFDELING PRODUKTIETECHNIEKEN,
MACHINEBOUW EN AUTOMATISERING
Celestijnenlaan 300B — B-3001 Heverlee (Leuven), Belgium

HIGH FREQUENCY VIBRATIONS : CONTRIBUTIONS TO EXPERIMENTAL AND COMPUTATIONAL SEA PARAMETER IDENTIFICATION TECHNIQUES

Jury :
Voorzitter : Prof. dr. ir. W. Dutré
Prof. dr. ir. P. Sas
Prof. dr. ir. G. Vermeir
Prof. dr. ir. D. Vandepitte
Prof. dr. ir. H. Van Brussel
Prof. dr. ir. J.P. Coyette
Prof. dr. ir. J. Wijker

Proefschrift voorgedragen tot
het behalen van het doctoraat
in de toegepaste wetenschappen

door

ir. Koenraad DE LANGHE

U.D.C. 534

Februari 1996

DANKWOORD.

Mocht je ooit bekoord worden door de gedachte om een doctoraat aan te vatten, bezin voor je begint. Je weet waar je begint, maar je weet niet waarààn je begint. Waar je uiteindelijk belandt, besef je pas wanneer je de gedrukte versie in handen hebt.

In dit proces ben je niet altijd in "blijde" verwachting : niet steeds immers is de inzet evenredig met het opzet, grootse momenten (dikwijls denkbeeldig) wisselen zich af met nog grotere twijfels. Thans is het eindelijk geboren, misschien ietwat overtijd en met enkele "zware" naweeën, maar plegen we dit niet een klassieke geboorte te noemen ? De beoordeling van de pas-geborene laat ik over aan de lezer.

Verwacht geen volledigheid, verwacht niet de "sleutel" tot de oplossing van het hoog-frekwent trillingsprobleem. Mijn bedoeling was om in de SEA puzzel enkele stukjes in te passen. Wellicht zullen anderen later, nadat de meeste stukjes van de puzzel gelegd zijn, een meer synthetische bijdrage kunnen leveren tot het SEA probleem.

Mijn oprechte dank gaat uit naar mijn promotor prof. Sas voor het vertrouwen dat hij me schonk om een boeiend onderwerp in de vibro-akoestiek uit te diepen. Zonder zijn kritische geest, met de eigenschap om de essentie terug te vinden in een moeras van ideeën, experimenten, formules en artikels, was ik wellicht meerdere malen van het rechte pad afgedwaald. Mijn welgemeende dank gaat tevens uit naar prof. Vandepitte voor de inspirerende bijdrage tot de numerische kant van SEA. De samenwerking met het secretariaat en de sfeervolle werkomgeving van de afdeling PMA, in het bijzonder van de "modale groep", hebben in grote mate bijgedragen tot het uiteindelijk resultaat.

Tenslotte diegenen achter de schermen. Mijn ouders en familie ben ik erkentelijk voor hun steeds aanwezige begrip en vertrouwen in de goede afloop.

Verder zou ik Gaëtane willen bedanken voor die verrukkelijke italiaanse gerechtjes die tussen enkele moeizame experimenten door, steeds weer de nodige rust en inspiratie brachten.

Tot slot gaat m'n dank uit naar m'n vrienden voor hun onrechtstreekse, maar daarom niet minder wezenlijke, steun tijdens de afgelopen jaren.

ABSTRACT.

Vibro-acoustic problems meet serious limitations at high frequencies due to the frequency dependent wavelengths of the oscillatory response. For high-frequency studies dominated by high modal densities, SEA has become a useful technique providing a solution in statistical terms. SEA yields a single space averaged energy value for every single subsystem and is generally applicable for broadband excitation. The model parameters relate energy levels, energy flow, energy dissipation and power input of the different subsystems. The main SEA parameters are correspondingly : the internal loss factor, the coupling loss factor, the modal density associated with the subsystems.

The main objective is the identification of the SEA parameters, constituting the background for this dissertation. More specifically, emphasis will be given to two approaches for identifying the SEA parameters :

- Experimental approach.
- Computational approach.

The basis of the experimental method is the Power Injection Method. Computational procedures are based on analytical formulae and on the finite element method.

While analytical expressions for SEA parameters exist for a variety of simple structures, it has not been possible to extend these expressions to include general complex structures. One possibility to study complex structures is to experimentally identify the model parameters, a procedure which naturally lacks the notable advantages of the purely predictive approaches. Nevertheless, vibration transmission paths in a structure in operating conditions can be recovered and effective measures can be taken to reduce noise and vibration levels of the structure. It will be shown that by applying existing and optimized techniques, an accurate though affordable study of the high frequency dynamics can be undertaken. Several methodologies to optimize specific aspects of the experimental identification procedure are examined and developed. Advantages, disadvantages are addressed and illustrated by means of some relevant examples. Together, these specific methods make up a powerful tool to effectively identify the SEA parameters on a structure in situ.

Computational modeling procedures constitute the second main aspect of this dissertation. Historically, computational identification procedures are fifteen years ahead compared to the experimental procedures in SEA. The main notable advantage of the computational procedures is the ability to perform noise and vibration prediction and to suggest the modification of structural properties in order to reduce noise and vibration levels, *in the early design stage of structures*. The application of analytical methods which are covered in this thesis allows to evaluate the dynamics of simple structures in the high frequency range. Complex structures can not be handled purely by analytical methods. Numerical procedures which include structural details in a detailed extent (like finite elements) should be employed. In this respect, this dissertation addresses an approach developed and worked out in the framework of the SEA research to identify vibration transmission properties of complex junctions, allowing one to evaluate more precisely the noise and vibration characteristics of a complex structure in the design stage.

For SEA, one should roughly distinguish between two fields :

- Noise and vibration evaluation of complex structures in operating conditions. The Power Injection Method (PIM) is the underlying method to perform the identification of the model parameters of a structure in situ, i.e. without the need to decouple the structure. Effective control measures can be taken to reduce excessive noise and vibration levels, based on the vibration transmission paths in the structure. Complex structure include cars, trucks, trains etc.
- The second main application field is situated in the design stage of structures. By applying finite element techniques to identify transmission properties of junctions (see chapter *6*), one is not restricted to the exhaustive list of simple substructure couplings which are implemented in the commercially available softwares at present.

Contents.

- ***Chapter 1***

  Chapter *1* covers the background of high frequency modeling of structures. It is shown that many industrial structures exhibit problems with respect to the evaluation of high frequency dynamics. The latter can not be treated by means of classical so-called deterministic methods, including finite elements, boundary elements and classical experimental modal analysis. In order to put the problems into a clear perspective, the example of a car will be addressed briefly, though similar structures could be considered as well. A survey of the literature is presented in chapter *1*. This literature overview covers the main methods which are dealing with the modeling of high frequency vibrations.

- ***Chapter 2.***

  Chapter 2 intends to give an in depth view on SEA. It focuses in particular on the SEA parameters, namely modal densities, coupling loss factors and internal loss factors. The SEA equations are derived for a two-subsystem model and are extended to models including an arbitrary number of subsystems. Several important issues are addressed such as :

  ◊ Modes of application.

  ◊ The choice of subsystems.

- ◊ Wave-mode duality.
- ◊ Averaging.
- ◊ Non-stationary SEA.
- ◊ Non-resonant transmission.
- ◊ Advantages and disadvantages.

As such, chapter *2* enlightens the background of chapter *3* to *6*.

- ***Chapter 3.***

Chapter *3* presents the background and implementation of experimental SEA. The experimental identification of SEA parameters is based on the steady state power injection method. Basically, the method consists of a series of input-output measurements. The measured data are inverted to yield the model parameters. The way to measure the energies and power inputs is addressed. Notes are presented concerning the updating of the measurements (and hence of the model). The application of FRF techniques is covered briefly.

- ***Chapter 4.***

Chapter *4* presents the statistical and sensitivity aspects of the Power Injection Method (PIM) and includes the following main issues :

- ◊ Confidence levels of PIM.
- ◊ Influence of measurement errors.
- ◊ Sensitivity analysis.
- ◊ Consequences of neglecting response measurements.
- ◊ Identification of specific SEA parameters.

The procedures developed in chapter *4* are illustrated by means of experimental results on a box structure.

- ***Chapter 5.***

Chapter *5* attacks the computational prediction of the SEA parameters. In particular the evaluation of coupling loss factors is covered extensively. General, flexible formulations concerning the evaluation of the coupling loss factors of beam-beam junctions and plate-plate junctions are presented. Some examples are foreseen. In addition, a brief description of the state of the art existing techniques concerning the evaluation of modal densities and internal loss factors, the way it is implemented into the SEA program SEAPACK (developed in the framework of this thesis) is given.

- ***Chapter 6.***

The research which is presented in chapter *6* contributes to the integration of numerical methods to analyze complex junctions in the higher frequency range. Numerical techniques, based on local finite element models of junctions are applied and shown to be essential and valuable in the high frequency range. The theory developed in chapter *6* is illustrated by means of some relevant examples.

TABLE OF CONTENTS.

NOMENCLATURE.

a_i	Generalized wave coordinate of wave i.
c	Speed of sound.
c_p	Phase velocity of a wave.
c_g	Group velocity of a wave.
f	Center frequency of frequency band.
$f(t)$	Measured force signal.
$f_{x,y,z}(t)$	Forces in the x, y respectively z direction as a function of time.
g_{12}	Parameter expressing the strength of coupling between two coupled oscillators.
k	Stiffness constant.
$k_{x,y}$	Wavenumbers associated with x and y directions.
m	Mass.
$m_{x,y,z}(t)$	Moments about the x, y respectively z direction as a function of time.
n	The number of subsystems.
n_i	Modal density of subsystem i.
p	Pressure.
q_r	Generalized coordinate associated with mode r.
$\{q\}$	12 × 1 vector of basic variables.
s_x^2	Variance of variable x.
t	Thickness of a plate.

$u_{x,y,z}(t)$	Particle displacement in the x, y respectively z direction as a function of time.
$v(t)$	Measured velocity signal.
$v_{x,y,z}(t)$	Particle velocity in the x, y respectively z direction as a function of time.
$w_{x,y,z}(t)$	Angular velocity about x, y respectively z direction.
E	Modulus of elasticity.
$\{E\}$	$n \times 1$ vector of energy levels.
E_i	Spatial and frequency averaged energy of vibration of subsystem i.
E_k	Kinetic energy.
E_p	Potential energy.
E_{ij}	Energy level of subsystem i when exciting subsystem j.
E_{ij}^c	Contribution of subsystem j with respect to the energy level of subsystem i.
$[E^n]$	Normalized energy matrix.
$F_{x,y,z}(f)$	Frequency representation of the forces.
$\{F^+\}$	6×1vector of internal forces associated with positive going waves.
$G(f)$	Conductance function = real part of mobility.
H_{12}	FRF between two signals : X_1 / X_2.
$I_{x,y,z}$	Second moment of area about x, y respectively z direction.
$[K_\infty^+]$	Wave dynamic stiffness of positive going wave.
$[K^d]$	Dynamic stiffness matrix.
$K_{y,z}$	Shear coefficient in the y respectively z direction.
L	Length of a one-dimensional subsystem.
M_i	Modal overlap factor of subsystem i.
$M_{x,y,z}(f)$	Frequency representation of the moment.
$N_i = \Delta f \cdot n_i$	Mode count of subsystem i : number of modes in a frequency band.
N_e	The number of excitation locations / subsystem.
N_r	The number of response locations / subsystem.
N_s	The number of subsystems on which response instruments are located.
$\{P\}$	$n \times 1$ vector of power input levels.
$P_{i,diss}$	Frequency averaged dissipated power in subsystem i.
$P_{i \to j}$	Frequency averaged energy flow from subsystem i to subsystem j.

P_{ij}	Net frequency averaged energy flow from subsystem i to subsystem j.
P_i	Frequency averaged power input into subsystem i.
$R(f)$	Input resistance of a cavity = real part of the impedance (pressure / volume velocity).
S	Area of a surface.
$S_{fv}(f)$	Crosspower spectrum between force and velocity.
$S_{fa}(f)$	Crosspower spectrum between force and acceleration.
V	Volume of a cavity.
$\{U^+\}$	6 × 1vector of particle displacement associated with positive going waves.
$U_{x,y,z}(f)$	Frequency representation of the particle displacement.
$V_{x,y,z}(f)$	Frequency representation of the velocity.
$W_{x,y,z}(f)$	Frequency representation of the angular velocity.
$Y(f)$	Mobility function = velocity / force.
$Z(f)$	Impedance function = force / velocity.
α	Energy correction coefficient.
$\alpha_{i,jk}$	Sensitivity parameter.
γ	Decay rate.
η_{ij}	SEA coupling loss factor expressing strength of coupling between wave fields in subsystem i to wave fields of subsystem j.
$\eta_i = \eta_{ii}$	Internal loss factor of subsystem i.
η_s	Structural loss factor.
η_{rad}	Acoustic radiation loss factor.
η_b	Loss factor expressing damping at the boundaries of a subsystem.
$[\eta^o]$	Total loss factor matrix.
λ_i	Eigenvalue of total loss factor matrix, multiplied by ω.
λ_c	Critical wavelength.
ν	Poisson's ratio.
ρ	Material density.
σ	Radiation ratio.
$\theta_{x,y,z}(t)$	Rotation about x, y respectively z direction as a function of time.
ω	Angular center frequency of frequency band.

ω_o	Undamped natural angular frequency.
$\Theta_{x,y,z}(f)$	Frequency representation of the rotation.
$[\Psi]$	Matrix of eigenvectors.
$\bar{}$	Averaging with respect to time.
$\langle \rangle_s$	Operator expressing spatial averaging.

SAMENVATTING PROEFSCHRIFT.

Inleiding.

Mede door de wetenschappelijke en technologische vooruitgang stelt de verbruiker hogere eisen aan zijn koopwaar. De markt verwacht snelle en krachtige wagens, betere wegligging gepaard aan een steeds hoger comfort zoals bijvoorbeeld op het gebied van geluid en trillingen enz. Producenten van huishoudapparaten streven naar het ontwikkelen van toestellen met een hoog gebruikerscomfort en een hoog energetisch rendement. Tegelijkertijd dienen de toestellen compact en geluidsvriendelijk te zijn. In de werkplaats wordt gestreefd naar een hogere veiligheid en betere werkomstandigheden. Aanvaardbare geluidsniveaus voor de werknemers staan in deze problematiek centraal. Om tegemoet te komen aan de hoge verwachtingen van de consumenten en om tevens de steeds strenger wordende normen opgelegd door goevernementele organisaties na te komen, dienen nieuwe, complexe technieken te worden ontwikkeld en bestaande methodes geoptimaliseerd.

Het modelleren en kwantificeren van het *structuurgeluid* en het nagaan van de *trillingspaden* in een structuur in het volledige audio-gebied kan hiertoe bijdragen. Indien de trillingswegen in een structuur kunnen bepaald worden, is het mogelijk om efficiënte maatregelen te nemen om het geluids-en trillingsniveau te reduceren. De klassieke en minder efficiënte oplossing voor dit soort problemen is het aanbrengen van dempingsmateriaal over grote delen van de constructie : bijvoorbeeld over de volledige romp van een vliegtuig om het geluidsniveau in het vliegtuig te verminderen. Een alternatieve, meer efficiënte oplossing van het probleem bestaat erin selectief dempingsmateriaal aan te brengen gebaseerd op de analyse van de voortplantingswegen van de trillingen in de structuur. Zo kunnen niet alleen belangrijke geluidsredukties verkregen worden maar tevens leiden deze maatregelen tot signifikante gewichtsbesparingen en kostenverlagingen : bijvoorbeeld een energetisch efficiënter vliegtuig.

Een algemene methode om geluids-en trillingsniveaus in constructies zoals voertuigen, vliegtuigen, schepen, huishoudtoestellen (wasmachines) enz. te voorspellen in het

volledige audio-gebied (*20* Hz - *20* kHz) bestaat heden niet. De eindige elementen-methode, randelementenmethode en experimentele modale analyse zijn thans de meest gebruikte methodes om geluids- en trillingsproblemen te analyseren. In het gebied van de lage frekwenties[*] zijn deze zogenaamde deterministische methodes geschikt en worden algemeen gebruikt. Zo kunnen de globale trillingsfenomenen in wagens met eindige elementen gemodelleerd worden tot *150* Hz, voor schepen is de frekwentielimiet enkele tientallen Hz, voor vliegtuigen is dit lager dan *100* Hz. In het gebied van de hoge frekwenties (golflengte < globale afmeting) zijn de klassieke deterministische methodes niet geschikt door hoofdzakelijk :

- De grootte van de modellen, resulterend in niet te verantwoorden hoge rekentijden, extensief modelleringswerk, gigantische databanken om het probleem te beschrijven en de resultaten te stockeren, enorme naverwerkingstijden en het bijna in de onmogelijkheid zijn om een praktisch bruikbare sensitiviteitsanalyse door te voeren.
- De onzekerheid op structurele details en materiaaleigenschappen, de onzekerheid op de omgevingscondities zoals temperatuurschommelingen, de onzekerheid op de randvoorwaarden van de structuur (ingeklemd, vrij, akoestische impedantie), de onzekerheid op de inwerkende belasting enz.

Als gevolg van deze onzekerheden zal de respons van individuele, nominaal identische structuren in het hoogfrekwente gebied sterk van elkaar verschillen. Uiteindelijk leiden deze onzekerheden ertoe dat de performantie die kan verwezenlijkt worden bij de klassieke analyse van een groot complex model, zelfs met ingewikkelde eindige elementenmodellen, in het geval dat meerdere modes signifikant tot de respons bijdragen, eerder schijnbaar is.

Zelfs al is het mogelijk vanuit rekentechnisch standpunt om FRF's (amplitude en faze) te berekenen in het hoogfrekwente gebied en zelfs al is het mogelijk om sensitiviteitsanalyses met klassieke deterministische methodes uit te voeren, uiteindelijk zal men toch de resultaten middelen om interpreteerbare, aanvaardbare resultaten op te leveren. Het ligt eigenlijk met andere woorden voor de hand om het relevante stelsel vergelijkingen op te lossen gebaseerd op reeds gemiddelde grootheden ipv de analyse uit te voeren op lokale grootheden en pas achteraf te middelen. Dit belangrijke verschil tussen de deterministische en statistische analysetechnieken wordt voorgesteld in figuur *1*.

---

[*] Een veel voorkomende definitie van het laag frekwente trillingsgebied is : het frekwentiegebied waarin de golflengte van de trilling (hetzij structureel of akoestisch) niet veel kleiner is dan de afmeting van de structuur of caviteit.

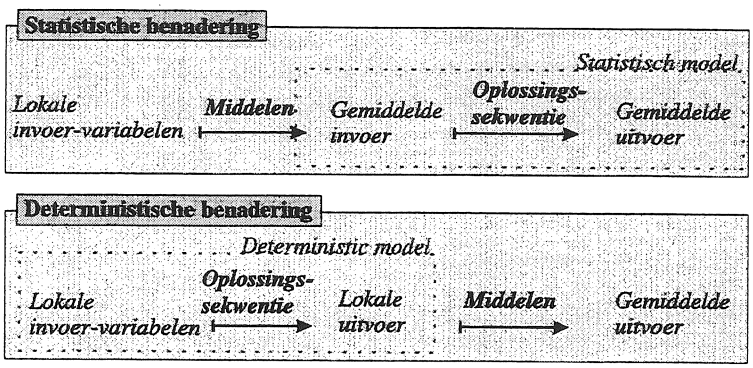

Figuur 1 : Schematische voorstelling van het verschil tussen een deterministisch model en een statistisch model.

Deze figuur illustreert duidelijk dat als een statistische benadering wordt aangewend, de problemen eigen aan de deterministische methodes vervallen :

- Grote rekentijd : gezien de variabelen en parameters worden gemiddeld zal de grootte van het resulteren stelsel vergelijkingen aanvaardbaar uitvallen.
- Duur modelleringswerk : er is niet langer de nood om elk detail van een structuur te modelleren. In het geval van een wagen zal het dak gemodelleerd worden als een vlakke plaat met een bepaalde dikte en met specifieke materiaaleigenschappen. Verbindingen daarentegen zullen in bepaalde gevallen nauwkeuriger moeten gemodelleerd worden.
- Enorme naverwerkingstijden : gezien slechts enkele variabelen meespelen in de analyse zullen de resultaten eenvoudig te interpreteren zijn en hoeven als dusdanig niet extensief naverwerkt te worden.
- Onzekerheid op de respons : gezien gemiddelde worden berekend zullen de hoge onzekerheidsniveaus verdwijnen. In het deterministische model heeft men te kampen met een grote onzekerheid omdat punt-responsies (op een specifieke plaats bij een specifieke frekwentie) worden berekend.
- Grote database : verdwijnt als gevolg van het klein aantal parameters en variabelen.
- Onpraktisch voor sensitiviteitsanalyses : gezien slecths enkele parameters worden beschouwd, zal de invloed van structurele veranderingen vlug kunnen gebeuren. De oplossingssekwentie is goedkoop en vlug, resultaten zijn gemakkelijk te interpreteren.

De voorgaande beschouwingen illustreren duidelijk de voordelen van een statistische benadering. De vraag kan nu worden gesteld hoe men een statistisch model kan opstellen : wat zijn de parameters? Hoe zijn de parameters gerelateerd met physisch interpreteerbare grootheden? Hoe zijn de invoer-variabelen en uitvoer-variabelen met elkaar verbonden ?

Stand van zaken.

Tijdens de laatste decennia is heel wat onderzoek verricht betreffende het ontwikkelen van technieken om hoogfrekwente trillingsproblemen adequaat te kunnen analyseren.

Enkele van deze methodes worden voorgesteld in hoofdstuk *1*. De procedures, voor-en nadelen worden kort toegelicht in het desbetreffende hoofdstuk. De belangrijkste methodes zijn : statistische energie analyse, asymptotische modale analyse, energiestroom eindige elementen-analyse, energie-modellen op basis van omhullenden, mobiliteits-energiestroom, algemene energie-formulering, "straal" technieken en intensiteitsmodellen.

In deze samenvatting wordt slechts een korte beschrijving gegeven van de techniek die verder in dit werk wordt aangewend, namelijk "statistische energie analyse".

Statistische Energie Analyse (SEA).

SEA beschrijft de trillingstoestand in termen van opgeslagen, gedissipeerde en uitgewisselde energie. Door energie te weerhouden als primaire variabele, kunnen akoestisch en structurele problemen op overeenkomstige manier behandeld worden. SEA stelt dat trillingsenergie zich op dezelfde manier gedraagt als warmte-energie. De trillingsenergie diffundeert van "hete" plaatsen naar "koele" plaatsen proportioneel met het verschil in temperatuur. Deze thermische constante wordt de thermische conductiviteit genoemd. Dit thermisch model wordt gerelateerd met het trillings-model door de gemiddelde modale trillingsenergie in een substructuur te beschouwen als maat voor de temperatuur. De koppelingsfaktor begroot de sterkte van de koppeling tussen twee subsystemen. De thermische capaciteit van een subsysteem wordt vertaald in de modale densiteit (i.e. het aantal modes per frekwentie-eenheid).

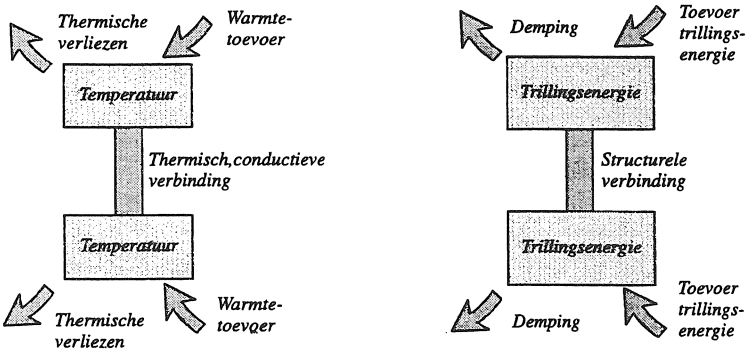

Figuur 2 : Vergelijking thermisch en vibro-akoestisch energiemodel.

Voor elk subsysteem (= opslagplaats van trillingsenergie) wordt een energiebalans opgesteld : de ingevoerde energie is gelijk aan de energie getransporteerd naar de aanliggende subsystemen en de energie gedissipeerd door interne demping. Het SEA concept wordt geïllustreerd in het geval van 3 gekoppelde platen :

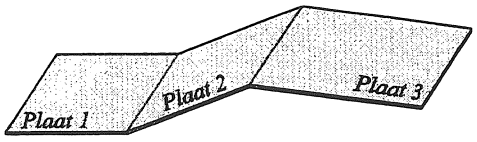

Figuur 3 : Physisch model : 3 gekoppelde platen.

Figuur *4* stelt schematisch het overeenkomstige SEA model voor.

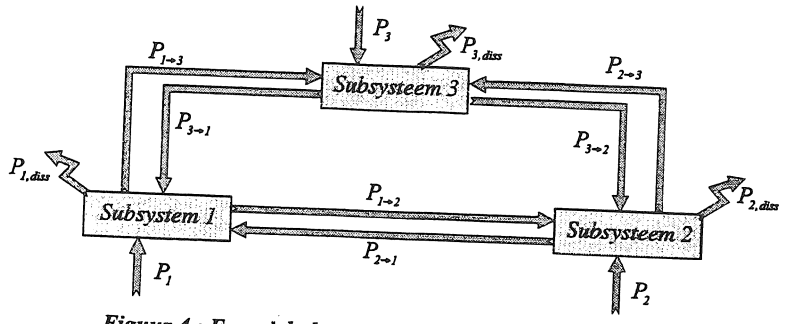

Figuur 4 : Energiebalans van een drie-subsystemen model.

De drie verschillende blokken van figuur *4* worden de SEA subsystemen genoemd. Het energie-niveau in een subsysteem i wordt voorgesteld door E_i. De energiestroom van een subsysteem i naar een nabij gelegen subsysteem j wordt voorgesteld door de pijlen $P_{i\to j}$. De externe energietoevoer naar subsysteem i wordt voorgesteld door P_i. De energie die wordt gedissipeerd in i, wordt gegeven door $P_{i,diss}$. Deze variabelen worden tijds-, frekwentie- en ruimtelijk gemiddelde beschouwd.

De SEA basisveronderstellingen en de eraan gekoppelde vergelijkingen betreffen enerzijds energiedissipatie in een subsysteem en anderzijds energie-uitwisseling tussen de subsystemen. De eerste basisveronderstelling (dissipatie) wordt vertaald in :

$$P_{i,diss} = \omega \cdot \eta_{ii} \cdot E_i \qquad (1)$$

Hierin stelt η_{ii} de interne verliesfactor van het subsysteem i voor. ω staat voor de centerfrekwentie van de beschouwde frekwentieband. Met andere woorden, het gedissipeerde vermogen is proportioneel met de excitatiefrekwentie en met de globale trillingsenergie van het subsysteem.

De energiestroom tussen twee individuele subsystemen (i & j) wordt proportioneel verondersteld met het verschil in modale energie (energie / mode). Mathematisch wordt dit laatste vertaald in :

$$P_{ij} = \omega \gamma_{ij} \left(\frac{E_i}{N_i} - \frac{E_j}{N_j} \right) \qquad (2)$$

De parameter N_i stelt het aantal modes van subsysteem i in de frekwentieband voor. γ_{ij} is een evenredigheidsfaktor.

Verglijking (2), bevattende drie parameters van het systeem, wordt quasi altijd geschreven in de vorm van twee vergelijkingen met vier onbekenden :

$$\begin{cases} P_{ij} = \omega(\eta_{ij} E_i - \eta_{ji} E_j) \\ n_i \eta_{ij} = n_j \eta_{ji} \end{cases} \qquad (3)$$

In vergelijking (3), stelt de n_i de modale densiteit voor. η_{ij} staat voor de koppelingsfaktor tussen subsysteem i en j.

De bedoeling van dit proefschrift is nu om de SEA parameters, zijnde de interne verliesfaktor, de koppelingsfaktor en de modale densiteit te bepalen. Hiervoor worden experimentele (hoofdstuk *3* & *4*) en rekenkundige technieken (hoofdstuk *5* & *6*) aangewend.

Geassembleerde vergelijkingen. Verder kan de globale energiebalans van de structuur geschreven worden als :

$$P_i = P_{i,diss} + \sum_{j \neq i}^{n} P_{i \to j} - \sum_{j \neq i}^{n} P_{j \to i} \qquad (4)$$

Vergelijking (4) houdt geen hypothese in, maar stelt een algemeen geldende energiebalans voor.

Gebruik makend van de basisveronderstellingen van SEA (betreffende energiedissipatie en energie-uitwisseling), verkrijgt men :

$$P_i = \omega \eta_{ii} E_i + \sum_{j \neq i}^{n} \omega(\eta_{ij} E_i - \eta_{ji} E_j) \qquad (5)$$

en

$$n_i \eta_{ij} = n_j \eta_{ji} \qquad (6)$$

Of in matrix vorm :

$$\{P\} = \omega \cdot [\eta^o] \cdot \{E\} \quad en \quad n_i \eta_{ij} = n_j \eta_{ji} \qquad (7)$$

Vergelijking (6) stelt de reciprociteitsvergelijking voor. De vergelijkingen (7) worden uitgebreid behandeld in hoofdstuk 2.

Applikaties met betrekking tot SEA.

Zodra de SEA parameters geïdentificeerd of geëvalueerd zijn (via experimentele of prediktieve methodes), heeft men de mogelijkheid om het SEA model aan te wenden om trillingsanalyses uit te voeren. Een SEA model kan in het ontwerpstadium van een structuur of tijdens het in gebruik zijn van een structuur gebruikt worden. De volgende paragrafen gaan dieper in op enkele applikatiedomeinen van SEA.

Prediktie van de respons.

SEA laat toe om bij gekend zijnde SEA parameters en bij gekend zijnde vermogentoevoer naar de verschillende subsystemen, het energieniveau in elk subsysteem te begroten. De vergelijkingen zijn linear algebraisch. De energieniveaus kunnen in bepaalde omstandigheden omgerekend worden naar secundaire variabelen van belang : geluidsniveaus, spanningsniveaus, rekwaarden etc. Mathematisch worden de energieniveaus berekend volgens :

$$\{E\} = \frac{1}{\omega} \cdot [\eta^o]^{-1} \cdot \{P\} \qquad (8)$$

Partiële contributies. Een eenvoudige manipulatie laat toe om de partiële contributies van de trillingsbronnen met betrekking tot het energieniveau in een subsysteem te quantificeren. De volgende vergelijking stelt deze contributies voor :

$$E_{ij}^{c} = \frac{1}{\omega} \cdot \eta_{ij}^{o-1} \cdot P_j \qquad (9)$$

In vergelijking (9) stelt E_{ij}^{c} de contributie van de vermogentoevoer in subsysteem j tot het energieniveau in subsysteem i voor.

Bronlokalizatie.

Op basis van gekend zijnde SEA parameters van een systeem en van gekend zijnde energieniveaus van de verschillende subsystemen, kan men de vermogentoevoer naar de verschillende subsystemen berekenen :

$$\{P\} = \omega \cdot [\eta^{o}] \cdot \{E\} \qquad (10)$$

Begroting van de energiestromen.

De meest praktische applikatie van SEA betreft het bepalen van de energiestromen van het punt van excitatie, doorheen de subsystemen naar verder gelegen subsystemen. Het begroten van deze energiestromen is essentieel om te komen tot efficiënte trillings- en geluidsreducerende maatregelen.

Eén van de basisvergelijkingen van SEA betreft de uitwisseling van trillingsenergie tussen subsystemen. Van zodra de SEA parameters en de vermogentoevoer naar de verschillende subsystemen gekend zijn, kunnen alle energiestromen in een systeem berekend worden volgens vergelijking (3). De volgende figuur stelt een typische energiestroom in een wagen voor.

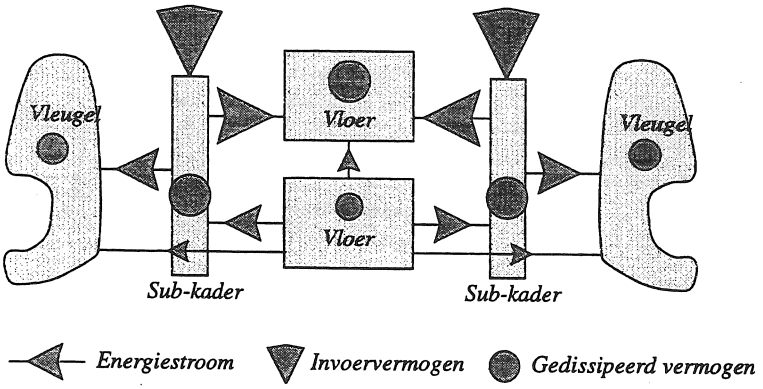

Figuur 5 : Representatie van energiestromen in een deel van een wagen.

Sensitiviteits-analyse.

Vermits het aantal parameters en variabelen dat in SEA gebruikt wordt vrij laag is (ttz. Significant lager dan de deterministische methodes), is het uitvoeren van sensitiviteitsberekeningen eenvoudig en weinig rekenintensief. Hier staat wel tegenover dat men met gemiddeld grootheden werkt, zodat ruimtelijke informatie verloren gaat.

Bij gekend zijnde SEA parameters en vermogentoevoer, kan de sensitiviteit van de energie in een subsysteem i met betrekking tot een model parameter als volgt berekend worden :

$$\frac{\partial E_i}{\partial \eta_{jk}} = -\frac{1}{\omega} \cdot \sum_{m=1}^{n} \left[\left[\eta^o\right]^{-1} \cdot \frac{\partial \left[\eta^o\right]}{\partial \eta_{jk}} \cdot \left[\eta^o\right]^{-1} \right]_{im} \cdot P_m \qquad (11)$$

Uitdrukkingen voor deze vergelijking worden gegeven in hoofdstuk *4*.

Keuze van de subsystemen.

Bij het aanwenden van SEA wordt een systeem conceptueel verdeeld in subsystemen. Sommige subsystemen worden direct geëxciteerd, andere indirect via de koppelingsmechanismen. De eerste en dikwijls heel belangerijke stap bij het aanwenden van SEA heeft betrekking op de keuze van de subsystemen.

Een subsysteem wordt gedefinieerd als een element van een SEA model corresponderend met een substantiële energie-opslagplaats. Twee condities dienen in overweging genomen te worden bij de keuze van de subsystemen : similariteit en signifikantie.

Similariteit : de set van modes in een subsysteem dienen in de mate van het mogelijke aan similariteit te voldoen, ttz. er mag geen enkele mode in de set zijn die een veel meer beduidende respons heeft dan de andere modes van de set. Bovendien wordt er verlangd dat de demping van de modes in de set van dezelfde grootteorde is.

Signifikantie : indien een subsysteem een marginale rol speelt in het SEA model omdat het niet is geëxciteerd, omdat de energiestromen van en naar dit subsysteem te verwaarlozen zijn en omdat het energieniveau laag is, dan dient men dit subsysteem niet in beschouwing te nemen. Voorbeeld : voor gekoppelde platen kan men in principe drie subsystemen per plaat beschouwen, ttz. afschuifenergie in het vlak, longitudinale energie in het vlak en buigingsenergie uit het vlak. In het laagfrekwentie gebied zijn echter de in-het-vlak werkende trillingen niet significant en moeten als dusdanig niet in rekening worden gebracht. In het hoogfrekwente gebied is het soms aangewezen om de in-het-vlak werkende energie in rekening te brengen.

Hier dient opgemerkt te worden dat de regels die gebruikt worden om SEA subsystemen te kiezen niet eenduidig zijn. Veel hangt af van ervaring. Een typisch probleem dat kan optreden bij de keuze van subsystemen wordt hieronder weergegeven. De structuur betreft het dak en de C-pillar van een wagen. Ter plaatse van de verbinding kan zich een afronding bevinden zoals weergegeven in de volgende figuur.

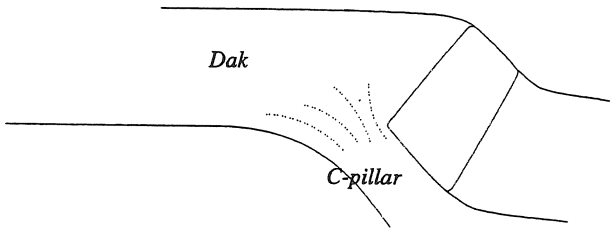

Figuur 6 : Verbinding tussen het dak en de C-pillar van een wagen.

Door de aanwezigheid van de afronding is de keuze van de subsystemen niet eenduidig : waar begint of eindigt een subsysteem juist ? In het hoogfrekwente gebied zullen bovendien de golven die invallen op het dak (vanuit de C-pillar) minder teruggekaatst worden, zodat de koppeling tussen C-pillar en dak minder zwak wordt, wat gevolgen heeft op de toepasbaarheid van SEA.

Voor- en nadelen.

Tot slot worden enkele voor- en nadelen van SEA opgesomd.

Voordelen.

- Gezien de dimensie van het vibro-akoestisch model drastisch gereduceerd is als gevolg van de middeling met betrekking tot plaats en frekwentie, zullen veranderingen aan het model gemakkelijk en vlug kunnen doorgerekend worden. Dus, SEA is uiterst bruikbaar in de ontwerpfaze van structuren.
- Prediktieve SEA (hoofdstuk *5-6*) gebruikt slechts enkele parameters van een subsysteem. Bijvoorbeeld, de modale densiteit van een plaat wordt gedetermineerd door slechts enekele parameters zoals dikte en materiaal karakteristieken.
- SEA is gebaseerd op energie conservatie. Elke afwijking van dit principe kan gemakkelijk gedecteerd worden, de vergelijkingen zijn physisch uiterst gemakkelijk te interpreteren.
- SEA biedt een excellent kader voor transmissiepadanalyse. SEA biedt de ingenieur de mogelijkheid om efficiënte maatregelen te nemen om trillingen te reduceren.

Nadelen.

- Heden zijn nog geen algemene aanvaardbare methodes ontwikkeld met betrekking tot het nagaan van betrouwbaarheidsintervallen en nauwkeurigheid.
- Een juiste keuze van subsystemen is van essentieel belang. Nochtans zijn heden nog geen criteria ter beschikking om de keuze van subsystemen te verantwoorden.
- Onderzoek is gaande omtrent smalband-excitatie.
- Klassieke SEA biedt niet de mogelijkheid om een nauwkeurige schatting te geven van lokale trillingsniveaus, wellicht één van de belangrijkste nadelen van SEA.
- Tunneling blijft een vraagteken.

- SEA veronderstelt een reverberent veld om de vergelijkingen aan te wenden. Hoedanook, als de trilling sterk en lokaal gedempt zijn (zoals het geluidsveld in een caviteit met sterk absorberende wanden) zullen de reverberente karakteristieken verdwijnen.
- Het verband tussen de SEA parameters en physische eigenschappen van een systeem zijn niet altijd even duidelijk. Bijvoorbeeld, een koppelingsfaktor die experimenteel bepaald is, is een min of meer onbekende funktie van de koppeling.

Experimentele identificatie van de SEA parameters.

Voor complexe structuren kunnen de SEA parameters niet altijd op een nauwkeurig prediktieve manier bepaald worden. In andere gevallen kan het opportuun zijn om de energiestromen tijdens operationele omstandigheden in bestaande structuren na te gaan teneinde doeltreffende maatregelen te treffen met betrekking tot het dynamisch optimaliseren van de structuur. Vaak zijn deze structuren complex (zoals een wagen) en analytische formules voor de SEA parameters zijn zelden aanwezig. Soms kan het ook noodzakelijk zijn om computationele SEA modellen te verifiëren. In deze gevallen is het dan ook aangewezen om de SEA parameters te bepalen aan de hand van metingen op de desbetreffende structuur. De vermogeninjectiemethode, kortweg PIM, vormt de basis van experimentele SEA. PIM is gebaseerd op het uitvoeren van een set van relevante responsmetingen op de structuur.

Vanuit een mathematische invalshoek, correspondeert PIM met het identificeren van de transformatiematrix tussen het *energie-domein* en het *vermogentoevoer-domein*, i.e. :

$$\{P\} = \omega \cdot [\eta^o] \cdot \{E\} \tag{12}$$

De meest voor de hand liggende manier om de transformatiematrix $\omega \cdot [\eta^o]$ te bepalen is via het bepalen van de beelden van set van orthogonale eenheidsvectoren. Elk van deze beelden vormt een kolom van de transformatiematrix. Praktisch zal de tranformatiematrix niet voorgesteld worden door $\omega \cdot [\eta^o]$, maar door de inverse, ttz :

$$\frac{1}{\omega} \cdot [\eta^o]^{-1} = \frac{1}{\omega} \cdot [E^n] \tag{13}$$

De procedure wordt hieronder kort toegelicht in het geval van een twee-subsysteem SEA model (figuur 7).

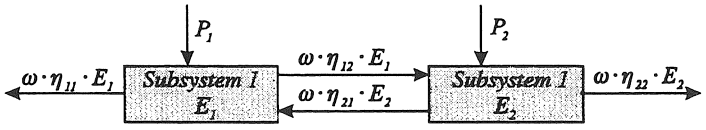

Figuur 7 : Twee-subsysteem SEA model.

The basisvergelijkingen van SEA zijn :

$$\begin{Bmatrix} P_1 \\ P_2 \end{Bmatrix} = \omega \begin{bmatrix} \eta_{11}^o & \eta_{12}^o \\ \eta_{21}^o & \eta_{22}^o \end{bmatrix} \begin{Bmatrix} E_1 \\ E_2 \end{Bmatrix} \tag{14}$$

Vooreerst wordt vermogen aangelegd aan het eerste subsysteem. Vergelijking (14) resultaat diengevolge in :

$$\begin{Bmatrix} P_1 \\ 0 \end{Bmatrix} = \omega \begin{bmatrix} \eta_{11}^o & \eta_{12}^o \\ \eta_{21}^o & \eta_{22}^o \end{bmatrix} \begin{Bmatrix} E_{11} \\ E_{21} \end{Bmatrix} \tag{15}$$

Hierbij stelt E_{ij} de gemeten energie in subsysteem i voor bij excitatie van subsysteem j. Het gemeten, aangelegd vermogen aan subsysteem j wordt voorgesteld door P_j.

Na de excitatie van het eerste subsysteem wordt vermogen aangelegd aan het tweede subsysteem, resulterend in een stelsel gelijkaardige vergelijkingen.

$$\begin{Bmatrix} 0 \\ P_2 \end{Bmatrix} = \begin{bmatrix} \eta_{11}^o & \eta_{12}^o \\ \eta_{21}^o & \eta_{22}^o \end{bmatrix} \begin{Bmatrix} E_{12} \\ E_{22} \end{Bmatrix} \tag{16}$$

Na het combineren en normaliseren (tov een eenheidsvermogen) van deze vergelijkingen bekomt men :

$$\begin{bmatrix} 1 & 0 \\ 0 & 1 \end{bmatrix} = \begin{bmatrix} \eta_{11}^o & \eta_{12}^o \\ \eta_{21}^o & \eta_{22}^o \end{bmatrix} \begin{bmatrix} E_{11}^n & E_{12}^n \\ E_{21}^n & E_{22}^n \end{bmatrix} \quad met \quad E_{ij}^n = \frac{\omega \cdot E_{ij}}{P_j} \tag{17}$$

De SEA parameters kunnen nu verder bekomen worden volgens :

$$\begin{cases} \eta_{11} = \eta_{11}^o + \eta_{21}^o & \eta_{12} = -\eta_{21}^o \\ \eta_{21} = -\eta_{12}^o & \eta_{22} = \eta_{22}^o + \eta_{12}^o \end{cases} \tag{18}$$

Deze techniek kan zonder enig probleem uitgebreid worden naar een groter aantal subsystemen.

Meten van energie en vermogentoevoer.

Om de genormaliseerde energiematrix te kunnen inverteren is het nodig om de vermogentoevoer naar elk van de subsystemen te meten en tevens de energieën van de verschillende subsystemen te begroten.

Meten van energie.

Gezien de totale reverberente energie in een subsysteem gelijk is aan het dubbele van de kinetische energie, zal de totale energie berekend worden uit de kinetische energie. Voor structurele subsystemen wordt de totale trillingsenergie dan ook benaderd door de som van de gekwadrateerde snelheden vermenigvuldigd met de massa van dat deel van het subsysteem waar een snelheidsmeting gebeurt.

$$E = \int_A \rho v^2 \, dA \cong \delta M_1 \cdot v_1^2 + \delta M_2 \cdot v_2^2 + \cdots + \delta M_N \cdot v_N^2 \tag{19}$$

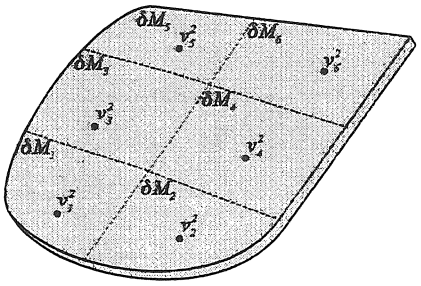

Figuur 8 : Energiemeting via discrete snelheidsmeting.

Vergelijking (19) kan omgezet worden in acceleratiespectra volgens :

$$E_{\omega_1,\omega_2} \cong M \cdot \frac{1}{N} \cdot \frac{1}{\omega^2} \cdot \sum_{i=1}^{N} \int_{\omega_1}^{\omega_2} S_{i,aa}(\omega) d\omega \qquad (20)$$

De grootheid E_{ω_1,ω_2} stelt de trillingsenergie in de frekwentieband $[\omega_1, \omega_2]$ voor. $S_{i,aa}(\omega)$ is het opgemeten acceleratiespectrum van accelerometer i.

Voor akoestische subsystemen gelden gelijkaardige formules. De akoestische energie wordt hierin opgemeten met behulp van microfoons.

Meten van vermogentoevoer.

Om de genormaliseerde energiematrix te kunnen inverteren, dient de vermogentoevoer naar elk van de subsystemen te worden opgemeten. De excitatie van de subsystemen geschiedt via het aanwenden van een shaker, hamer of een "horndriver", naargelang de aard van het subsysteem. Enkel structurele vermogentoevoer wordt hier verder besproken.

De vemogentoevoer als gevolg van puntexcitatie is voorgesteld in de volgende figuur.

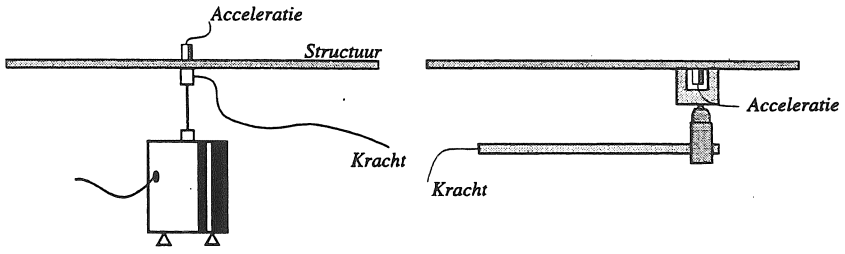

Figuur 9 : Vermogentoevoer en meting voor shaker en hamer excitatie.

De vermogentoevoer op elk moment t wordt gegeven door :

$$f(t) \cdot v(t) \qquad (21)$$

In spectrale gedaante en gebuik makend van acceleraties ipv snelheden, wordt de vermogentoevoer in de frekwentieband $[\omega_1, \omega_2]$ voorgesteld door :

$$P_{\omega_1,\omega_2} = \frac{1}{\omega} \cdot Im\left[\int_{\omega_1}^{\omega_2} S_{qf}(\omega) d\omega\right] \qquad (22)$$

De formules (20) en (22) zijn niet als dusdanig geïmplementeeerd in het SEA programma SEAPACK. In dit programma is gebruik gemaakt van FRF's ipv. vermogenspectra. Op die manier worden equivalente energieën en een equivalente vermogentoevoer verkregen. Zo kan het aangetoond worden dat de trillingsenergie proportioneel is met het kwadraat van de amplitude van de niet-diagonale termen van de FRF matrix (indirect FRF's).

$$E_{ji} \approx \left|H_{ji}\right|^2 = \left|\frac{A_j}{F_i}\right|^2 \qquad (23)$$

De vermogentoevoer is proportioneel met het imaginair gedeeld van de directe FRF's (acceleratie over kracht) :

$$P_{in} \approx Im\left[H_{ii}\right] = Im\left[\frac{A_i}{F_i}\right] \qquad (24)$$

Correctiecoëfficiënt met betrekking tot de opgemeten energie.

Formule (20) die het verband aangeeft tussen het acceleratiespectrum en de energie geldt slechts bij benadering aangezien :

$$E = 2 \cdot E_k = \int_V \rho v^2 \cdot dV \neq M \cdot < v^2 > \qquad (25)$$

Een correctiecoëfficiënt kan ingevoerd worden om de benadering van de opgemeten energie te elimineren volgens :

$$\int_A \rho v^2 \cdot dA = \alpha \cdot M \cdot < v^2 > \qquad (26)$$

Hierin stelt α de correctiecoëfficiënt voor. Via het aanwenden van "decay" metingen en het bepalen van "decay" karakteristieken van een subsysteem kan α bepaald worden. Een typisch voorbeeld van de enegieafname wordt voorgesteld in figuur *10*. De excitatie bestaat uit ruis in de band *1187.5 - 1312* Hz die op een specifiek ogenblik $t = 0.35\,s$ wordt uitgeschakeld.

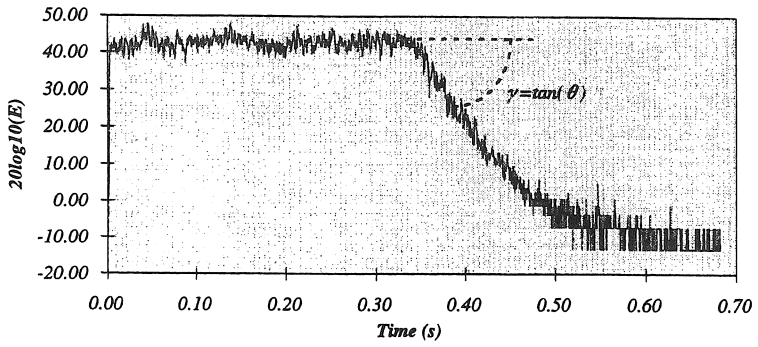

Figuur 10 : Afname van energie in een lin-log schaal.

Het aanwenden van een correctiecoëfficiënt is noodzakelijk wanneer in een subsysteem de masss niet gelijkmatig is verdeeld met dien gevolge dat vergelijking (20) minder bruikbaar wordt.

Een uitbreiding van voorgaande techniek is uitgewerkt in het kader van dit proefschrift en behandelt het "updaten" van de PIM meetresultaten via het aanwenden van (reeds aanwezige) informatie over specifieke subsystemen. Twee typische meetresultaten die in beschouwing kunnen genomen worden met betrekking tot het updaten zijn : energie-correctiecoëfficiënt en de vermogentoevoer in akoestische subsystemen.

Het tweede voorbeeld is uitgewerkt in het proefschrift. Voor een akoestische caviteit van een structuur is de verliesfaktor berekend uit de uitsterftijden van de caviteit. Door substitutie van deze verliesfactor in het globale SEA stelsel kan het meten van de vermogentoevoer in de akoestische caviteit vermeden worden. De algebraïsche vergelijkingen worden uitgebreid behandeld in hoofdstuk 3.

Meetstrategieën.

Het uitvoeren van een PIM meting op een grote, complexe structuur vergt het opmeten van een omvangrijk aantal spectra. De parameters die bij PIM metingen essentieel geacht worden zijn : het aantal subsystemen, het aantal excitatie- en responspunten (met betrekking tot de geometrische middeling) en het aantal beschikbare kanalen. Verschillende meetopstellingen zijn mogelijk :

- Concentratie van alle instrumenten op één subsysteem.
- Het plaatsen van een responsinstrument op elk subsysteem.
- Hybride meetopstelling (combinatie van de twee voorgaande).

De drie meetstrategieën hebben elk intrinsieke voor- en nadelen. Voor de eerste meetopstelling kan men per acquisitie een groter aantal spectra opmeten. Het nadeel van deze meetopstelling is dat de volledige set van metingen dient te gebeuren vooraleer de opgemeten genormaliseerde energiematrix kan geïnverteerd worden. De tweede meetopstelling laat toe om tijdens de metingen reeds de energiematrix te inverteren. Van zodra de vereiste nauwkeurigheid (in termen van betrouwbaarheidsinternvallen) is

bereikt kunnen de metingen worden stopgezet. Nadeel is dat men een kleiner aantal FRF's kan opmeten per acquisitie. De derde meetopstelling is een hybride van de beide voorgaande en bevat als dusdanig de voor- en nadelen van beide voorgaande meetopstellinen.

Modale densiteits- en modal overlappingsmetingen.

Eén van de basisparameters van SEA is de modale densiteit (aantal modes per Hertz). Deze parameter drukt uit hoe ontvankelijk een subsysteem is voor trillingsenergie : hoe hoger de modale densiteit, des te meer modes liggen er in de frekwentieband des te gemakkelijker kan energie opgeslagen worden in een subsysteem. Bovendien is de modale densiteit gerelateerd met de modale overlapping (getal dat de graad van overlapping van de modes uitdrukt) via :

$$M = \omega \cdot \eta \cdot n \tag{27}$$

De meest gebruikte techniek om modale densiteiten experimenteel te bepalen bestaat erin om het reëel deel van de puntmobiliteit (kracht over snelheid) op te meten (het reëel deel van de puntmobiliteit is op zichzelf een maat voor de ontvankelijkheid van een subsysteem voor energie en dus een maat voor de modale densiteit). Het verband tussen beide grootheden wordt gegeven door :

$$n(\omega) = \frac{4m}{\Delta\omega} \cdot \int_{\omega_1}^{\omega_2} < Re[Y(\omega)] > d\omega \tag{28}$$

Hierin stelt $Y(\omega)$ de puntmobiliteit van de structuur voor. m is de massa van het subsysteem.

Statistische analyse van PIM.

Gezien het middelen van de energie en vermogentoevoer geschiedt met inbegrip van een eindig aantal meetpunten, zal er diengevolge een onzekerheid bestaan op de gemiddelde energie en het gemiddeld toegevoerd vermogen in elk subsysteem. Daarom is het noodzakelijk om naast de gemiddelde waarden tevens de betrouwbaarheidsintervallen die kunnen geassocieerd worden met PIM te bepalen. Formuleringen zijn opgesteld om uitgaande van de meetresultaten, de betrouwbaarheidsintervallen van de genormaliseerde energieën, van de SEA parameters en van de SEA predikties te bepalen in funktie van het aantal meetpunten op de structuur.

In een eerste stap worden de betrouwbaarheidsintervallen van de genormaliseerde energieën begroot uitgaande van de opgemeten grootheden, resulterend in :

$$s^2_{E_{ij}} = \frac{1}{\overline{P}_j^2} \cdot s^2_{E_{ij}} + \frac{\overline{E}_{ij}^2}{\overline{P}_j^4} \cdot s^2_{P_j} \tag{29}$$

Hierin stellen $s^2_{E_{ij}}$ en $s^2_{P_j}$ de varianties van de opgemeten energieën respectievelijk toegevoerde vermogens voor. $s_{E^n_{ij}}$ is de variantie van de genormaliseerde energie.

De statistiek met betrekking tot de genormaliseerde energieën wordt omgezet naar statistiek met betrekking tot SEA parameters. De varianties van SEA parameters wordt

geschreven in funktie van varianties van genormaliseerde energieën via het aanwenden van een eerste orde Taylor benadering, resulterend in :

$$s^2_{\eta_{ij}} \cong \sum_{l,m=1}^{n} \left(\overline{\eta}^o_{jl} \cdot \overline{\eta}^o_{mi}\right)^2 \cdot s^2_{E^n_{lm}} \quad \textit{voor koppelingsfaktoren} \tag{30}$$

$$s^2_{\eta_{ii}} \cong \sum_{l,m=1}^{n} \left(\overline{\eta}^o_{mi} \cdot \overline{\eta}_{il}\right)^2 \cdot s^2_{E^n_{lm}} \quad \textit{voor verliesfaktoren} \tag{31}$$

Van zodra het SEA model geïdentificeerd is, kan het aangewend worden om predikies (energieën, vermogentoevoer etc.) door te voeren. De statistiek met betrekking tot de SEA predikties kan op aanverwante (zoals de statistiek met betrekking tot de SEA parameters) manier uitgevoerd worden.

Sensitiviteitsanalyse.

Een intrinsieke, belangerijke eigenschap van SEA is dat slechts een gering aantal variabelen en parameters in het model terug te vinden zijn. Het immense model dat zou verkregen worden met eindige elementen wordt bij SEA significant kleiner als gevolg van het middelen. Het grote voordeel van SEA aan de andere kant is dat, gezien slechts een gering aantal variabelen en parameters meespeelt, dat het uitvoeren van een sensitiviteitsanalyse relatief goedkoop en eenvoudig wordt. Het doorrekenen van het probleem voor verschillende configuraties vergt slechts een fraktie van de tijd die hieraan gespendeerd wordt bij eindige elementen.

Deze paragraaf is gefocuseerd op de applikatie die vanuit praktisch hoek als essentieel kan worden beschouwd. Als men de trillings- en geluidsniveaus van structuren en caviteiten wenst te controleren, dan is het essentieel om te weten waar en in welke mate structurele veranderingen door te voeren, ttz. men dient te kunnen nagaan in hoeverre de energieën veranderen bij veranderende parameters van het probleem. In het geval van PIM worden de sensitiviteitsformules vertaald in het zoeken naar een gepaste uitdrukking voor de volgende afgeleide :

$$\frac{\partial E_i}{\partial \eta_{jk}} \tag{32}$$

Na een vereenvoudiging van vergelijking (32) bekomt men de volgende resultaten voor koppelingsfactoren respectievelijk verliesfactoren :

$$\frac{\partial E_i}{\partial \eta_{jk}} = \left(E^n_{ik} - E^n_{ij}\right) \cdot E_j \qquad en \qquad \frac{\partial E_i}{\partial \eta_{ji}} = -E^n_{ij} \cdot E_j \tag{33}$$

Met behulp van formules (33) kan men op een eenvoudige manier nagaan welke SEA parameter η_{jk} (en dus structuurparameter) het meest gevoelig is met betrekking tot het energieniveau E_i van een specifiek subsysteem i.

Tenslotte dient vermeld te worden dat de sensitiviteitsformules niet direct betrekking hebben op physische grootheden. Men kan met andere woorden niet nagaan wat de invloed is van bijvoorbeeld het veranderen van de dikte van een substructuur op het energieniveau in een ander specifiek subsysteem. Dit laatste is niet mogelijk voor

experimentele SEA modellen vermits het verband tussen SEA parameters en physische grootheden niet voorhanden is.

Invloed van meetfouten.

Bij het aanwenden van PIM is het essentieel om een idee te hebben van de invloed van meetfouten op de SEA parameters en predikties. Hieronder vallen de meetfouten op energieën en meetfouten op toegevoerde vermogens. In het proefschrift worden de verschillende gevallen uitgebreid behandeld, ttz. meetfouten van energieën en vermogens op SEA parameters en op SEA predikties. Als voorbeeld wordt de invloed van meetfouten van toegevoerde vermogens met betrekking tot de SEA parameters gegeven. In de veronderstelling dat het opgemeten aangelegd vermogen van subsysteem i tijdens PIM systematisch verkeerd is volgens : $E_{ki}^{n,exact} = \alpha \cdot E_{ki}^{n,gemeten}$, dan kan de invloed van deze meetfout op de SEA parameters begroot worden met behulp van de volgende afgeleide :

$$\frac{\partial \eta_{kj}}{\partial \alpha} \tag{34}$$

Vergelijking (34) kan vereenvoudigd worden tot :

$$\begin{cases} \dfrac{\partial \eta_{kj}}{\partial \alpha} = -\dfrac{\eta_{ik}^{o}}{\alpha} \cdot \delta_{j,i} = \dfrac{\eta_{ki}}{\alpha} \cdot \delta_{j,i} & k \neq j \\ \dfrac{\partial \eta_{jj}}{\partial \alpha} = \displaystyle\sum_{l=1}^{n} \dfrac{\eta_{ij}^{o}}{\alpha} \cdot \delta_{l,i} = \dfrac{\eta_{ij}^{o}}{\alpha} \sum_{l=1}^{n} \delta_{l,i} = \dfrac{\eta_{ij}^{o}}{\alpha} \end{cases} \tag{35}$$

Besluit : in het geval van koppelingsfaktoren η_{kj}, zal er enkel een invloed van meetfouten zijn indien $j=i$. In het geval van interne verliesfactoren worden deze laatste allemaal beïnvloed volgens :

$$\Delta \eta_{jj} = \frac{\Delta \alpha}{\alpha} \cdot \eta_{ij}^{o} \tag{36}$$

Vergelijking (36) wordt maximaal indien j=i. *Grafisch kunnen de voorgaande besluiten voorgesteld worden door :*

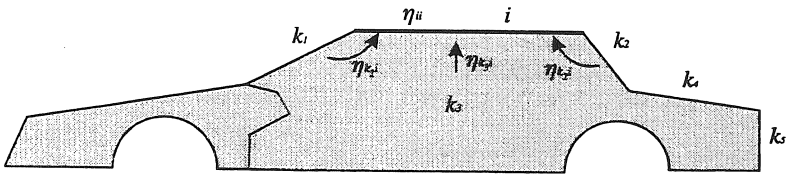

Figuur 11 : Invloed van meetfouten op de SEA parameters.

Enkel de koppelingsfaktoren tussen subsysteem i en de subsystemen palend aan subsysteem i zullen beïnvloed worden door meetfouten op de ingevoerde energie van subsysteem i, i.e. $\eta_{k,i}, \eta_{k,i}, \eta_{k,i}$. Verder zullen alle interne verliesfaktoren beïnvloed worden.

Terugvoeren van het aantal responsemetingen.

Eén van de nadelen van PIM voor een systeem met een groot aantal subsystemen (typisch *50* in het geval van een wagen) heeft betrekking op de lange meettijden. Iedere significante reductie van de meetsequentie draagt substantieel bij tot het optimaliseren van PIM. Eén van de mogelijkheden om de experimentele inspanningen te verminderen heeft betrekking op het aantal subsystemen dat in beschouwing wordt genomen voor responsmetingen. Strict gezien is het noodzakelijk om bij excitatie van een subsysteem, de respons van elk subsysteem op te meten, teneinde de genormaliseerde energiematrix te kunnen inverteren. Soms is het echter al voldoende om de energieën van dichtbij gelegen subsystemen (tov de subsystemen die geëxciteerd worden) op te meten en aldus de contributies van subsystemen die veraf gelegen zijn te verwaarlozen tijdens de PIM metingen. Dit conept wordt kort toegelicht in het volgende voorbeeld.

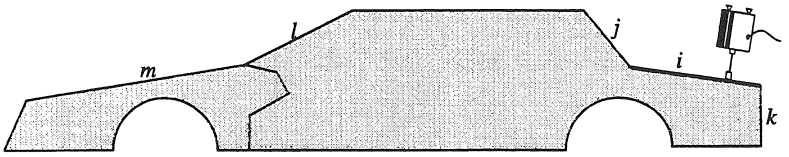

Figuur 12 : Verwaarlozing van de responsies in "veraf" gelegen subsystemen.

De energie die via subsysteem *i* de structuur binnenkomt, wordt getransporteerd naar veraf gelegen subsystem (subsystemen *l* en *m*) via de koppelingsmechanismen tussen de subsystemen. De energie in *l* en *m* dikwijls al vrij klein tov de energieën in de nabij gelegen subsystemen zodat de contributies van *l* en *m* kunnen verwaarloosd worden en bijgevolg het aantal reponsmetingen sterk verminderd wordt. In het proefschrift wordt uitgebreid ingegaan op de gevolgen van het verwaarlozen van responsmetingen op SEA parameters en op SEA predikties. Zo wordt aangetoond dat als de respons in een subsysteem *i* verwaarloosd wordt bij excitatie van subsysteem *j* (de genormaliseerde energie E_{ij}^{n} wordt op nul gesteld), dat de overeenkomstige parameter η_{ji} substantieel wijzigt en zelfs negatief wordt. De invloed met betrekking tot de parameters η_{j*} en η_{*i} is van tweede orde. De invloed op de andere parameters is nog een orde kleiner.

Met betrekking tot de invloed op de SEA predikties dient het volgende opgemerkt te worden : indien de energie van subsysteem *i* niet wordt opgemeten bij excitatie van subsysteem *j*, of indien de overeenkomstige E_{ij}^{n} op nul wordt gesteld dan kan men stellen dat het energieniveau van subsysteem *i* en de vermogentoevoer naar subsysteem *j* ontkoppeld zijn bij het aanwenden van het SEA model in een latere faze. Zo zal men nooit het energieniveau in *i* kunnen voorspellen bij excitatie van *j*.

Identifikatie van specifieke parameters.

Eén van de nadelen van PIM in zijn klassieke vorm is dat elk subsysteem dient geëxciteerd te worden en dat de respons van de subsystemen dient opgemeten te worden teneinde de parameters te kunnen bepalen, zelfs als men slechts geïnteresseerd is in één van de parameters. Zo bijvoorbeeld kan men geïnteresseerd zijn in de effectieve verandering van een koppelingsfactor na het doorvoeren van een physich structurele verandering. In die omstandigheden kan het aangewezen zijn om een benaderende

waarde te verkrijgen van een SEA parameter via het aanwenden van een eenvoudige meting waarbij slechts enkele subsystemen dienen geëxciteerd en opgemeten te worden.

De techniek voorgesteld in dit proefschrift maakt gebruik van een subset van de genormaliseerde energiematrix. Zo kan men bijvoorbeeld een eerste schatting bekomen van de koppelingsfaktoren η_{jk} η_{kj} en van de interne verliesfaktoren η_{jj} en η_{kk} door enkel rekening te houden met de subsystemen j en k. In dit geval hoeft men zich slechts te concentreren op de relevante 2×2 submatrix van de genormaliseerde energiematrix, zoals hieronder wordt weergegeven :

$$[E^n] = \begin{bmatrix} & E^n_{jj} & E^n_{jk} & \\ & & & \\ & E^n_{kj} & E^n_{kk} & \end{bmatrix} \begin{matrix} \\ \longleftarrow j \\ \\ \longleftarrow k \end{matrix} \Longrightarrow [E^n_{subset}] = \begin{bmatrix} E^n_{jj} & E^n_{jk} \\ E^n_{kj} & E^n_{kk} \end{bmatrix} \qquad (37)$$

De SEA parameters kunnen dan bepaald worden uitgaande van de inverse van de genormaliseerde submatrix.

Deze procedure kan uitgebreid worden zodanig dat meerdere subsystemen tijdens de metingen in beschouwing genomen worden om specifieke parameters te bepalen. Door metingen uit te voeren op een subset van drie subsystemen kan men een meer nauwkeurige schatting bekomen van een specifieke parameter. PIM metingen waarbij *4,5* etc. subsystemen in rekening worden gebracht leveren nog een betere schatting van een specifieke parameter.

De voorgaande bemerkingen en ideeën kunnen in een mathematisch formalisme worden gegoten. Hierbij wordt de contributie van een specifiek subsysteem met betrekking tot een specifieke SEA parameter geëvalueerd. Dit laatste resulteert in de volgende vergelijking :

$$\eta_{jk,p} \cong \eta^o_{kp} \cdot \delta_{p,j} + \eta^o_{pj} \cdot \delta_{p,k} - E^n_{pp} \cdot \eta^o_{kp} \cdot \eta^o_{pj} \qquad (38)$$

In vergelijking (38) stelt $\eta_{jk,p}$ de contributie voor van het p^{de} subsysteem met betrekking tot de SEA parameter η_{jk}.

Figuur (12) geeft de contributies van de verschillende subsystemen met betrekking tot de parameter η_{15} weer. De structuur die gebruikt is voor deze meting staat weergegeven in figuur 3.3.

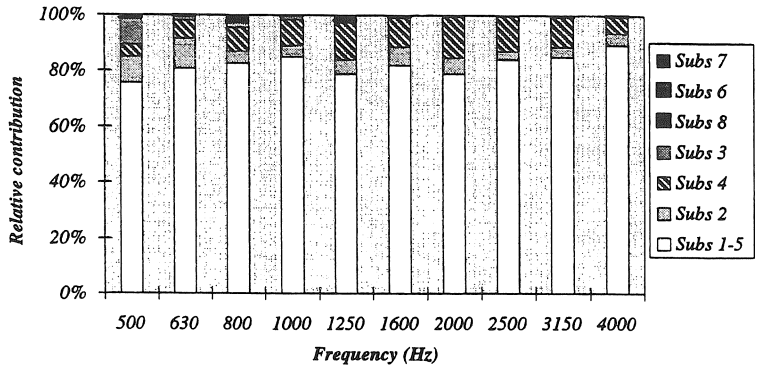

Figuur 12 : Contributies subsystemen met betrekking tot een SEA parameter.

Besluit : een substantiële reduktie van de meet-kost kan verkregen worden indien men enkel geïnteresseerd is in het nauwkeurig bepalen van een specifieke parameter tussen twee subsystemen.

Computationele evaluatie van de SEA parameters.

In vele gevallen kan het noodzakelijk zijn om de SEA parameters te bepalen in de beginfaze van het ontwerp. Dit kan gewenst zijn met de bedoeling om het geluidsniveau in een caviteit te verminderen of om eventuele vermoeiingsproblemen in ontwerpfase te analyseren. In de beginfaze van een ontwerp zijn dikwijls slechts enkele globale eigenschappen van de constructie gekend. Details van verbindingen tussen komponenten en dergelijke zijn in dit stadium nauwelijks gekend. De berekening van SEA parameters zal dan ook gebeuren met een beperkt aantal gekende grootheden. In sommige gevallen zullen zelfs gesloten analytische formules gebruikt worden.

Hoofdstuk 5 gaat dieper in op de evaluatie van SEA parameters op een klassieke manier. Meer bepaald wordt de evaluatieprocedure van de koppelingsfaktoren van balk-balk en plaat-plaat verbindingen uitgebreid behandeld. Terwijl de bestaande SEA pakketten een vrij beperkte lijst voorleggen van koppelingsfaktoren tussen structurele subsystemen is dit toch een kritische parameter om met behulp van SEA complexe structuren te modelleren. Hieronder wordt een kort overzicht gegeven van de methode om de koppelingsfaktor van balk-balk verbindingen te bepalen. Min of meer dezelfde procedure geldt voor plaat-plaat verbindingen.

Het golfmodel.

Klassiek worden de SEA vergelijkingen afgeleid gebaseerd op het modale model. Men zal de energie-uitwisseling tussen subsystemen begroten op basis van de energie-uitwisseling tussen de relevante modes van twee subsystemen. In de praktijk echter komt het vaker voor dat de koppelingsfaktoren bepaald worden steunend op een golfbeschrijving van de physische fenomenen. Deze beschrijving leent zich namelijk gemakkelijker tot het bepalen van koppelingsfaktoren voor een groot aantal verbindingen. De trillingen worden beschreven door vlakke golven, die partieel

gereflecteerd of doorgelaten worden aan structurele discontinuiteiten etc. Van primair belang in dit model is het bepalen van de transmissiecoëfficiënten van de verbinding ✎. De omzetting van transmissiecoëfficiënten naar koppelings-faktoren is over het algemeen vrij voor de hand liggend.

Balk-balk verbindingen.

De balk-balk junkties die hier beschouwd worden zijn vrij algemeen in die zin dat een willekeurig aantal Timoshenko balken onder willekeurige hoek met elkaar verbonden, kunnen behandeld worden. Longitudinale, buigingsenergie (volgens de hoofdrichtingen) en torsie-energie wordt in rekening gebracht.

Dynamische golfstijfheid van een balk.

Een eerste stap in het berekeningsproces van de transmissiecoëfficiënt betreft het bepalen van dynamische golfstijfheid van de balk : het verband tussen de inwendige krachten in de balk en de overeenkomstige verplaatsing bij aanwezigheid van een golfveld bestaande uit golven in een bepaalde richting. Deze stijfheid kan bepaald worden op de volgende manier :

- Opstellen van het stelsel dynamische differentiaalvergelijkingen van de balk.
- Substitutie van de golfoplossing $e^{j(\omega t - kx)}$ in het stelsel, resulterend in een eigenwaardenprobleem.
- Een eenvoudige wiskundige manipulatie van de eigenvectoren resulteert in de golfstijfheid van de balk.

De golfstijfheid wordt vervolgens beschouwd in een globaal coordinatensysteem.

Transmissiecoëfficiënt.

In elke balk van een verbinding kunnen vier types golven onderscheiden worden : longitudinaal, 2 ×buiging en torsie. Deze golven kunnen ontstaan ter plaatse van een verbinding of van een sructurele discontinuiteit. Om de transmissiecoëfficiënt te berekenen is het nodig om een golf met een gekende energie te laten invallen op de verbinding. Deze golf wordt partieel gereflecteerd en wordt gedeeltelijk teruggevonden in de andere balken. De verhouding van de energie van een uitgaande golf en de energie van een invallende golf bepaalt de transmissiecoëfficiënt.

Een eerste stap in het bepalen van transmissiecoëfficiënt bestaat erin om evenwicht en compatibiliteit van de golven ter plaatse van de verbinding uit te drukken. Combinatie van evenwicht en compatibiliteit resulteert in een verband tussen de vector van verplaatsingen van de invallende golven en de vector van verplaatsingen van de uitgaande golven.

$$\{U^+\}_i = [A] \cdot \{U^-\}_i \qquad (39)$$

✎ Een transmissiecoëfficiënt wordt gedefinieerd als de verhouding van de energie van een getransmitteerde golf en van een invallende golf op een structurele discontinuïteit.

Het plusteken betreft uitgaande golven (=weg van de verbinding). Het minteken betreft invallende golven. De vectoren van verplaatsingen $\{U\}$ bevatten de verplaatsingen van alle balken ter plaatse van de verbinding. Deze verplaatsingen kunnen omgezet worden naar veralgemeende golfcoordinaten ✎. Het verband tussen de veralgemeende golfcoordinaten van de invallende golven en de uitgaande golven wordt als dusdanig :

$$\{a^+\}=[B]\cdot\{a^-\} \qquad (40)$$

Vergelijking (40) maakt het met andere woorden mogelijk om voor elke invallende golf (met gekende veralgemeende coordinaten), de uitgaande golf te berekenen. De omzetting van veralgemeende golfcoordinaten naar energieen is de laatste stap om te komen tot de transmissiecoëfficiënt.

Koppelingsfaktoren.

Het verband tussen de SEA koppelingsfaktoren en de transmissiecoëfficiënten wordt hierna behandeld voor een balkennetwerk (figuur 13).

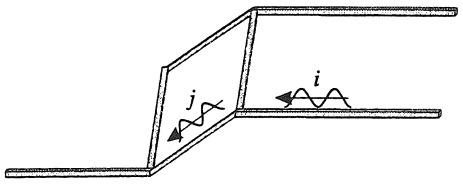

Figuur 13 : SEA balkennetwerk.

Veronderstel dat de energie van subsysteem i gegeven wordt door E_i. De groepsnelheid van de corresponderende golf is $c_{i,g}$. De lengte van subsysteem i is L_i. Er wordt verder verondersteld dat de energiestromen in de positieve en negatieve richting gegeven worden door P_i^+ en P_i^- ; beiden worden gelijk verondersteld. Hieruit kan het verband tussen de energie E_i en de energiestroom P_i berekend worden :

$$E_i = L_i \cdot \frac{2 \cdot P_i}{c_{i,g}} \qquad (41)$$

Uit de definitie van SEA koppelingsfaktoren volgt tevens : $P_{i\to j} = \omega \cdot \eta_{ij} \cdot E_i$. De definitie van transmissiecoëfficiënt resulteert in : $P_{i\to j} = \tau_{ij} \cdot P_i^-$. Via het combineren van de relevante vergelijkingen bekomt men het verband tussen SEA koppelingsfaktor en transmissiecoëfficiënt van een verbinding :

$$\eta_{ij} = \frac{\tau_{ij}}{\omega n_i(f)} \qquad (42)$$

Voorbeeld.

In vele gevallen van koppeling tussen balken wordt de koppeling tussen de verschillende types golven niet in rekening gebracht. Met andere woorden, bij het berekenen van de koppeling tussen de buigingsgolven van twee gekoppelde balken worden de contributies

---

✎ complexe coordinaat behorend bij een specifiek golf.

van de longitudinale en torsiegolven achterwege gelaten. Het volgende voorbeeld toont de invloed van de koppeling en wijst op de noodzaak om een volledig gekoppelde analyse door te voeren in het geval van balk-balk verbindingen.

De stuctuur bestaat uit twee gekoppelde balken waarvan de eigenschappen hieronder worden weergegeven.

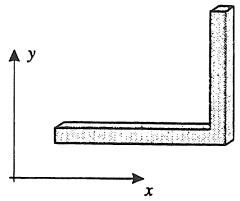

Balk eigenschappen	*Waarde*
Afschuif-coëfficiënt	*0.833*
Balkdoorsnede	$10 \times 10\ mm^2$
Materiaal	*Rigid PVC*

Figuur 14 : Eigenschappen van de structuur.

Een vergelijking wordt gemaakt tussen het geval waarbij geen koppeling van de golven wordt beschouwd en het geval waarbij een volledige koppeling in rekening wordt gebracht. De transmissiecoëfficiënten die hier worden weerhouden relateren buigingsgolven in balk *1* met buigingsgolven in balk *2* en relateren buigingsgolven in balk *1* met longitudinale golven in balk *2*.

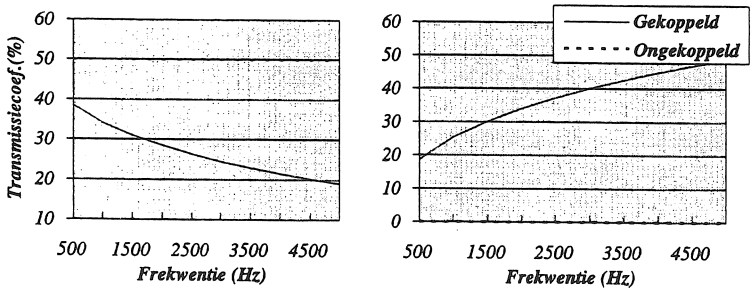

Figuur 15 : Transmissiecoëfficiënt van buiging naar buiging (links) en buiging naar longitudinale energie (rechts).

De resultaten wijzen op de noodzaak om een volledig gekoppelde berekening door te voeren, vooral in het hoogfrekwente gebied.

Plaat-plaat verbindingen.

Hoewel de berekening van de SEA koppelingsfaktoren voor plaat-plaatverbindingen in principe equivalent is met de balk-balk verbindingen, dienen hier toch enkele opmerkingen gemaakt te worden. Vooreerst kan gewezen worden op het feit dat het aantal energie-transporterende golven gelijk is aan drie : *1* buigingsgolf, *1* longitudinale golf in het vlak en *1* afschuif-golf in het vlak van de plaat. Deze golven kunnen echter onder variable hoek invallen op de verbinding. Diengevolge verkrijgt men voor plaat-plaat verbindingen een bijkomende vrijheidsgraad, namelijk de invalshoek van de golf.

Men zal dan ook de transmissiecoëfficiënt berekenen als funktie van de invalshoek van de golf. Na middeling over de invalshoek, volgt de gemiddelde transmissiecoeffcient die dan kan omgezet worden in een SEA koppelingsfaktor op een identieke manier als voor een balk-balk verbinding.

De volgende figuur toont de transmissiecoëfficiënt van een plaat-plaat verbinding bestaande uit twee loodrecht gekoppeld PVC platen met een dikte van *10 mm*. Bemerk de discontinuiteiten die optreden als funktie van de invalshoek van de golf.

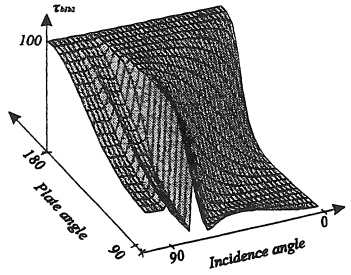

Figuur 16 : Transmissiecoëfficiënt van een plaat-plaat verbinding

In een volgend voorbeeld worden de berekende energieniveaus vergeleken met de experimenteel bepaalde energieën. De structuur bestaat uit twee gekoppelde aluminium platen van *1* mm dikte. De koppelingshoek bedraagt *135°*. Vermogen wordt aangelegd aan het eerste subsysteem in de frekwentieband *100 - 1000* Hz. Het energieniveau van beide platen wordt voorgesteld in de volgende figuur. De grafiek links bevat de gegevens van het eerste subsysteem. Rechts worden de data van het tweede subsysteem voorgesteld.

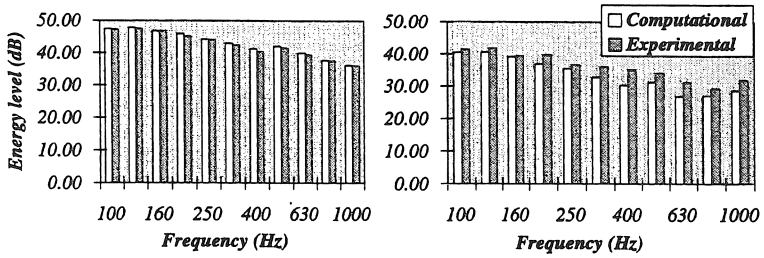

Figuur 17 : vergelijking tussen berekende en experimenteel bepaalde energieniveaus.

Gebruik van eindige elementen.

Eén van de belangrijkste nadelen van de klassieke rekenkundige technieken om transmissiecoëfficiënten van verbindingen te bepalen, betreft de onmogelijkheid om structurele details ter hoogte van de verbinding te modelleren. Met andere woorden, klassiek gaat men uit van een sterkt geïdealiseerde verbinding : bijvoorbeeld het star zijn van een verbinding. Structurele details kunnen echter significant worden in het hoogfrekwente gebied. Een typisch voorbeeld betreft een hoek met een afronding (figuur 18). Het is namelijk zo dat als de straal van de afronding van dezelfde grootte-orde is als

1. INTRODUCTION AND STATE OF THE ART IN HIGH FREQUENCY MODELING.

1.1 Motivation.

1.1.1 Background.

As the expectations of consumers steadily increase and as intensifying government regulations become effective, the engineer faces continuously new yet promising challenges. These are most often determined by the compulsion to accomplish contradictory needs and to fulfill several constraints demanded by the market. For example, from the automotive side, one can expect cars to be more powerful and faster as well as less energy consuming, safer, quieter. The aerospace industry continuously looks for engineering tools to increase the safety and quality of men and instruments. With respect to the development of space stations, one requires the prediction of vibration levels to assess the fatigue life of critical components as well as the noise suppression to increase the work efficiency, hearing conservation and comfort of the crew members. Optimized vibration and noise prediction tools are needed to control excessive noise and vibration levels in order to provide a safe environment conducive for communication, comfort and work efficiency.

One of the critical issues in this field deals with the identification of vibration transmission paths. By correctly identifying these paths, proper vibration and noise control measures can be taken to ultimately and efficiently reduce the vibration and noise levels. For example, instead of applying damping treatment to the entire fuselage of an airplane to reduce noise in the cabin, selective damping treatments can be applied based on the predicted vibration transmission paths, in such a way that besides the increased comfort, one can achieve weight savings and a more efficient aircraft design. Careful optimization of design details (e.g. optimization of junctions) is essential for obtaining cost-effective modifications leading to appropriate noise and vibration characteristics.

Automotive vehicles, airplanes, ships, busses, trains etc. constitute complex structures for which no simple methods exist for the prediction of noise and vibration in the entire audible frequency range. Some so-called deterministic methods such as the finite element method and the boundary element method have become widely established numerical tools regarding noise and vibration prediction. These methods are reasonably effective for the prediction of noise and vibration characteristics in the lower frequency range, especially when in addition model updating techniques based on experimental modal models are applied. A frequently encountered definition of high frequency range is given by : *the frequency range for which the wavelength (acoustical and structural) is small compared to the structural dimensions*. The low frequency range complements the high frequency range. A small number of modes will be involved in the low frequency range, thereby making it possible to apply the finite element method, the boundary element method and classical modal analysis procedures; techniques which are generally used today by all automotive, truck, airplane, etc. manufacturers.

1.1.2 Deterministic methods.

This section covers the applicability, advantages and disadvantages of the more conventional deterministic methods, including the finite element method, the boundary element method and experimental modal analysis for the prediction of noise and vibration in the high frequency range.

As stated before, design improvement and tuning of critical components for low noise and vibration characteristics require the ability to model the *overall* system response over a *wide frequency* range in a reliable and especially affordable way. The global system includes the dynamics of the structural parts, acoustic cavities and critical dynamic components which are contributing to the excitation (such as gears, exhaust, engine etc.). The noise and vibration concerns occur over a wide frequency range and are governed by low as well as high modal densities and modal overlap. Theoretically, there is no fundamental reason why the finite element method can not be applied to examine vibro-acoustic problems in the entire frequency range of interest. The finite element method can be used to determine frequency response functions, transient response functions, eigenfrequencies, eigenmodes etc. Solutions are obtainable at *discrete locations*, at *discrete frequencies* or at *discrete moments in time*. Although the finite element method has been effective at low frequencies for the prediction of structure-borne noise and vibration in built-up structures, it has not been effective at high frequencies even with today's increasing computing speed and the sophisticated enhancements of the finite element implementations. At high frequencies, the wavelength of the vibration pattern decreases and hence the element size of the finite element mesh should decrease in the same order of magnitude in order to faithfully capture the structural deformations. Therefore, the finite element method inherently leads to extremely huge and expensive models in the high frequency range. For example, a very detailed finite element model of an automotive vehicle for noise and vibration prediction purposes requires several manmonths to be developed. Enormous computational effort evolves such that most often the application of the finite element method is practical and justified only up to *200* Hz in the case of for example automotive vehicles.

It can be concluded that the computational cost is prohibitive for high frequency vibration analysis. Furthermore, for a design optimization, a mathematical model of a

structure is used to estimate the sensitivity of vibration levels in relation to parametric modifications of the model. Clearly, as the number of parameters increases when using the finite element method to accurately model the vibration pattern, the more ill-favored it becomes to apply these finite element models. The computational expenses for performing sensitivity analyses in the higher frequency range are crucial and most often unjustified. LANDMAN and TILLEMA [73] discuss the use of the finite element method for predicting the dynamic characteristics of an engine-airframe-acoustic cavity system in an attempt to define an acceptable minimum finite element model size. The finite element predictions of a *727-100* airplane were compared to the data obtained from ground vibration tests. Results showed that the finite element model was capable of making accurate noise predictions for large commercial airplanes in the frequency range *0-40* Hz. The authors noted however that the large size of the finite element model (*23* substructures comprising *12200* nodes and *11000* elements) made model checkout and turn around of predicted results time consuming and expensive.

LIM and STEYER [27] point out that a structural-acoustic finite element analysis of an automotive vehicle is feasible in the *0-200* Hz frequency range. Nonetheless, most noise and vibration problems occur in the *200-1000* Hz frequency range. The following example illustrates vibro-acoustic problems encountered in cars in the audible frequency range.

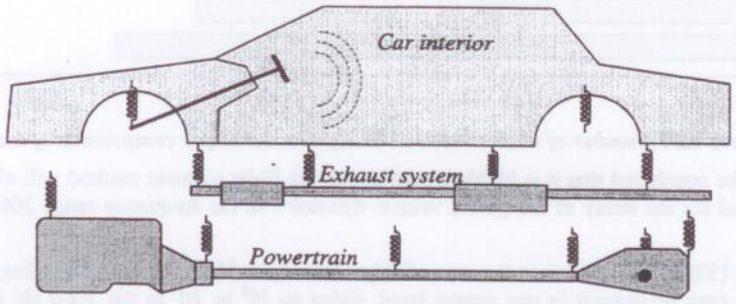

Figure 1.1 : Schematic representation of the principal parts of an automotive vehicle with respect to vibro-acoustic modeling.

Figure *1.1* pictures an automotive vehicle which is composed of several major dynamic components and shows their structural paths contributing to the interior noise. A brief description of these types of structure-borne noise problems is given below :

- Gear whine is caused by gear manufacturing, load induced deflection, casing machining, and assembly errors characterized by the transmission error of mating gear teeth. Gear whine occurs at harmonics and sidebands of mesh frequencies between *100-1000* Hz. It does not contribute significantly to the interior noise level, but its presence usually causes poor sound quality.
- Tire or road noise problems is predominant during constant operating speed in the frequency range of *100-500* Hz where other types of structure-borne noise may be low. It is generated at the tire and road contact regime due to roughness on the tire or road surface profile.

- Engine acceleration and boom noise problems are both caused by engine dynamics. These engine noise frequencies are associated with various engine harmonics and half orders. Engine acceleration noise occurs between *300-1000* Hz. Boom noise occurs between *50-300* Hz.
- Structure-borne exhaust noise occurs between *50-800* Hz and is caused by gas pressure pulsation in the acoustic cavity of the exhaust system. The gas dynamics induce structural resonance's in the exhaust system.

In addition, beyond *200* Hz, the vehicle exhibits a high modal density as illustrated in figure *1.2* (after LIM and STEYER).

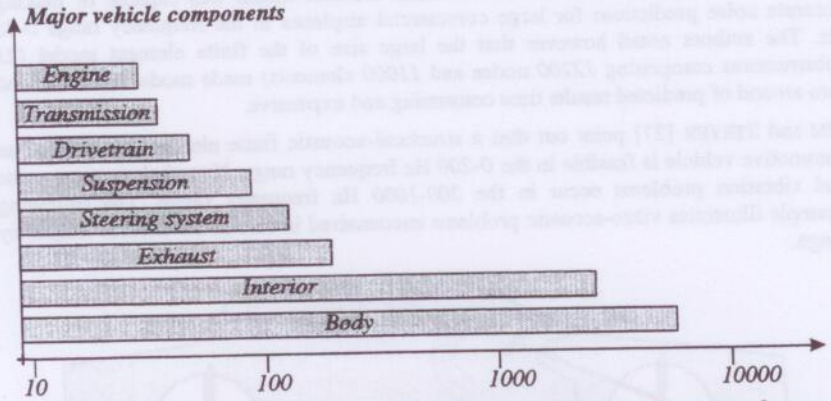

Figure 1.2 : Number of modes below 1000 Hz of some major components of a car.

It can be concluded that it is highly doubtful that the finite element method will ever by practical for the study of the global vehicle dynamics in the frequency range *200-1000* Hz.

PLUNT [32] points out that in the case of ships, already at *50* Hz 10^3 to 10^4 bending wave modes may be present in one octave band, rising to 10^5 to 10^6 in the *1000* Hz octave band. The frequencies of interest will range from about *10* Hz to a couple of kHz. The practical utilization of e.g. a dynamic finite element analysis will necessarily be restricted to the frequency range below *10* Hz if the vibrations of the entire aft body are to be studied or in other words if one has to calculate the forced vibration response in sufficient detail of the *global* structure to a number of complex force inputs. Still it should be mentioned that the classical deterministic methods will be excellent tools, whenever detailed vibrational behavior of certain complicated substructures of limited extension, like e.g. double bottoms in ships are to be studied.

The boundary element method is a more recently developed method for solving engineering problems. It can be applied to structural, electromagnetic and other physical problems and is particularly well suited for acoustic applications. The boundary element method makes it possible to model radiation problems in infinite media without resorting to artificial boundary conditions. Considerable literature has been accumulated over the last decade. The boundary element method distinguishes between two main implementations, called direct and variational. For the direct implementation, the volume

surface must be closed, while the variational technique can model open surfaces. The direct formulation can be derived through a direct application of Gauss' divergence theorem. The variational approach, as the name suggests, is based on the application of variational methods. There are a variety of implementation issues unique to each technique. Nevertheless both approaches use similar surface geometry modeling techniques. If the variational method is used, interior and exterior acoustic domains can be modeled simultaneously. The direct approach on the other hand implies the modeling of openings as a radiation impedance condition. The pressure at the opening is then used as a boundary condition for the exterior calculation.

Although theoretically it is possible to apply the boundary element method in the entire frequency range of interest[*], CPU and memory resource limitations restrict its use to low frequencies. The density of the surface discretisation and hence the number of degrees of freedom is directly proportional to the frequency. The stiffness matrices are fully populated, making it impossible to utilize the optimized solution sequences which are applied in the case of sparse matrices. Hence the boundary element model becomes increasingly expensive to be applied in the high frequency range.

In addition to the computational problems when dealing with deterministic methods, there are other motivations why these deterministic methods are not applicable for noise and vibration analysis in the high frequency range. One of the most important motivations deals with the sensitivity of the response to small variations of component properties and with the sensitivity to assembly tolerances. It is shown by RADCLIFFE and HUANG [30] that a substantial variation regarding the dynamic properties of structures can be noticed if some parameters of the structure are slightly changed. In that way, the deterministic dynamic predictions of a structure become increasingly dependent upon the accuracy of the modeling of structural details such as joints and boundaries conditions.

As a first example in this respect, the statistical distributions of the eigenfrequencies of a free-free flat plate are calculated as a function of the statistical distribution of a specific structural property, in particular the thickness of the plate. The thickness is assumed to be taken out of a population with a given normal distribution. The essential properties of this problem are listed in table 1.1.

Parameter	*Value*
Thickness t	*Mean : 5 mm*
	Deviation : 3% of mean value
Dimension a x b	*1600 × 1000 mm*
Material	*Aluminum*

Table 1.1 : Properties of the analysis.

The statistical distribution of the thickness is in accordance with a typical engineering variation. The eigenfrequencies (for the undamped case) are calculated analytically according to the formula :

[*] As it is for the finite element method.

$$f_{m,n} = t \cdot \sqrt{\frac{E}{12 \cdot (1-\nu^2) \cdot \rho}} \cdot \left[\left(\frac{\pi}{a}\right)^2 \cdot m^2 + \left(\frac{\pi}{b}\right)^2 \cdot n^2 \right] \qquad (1.1)$$

Where $f_{m,n}$ represents the eigenfrequency of mode (m,n).

The following figure pictures the corresponding probability functions of the eigenfrequencies for mode *1,2,13,15,16*.

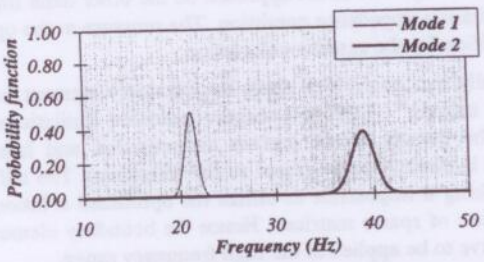

Figure 1.3 a : Probability function of eigenfrequencies; lower order modes.

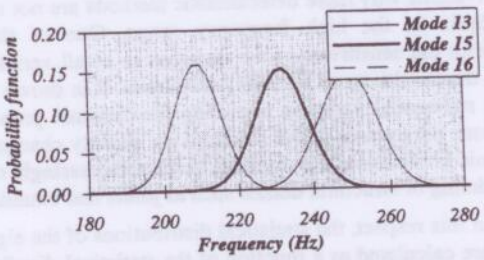

Figure 1.3 b : Probability function of eigenfrequencies; higher order modes.

Figure *1.3 a* clearly shows that a low frequencies, the statistical distributions of the eigenfrequencies are well separated whereas for the higher order modes (figure *1.3 b*), overlapping of the probability functions occurs. In other words, if two plates from an ensemble of plates with a thickness distribution as assumed above are excited in a frequency band around the 15^{th} or so mode , then one can not retrieve the dominant vibration pattern : for one specific plate the vibration pattern could be dominated by 15^{th} mode, while for another plate the vibration pattern could be dominated by the 16^{th} mode. Let's now consider a rigid coupling between two such plates (figure *1.4*).

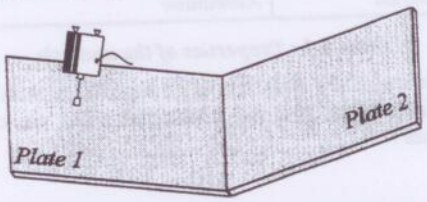

Figure 1.4 : Structure composed of two coupled plates.

If the first plate is excited at a certain point, then the second plate will be excited through the interaction forces at the coupling between both plates. In the higher frequency range, one can not ascertain **if** nor **which** mode will be excited at a certain frequency because of the statistical variation of the eigenfrequencies of both according to figure *1.3*. Suppose plate one is excited at an eigenfrequency, resulting in a resonant response. If plate two has exactly the same properties as plate one, then both plates exhibit a resonant behavior[*]. If on the other hand some properties of the second plate are slightly different (e.g. according to the thickness distribution mentioned above), then this plate could eventually not exhibit a resonance at the exciting frequency. In that case, the coupling between the two plates is much weaker than in the case of coinciding eigenfrequencies. Moreover, it is even conceivable that at the exciting frequency, the second plate exhibits a different mode compared to the first plate. In that case, the coupling between the two plates will be stronger, yet the deformation patterns of both plates would be different.

Due to the high modal density and modal overlap at high frequencies, more than one mode contributes significantly to the total response at any one frequency. The phase of the modal response however varies rapidly near resonance. Besides, how much detailed a model is built, and how much sophisticated computational procedures are, any one physical realization of the system will differ in detail from the idealized model. Consequently, the relative amplitudes and phases of the higher order modal responses at any one frequency cannot be predicted correctly. Figure *1.5* depicts the phase of the - by means of finite elements computed - frequency response function between acceleration and driving force at specific locations of the plate. Note that a similar curve holds for the amplitude of the frequency response function.

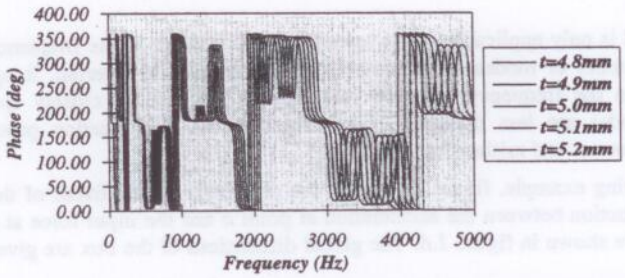

Figure 1.5 : Phase representation of the FRF between acceleration and force two arbitrary locations of a plate.

The relative amplitudes and phases of the substantial modes are crucial with respect to the global response. Hence, there exists an inherent uncertainty in the degree of correspondence between the predicted response at any one frequency and any one position of a model compared to that observed in an individual physical counterpart.

With respect to the uncertainty resulting from the deterministic methods, WOOD and JOACHIM [44] measured structural-acoustic transfer functions of nominally identical sedans and wagons which shared the same front structure, in order to evaluate the

[*] Under the assumption that the dynamical behaviour of the coupled plates can be approximated by the dynamics of the two uncoupled plates.

interior noise level scatter. The structural-acoustic transfer functions were measured using an impact excitation at the front passenger side engine mount location. Acoustic pressures were recorded at the front and rear seat locations. They observed that the interior noise level scatter can be as high as *10* dB to *15* dB in the frequency range *50-250* Hz.

KOMPELLA and BERNHARD [74] measured the frequency response functions of structure-borne and air-borne paths on *99* identical Isuzu Rodeos and *57* identical Isuzu pickup trucks. Impact excitation with an instrumented hammer was used at the left front wheel for measuring the structure-borne transmission paths into the vehicle interior. A loudspeaker excited by a band-limited random noise was used for measuring the air-borne transmission paths. Two microphones were placed inside the vehicle to measure the interior acoustic response. The structure-borne and air-borne frequency response functions of the vehicles showed relatively low variation at low frequencies but variation of *8* to *10* dB above *200* Hz. The authors state that the usefulness of a noise control treatment at high frequencies based on the analysis of a single vehicle will be uncertain for other nominally identical vehicles.

Besides the deterministic computational methods, there are also no experimental modal methods suitable for analyzing the dynamic behavior of complex, highly damped structures in the higher frequency range. Experimental modal analysis, a method which has been around for several decades, is aiming at the identification and analysis of the dynamic behavior of an existing structure, already in use, in a prototype or a design stage. The method is based on extracting and interpreting modal characteristics which are obtained through experiments. First, the relevant frequency response functions are estimated. In a next phase, the modal parameters are identified from the measured input-output data.

The method is only applicable in the lower frequency range. If the frequency increases, then the number of modes increases and the modes tend to overlap. Response peaks appearing in the frequency response functions in the case of closely spaced highly damped modes are less distinct. Experimental modal identification procedures will produce incorrect and misleading results.

As a clarifying example, figure *1.7* shows the amplitude (normalized) of the frequency response function between the acceleration at point *a* and the input force at point *b* of a box structure shown in figure *1.6*. The global dimensions of the box are given in section *3.3*.

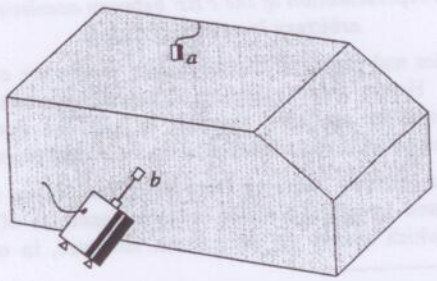

Figure 1.6 : Box structure excited at a side wall.

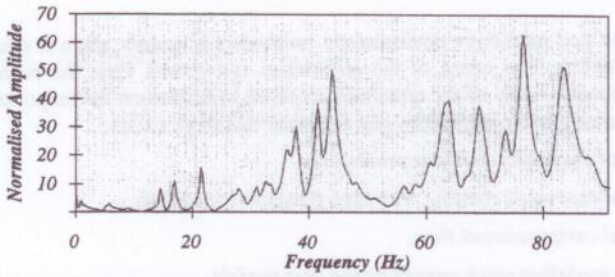

Figure 1.7a : Normalized amplitude of the FRF : low frequency range.

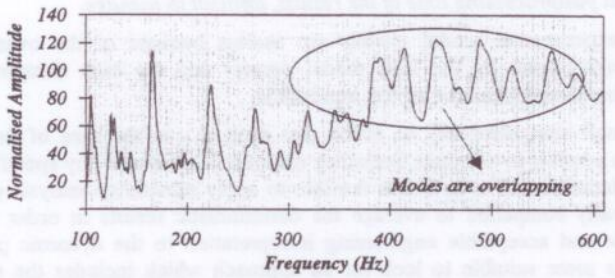

Figure 1.7b : Normalized amplitude of the FRF : mid frequency range.

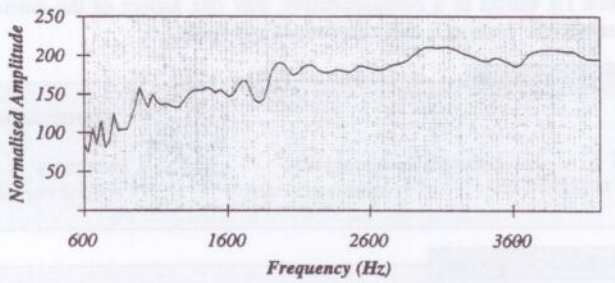

Figure 1.7c : Normalized amplitude of the FRF : high frequency range.

Clearly at low frequencies : *0-100* Hz, the peaks are distinct and the application of modal methods is suggested. However at higher frequencies : > *100* Hz, the modes tend to overlap. In the frequency range *600-4000* Hz, no individual peaks can be noticed any longer, the modes are overlapping and the classical modal extraction procedures will fail.

The shortcomings of the deterministic methods as explained above in mind, it is unrealistic to try to predict the detailed frequency response function at a specific location on a real system with a high degree of accuracy in the high frequency range.

Summary.

It can be stated that predictive deterministic methods are useless when it comes to high frequency modeling. The cause of the difficulties is twofold. First the models are too extensive. Secondly, many of the quantities required to determine the response cannot be accurately obtained. More explicitly, one can state that there exists :

- *Impractical sensitivity analysis procedures.*
- *Huge databases when dealing with high frequency problems.*
- *Unjustified computational time.*
- *Expensive modeling work caused by the vast models.*
- *High uncertainty of the model to local structural variations.*
- *Substantial postprocessing time of the results, difficult to manage.*

In addition, experimental modal models are useless because of the overlapping of individual peaks caused by the high modal density and the high damping, thereby making a distinction between the modes impossible.

It should though unquestionably be stated that even if - in the case of deterministic methods - it is possible to calculate frequency response functions at any specific response or excitation location and even if it is feasible to apply sensitivity analysis procedures, one is practically compelled to average the deterministic results in order to give an understandable and acceptable engineering interpretation to the dynamic phenomena. Therefore it is more suitable to look for an approach which includes the statistics in advance, i.e. before the solution sequence, such that the model includes statistical, meaningful variables and parameters. Statistical Energy Analysis constitutes such an approach. Figure 1.8 shows in a comprehensive way one aspect of the main difference between a deterministic approach and a statistical approach.

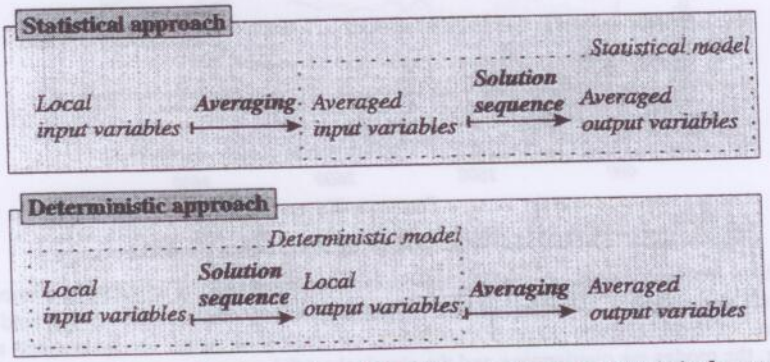

Figure 1.8 : Schematic representation of the difference between a statistical approach and a deterministic approach.

Hence, if a statistical approach is followed, then the following problems encountered when using a deterministic approach vanish :

- *Unjustified computational time* : Because the input variables are averaged (with respect to frequency, time, location) only few parameters will be involved in the calculation phase and thus the solution sequence demands less CPU time which makes a statistical approach interesting and economically justified.
- *Expensive modeling work* : There will be no need any longer to model all parts of a structure in detail as would be the case when applying the finite element method. For example, a flat plate could eventually be modeled by using a few lumped parameters such as thickness, type of material, dimensions etc. Other parts such as connections should in some occasions be modeled in detail.
- *Enormous postprocessing time* : Only a few number of variables and parameters will be involved in the postprocessing phase.
- *Uncertainty* : Because averaging is involved, high variation of the response to small structural modifications will disappear. In the case of deterministic models, the high uncertainty was caused by the fact that *single point* responses (single frequency and single location) were taken.
- *Huge database* : Disappears because of the few parameters and variables which are involved.
- *Impractical for sensitivity analysis* : Because only few parameters are involved, the effect of structural modifications can be examined very easily, the solution is cheap and quick, the results are easy to interpret.

The considerations mentioned above illustrate the benefits of a statistical approach. The following question can now be raised : how can such a model be built ? What are the variables (displacements, velocities, energies etc.) ? what are the parameters of the statistical model ? What is the physical significance of the parameters used in an appropriate statistical approach ?

1.2 Survey of the literature.

During the last two decades, a lot of effort has been spent on improving and developing methods to model high frequency vibrations of elastic and acoustic media. The intention of this section is to give an overview of the present-day existing methods with respect to the analysis of mid to high frequency vibrations in order to put the approach followed in this dissertation (namely SEA) in a more broad perspective. The prediction procedure, potential benefits and drawbacks will be discussed in the case of each method.

The following methods are covered :

- Statistical Energy Analysis : SEA.
- Energy Flow (Finite Element) Analysis : EF(FE)A.
- Asymptotic Modal Analysis : AMA.
- Mobility Energy Flow (Finite Element) Analysis : MEF(FE)A.
- Energy flow analysis using classical finite element.
- General Energy Formulation Method : GEFM and Smooth Energy Formulation (SEM).
- Energy (Phase) Envelope Model : E(P)EM.
- Ray Tracing.

1.2.1 Statistical Energy Analysis (SEA).

SEA is one of the main methods for quality vibro-acoustic analysis in the high frequency range. For SEA, the state of vibration is expressed in terms of stored, dissipated and transmitted *energies* of and between substructures. The frequency bands are wide enough to contain a large number of eigenfrequencies. Input power into the subsystems forms the excitation (input) of the model. The subsystem energy is the response coordinate. By using energy as a primary variable, both the structural and acoustic subsystems can be modeled using the same type of variable. The basic premise of SEA is that vibrational energy behaves in the same way as heat energy. The vibrational energy diffuses from the hotter places to the cooler places at a rate proportional to the difference in temperature. The thermal constant of proportionality is called the thermal conductivity. To relate the thermal model to vibrations, the modal energy in each subsystem is regarded as a measure of the temperature. The thermal conductivity parameter which measures the strength of coupling of the subsystems is given by the *SEA coupling loss factor*. The thermal capacity of a subsystem is expressed by the *modal density* (i.e. the number of modes / Hz). Convection is quantified by the *internal loss factor*.

For all subsystems, an energy balance is performed. The energy input into a subsystem equals the energy transferred to the contiguous subsystems and the energy dissipated due to internal damping. The global energy equations can be solved for the averaged energy in each subsystem. SEA is illustrated by means of a structure consisting of *3* coupled plates (figure *1.9*).

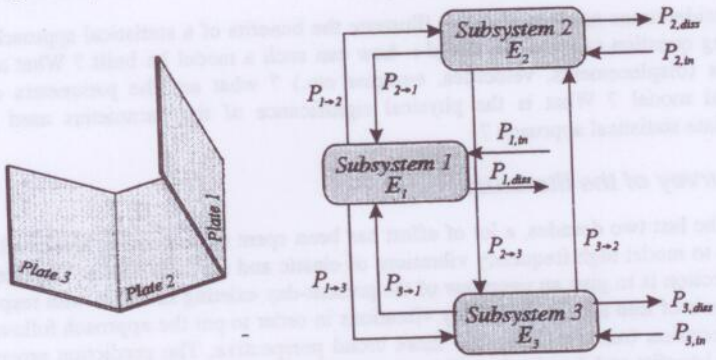

Figure 1.9 :Three subsystem SEA model of three coupled plates.

The three different blocks of figure *1.9* are called the SEA subsystems. The energy storage of subsystem *i* is represented by E_i (space and frequency averaged). The energy flow from one subsystem to the other is shown by the arrows labeled $P_{i\to j}$. The external energy input is given by $P_{i,in}$. The frequency averaged energy which is dissipated in subsystem *i* by the damping mechanism of the system is represented by $P_{i,diss}$.

The SEA method applies lumped dynamic variables and parameters to model the dynamic behavior of continuous linear systems. Consequently, a *simple* and *small* algebraic equation can be used to describe the state of vibration. In addition, because the number of subsystems is not dependent upon the frequency, the size of the model for higher frequencies can be kept relatively small. The relatively small number of

subsystems facilitates model check-out and design sensitivity analysis. However, because of the use of *lumped* dynamic characteristics, only one single energy value can be predicted for each subsystem. Any spatial information of energy in a subsystem is lost. In addition, modeling of localized effects such as local damping treatments and point forces is not straightforward using SEA. Chapter *2* focuses extensively on the SEA theory. A few basic notions concerning SEA are nevertheless given below.

The development of space technologies in the *'60s* led to the earliest applications of SEA. In order to avoid the malfunctioning of rockets due to vibration damage, one has applied SEA in the early design stage. SEA forms a excellent modeling tool to be used in the conceptual design stage of structures as the approach requires only few gross structural properties in order to build the model. At a later stage of the design, more information concerning structural details becomes available to the designer, making it possible to gradually perform a fine-tuning of the model.

In the *'70s* and *'80s*, SEA has mainly been applied to analyze structure borne sound in ships and buildings. As for the time being, many of the shipbuilding companies today have their own SEA program. Recently, interest is growing in new applications including helicopters, airplanes, cars and even engines.

During the last decade, an experimental counterpart of predictive SEA has been developed. For experimental SEA, the aim is to analyze the energy flow in existing structures or in prototypes by performing in situ measurements on the structure. In this way, it is possible to evaluate the transmission paths in complex structures during operating conditions. The experimental approach will be applied at a later stage of the design and can therefore be considered as a trouble-shooting tool.

At present, SEA is the only one method which can handle high frequency vibrations in an sufficiently accurate way - at least for some structures - and which is commercially available (software : AUTOSEA, VAPEPS, SEAM).

Although the appeal of SEA, it's long lasting history (more than *30* years) and the satisfactory results in many occasions with respect to high frequency modeling, some aspects of SEA (experimental as well as predictive) still need to be worked out.

Chapter *2* covers in a more comprehensive way the SEA method, its weaknesses and shortcomings. Chapters *4* to *6* aim at contributing to the SEA research by presenting some procedures which are originally developed in the framework of this thesis.

1.2.2 Energy Flow (Finite Element) Analysis (EFA or EFFEA).

EFA is initiated by BELOV et al. [45]. Using this approach, the flow of vibrational energy is modeled similar to the flow of heat in a structure. A heat conduction type differential equation describes the state of vibration. BELOV uses this type of differential equation to analyze the propagation of flexural and longitudinal vibrational energy in a plate reinforced by a beam. Recently, NEFSKE and SUNG [22] implemented a finite element formulation (EFFEA) of the heat conduction differential equation applied to structural vibrations. The EFA approach developed by NEFSKE and SUNG takes into consideration the spatial variation of the energy in the individual subsystems as well as the energy flow between subsystems. Instead of characterizing each subsystem by a single energy value, EFA describes the dissipation and conduction of vibrational energy *within* each subsystem. By solving the suitable energy equations for the energy density distribution in

each subsystem, the spatial variation of the vibrational response (in terms of acceleration, strain, sound pressure levels etc.) can be obtained.

The basic premise of EFA is that the state of vibration can be represented by stored, dissipated, and transferred energies. EFA predicts the spatially and frequency averaged vibrational behavior of a structure similar to SEA. However, EFA makes use of a differential volume approach to derive a governing equation for the energy density of a subsystem. One of the benefits of using a differential equation to describe the state of the farfield vibrational energy is that modeling localized effects such as local damping and point forces is feasible. Another major advantage is that the *spatial variation* of the farfield energy densities and energy flow can be obtained. A small tradeoff for acquiring the capability to predict a spatial distribution of farfield energy densities and energy flow is the more intensive computational time, relatively speaking, when compared to SEA.

The following example demonstrates the derivation of an EFA model in the case of beams. From the theory of continuum mechanics, it follows that the energy distribution in structures must obey conservation of energy. The energy conservation principle in general elastic media can be stated as (after BOUTHIER et al. [21]) :

$$\frac{\partial e}{\partial t} + \nabla \cdot \vec{q} + p_{diss} = 0 \qquad (1.2)$$

Where e is the energy density, $\vec{q}$ is the vibrational intensity vector and p_{diss} represents the dissipated energy. For steady state conditions, the time derivative is ignored. One of the simplest models of dissipation of energy through damping (like hysteresis damping) reads :

$$p_{diss} = \omega \cdot \eta \cdot e \qquad (1.3)$$

Equation (1.3) is not exact since hysteresis damping is proportional to strain and not to energy. However, equation (1.3) seems to be a fairly good representation of the spatial averaged damping in a structure, particularly at high frequencies.

For thermal systems (thermal analogy !) it generally holds that energy flows from locations of high temperature (or analogously energy density) to locations of low temperature. This behavior is modeled as :

$$\vec{q} = \alpha \cdot (-\nabla e) \qquad (1.4)$$

Where α represents the conductivity coefficient.

By combining equations (1.2), (1.3) and (1.4), the energy equation for thermal systems can be written as :

$$\alpha \cdot \nabla^2 e = \omega \cdot \eta \cdot e \qquad (1.5)$$

It has been shown that similar equations can be obtained to model energy distributions in structures. Two main difficulties arise when dealing with complex structures :

- A consistent relationship between energy density and intensity (equation (1.4)) should be developed for several types of structures : rods, beams, membranes, plates, cavities etc. In mathematical terms : $\vec{q} = f(e)$
- The coupling between subsystems can be quantified by transmission coefficients and should be developed for all types of junctions.

In the case of beams, the energy equation regarding the farfield local space averaged energy density is given by :

$$\nabla^2 e - \left(\frac{\omega \cdot \eta}{4 \cdot c_f}\right)^2 \cdot e = 0 \qquad (1.6)$$

Where c_f represents the flexural wave speed in the beam, η represents the loss factor, ω denotes the angular frequency.

The energy differential equations can be solved analytically or by using finite element implementations. In some cases, one can eventually use the thermal finite element software because of the similarity between the vibrational energy flow equations and the thermal equations. One of the major advantages of EFFEA is the fact that the models can become small[`] yet as accurate - in the higher frequency range - compared to the classical displacement finite element approach. The following figure shows an EFA model in the case of a beam. The upper side of figure *1.10* pictures the classical finite element model, the lower side of figure *1.10* depicts the corresponding EFA model. The results of both methods are presented in figure *1.11* and are compared to the SEA results.

Parameter	*Value*
Length	*1 m*
Section	*17.3 x 17.3 mm*
Material density	*7860 kg/m³*
Young's modulus	*200 GN/m²*

Table 1.2 : Properties of the analysis.

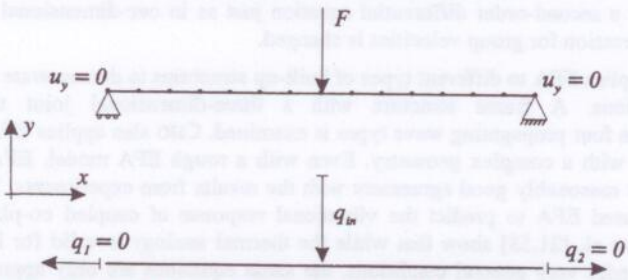

Figure 1.10 : FE model versus EFFEA model of a beam excited by a point load.

[`] For the classical finite element models, one requires at least *5* elements / wavelength in order to capture the structural deformation. For EFFEA, the latter requirement is not necessary any longer.

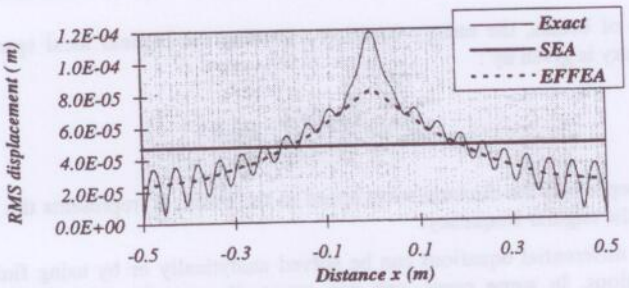

Figure 1.11 : Displacement in the y-direction along the beam.

NEFSKE and SUNG [22] use EFFEA to predict the vibrational response of an uncoupled beam excited by a point harmonic force and two coupled beams for which the source beam is excited by a point harmonic force. The results revealed a good agreement with SEA in the higher frequency range. In addition, the spatial distribution of the vibrational response of the structure is obtained thereby eliminating one of the main shortcomings of SEA. The authors assume that the vibrational intensity is proportional to the group velocity and to the total energy density of the structure. This relationship is correct for infinite structure. The authors use this relationship to derive the governing heat conduction type differential equation which is then used to predict the vibrational response of finite beam structures. WOHLEVER [53], in his study of vibrational energy flow in rods and beams, discovers that for finite beams the energy flow is *not* proportional to the gradient of the total energy density when both quantities are space and time averaged in a local sense. BOUTHIER [46] extends the work of WOHLEVER to include energy flow in membranes, thin plates and acoustic cavities. BOUTHIER states that the vibrational energy flow in two-dimensional structures and acoustic cavities is governed by a second-order differential equation just as in one-dimensional structures; only the expression for group velocities is changed.

CHO [48] applies EFA to different types of built-up structures to demonstrate its benefits and limitations. A frame structure with a three-dimensional joint taking into consideration four propagating wave types is examined. CHO also applies EFA to a light truck frame with a complex geometry. Even with a rough EFA model, EFA predicted results show reasonably good agreement with the results from experiments. In addition, the author used EFA to predict the vibrational response of coupled co-planar plates. BERNHARD et al. [21,53] show that while the thermal analogy is valid for longitudinal vibrations under very general conditions, the same equations are only approximate for flexural vibrations of beams and plates. Particularly, for flexural waves, the heat conduction equation can be obtained provided that the near field and spatially harmonic terms of the time averaged energy density are neglected.

Conclusion.

EFA is applicable for the prediction of frequency-averaged structure-borne noise and vibration problems in built-up structures in the high frequency range. EFA can be used to predict the spatial distribution of the energy density and energy flow in built-up structures such that local effects can be modeled in a straightforward manner. Also, EFA is amenable to a numerical implementation such as the finite element method. Thus

eventually, traditional finite element models which are used to predict the vibrational response at low frequencies in terms of motion variables, can be used at high frequencies in terms of energy variables. One of the immediate objectives of the researchers is the dynamic modeling of different types of joints i.e. the identification of transmission coefficients. The joints that should be analyzed include complex plate joints, beam-plate couplings, finite plate-acoustic cavity couplings, flexible and damped joints (smart joints). Novel procedures, eventually based on numerical techniques are necessary to identify the transmission characteristics of these joints. It should nevertheless be noted that the accurate evaluation of transmission and reflection coefficients likewise represents one of the difficulties encountered by SEA. Therefore, the advantage of the energy flow method compared to SEA looks modest, being limited to yield, for each structural component a slow decaying trend of the energy density due to dissipation effects. Still it is felt that EFFEM deserves close attention in order to be applied on more complex structures.

1.2.3 Asymptotic Modal Analysis (AMA).

Classical modal analysis involves consideration of each individual mode of a system within a given frequency band : the acoustic modes of a cavity, the structural modes etc. SEA is complementary to classical deterministic modal analysis when a large number of modes is involved, since only averaged quantities regarding the systems dynamics are considered. Because for SEA the results are given in terms of lumped quantities, detailed information with respect to frequency and location cannot be obtained. AMA is developed by PERETTI and DOWELL [20] and constitutes a hybrid of classical deterministic modal analysis and SEA. The equations involved are systematically derived from classical modal analysis and therefore AMA contains several levels of approximation and generality.

AMA is basically a modal summation method for which several essential approximations can be carried out if a large number (theoretically an infinite number) of modes is observed. AMA possesses the computational advantages of SEA, in that the individual modal characteristics do not play a role in the asymptotic analysis. AMA in addition can predict local response peaks or intensification zones, results unobtainable using SEA. Besides, it can be noted that the space averaged AMA results are identical to the SEA results. The systematic derivation of the AMA equations allows for an assessment of the assumptions and consequent simplifications which are made in SEA. One of the important contributions of AMA is the systematic way in which it is shown that the boundary conditions of vibrating systems do not influence the mean square response of the system at high frequencies.

DOWELL and KUBOTA [24] apply AMA to study the high frequency dynamics of a rectangular plate. The experimental results approach the results predicted by AMA as the frequency band becomes large. AMA in the case of an acoustic cavity is addressed by KUBOTA, DIONNE and DOWELL [25].

PERETTI and DOWELL [20] analyze the acoustic field inside a rectangular cavity with five rigid walls and a vibrating sixth wall. Their work revealed a good agreement (in terms of the interior noise levels) between the results obtained by AMA and by classical modal analysis. In the process of obtaining the AMA results, it is assumed that the frequency interval of interest is small such that the modal characteristics (modal masses,

frequencies and damping) do not vary rapidly within the frequency band. Also it is assumed that the frequency band is sufficiently large to include many resonant modes. Since the number of resonant modes increases with the increase of the frequency bandwidth, there will be a compromise to keep the frequency band small yet large enough to have sufficient resonant modes.

Conclusion.

It has been shown that AMA can be used effectively for the prediction of the mid and high frequency vibrational response of structural and structural-acoustic systems. PERETTI and DOWELL state that AMA is applicable to any linear dynamic system at high frequencies regardless of geometry assuming that the damping is small. AMA has nonetheless not yet (September *1995*) been applied for general complex vibro-acoustic systems. Only very simple systems have been reported on in literature, the latter being a substantial disadvantage compared to SEA. According to PERETTI and DOWELL, AMA can bridge the gap between classical modal analysis and SEA in terms of computational requirements and predictive capabilities. The main advantage of AMA is the possibility to model local intensification zones, hence making it possible to obtain information on the distribution of the energy along the subsystem.

1.2.4 Mobility Energy Flow (Finite Element) Analysis (MEFA).

PINNINGTON and WHITE [50] investigated in a theoretical way the parameters controlling the energy transmission from a mass to a finite beam structure via a spring-like isolator. A useful mathematical model for the mobility of a finite beam structure is developed making it possible to develop simple formulae for peak and averaged energy transmission from a mass to a finite beam via spring-like isolators. In addition, the authors showed that the finite structure can be modeled by an equivalent structure of infinite extent for frequency averaged energy transmission calculations.

CUSHIERI [49] developed a method to analyze the vibrational response and structure-borne vibration transmission between elements of connected structures based on the work by PINNINGTON and WHITE [50]. Using the MEFA approach, the global structure is subdivided into substructures. Mobility functions are used to characterize the coupling of the substructures using vibrational energy flow as the linking parameter. MEFA uses a mobility representation of the modal response of the individual substructures that make up the global system. The mobility functions are then applied in conjunction with the global boundary conditions to obtain the response of the global system. The type of mobility functions to be used for a particular substructure depends on the type and configuration of the joints.

In 1990, MCCOLUM and CUSHIERI [37] report on the application of MEFA for two coupled plates. Using MEFA, the structure is subdivided into two substructures and the energy transmission is described in terms of the input and transfer mobility's of the substructures. The source plate is excited by a point harmonic source and a pinned type joint is considered for the analysis. The use of pinned joints allows the in-plane modes to be neglected. It has been shown that accurate results and a reduced computational effort can be achieved compared to the classical finite element method when applied in the higher frequency range.

This far MEFA has been successfully applied in the case of simple bending transmission between beams and plates. Research is going on to extent the applicability to incorporate structures with complex geometry and complicated joint configurations. One of the main advantages of MEFA is the possibility to obtain a spatial distribution of the energy of vibration along the subsystems. Furthermore, frequency averaging is not required. MEFA has shown to be especially useful in the mid frequency range, between the optimum frequency regime for finite elements and SEA.

1.2.5 Energy flow method using classical finite elements.

FREDÖ [33,39] demonstrates the possibility of using classical finite elements for evaluating the energy flow within and between substructures. The energy flow approach followed by FREDÖ is outlined briefly in the case of a two-subsystem model. The basic equations used for the approach consist of the classical energy balance equations which are also used for SEA purposes :

$$\omega \cdot \begin{bmatrix} \eta_{12} & -\eta_{21} \\ -\eta_{12} & \eta_{21} \end{bmatrix} \cdot \begin{Bmatrix} E_1 \\ E_2 \end{Bmatrix} = \begin{Bmatrix} P_1 \\ P_2 \end{Bmatrix} - \begin{Bmatrix} P_{1,diss} \\ P_{2,diss} \end{Bmatrix} \qquad (1.7)$$

Where ω is the angular frequency, the matrix $[\eta]$ represents the energy flow coefficient matrix (EFC matrix). The vector $\{E\}$ denotes the subsystems vibrational energy vector, $\{P_i\}$ represents the input energy and $\{P_{i,diss}\}$ the dissipated energy. The set of equations (1.7) is used to obtain the EFC's. The latter can be done in the following way. A finite element model of *specific* coupled subsystems of a n-subsystem model (not the *entire* system !) is used to extract the energy input, the dissipated energy and the kinetic energy of the two subsystems. In a first calculation, a dynamic force is applied on subsystem *1* and the corresponding $\{P_{in}\}$, $\{E\}$ and $\{P_{diss}\}$ are calculated. The similar procedure is followed in case of the excitation of the second subsystem. The results are substituted into the basic equation (1.7), which can be solved to yield the EFC's of the model. In fact, the computational approach which is followed by FREDÖ is similar to the one used for experimental SEA (see chapter 3), despite the fact that the latter method is purely experimental. Note that frequency band averaging is not necessary in order to solve the basic equation. Once the parameters (EFC's) of the model have been identified, it is possible to examine the energy flow between the different subsystems and to identify vibration transmission paths in structures.

One of the main advantages is that non-resonant transmission can be taken into account. Moreover the applicable frequency range has been decreased even to include frequencies below the first eigenfrequency. FREDÖ's results confirm the tendencies of the energy flow coefficients to converge for higher frequencies to the SEA coupling loss factors. The energy flow coefficients are unfortunately case specific, i.e. dependent on the global system properties and dependent on the excitation, whereas the SEA coupling loss factors are assumed to be only dependent on the subsystem properties. Even so, the existence of negative EFC's is exemplified at low frequencies. Consequently, the classical heat analogy is considered not applicable for direct interpretation of EFC's at frequencies where a low modal overlap exist. The main drawback of the method is it's applicability to rather small structures since each subsystem has to be modeled in detail by finite elements. Classical finite element implementations and classical finite element models with ± 5 elements/wavelength can be used. It is quite impractical to extend the

method to large systems because for every single connection, the energy flow coefficients should be calculated by modeling in detail all essential subsystems. At present however, the method has only been applied on simple geometry's : e.g. two right angled thin plates. Research is spent on incorporating more complex subsystems. It can be concluded that the energy flow approach offers a good understanding of some of the simplifications and assumptions made in SEA and offers the possibility to complement classical SEA for specific cases, i.e. modeling of non-resonant transmission of energy and including the mid-frequency range. Nevertheless, the method is not developed sufficiently in order to include complex, industrial relevant systems which are analyzed by SEA these days.

1.2.6 General Energy Formulation Method (GEFM) and Smooth Energy Formulation (SEF).

LEBOT [51], LEBOT and JEZEQUEL [47], LASÉ and JEZEQUEL [52] have developed GEFM for the prediction of the steady-state vibrational response of one-dimensional structures. The formulation is entirely energetic with energetic boundary conditions from low up to high frequencies. GEFM formulates the vibrational problem of one-dimensional structures in a purely energetic form without approximation. Hence, the results obtained using GEFM for one-dimensional structures are similar to the results obtained using the displacement solutions of the dynamic equations of one-dimensional structures. The keys to GEFM are that the complex energy (i.e. active and reactive) is modeled and that total and Lagrangian[`] energy densities are used to describe the flow of vibrational energy in the one-dimensional structures. The total energy density is defined as the sum of the kinetic and the potential energy densities. Two second-order differential equations are required to predict the response of a longitudinally vibrating rod instead of one second-order energy differential equation for motion variables. Similarly, two eight-order energy differential equations are required to predict the response of a transversely vibrating Bernoulli-Euler beam instead of one fourth-order differential equation when classical motion variables are applied. Eventually one can obtain a smoothed solution at low up to high frequencies by introducing a smoothing function with values between *0* and *1*. Hence, GEFM is more computationally intensive compared to the classical finite element methods. The reason for pursuing GEFM is not its computational efficiency but rather its capability for handling vibrational problems in a purely energetic form and in a mathematically formal manner without approximations. By studying the exact flow of vibrational energy using GEFM, the importance of various energy components (i.e. active and reactive energy component, nearfield and oscillating component) can be assessed in the case of energy transmission from one structural element to the other. At present-day, the challenges for the researchers are related to the development of general energy formulations for higher-order structures such as thin plates and cylinders and the development of coupling relationships for coupled structures. The GEFM formulation is presented hereafter for a transversely vibrating Bernouilli-Euler beam. The expressions for active and reactive power in terms of the total and Lagrangian energy density are given by :

[`] The Lagrangian energy (L) equals difference between kinetic and potential energy. In the case of SEA and PFFEM, kinetic and potential energy are assumed to be equal and hence $L=0$.

$$\begin{Bmatrix} P \\ Q \end{Bmatrix} = -\frac{\omega}{8\eta^3} \cdot \begin{pmatrix} \frac{(1+\eta^2)^2}{k_o^2} \cdot \begin{bmatrix} 8+2\eta^2 & -2\eta^2 \\ 4\eta & 0 \end{bmatrix} \cdot \frac{\partial^7}{\partial x^7} \begin{Bmatrix} W \\ L \end{Bmatrix} + \\ \frac{(1+\eta^2)}{k_o^2} \cdot \begin{bmatrix} -128-80\eta^2 & 32\eta^2 \\ -64\eta-24\eta^3 & 24\eta^3 \end{bmatrix} \cdot \frac{\partial^3}{\partial x^3} \begin{Bmatrix} W \\ L \end{Bmatrix} \end{pmatrix} \qquad (1.8)$$

Where k_o is the real part of the complex flexural wavenumber, P, Q, W, L represent respectively the active power, reactive power, total energy density and Lagrangian energy density. When this equation is substituted into the general energy balance equation, a linear system of two eight-order differential equations is obtained :

$$\frac{\partial^8}{\partial x^8} \begin{Bmatrix} W \\ L \end{Bmatrix} - k_o^4 \begin{bmatrix} 16 & -6\eta^2 \\ 6\eta^2 & 0 \end{bmatrix} \cdot \frac{\partial^4}{\partial x^4} \begin{Bmatrix} W \\ L \end{Bmatrix} + k_o^8 \begin{bmatrix} 0 & 4\eta^2 \\ -4\eta^2 & 16 \end{bmatrix} \cdot \begin{Bmatrix} W \\ L \end{Bmatrix} = \begin{Bmatrix} 0 \\ 0 \end{Bmatrix} \qquad (1.9)$$

The general solution for W and L of this equation each have eight independent terms. Hence, a total of sixteen boundary conditions are needed to completely describe the flexural vibrational energy flow in a beam. However, according to LEBOT [51], only ten of the sixteen terms are needed to accurately describe the flow of vibrational energy.

Conclusion.

The GEFM tries to evaluate the response of a system for low as well as high frequencies and in addition considers different types of boundary conditions of the system. The latter being a substantial advantage compared to SEA. The method enables one to predict a spatial variation of the vibration response within each subsystem as well as throughout the entire system and to evaluate the structure entirely in the energetic formulation with energetic boundary conditions. However, one again, this method has only been applied for very simple structures : beam-beam couplings incorporating longitudinal motion. Further research is required to extend the method in order to include complex, industrial relevant structures.

1.2.7 Energy (Phase) Envelope Method (E(P)EM).

CARCATERRA and SESTIERI [40,41] state that some terms in the equations of the energy flow analysis (EFA) discussed in paragraph 1.2.2 when dealing with flexural waves in beams or plates, are neglected, hence increasing the discrepancy between the experimental results and the results obtained by using EFA. Even in simple cases, the energy flow does not show a thermal behavior and the equations involved are non-linear with respect to the energy density. CARCATERRA and SESTIERI clarify the mechanism of energy transmission in mechanical structures and reveal the limits of the thermal analogy. Drawbacks of the energy formulations are the non-linear terms and an oscillating behavior of the energy density which becomes a serious limit at high frequencies. The use of an approximated solution showing a smooth non-oscillatory trend, provides a useful and convenient description of dynamic problems at high frequencies and avoids numerical pitfalls. Discussing the highly non-linear character of the energy density equations whose solution would require a much larger effort than the one necessary to solve the displacement equation, an envelope energy model was determined through an appropriate use of the Hilbert transform.

An approximate envelope kinetic energy can be defined through the Hilbert transform which is an integral operator whose kernel is $1/\pi x$:

$$H(f)=\int_{-\infty}^{\infty}\frac{f(\xi)}{\pi(x-\xi)}d\xi=f*\frac{1}{\pi x} \qquad (1.10)$$

The Fourier transform of the Hilbert transform is :

$$\Im(H(f))=\Im(f)\cdot\Im\left(\frac{1}{\pi x}\right) \qquad (1.11)$$

Therefore, the Hilbert transform is an operator that shifts all harmonic components of $f(x)$ by $\pi/2$. Thus through the application of the Hilbert transform, an envelope $E(x)$ of an analytical function $f(x)$ can be defined as :

$$E(x)=\frac{\kappa_T}{2}\sqrt{f^2(x)+H^2(f)} \qquad (1.12)$$

With κ_T a constant depending on the inertial and geometrical properties of the structure.

Unlike EFA and GFFEM, the envelope model provides different order equations : a second order for longitudinal wave, a fourth order for flexural wave :

$$\frac{d^2E}{dx^2}-\left(\frac{\eta\omega}{c}\right)^2E=0 \qquad (1.13)$$

The envelope $E(x)$ tends to cancel the harmonic components of $f(x)$, performing a smoothing operation. Clearly, the Hilbert transform forms the kernel of the envelope energy method. It has been shown that an approximate definition of the envelope energy permits to obtain a very effective equation whose solution replies to the exigencies of classical high frequency modeling methods (SEA, EFA, GFFEM). The smoothing trend of the envelope can be determined using a finite element model, without requiring a fine mesh of the structure.

Conclusion.

It can be stated that EEM shows similar characteristics compared to EFA. The approach which has been followed by SESTIERI to obtain the envelope equation is however different due to the use of Hilbert transforms. The main application of the envelope method is situated in the mid to high frequency range since local oscillating vibration patterns are eliminated and therefore one can make use of existing coarse finite element models of structures which are used in the lower frequency range. No applications on complex systems have been found in literature. The applications which have been reported at present are dealing with simple structures such as longitudinal motion in beams. The optimization of the method and the extension to flexural waves in beams which is under development does not - according to the Carcaterra - seem to present difficulties. The possibility of a generalization to two and three dimensional structures is considered, and though it is not a trivial extension of the one-dimensional technique, it is, according to the researchers, quite promising

1.2.8 Ray Tracing.

Ray tracing techniques are appropriate to apply in the high frequency range because the wavelength is small enough to ignore local interference patterns (No phase information !!). Ray tracing techniques make several simplifying assumptions. For example a sound field can be represented by a series of discrete rays similar to light rays. Each ray reflects from boundary walls, losing energy in proportion to a surface absorption coefficient and to the distance traveled along the path. The intensity at a particular location is the sum of all rays traversing through a small surface area or volume. Usually, a second assumption is that the sound field has a high modal density and is diffuse, i.e. independent of measurable phase cancellation effects. At high frequencies, where the wavelength is small compared to linear dimensions and volumes, ray intensity values can be integrated to obtain representative levels. If the average room absorption is small, the sound field far from the source will be diffuse. An implication of diffuse fields for ray modeling is that wall reflections are proportional to the cosine of the incident and reflected angles (Lambert's law). Some ray analysis codes can model this behavior. It is quite unusual to model small volumes using ray tracing techniques. The main advantage of the ray tracing technique is that the frequency range is not limited. High frequency analyses of rooms is perfectly possible and the technique is implemented in some commercial codes. However, a complex vibro-acoustic system (such as car) can not be modeled by ray tracing techniques as the method is restricted to acoustic cavities.

1.3 Conclusion.

Traditional analyses of mechanical vibration of structures focus on the low frequency range. This is because the frequencies of excitation are usually fairly low and low frequency modes have the greatest displacement response and therefore stress. The advent of fairly large and lightweight aerospace structures in the '60s, and their attendant high frequency broad band loads has brought attentions to frequencies well above the fundamental resonant frequency. Classical modal analysis, which has been applied well in studying low frequency vibrations, is valid, in principle, to all frequencies. However, its applications to high frequencies are usually impractical. SEA on the other hand, provides a simple and meaningful approach for understanding and estimating the high frequency multi-modal vibration of complex systems. This approach takes averages initially and then carries out calculations in terms of averaged quantities.

SEA was initiated in the early '60 by Lyon and Beranek and constitutes nowadays the most widely applied method with respect to high frequency modeling. Recently however, many researcher are investigating alternative techniques to get rid of the weaknesses of SEA. For example, one major weakness of SEA deals with the impossibility to model local vibration patterns. Only global, spatially averaged vibrations patterns can be obtained by SEA. The alternative methods (paragraphs 1.2.2-1.2.10) are aiming at complementing SEA in this respect. Still and all, these alternative[`] methods have not tackled the problem of analyzing high frequency vibrations of complex structures. Simple structures are analyzed such as two coupled beams or flat plates. Research is spent on extending these methods to incorporate *complex* structures which are relevant from the practical engineering viewpoint. Nevertheless, these techniques (except for

[`] Compared to SEA

SEA) are mainly examined only during the last decade in a small extent in very specialized research laboratories. Although each individual technique explained briefly in this introduction deserves further attention, it can not be guaranteed that it will be accepted by the engineering community as a significant tool to solve high frequency vibrations, the latter being one of the reasons why one the alternative methods has not been taken as the research topic of this dissertation.

SEA on the other hand is around for thirty years. Predictive SEA led to many interesting applications in aerospace industry, shipbuilding industry and building acoustics. Recently, other industries are focusing on SEA. Major car builders are looking for adequate techniques to finally solve the high frequency puzzle. Attention comes from the helicopter, train, engine- and many more - constructors.

Whereas for the classical SEA applications (building acoustics, shipbuilding, aerospace industry), gross of the research has already been performed and more or less satisfactory results are obtained, the latter does not hold for the newcomers in the field. Novel and adequate SEA formulations (as well as for experimental and computational SEA) have to be developed in order to be able to model the high frequency vibrations. Because of SEA being promising and backed by a lot interest of companies on one hand and because of the fact that SEA is still missing some essential features on the other hand, the option has been taken to apply SEA for modeling high frequency vibrations in the framework of this dissertation.

One of the recently developed SEA related techniques deals with the *experimental* identification of the SEA model. No in depth research has been performed in this respect, in particular in the area of statistics, confidence and sensitivity. A comprehensive description of this method is unquestionably needed. Chapter *3* and *4* contribute to this field of the research by presenting formulations to perform a statistical analysis of the SEA predictions and parameters in order to qualify the confidence of the model. Chapter *4* also concentrates on an optimization of experimental SEA from the point of view of measurement effort.

From the predictive side, the library of types of couplings between subsystems needs to be extended in order to include complex couplings which are encountered in cars, trains etc. Whereas formulas dealing with simple (e.g. right angled) junctions are well described in literature (See CREMER and HECKL [79]), some couplings are not. Chapters *5* and *6* clarify the efforts which have been performed in this respect in the framework of this thesis.

2. STATISTICAL ENERGY ANALYSIS.

2.1 Introduction - history - state of the art.

The name Statistical Energy Analysis (SEA) was coined in the early *60's* to emphasize certain aspects of a, at that time, new field of study.

Statistical : meaning that the SEA variables and parameters are drawn from a statistical population.

Energy : emphasizing that energy constitutes the primary variable of interest. Other variables such as velocity, strain, stress, sound pressure level etc. can be obtained from the energy variable.

Analysis : denoting that SEA is more a framework of study or an approach, rather than a particular technique.

The vibration of walls and floors in the higher frequency range has been of interest for a long time especially in the civil engineering community. From the early *60's*, when mechanical engineers started to be aware of the problems dealing with large and lightweight structures and their attendant broadband loads, became SEA a general approach of interest, mainly for the *aerospace* engineering industry. There was however already some experience in the early days concerning dynamic systems described by random parameters :

- ***Room acoustics*** : dealing with the excitation of very many degrees of freedom of cavities. In an ordinary room there may be over millions of modes as illustrated by the following formula[`] .

$$N(f) = \frac{4\pi f^3 V_0}{3c^3} \qquad (2.1)$$

  Where $N(f)$ represents the number of modes in the frequency range $[0\text{-}f]$, V represents the volume of the cavity and c denotes the velocity of sound. In the case of a room with dimensions $3x6x9m$, the number of modes below *8000* Hz

[`] this formula is derived in chapter 5.

equals $9*10^6$. Because of the large number of modes, a classical modal approach to model the acoustics becomes impossible.

The very large number of degrees of freedom is an advantage from the statistical point of view : it tends to diminish the fluctuations of the response.

- ***Statistical mechanics*** : dealing with systems with few or many degrees of freedom. The theory of statistical mechanics shows that - in the case of thermal systems - energy always flows from hotter to cooler places.

As such, SEA can be considered as a combination of three different techniques : modal & wave superposition techniques, room acoustics and statistical mechanics.

The earliest, identifiable work with respect to SEA (although the name SEA was not adopted yet) dates back to *1959*. At that time, LYON [59] and SMITH [58] independently carried out calculations which were SEA related. Lyon was studying the energy flow between *two* lightly coupled oscillators. Smith examined the response of a resonator excited by a diffuse, broadband sound field. Smith found that the response of his resonator reached a limit. If a resonator is excited by a broadband noise source and if the internal damping equals zero, then the response tends to infinity. However, due to the reaction of the sound field on the resonator, the response remains finite. Lyon and Smith joined and they found that Smith's limiting vibration amounted an equality of energy between the resonator and the averaged modal energy of the sound field, a result which was consistent with the former results of Lyon concerning the energy flow between two coupled oscillators. In the *'60s,* Lyon's and Smith's work was extended and formulas were derived to quantify the interaction of single modes of a system with many modes of another system. This work and results stressed the importance of some basic parameters for response predictions : *modal densities, internal loss factors and coupling loss factors*. These parameters are further referred to as SEA parameters.

The pioneer applications of SEA were dealing with sound-structure interaction, mainly because it seemed obvious that SEA would work best when a sound field, which includes many degrees of freedom, was involved. In this respect MAIDANIK [90] studied the radiation of reinforced plates. MANNING and MAIDANIK [91] investigated the radiation of sound by cylinders.

Very soon, structure-structure interactions were examined, being still one of the attracting and challenging topics of SEA. An extension of the early theory which was developed for two subsystems, was made by EICHLER [60] who predicted the flow of vibrational energy through three substructures connected in tandem. The applications on structural vibration transmission were dealing with electronic package vibration during the launch phase of a satellite. A related "SEA paper" by LYON and EICHNER [61] investigates plate-beam interactions, plate-plate interactions and a three subsystem plate-beam-plate model. Soon it was found out that the major problem with respect to building a reliable SEA model, was the evaluation of the model parameters for a large variety of substructures and junctions between substructures

The most active uses of SEA have been in aerospace industry, shipbuilding industry and building acoustics. In all of these fields, structure-borne sound in particular is of the utmost importance and a substantial effort has been undertaken to model vibration transmission through structural junctions. These couplings mainly include right angle plate junctions : L, T and cross junctions (See also chapter *5*). Whereas for ship

structures (including many simple connections : e.g. right angled plate junctions for which the SEA parameters can be calculated without too many problems), the SEA models are quite accurate, the latter is still not the case for very complex structures including complex junctions and subsystems, such as cars and engines. The many calculations of force and moment impedances of beams and plates performed by building acousticiens has allowed already a wide variety of systems and junctions to be evaluated.

To date, the potential areas of interest to SEA have been increased significantly compared to the early days. During the last decade, car, truck and train builders, helicopter manufacturers and engine constructors became interested and became involved. Along with the advent of their novel, more complex structures arose the need to extend the range of applicability of SEA. As a consequence, the number of different types of couplings and substructures which is analyzed has been increased and still needs to be increased in the future.

SEA applications can roughly be divided into two groups covering :

- The utilization of experimentally identified models.
- The application of predictive SEA schemes.

The *experimentally* identified models are primarily based on a technique referred to as the Power Injection Method (PIM). PIM allows for an identification of the SEA parameters on a structure in situ, without having to decouple the structure. Chapter *3* & *4* addresses extensively the application and optimization of PIM. These days, PIM is being applied to cars, trucks, helicopters and other complex structures. STIMPSON [10] describes the use of experimental energy techniques for the prediction of machinery noise with emphasis on a diesel engine. The author concludes that this type of analysis can be performed in a economic way, on a simple computer, that it provides a good picture of an engine's noise radiation characteristics and that it provides a valuable insight into the important vibrational transmission paths. WU et al. [55] report on the use of experimental SEA techniques to study the vibrational energy flow in engines. Although their results are still not sufficiently adequate, the techniques looks promising and deserves further attention. HANISH [28] addresses the application of PIM applied to a car body for the identification of the major vibrational transmission paths and for the evaluation of the power sources (source localization). As a general remark, it can be stated that the number of applications dealing with experimental SEA has been small compared to the number of applications dealing with predictive SEA. No in-depth research on this topic has been performed so far. Especially sensitivity and statistical aspects, aspects with respect to measurement strategies and practical implementation aspects need to be clarified. As such, chapter *3* and *4* contribute to this field of research by presenting an in-depth investigation into experimental SEA.

Predictive SEA aims at evaluating the SEA parameters on a theoretical basis and is therefore aimed to be employed in the early design phase of structures. Although not all parameters can be determined computationally - the internal loss factors is difficult to evaluate by using exclusively computationally procedures - it has been shown that it is possible to calculate modal densities and coupling loss factors for a whole branch of subsystems and connections (see Chapter *5* & *6*). Promising and successful applications have been reported on ships (see LYON [18] and PLUNT [32]), buildings (see CRAIK

[29]), aerospace structures (see TANNER [88] and THINCH [89]) and helicopters (see HERON [23]). LIM [11] even describes the application of predictive SEA to a gearbox with emphasis on the bearing path. The model includes a theoretical coupling loss factor calculation associated with the transmission of vibrational energy through the dominant path, i.e. rolling element bearings. Although many simplifying assumptions are involved, experimental results are in reasonable agreement with the proposed SEA model.

In order to fully understand the SEA assumptions and hypotheses, it is essential to obtain a good understanding of the basic theory of SEA. The next section intends to give a in-depth view on SEA.

2.2 Energetics of coupled subsystems.

2.2.1 Introduction.

This section is concerned with the exchange of energy in coupled vibrating systems. The goal is to reveal how certain quantities of coupled vibratory oscillators can be derived from the energetic viewpoint. Linear systems and some interesting measures of response that are particularly related to vibrational energy : *mean square velocity* will be focused on. The first part of section 2.2 covers the energy exchange between two coupled linear resonators. The second part examines how the two-subsystem model can be extended to a multi-modal system in which energy is exchanged between every mode of the first subsystem and every mode of the second subsystem. The excitation force is assumed to be random. Some parameters which are unique to the energetic description of vibrating systems, namely the SEA parameters, will be addressed.

The meaningful and pervasive concept of a *statistical* description of modal parameters is introduced. Relationships between modal parameters and their statistical equivalence will be established.

2.2.2 Energy exchange between two resonators.

To begin the discussion, the energetics of one simple linear resonator (figure 2.1) are clarified.

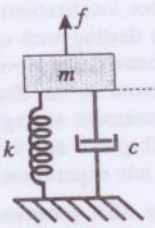

Figure 2.1 : Single degree of freedom system.

The equations involved are :

$$m\ddot{x}+c\dot{x}+kx=f \quad or \quad \ddot{x}+\omega_o\eta\dot{x}+\omega_o^2 x=\frac{f}{m} \tag{2.2}$$

Where $\omega_o = \sqrt{k/m}$ represents the undamped natural angular frequency. $\eta = c/\omega_o m$ represents the loss factor.

In the case of free vibration without damping, it holds that :

$$\ddot{x} + \omega_o^2 x = 0 \tag{2.3}$$

For which the general steady-state solution $x = A \cdot sin(\omega_o t + \varphi)$ can be substituted into the expression of kinetic energy :

$$E_k = \frac{1}{2} m \dot{x}^2 = \frac{1}{2} m A^2 \omega_o^2 cos^2(\omega_o t + \varphi) \tag{2.4}$$

The potential energy at any time is given by :

$$E_p = \frac{1}{2} k x^2 = \frac{1}{2} k A^2 sin^2(\omega_o t + \varphi) \tag{2.5}$$

Since a free linear system without damping is concerned, it is evident that the total vibrational energy is time independent. If the kinetic and potential energy are time averaged, then :

$$E = \frac{1}{T} \int_0^T (E_k + E_p)\, dt = \frac{1}{4} m A^2 \omega_o^2 + \frac{1}{4} k A^2 = \frac{1}{2} k A^2 \tag{2.6}$$

Therefore, the time averaged kinetic and potential energy are both equal to *1/2* of the global energy of vibration, a result which is important for SEA since it allows to evaluate global energies by evaluating kinetic energies.

In the presence of damping, the kinetic and potential energy can be calculated in the same way as in the undamped case though they are slightly more complicated compared to the undamped case. The formulas substantially simplify if the average is taken over a cycle of oscillations, neglecting the slight change in amplitude in this period due to the exponential multiplier.

$$E(t) = \frac{1}{2} k A^2 e^{-\omega_o \eta t} \tag{2.7}$$

Next, a broadband random excitation is applied to the oscillator (most of the SEA applications that are of concern are dealing with situations for which the excitation is random). Notwithstanding the introduction of broadband excitation, it is worthwhile and necessary to mention that SEA is perfectly applicable to systems excited by pure tones if one considers appropriate statistical descriptions of the system and a suitable description of the response.

LYON [1] shows that for a random excitation of a system of the kind previously described, one can easily deduce that :

$$\langle \ddot{x}^2 \rangle_t \cong \omega_o^2 \langle \dot{x}^2 \rangle_t \tag{2.8}$$

meaning that, sinusoidal input excitation and random input excitation both produce the same relationship between time averaged squared displacement, velocity and acceleration. This result is useful in the sense that it allows to transform from one

response variable to another without having to concern for the exact nature of the excitation.

Next, the energy flow between two oscillators with stiffness coupling is evaluated (figure 2.2).

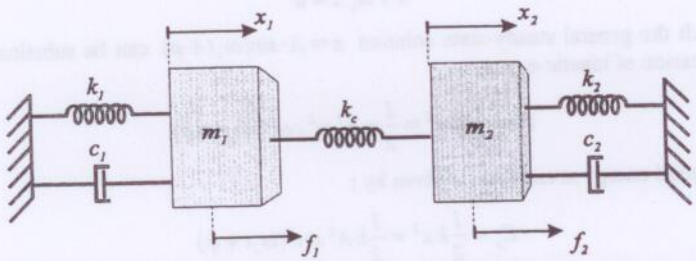

Figure 2.2 : Two linear resonators coupled by a spring element.

Where k_c represents the stiffness coupling.

The global equations of motion are given by :

$$\begin{cases} m_1 \ddot{x}_1 + c_1 \dot{x}_1 + (k_1 - k_c) x_1 + k_c x_2 = f_1 \\ m_2 \ddot{x}_2 + c_2 \dot{x}_2 + k_2 - k_c) x_2 + k_c x_1 = f_2 \end{cases} \qquad (2.9)$$

In this section, we are concerned with the response of the two resonators and with the energy flow between the resonators, excited by the white noise forces f_1 and f_2.

The white noise forces are assumed to be statistically independent. The reader is referred to [1] for a complete derivation of the equations involved. The time averaged energy flow from subsystem *1* to subsystem *2* equals :

$$\langle P_{12} \rangle_t = \langle \dot{x}_1 \cdot k_c \cdot (x_2 - x_1) \rangle_t \qquad (2.10)$$

Since $\langle \dot{x}_1 \cdot x_1 \rangle_t = 0.5 \langle d x_1^2 / dt \rangle_t = 0$ for stationary processes, it follows that :

$$\langle P_{12} \rangle_t = k_c \langle \dot{x}_1 \cdot x_2 \rangle_t \qquad (2.11)$$

The next step is to evaluate expression (2.11) in terms of the spectral densities of the loads and of the system parameters. The derivation of the related formulas can be found in [1] where it is shown that the time averaged energy flow is proportional to the difference in time averaged energy (two times kinetic energy or two times potential energy) of both resonators. If the time averaged energy of resonator *1* and *2* is respectively given by E_1 and E_2, then the time averaged energy flow between the two subsystems reads :

$$\langle P_{12} \rangle_t = g_{12} \cdot (E_1 - E_2) \qquad (2.12)$$

Where g_{12} represents a parameter depending only upon the system properties :

$$g_{12} = \frac{\kappa^2 (\beta_1 + \beta_2)}{(\omega_1^2 - \omega_2^2)^2 + (\beta_1 + \beta_2) \cdot (\beta_1 \omega_2^2 + \beta_2 \omega_1^2)} \qquad (2.13)$$

With :

- $\omega_{1,2}^2 = (k_{1,2} + k_c)/m_{1,2}$ (2.14)
- $\beta_{1,2} = \eta_{1,2}\omega_{1,2}$ (2.15)
- $\eta_{1,2} = c_{1,2}/m_{1,2}$ (2.16)
- $\kappa = k_c/\sqrt{m_1 \cdot m_2}$ (2.17)

Equation (2.12) is very useful because it allows to calculate the time averaged energy flow between subsystems from the energy levels of the subsystems. Important annotations which can be made in this respect are given below :

- The parameter g_{12} is strictly *positive;* in addition, it holds that $g_{12} = g_{21}$. Therefore energy flows from the more energetic resonator to the less energetic one and one may state that the energy flow is reciprocal.
- If only one resonator is directly excited, the largest possible value of the energy of the second resonator equals that of the first resonator.
- The constant of proportionality g_{12} is a function of the oscillator parameters and is independent of the source strength of the excitation. The analysis holds for coupling of arbitrary strength with *stiffness*, *inertial* and *gyrostatic*[`] elements, as long as there is no dissipation in the coupling. If inertial and gyrostatic coupling elements are present, then equation (2.13) takes a more complicated form. Nonetheless, the remarks made in here do not change. In practice, when systems have interface damping at the connection between subsystems the associated damping is split between subsystems.
- The constant of proportionality g is very sensitive to the difference in blocked[``] natural frequencies ω_1 and ω_2. Oscillators having close blocked natural frequencies exchange energy more easily than those having remote natural frequencies.
- g is damping dependent ($\beta = \eta \cdot \omega$). Hence, in principal the coupling loss factor will also be damping dependent.

2.2.3 Energy exchange between two multi-degree of freedom systems.

As the systems of interest to engineers are much more complicated than two coupled linear resonators, the findings of the previous section should be extended to include multi-modal (distributed) systems. Before deriving the SEA equations dealing with the energy flow between multi-modal systems, it is essential to obtain a basic understanding of their energy behavior.

2.2.3.1 Energetics of a distributed system.

For general physical structures, the stiffness, inertia and dissipation mechanism should be modeled distributed along the structure. The global differential equation of a multi-modal linear system can be given in terms of displacements x by :

[`] the acoustic coupling between a fluid and a structure takes a gyrostatic form.

[``] meaning that the degrees of freedom at the connection between subsystems is set motionless.

$$\rho \ddot{x} + c\dot{x} + \Lambda x = f(\vec{r}, t) \tag{2.18}$$

Where ρ is the mass density, c is the damping factor and Λ is a linear operator consisting of differentiations with respect to space. $f(\vec{r}, t)$ represents the excitation at a certain location $\vec{r}$ and x stands for the displacement. In the case of a flat plate, ρ is the mass per unit area of the plate and $\Lambda = B\,\nabla^4$; where B represents the bending rigidity.

The solution of equation (2.18) is frequently sought by a modal expansion approach. The response is expanded in eigenvectors (modal summations) and equation (2.18) can be transformed into uncoupled equations of the following form :

$$\ddot{q}_r + \omega_r \eta_r \dot{q}_r + \omega_r^2 q_r = f_r \tag{2.19}$$

Where q_r represents a generalized coordinate, ω_r denotes the resonance angular frequency, $\omega_r \eta_r$ represents the damping and f_r stands for the excitation. Subscript r denotes the mode number.

Hence, each modal response amplitude obeys the equation of a linear resonator of the sort discussed in the previous section. This result, in conjunction with the spatial orthogonality of the mode shapes leads to the concept of a complex dynamic system as a group of independent resonators of mass m_r, stiffness $\omega_r^2 m_r$ and mechanical resistance $\omega_r \eta_r m_r$.

The kinetic energy of vibration of the global system is given by :

$$E_k(t) = \frac{1}{2}\int_V \rho \dot{x}^2\, dV = \frac{1}{2}\sum_r m_r \dot{q}_r^2 \tag{2.20}$$

Hence by using the orthogonality relationship between the modes of vibration, the kinetic energy of the modes add separately to yield the global kinetic energy of the system. As the time averaged kinetic and potential energies of each single resonator are equal, the total energies of the modes simply add to form the global system energy.

2.2.3.2 *Energy exchange between two multi-degree of freedom systems.*

In this section, two multi-modal subsystems connected by means of a non dissipative coupling are considered and the energy flow between them is calculated. The two subsystems are responding to their own excitation and to the interaction forces acting at the junction. Assume a white noise excitation and suppose that within the frequency range of interest subsystem i exhibits N_i modes. In addition, the following hypotheses are made :

- The modes are equally distributed in the frequency interval represented by Δf (or by $\Delta\omega$ in angular form).
- All modes of a subsystem are equally energetic and the modal responses are incoherent.
- Damping values of the modes of a subsystem are assumed to be approximately similar.

The coupled subsystems, including the interaction of the different modes may be represented as shown in the following figure.

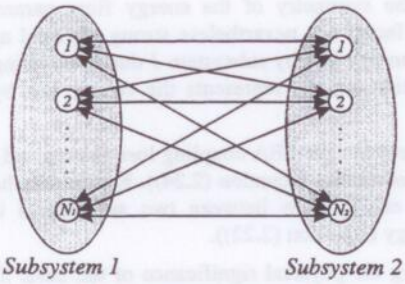

Figure 2.3 : Interaction of mode pairs.

LYON [1] has shown that energy modal pair interaction, when averaged over the ensemble of systems will act like a white noise generator. Mode i of subsystem *1* and mode j of subsystem *2* have energies $E_{i,1}$ respectively $E_{j,2}$ as a result of these white noise generators. Furthermore, the modal energies within each individual subsystem are equal (based on the hypotheses mentioned above). Therefore :

$$E_{1,1} = E_{2,1} = \cdots = E_{N_1,1} = \frac{E_1}{N_1} \quad and \quad E_{1,2} = E_{2,2} = \cdots = E_{N_2,2} = \frac{E_2}{N_2} \tag{2.21}$$

Note that $E_{i,j}$ are modal energies (energy / mode). N_i represents the mode count.

The modes of the global system are a linear combination of the modes of the individual subsystems. Each mode of the first subsystem is coupled to all of the relevant modes of the other subsystem. The total energy flow is the sum of the individual mode-to-mode energy flows evaluated as independent isolated pairs of oscillators. If the significant coupling is assumed to occur in a limited frequency band Δf, then the net energy flow can be found by averaging the value of g (equation (2.13)) over Δf and using subsystem modal energies, resulting in :

$$P_{12} = \langle g \rangle \, N_1 \, N_2 \left(\frac{E_1}{N_1} - \frac{E_2}{N_2} \right) \tag{2.22}$$

The energy flow is proportional to the difference in *modal* energy, and not to the difference in total energies. Hence, if the time averaged total energy of the subsystems *1* and *2* is given by E_1 respectively E_2 then equation (2.22) can be written as :

$$P_{12} = \omega \left(\eta_{12} E_1 - \eta_{21} E_2 \right) \tag{2.23}$$

and :

$$n_1 \eta_{12} = n_2 \eta_{21} \tag{2.24}$$

Where ω represents the band center frequency, $n_i(f) = N_i / \Delta f$ the modal density of subsystem i. The quantities η_{12} and η_{21} are called the SEA coupling loss factors associated with subsystems *1* and *2* defined by :

$$\eta_{12} = \frac{\langle g \rangle n_2 \, \Delta f}{\omega} \tag{2.25}$$

By introducing them, the symmetry of the energy flow parameters η_{ij} is lost, i.e. $\eta_{ij} \neq \eta_{ji}$. The coupling factor has nevertheless strong physical appeal. The expression $\omega \eta_{12} E_1$ represents the energy lost by subsystem *1* due to coupling with subsystem *2*, in a similar way the quantity $\omega \eta_1 E_1$ represents the energy lost by subsystem *1* due to damping.

The basic relationship between the SEA coupling loss factors and the modal densities is called the reciprocity relationship (equation (2.24)). Reciprocity has basically originated from the fact that the energy flow between two subsystems is proportional to the difference in *modal* energy (equation (2.22)).

A short example showing the physical significance of the basic SEA equation (2.23) is given below :

Consider a two-subsystem model of which one subsystem is driven by external forces and the other is driven only through the coupling. This situation represents a problem which is frequently encountered. The energy balance is given by :

$$\begin{cases} P_1 = \omega \eta_1 E_1 + \omega \eta_{12} E_1 - \omega \eta_{21} E_2 \\ 0 = \omega \eta_2 E_2 + \omega \eta_{21} E_2 - \omega \eta_{12} E_1 \end{cases} \tag{2.26}$$

The energy ratio between the two subsystems reads :

$$\frac{E_2}{E_1} = \frac{\eta_{12}}{\eta_2 + \eta_{21}} \tag{2.27}$$

Equation illustrates that :

- If $\eta_2 << \eta_{21}$, then irrespective of the actual magnitude of the coupling, the energy ratio converges to η_{12} / η_{21} or to n_2 / n_1 (by using reciprocity) i.e. the ratio between the subsystems modal densities. One of the practical results is that the application of additional damping will not be effective unless η_2 is of the same order of magnitude as η_{21}. The condition for which it holds that $E_1 n_2 = E_2 n_1$ is referred to as equipartition of energy and is favored by close natural frequencies, small damping and large coupling. In the case of equipartition of energy, the energy flow between the subsystems will vanish.
- The modal energy of subsystem 2 never exceeds the modal energy of the driven subsystem since the coupling loss factors are positive.
- For $\eta_{21} << \eta_2$, the energy level of the second subsystem is *inversely* proportional to its damping and *directly* proportional to the coupling factor η_{12}. Hence, in some cases for which a low value of E_2 should be achieved, increasing the damping of the second subsystem will not be very effective and decreasing the coupling factor η_{12} should eventually be preferred.

2.2.4 General SEA equations.

In many practical situations, the system will comprise several multi-modal subsystems, in which case each subsystem may be physically coupled to more than one contiguous subsystem. Every single subsystem can be modeled as a set of modes, as discussed in the previous section, constituting energy storage locations. For example, in the case of beams, the flexural modes in a frequency band can be considered as a subsystem, the

longitudinal modes as another subsystem. Longitudinal and bending behavior should be considered separately (i.e. separate subsystems) from the energetic viewpoint because of their difference regarding characteristic impedances and modal densities. For SEA it is assumed that the energy flow between two single subsystems of a global system is given by the energy flow equation which holds for a two-subsystem model. Keeping in mind this hypothesis, one can represent the time-averaged energy exchange between two subsystems i and j as :

$$P_{ij} = \omega g_{ij} \left(\frac{E_i}{n_i} - \frac{E_j}{n_j} \right) \tag{2.28}$$

Equation (2.28) states that the energy flow between two subsystems of a multi-subsystem model is proportional to the difference in modal energy of both subsystems. Equation (2.28) comprising three parameters (g_{ij}, n_i, n_j) is usually written in the form of two equations containing four parameters $(\eta_{ij}, n_i, \eta_{ji}, n_j)$:

$$\begin{cases} P_{ij} = \omega(\eta_{ij} E_i - \eta_{ji} E_j) \\ n_i \eta_{ij} = n_j \eta_{ji} \end{cases} \tag{2.29}$$

The time averaged energy dissipated in a subsystem i is given by :

$$P_{i,diss} = \omega \eta_i E_i \tag{2.30}$$

Where η_i represents the loss factor of subsystem i. For reasons of clarity, η_i will occasionally be written as η_{ii} further on.

It should be emphasized though that not all damping mechanism can be treated by means of equation (2.30), e.g. non linear damping. However, most damping models, such as viscous damping, visco-elastic damping and acoustic radiation damping can be expressed by equation (2.30). Chapter 5 covers the evaluation of the loss factor more in detail.

The global SEA equations of a system can now be obtained through an energy balance of each individual subsystem (figure 2.4) :

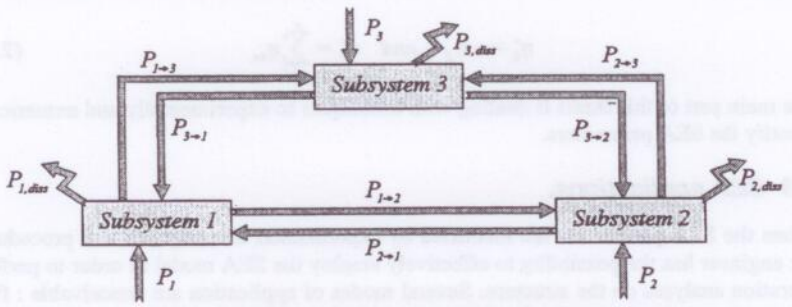

Figure 2.4 : Energy balance of a three-subsystem model.

Mathematically, the energy balance of every single subsystem i is given by :

$$P_i = P_{i,diss} + \sum_{j \neq i}^{n} P_{i \to j} - \sum_{j \neq i}^{n} P_{j \to i} \tag{2.31}$$

Substituting the basic SEA equations (2.29) and (2.30) concerning energy flow respectively energy dissipation into (2.31) results in :

$$P_i = \omega \eta_{ii} E_i + \sum_{j \neq i}^{n} \omega (\eta_{ij} E_i - \eta_{ji} E_j) \tag{2.32}$$

and in the reciprocity equation :

$$n_i \eta_{ij} = n_j \eta_{ji} \tag{2.33}$$

The set of equations (2.32) and (2.33) can eventually be written in a form more corresponding to the concept which states that *energy exchange is proportional to the difference in* ***modal*** *energy* :

$$\omega \cdot \begin{bmatrix} \left(\eta_{11} + \sum_{i=1}^{n} \eta_{1i}\right) \cdot n_1 & -\eta_{12} \cdot n_1 & \cdots & -\eta_{1n} \cdot n_1 \\ -\eta_{21} \cdot n_2 & \left(\eta_{22} + \sum_{i=2}^{n} \eta_{2i}\right) \cdot n_2 & \ddots & \vdots \\ \vdots & \ddots & \ddots & \vdots \\ -\eta_{n1} \cdot n_n & \cdots & \cdots & \left(\eta_{nn} + \sum_{i=n}^{n} \eta_{ni}\right) \cdot n_n \end{bmatrix} \cdot \begin{Bmatrix} E_1 / n_1 \\ E_2 / n_2 \\ \vdots \\ E_n / n_n \end{Bmatrix} = \begin{Bmatrix} P_1 \\ P_2 \\ \vdots \\ P_n \end{Bmatrix} \tag{2.34}$$

The matrix on the left hand side of equation (2.34) is symmetric because of the reciprocity relation.

Sometimes, it is convenient to write the global SEA energy balance equation in the following form :

$$\{P\} = \omega \cdot [\eta^{\circ}] \cdot \{E\} \quad and \quad n_i \eta_{ij} = n_j \eta_{ji} \tag{2.35}$$

Where :

$$\eta_{ij}^{\circ} = -\eta_{ji} \quad and \quad \eta_{ii}^{\circ} = \sum_{m=1}^{n} \eta_{im} \tag{2.36}$$

The main part of this thesis is dealing with techniques to experimentally and numerically identify the SEA parameters.

2.3 SEA applications.

When the SEA parameters are identified by experimental or computational procedures, the engineer has the possibility to effectively employ the SEA model in order to perform vibration analyses on the structure. Several modes of application are conceivable : from the prediction of subsystem energy levels to sensitivity analysis.

An SEA model can be used in the *preliminary design stage* or in the *operational condition stage* to obtain a quick and cheap understanding of the energy patterns in a system, to perform source localization or to reveal substantial transmission paths in the

structure. In the next sections, an overview is given of the main SEA applications. This overview is not exhaustive, though it covers the most important SEA applications.

2.3.1 Response prediction.

The SEA model allows one to calculate the energy level of each subsystem from a knowledge of the SEA parameters and from a knowledge of the power inputs. The simultaneous equations for the state of vibration in terms of energy are linear algebraic. The result of the energy calculation is the total resonant energy in a frequency band. The energy levels can then in some occasions be converted into the actual dynamic response of interest : sound pressure level, strain level, stress level etc. The relation between the response in energy terms and the response of interest is covered in section 2.9.2.

Mathematically, the energy levels are given by :

$$\{E\} = \frac{1}{\omega} \cdot [\eta^e]^{-1} \cdot \{P\} \qquad (2.37)$$

Partial contributions. A simple manipulation also allows for the assessment of the partial contributions of the sources. The contribution of specific sources to the vibration level of an individual subsystem can be evaluated by calculating the response due to the excitation of one specific subsystem (figure 2.5). Equation (2.38) mathematically represents the contribution in an efficient way :

$$E_{ij}^c = \frac{1}{\omega} \cdot \eta_{ij}^{e-1} \cdot P_j \qquad (2.38)$$

Where E_{ij}^c represents the part of the energy of subsystem i coming from subsystem j.

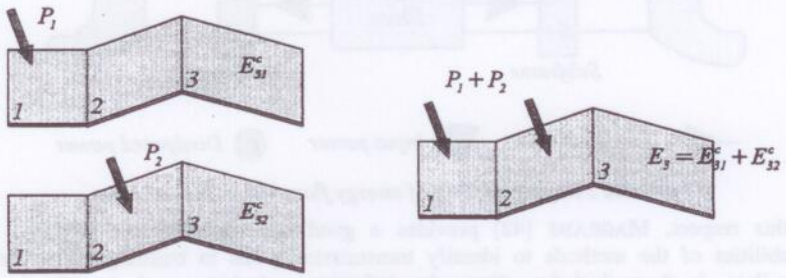

Figure 2.5 : Partial contributions of sources.

2.3.2 Source localization.

On the basis of the knowledge of the SEA parameters of a system and of the knowledge of the energy levels of the different subsystems, it is possible to perform a source localization. By applying equation (2.39), one can obtain an estimate of the power input levels and of the locations where the energy enters the structure.

$$\{P\} = \omega \cdot [\eta^e] \cdot \{E\} \qquad (2.39)$$

Equation (2.39) does not require the inverse of the SEA parameter matrix. When the sources have been localized, it is possible to calculate the partial contribution of the sources with respect to the energy level of the different subsystems according to equation (2.38).

2.3.3 Energy flow assessment.

The practical application of SEA often involves the flow of vibratory energy through intervening and parallel subsystems, before it gets to a vibration sensitive area. It is important therefore to be able to predict the energy flows and distributions in such cases in order to efficiently reduce the vibration levels of specific subsystems..

One of the basic SEA equations deals with the exchange of energy from one subsystem to the other. Hence, if the SEA model has been identified and if the energy levels or the power inputs are known, then it is possible to perform an energy flow analysis of the structure. This kind of analysis gives the engineer the possibility to assess main energy flow paths in the system and therefore provides a tool for optimal noise control measurements. A picture of how the energy flows in a system can be represented is shown below (after STIMPSON and LALOR [15]).

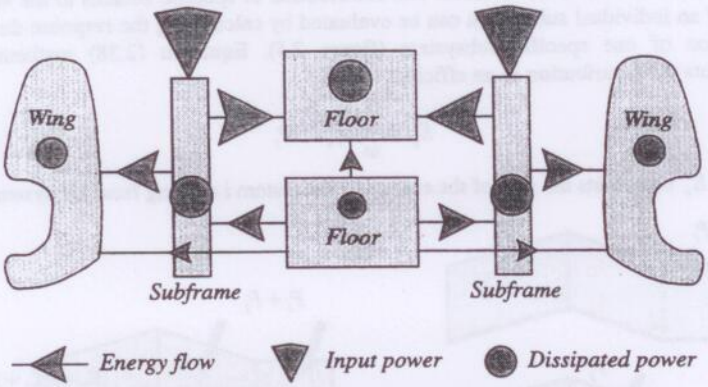

Figure 2.6 : Representation of energy flow within part of a car.

In this respect, MAGRANS [42] provides a good understanding and explores the capabilities of the methods to identify transmission paths in buildings. The author assimilates in theoretical formalisms the definition, calculation and classification of transmission paths.

In this, it is worthwhile mentioning the existence of a confusing semantic problem. Many authors use the term power flow instead of energy flow because of historic reasons : people are used to apply power flow because it is a generally well known term. However, the correct term representing the flow of energy between two subsystem is *energy flow*. The dimension of energy flow is *power*.

2.3.4 Sensitivity analysis.

Because SEA employs simple, idealized representations of the subsystems, and because the number of parameters is small, performing a sensitivity analyses is quite straightforward. This is in contrast to the form of output from large computational methods, which are difficult to manage in terms of parameter sensitivities. The penalty of the more primitive SEA approach is that the uncertainty of the resulting estimates is sometimes larger. SEA sensitivity analyses can be performed in the early design stage as well as in the operational stage, as long as an appropriate SEA model exists. The sensitivity are given in chapter 4.

Suppose the SEA parameters and the power input into the structure are assumed to be known. The energy level of a subsystem i emerging from this, is given by equation (2.37). The sensitivity parameter, relating a change of an SEA parameter to a change of an energy level is given by :

$$\frac{\partial E_i}{\partial \eta_{jk}} = -\frac{1}{\omega} \cdot \sum_{m=1}^{n} \left[\left[\eta^o\right]^{-1} \cdot \frac{\partial \left[\eta^o\right]}{\partial \eta_{jk}} \cdot \left[\eta^o\right]^{-1} \right]_{im} \cdot P_m \qquad (2.40)$$

further referred to as $\alpha_{i,jk}$.

2.4 SEA assumptions.

The attempts to better understand the theoretical basis of SEA and the limiting effect of its assumptions on the range of applications has kept a large number of researchers and engineers active for several decades. During the last two decades, engineers and researchers have been focused extensively on investigating the scope of validity of SEA. Section 2.4 gives a brief overview of the hypotheses made in SEA.

The SEA approach adopts one particular concept : vibrational energy varies from one subsystem to a contiguous one at a rate proportional to the difference in modal energy and in addition the vibrational energy is dissipated internally in each subsystem at a rate proportional to the subsystem vibrational energy.

As stated before, the assumptions adopted in SEA are mainly, forming the basis for the equation :

$$P_{i,diss} = \eta_{ii}\, \omega\, E_i \qquad (2.41)$$

and

$$P_{ij} = \omega\left(\eta_{ij} E_i - \eta_{ji} E_j\right) \qquad (2.42)$$

The assumption which comprises the *proportionality* of the dissipated energy with respect to the energy level of the subsystem is fairly familiar and is discussed in several books on damping.

The second assumption (equation (2.42)), which concerns the energy flow between subsystems, is based upon :

- **Weak coupling condition**. A practical criterion of weakly coupled subsystems is based upon the relative magnitude of the coupling loss factors and the internal loss

factor of the coupled subsystems. Coupling is weak if the ratio of the coupling loss factor to the internal loss factor of each oscillator is substantially less than unity (See SMITH [107]). Under weak coupling conditions, there is an energy flow - energy relationship between two sets of oscillators based upon on the difference of *uncoupled*[1] energies of the two sets of oscillators (see also NEWLAND [104] and [105]). This result can not in general be extended to *more* than two sets of coupled oscillators (See FAHY [5]). A simple example showing the latter statement is given. Consider three subsystems coupled in chain (figure 2.7).

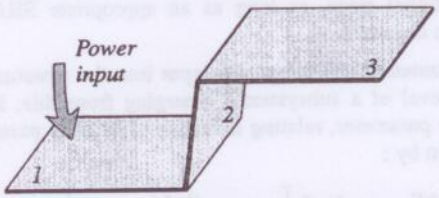

Figure 2.7 : Three subsystems coupled in chain.

If energy is fed into subsystem *1* only, then the *uncoupled* energies of subsystem *2* and *3* are zero and hence the energy flow between subsystem 2 and 3 equals zero (based on the premise that the energy flow is proportional to the difference of *uncoupled* energies). As a result of this consideration, the energy level of subsystem 3 is zero. Naturally, the actual energy is not zero. Nonetheless, in order to proceed with the analysis of multiple (more than two) sets of oscillators, many analysts have *assumed* that the uncoupled energies can be replaced by the actual coupled energies to be used for the basic SEA equation (see FAHY [5]). The replacement of the uncoupled energies by the actual coupled energies is justified for weakly coupled subsystems. Further research on this topic is definitely required in order to assess the consequences of violating the weak coupling condition.

From a wave point of view, the weak coupling condition is favored by high wave reflection coefficients, associated with large impedance discontinuities and large internal damping. The left side of figure *2.8* shows two subsystems (flexural plate energy) which are strongly coupled (2 plates more or less in line) and the right side of figure *2.8* illustrates weak coupling in the case of two more or less right angled coupled plates.

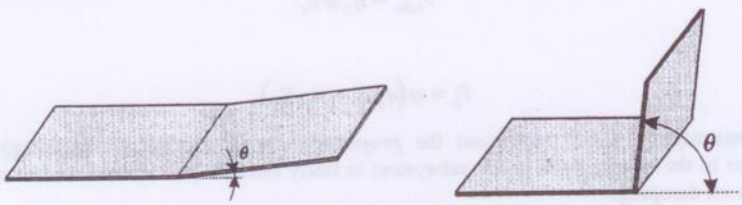

Figure 2.8 : Two coupled plates : strong and weak coupling.

[1] Uncoupled or blocked is defined by constraining the boundaries of each subsystem

- Input forces must be uncorrelated. In that case, energy levels and energy flow levels are additive, necessary to obtain the *linearity* of the SEA equations. If the excitation forces acting upon the subsystems would be correlated, then it holds that :

$$\langle v^2 \rangle_t = \langle (v_1 + v_2)^2 \rangle_t = \langle v_1^2 \rangle_t + \langle v_2^2 \rangle_t + 2 \cdot \langle v_1 \cdot v_2 \rangle_t \qquad (2.43)$$

  Where v_1 and v_2 represent the particle velocities at a certain point of the structure caused by the excitation of subsystem *1* and *2* respectively. The right term $< v_1 \cdot v_2 >_t$ does not vanish, resulting in non linear energy relations :

$$\langle v^2 \rangle_t \neq \langle v_1^2 \rangle_t + \langle v_2^2 \rangle_t \quad or \quad E \neq E_1 + E_2 \qquad (2.44)$$

- Natural frequencies should be equally distributed within the frequency interval of interest.
- The vibrational energy should be equally distributed over the modes of a subsystem in the frequency band of interest. This assumption embodies the similarity condition of subsystems, which will never be completely fulfilled in practical situations. Nevertheless, one should try to choose the subsystems in such a way to avoid the presence of modes exhibiting a much larger energetic response. For example, in the case of a beam, the bending and longitudinal modes do not fulfill the similarity condition.

2.5 Wave-mode duality.

The SEA equations which are derived in section 2.2 are based upon the so called *modal approach*, i.e. the exchange of energy between subsystems is described by the exchange of energy between their significant modes. Direct application of the average in equation (2.22) to determine the coupling loss factor is often not practicable, especially since the individual coupling coefficients g_{ij} can rarely be quantified.

An alternative way of describing high frequency vibrations and of deriving the SEA energy flow equations is based upon the application of wave theory, further referred to as the wave approach. Nor the wave approach nor the modal approach should be preferred to cover all types of complex vibro-acoustic problems in the high frequency range. In practice however, the wave approach is favored by the majority of the SEA community with respect to the identification of the model parameters, in particular the coupling loss factors. The evaluation of SEA coupling loss factors based upon the SEA wave approach is explained in detail in chapters *5* and *6*. Some points which illustrate the duality between modes and waves and which are interesting to be looked at from the SEA point of view are mentioned below.

A first item concerning the mode-wave duality deals with the averaged point impedance of structures. At high frequencies, the impedance computed by averaging over modes (or over frequency) of a *finite* plate is similar to the impedance obtained by considering waves radiated outward by exciting an *infinite* plate at one point. The fact that in the finite plate case the waves reflect from the boundaries and may return to the drive point is proved to be unimportant in affecting the drive point impedance because of their random phases. The following example clarifies this statement.

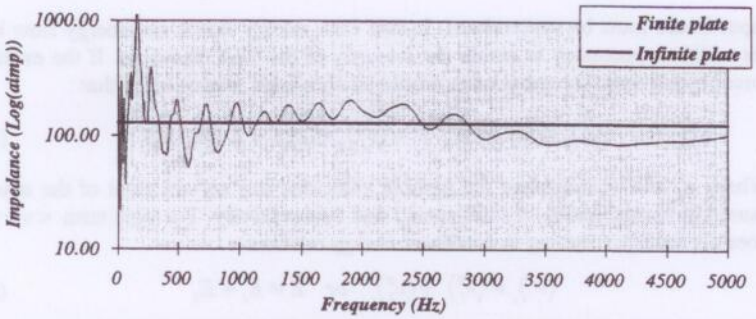

Figure 2.9 : Driving point impedance of an infinite and a finite plate.

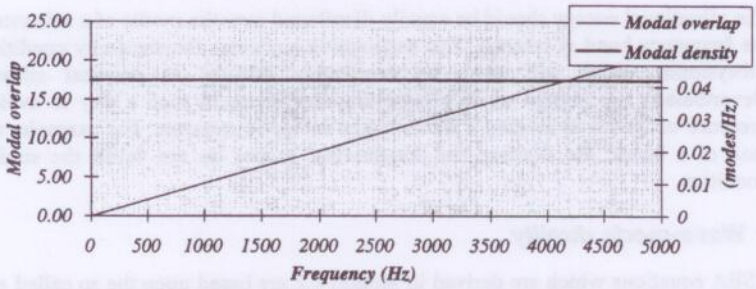

Figure 2.10 : Modal density and modal overlap for the finite plate.

An aluminium plate (thickness *2 mm* and dimension *500×500 mm*) is excited at one point. The driving point impedance Z is calculated by means of a finite element analysis. The excitation point is randomly located on the plate, the averaged impedance is calculated by means of the finite element model. The input impedance in the case of the corresponding infinite plate is calculated using the formula (after CREMER and HECKL [79]):

$$Z = \frac{8\rho t^2}{\sqrt{12\rho(1-\gamma^2)/E}} \qquad (2.45)$$

Where ρ represents the material density, t stands for the thickness of the plate, E denotes the modulus of elasticity, γ stands for the coefficient of Poisson.

Clearly, the impedances of the finite and of the infinite plate case match fairly well in the high frequency range (see figure *2.9*). This result is important for SEA because it allows us to calculate the power input into a plate based on the impedance of an infinitely extended plate and not on the actual impedance of the finite plate with its specific boundary conditions. As an aside, figure *2.10* pictures the corresponding model overlap (ratio between the half power bandwidth and the mode separation) and modal density (number of modes / Hz) of the plate.

A second important item with respect to mode-wave duality concerns damping. The modal approach incorporates damping by means the half-power bandwidth (or another modal related parameter) related to the loss factor by :

$$BW = \frac{\omega \eta}{2\pi} \tag{2.46}$$

If one considers waves propagating along a damped structure (e.g. a beam), then the amplitude of the wave will decrease, depending on the loss factor of the system.

$$U(x) = A \cdot e^{-\omega \eta x/c} \tag{2.47}$$

With U representing the transverse displacement.

The wave parameter which describes damping is called the wave attenuation factor, related to the loss factor by :

$$m = \frac{\omega \eta}{2c} \tag{2.48}$$

Both dissipation qualifiers, namely BW and m for respectively the modal and the wave description are not explicitly used in the SEA equations. Within the SEA framework, damping is described by the loss factor. In obtaining the loss factors of subsystems, one can apply a wave approach to extract the wave attenuation factor or one can apply the modal approach to evaluate the half power bandwidth. For high frequencies, for which modes are overlapping, it is quite difficult to identify the half power bandwidth from experimentally identified FRF's. The wave approach on the other hand can in these occasions be used to identify the attenuation factor and hence the internal loss factor.

Certain quantities that enter the modal description are equivalent to specific quantities associated with the wave description. For example : *modal energy* can be related to diffuse *wave intensity* for large modal overlap factors, giving rise to the relation between *SEA coupling loss factors* and *wave transmission coefficients* of junctions (see chapter 5).

As a final point of interest of this section, the difference between *direct* and *reverberant* wave field is addressed in relation to their modal counterparts namely the *coherent* and *incoherent* components of the modal summations.

Suppose a white noise force excites a large plate. It is fairly acceptable that the direct field is dominant near the excitation point and attenuates 3 dB per double distance geometrically and some attenuation caused by damping. At a certain distance away from the excitation point, the response will be determined by a large number of reflections coming from the boundaries. It can be assumed that the coherence with the *direct* field is lost due to the random phases of the reflections, particularly if the number of reflections is large and if the boundaries are geometrically irregular. The responses of the points located in the far field are dominated by the reflected waves composing the reverberant wave field. The vibration field can also be analyzed by means of a modal description of the response in which case it is possible to show that the *direct* and *reverberant* wave fields which arise in the wave approach have their counterparts in the *coherent* and *incoherent* components of the summations of the modal description especially when

many modes resonate within a band and have close natural frequencies in terms of modal bandwidth. In that case, the individual wave components which are forming the modal field may be considered to be incoherent and in uniform isotropic media, may be considered to travel with equal probability in all directions. The latter constitutes the ideal diffuse field.

The issues mentioned above are interesting in the sense that it is allowed to switch between a modal description and a wave description for the identification of the SEA model. The SEA coupling loss factors can be calculated by either wave transmission analysis or modal analysis. The practical implementation and corresponding examples concerning the calculation of SEA coupling loss factors by the wave approach is foreseen in chapter *5* and *6*.

2.6 Averaging.

The SEA equations express energy balance between subsystems. A major difference between the classical deterministic methods and SEA is that the former methods are concerned with field variables such as displacement, velocity, acceleration, pressure etc. at specific locations and frequencies, whereas SEA is concerned with averaged, global energy variables. Hence, SEA can never predict anything related to phase.

The seemingly strong limitation, namely the fact that not the response at particular points can be calculated but rather global values, is justified by the fact that SEA was essentially developed to overcome the problems described in chapter 1 and is therefore *aimed* at the prediction of averaged quantities.

Section 2.6 is concerned with the phrase *"on the average"* and its potentially different meanings, the relation between them and their interchangeability (ergodic aspect). Roughly, three main types of averaging can be considered :

- **Frequency averaging** : Over a frequency band. Most often third octave bands.
- **Spatial averaging** : The energy density of subsystems is integrated along the subsystems in order to obtain global vibrational energies.
- **Ensemble averaging** : Across different design realizations.

2.6.1 Time and Frequency averaging.

Time averaging. The aspect of time averaging is usually straightforward as stationary, broadband signals are *mainly* used to estimate the response. It will be assumed that when dealing with white noise excitation, the time signals are sufficiently long to remove the variations due to this cause. Hence, time averaging is implicitly present and causes no further restrictions on the applications of SEA. The application of transient signals has nevertheless been examined and will be addressed briefly in section 2.11.

Frequency averaging. The derivation of the SEA equations is directed towards the prediction of frequency averaged responses. Although there is no fundamental reason to apply a specific type of frequency band, most often third octave bands are taken. Eventually octave bands, fixed bandwidths bands or narrow bands can be taken as long as the basic SEA assumptions are not violated. Third octave bands are considered in this thesis.

While in principle SEA is amenable to time-harmonic excitation, the variance tends to be very large. This leads to statements such as *"SEA doesn't work for time harmonic excitation"*, such statements failing to recognize the inherent statistical nature of SEA predictions.

Finally, it should be stated that frequency averaging effects are mainly dependent on the mode count. Therefore, one can expect the number of modes in the frequency band to be the parameter determining the variance of the response. Hence, frequency averages should preferably be made over bandwidths containing a certain number of modes rather than over octaves or third octave bands. The structures which are considered in this dissertation all exhibit sufficient modes in third octave bands.

2.6.2 Spatial averaging.

SEA assumes global energies of subsystems, hence averaging needs to be performed along the extent of the subsystem. The spatial integral of the energy density of a subsystem yields the global vibrational energy. Although, it would be beneficial to know the energy density or the stresses at certain locations, it is generally not possible to derive the relation between the global energy and the energy density.

As an illustration of the consequences of the process of spatially averaging, consider a beam excited in its middle by a white noise force in the frequency band *500-1000* Hz. The properties of the analysis are stated in the table below.

Property	*Value*
Section	*2 × 2 mm*
Material	*Aluminium*
Length	*1000 mm*
Number of elements	*100 NASTRAN BAR*
Boundaries	*Clamped*

Table 2.1 : Properties of the analysis.

The displacement field is calculated using NASTRAN. Three graphs are retained :

- The energy density at one specific frequency.
- The frequency averaged energy density in the beam. Frequency averaging is performed in the band *500 - 1000* Hz.
- Spatial and frequency averaged energy in the beam. Spatial averaging is performed on the frequency averaged energy density and corresponds to the value which is obtained by SEA.

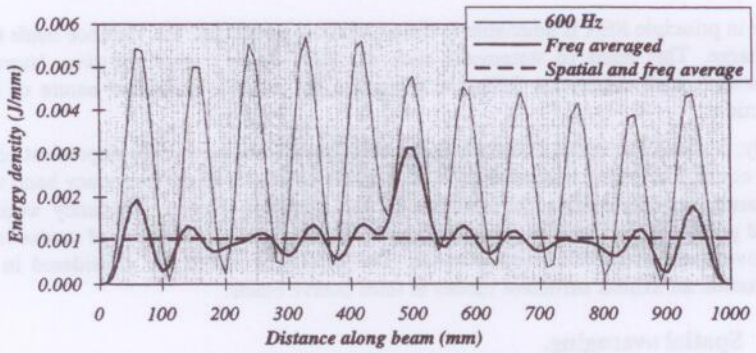

Figure 2.11 : Energy density of a beam.

Clearly, the actual energy density at one specific frequency - in particular 600 Hz - oscillates significantly around the averaged energy density obtained by SEA. If the frequency bandwidth becomes larger and if the frequency increases, then the response will be determined by the sum of the responses of an increasing number of higher order modes. The fluctuations of the averaged energy density of the beam tend to diminish. From figure *2.11*, it becomes clear that in the higher frequency range, it is acceptable to apply SEA and its inherent spatial averaging as the associated variance decreases. Therefore, it is possible to estimate the averaged energy of a subsystem by measuring responses at only a few locations. KUBOTA and DOWELL [24] showed that in the higher frequency range (theoretically infinite), a system with equally distributed mass, excited by white noise exhibits a *constant* energy density. In statistical terms : the variation of the response becomes smaller with the increase of the frequency and with the increase of the bandwidth.

2.6.3 Ensemble averaging.

From the engineering point of view, it would be desirable to be able to evaluate the mean response and the confidence limits for populations of nominal identical systems (ensembles). From the experimental viewpoint, it is practically not feasible to perform the required measurements for determining ensemble variability, including mean value and confidence levels. For example, car manufacturers are these days not even considering to perform expensive SEA experiments based on PIM on a set of nominally identical vehicles. Nevertheless, instead of performing statistical analyses on samples of *nominally identical* systems, one could think of evaluating the statistics with respect to *frequency* on *single artifacts* of the population and of relating the frequency statistics to ensemble quantities. This approach has the desirable consequence that a theory based on frequency and/or on spatial averaging concepts will in some sense also predict the ergodic mean.

The aspect of ensemble averages has received little attention to date. For experimental studies, the measurement results of the behavior of a single system are taken to be indicative of the behavior of both the ensemble average and that of a second subsystem. In such single-system applications, the frequency average is often taken to be equal, or nearly equal, to the ensemble average. However, frequency averages are not equal to

ensemble averages !! These differences are due to both the finite bandwidth and inherent differences between the idealized ensemble variations and those of a single system; e.g. the uniformly probable assumption for natural frequencies for the ensemble and the distribution of natural frequencies for a single system, for which there is a non-uniform joint probability density function. MACE [56] discusses the main difference between frequency averaging and ensemble averaging with emphasis on simple systems. In practice, many systems have enough inherent complexity that the variation in the response over frequency and location is *adequately* represented by the ensemble statistics.

2.7 Choice of subsystems.

For SEA, a global system is conceptually divided into subsystems. Some are directly excited, some indirectly through the coupling. For example, in the case of a car, energy partially enters the car through the mounts into the car body which excites the surrounding panels of the interior. The first step and generally the most critical one with respect to SEA modeling is the choice of the subsystems and the corresponding couplings. An appropriate breakdown of a global system into subsystems is essential to obtain a valuable SEA model.

A *subsystem* is defined as an element of an SEA model corresponding to a substantial energy storage location. As an aside, it can be noted that a *substructure* corresponds to a physical part of a structure. Two main rules should be carefully thought about when building an SEA model and when choosing the SEA subsystems : all modes in a set (=subsystem) should be *similar* and the energetics of a subsystem should be *significant*.

In order to build a reliable SEA model, subsystems should be chosen according to the principle of *similarity*. This means that the modes contained in a subsystem should be similar, in energetic terms (e.g. longitudinal and bending motion should be treated separately). Another criterion with respect to modal similarity is that the modes should have more or less the same order of damping. It is usually assumed as a rule of thumb that the individual modal loss factors of a set of modes should not vary by a factor of ten or more in a frequency band.

A second main item with respect to the choice of the subsystems deals with the *significance* of the subsystems. If a specific subsystem does not play a significant role in the energy balance, due to the fact that it is not substantially excited, due to the fact that the energy level is very low or due to the fact that the energy exchange between this subsystem and surrounding subsystems is marginal, then one should not take into account the contribution of this subsystem with respect to the energetics of the system. Practically, this rule is largely based on experience. A typical example on the *rule of significance* of a subsystem is given below.

In the case of a line coupling between two plates, it is quite obvious to take the connection line as the coupling element between both subsystems. In many occasions, the subsystems can be chosen to correspond to the set of flexural modes of both plates. In this case, two SEA subsystems arise, each corresponding to the set of flexural modes in a specific plate. It may however sometimes be necessary to include in-plane vibrations (in-plane longitudinal and in-plane shear waves), particularly if the in-plane energy is

substantial compared to the out of plane motion or if the external loads directly excite the in-plane modes. Hence, in this case, the two-plate problem is converted into a *six-subsystem* SEA model (figure *2.12*). A typical example for which in-plane vibrations are included deals with the energy transfer in ships. LYON and TRATCH [18] point out the importance of the in-plane vibrations (and hence the importance of the in-plane subsystems) with respect to the energy flow in ships. By including the in-plane vibrations into the SEA model, it follows that one specific substructure (a plate) gives rise to three SEA subsystems. In chapter *5* is shown how to incorporate the in-plane vibrations, i.e. how to calculate the coupling loss factors involved..

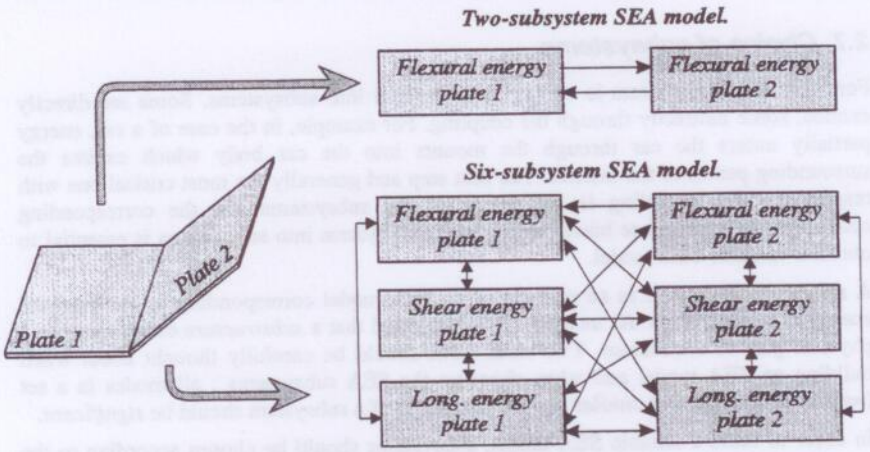

Figure 2.12 : Different SEA models of two coupled plates.

From the previous example it is found to be quite evident that the connection line between the plates serves as the coupling of the subsystems. The latter however is not always the case. The next example illustrates a typical difficulty that can arise when defining the subsystems of an SEA model. The structure, consisting of the roof and the C-pillar of a car, is roughly pictured in figure *2.13*.

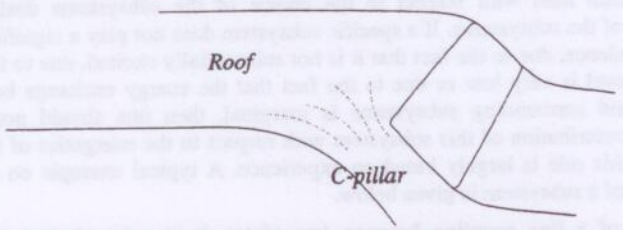

Figure 2.13 : Coupling between the roof and the C-pillar of a car.

The connection line between the roof and the C-pillar of the car is not distinct nor unique. Because of the round-off, it is not straightforward to define the connection line between the subsystems nor the subsystem boundaries. It is even conceivable to combine the roof and the C-pillar into one subsystem for very high frequencies because in that case the roof and C-pillar are strongly coupled : waves are not reflected at the

connection, hence weak coupling vanishes in a continuos way for increasing frequencies. Thus, the choice of subsystems and the number of subsystems can depend on the frequency band, making it sometimes very hard to specify how the division into subsystems should be accomplished. Again, experience is the key word for building a reliable SEA model.

As a final item on this topic, it is worthwhile mentioning that some *elements* of vibrating systems may not be considered as SEA subsystems. For example, a turbulent boundary layer does not represent an SEA subsystem as it can not be represented as a group of linear oscillators. An acoustic cavity may be treated as an SEA subsystem or it may not, depending on the reverberant characteristics of the cavity : the more reverberant, the more it tends to a separate SEA subsystem.

In summary, it can be stated that there are only two rules of thumb (similarity and significance) which are actually not well established to base the choice of subsystem on. Building a reliable SEA model will very often rely thoroughly upon the experience of the engineer.

For illustration purposes, two typical SEA models are presented (after CIMERMAN [108]). The first example deals with the sidewall of an aircraft which is typically a double wall construction (see figure 2.14).

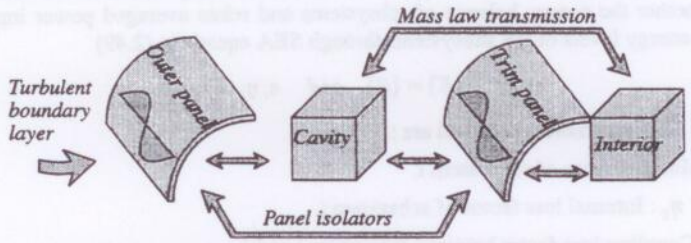

Figure 2.14 : SEA model of double wall configuration.

The in-flight condition gives rise to the appearance of an attached turbulent boundary layer which is modeled by means of a power input. Four SEA subsystems are retained : outer panel, trim panel, cavity between panels and the interior. Naturally, the model can be refined by including floor panel etc.

The second example deals with the roof-windscreen assembly of a car. Energy can flow within this part of a car through the roof, windscreen and the interconnecting beams as shown in the SEA network of figure 2.15. Energy enters the structure via the windscreen. Note that within this example, no in-plane motion is taken into account. The incorporation of in-plane motion can be considered as a further refinement of the model.

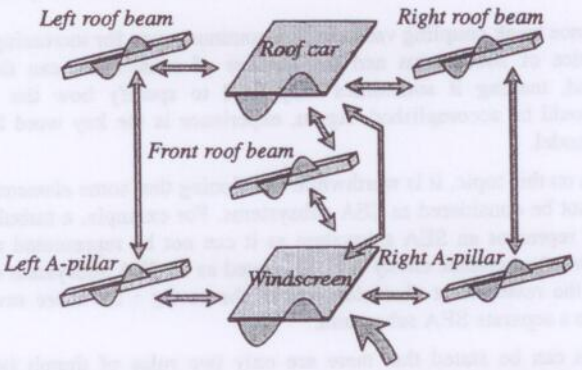

Figure 2.15 : SEA model of the roof-windscreen part of a car.

2.8 SEA parameters.

SEA is basically concerned with lumped energetics of systems. The fundamental key of SEA is related to the energy balance of subsystems including subsystem energy levels, dissipated energy, power input, energy flow. The basic SEA parameters describe in one way or another the energy balance of subsystems and relate averaged power inputs and averaged energy levels of the subsystems through SEA equations (2.49)

$$\omega \cdot [\eta^{\circ}] \cdot \{E\} = \{P\} \quad and \quad n_i \eta_{ij} = n_j \eta_{ji} \tag{2.49}$$

The basic SEA parameters involved are :

- n_i : Modal density of subsystem i.
- η_i or η_{ii} : Internal loss factor of subsystem i.
- η_{ij} : Coupling loss factor between subsystem i and j.

In the framework of this dissertation, all SEA parameters are considered in third octave bands.

In this section, some interesting features of the SEA parameters will be presented. The evaluation procedures, based on experimental or computational methods are given in chapter *3*, *5* and *6*.

2.8.1 Loss factor.

The loss factor η_i of subsystem i is defined as the ratio between the dissipated energy (dimension of power), the global subsystem energy and the center frequency :

$$\eta_i = \frac{P_{i,diss}}{\omega \cdot E_i} \tag{2.50}$$

The loss factor can be related to a number of other dissipation parameters that occur in vibration and noise analysis. These factors and the relation between them is given in table *2.2*.

Dissipation Descriptor	*Symbol*	*Relation to* η
Quality factor	Q	$1/\eta$
Critical damping ratio	ξ	0.5η
Reverberation time (for an acoustical subsystem only)	T_R	$13.82/\omega\eta$
Decay rate	DR	$4.35\omega\eta$
Logarithmic decrement	δ	$0.5\omega\eta$
Wave attenuation	m	$\omega\eta/2c_g$
Mechanical resistance	R	$\omega\eta M$
Damping bandwidth	BW	$\omega\eta/2\pi$
Imaginary part of E modulus	E_i	E,η
Acoustical absorption coefficient	α	$2\omega V\eta/cA$

Table 2.2 : Different types of damping descriptors.

Where c_g represents the group velocity, M represents the mass of a structure, V denotes the volume of a cavity and A depicts the surface of its surrounding walls.

The wide variety of parameters exists because of the importance of dissipation mechanism in many different fields and the natural ways of presenting damping in each field according to the equations involved or according to measurement procedures. Because in SEA, we are mainly concerned with a relation between the dissipated energy and the energy level of a subsystem, it is reasonable to employ the loss factor to describe damping phenomena.

Whilst analytical expressions of modal densities and some coupling loss factors are readily available in literature for a wide range of geometry's, analytical expressions are not generally available for the internal loss factor of structural components or acoustic cavities. The loss factor is recognized as the major source of uncertainty in the estimation of the dynamic response of systems based on predictive SEA.

The main damping mechanism to be considered are :

- *Structural damping* being a function of the material properties. This can take a hysteretic or a visco-elastic form.
- *Acoustic radiation damping* being associated with radiation losses from the surface of the structure into the surrounding medium.
- *Non-linear damping mechanism of built-up structures* at the subsystem interfaces. The latter includes gas pumping at joints and friction forces which are briefly covered in section *5.2*.
- Local internal damping due to friction.

As the damping mechanisms are independent, the global internal loss factor of a subsystem is composed of the partial contributions of the substantial loss factors :

$$\eta = \eta_s + \eta_{rad} + \eta_b \qquad (2.51)$$

Where η_s represents the losses *within* the subsystem (e.g. material losses), η_b is associated with the damping at the subsystem interfaces (partially attributed to each

subsystem of the junction) and η_{rad} is the acoustic radiation loss factor. A brief discussion of the relative importance of the different contributions follows.

The losses are mainly dominated by the material damping, added damping treatments and the acoustic radiation. The acoustic radiation can become dominant for lightweight structures with high radiation ratios and low internal damping. Typical values for material loss factors can be found in section *5.2.1* for some important materials. The evaluation of the acoustic radiation loss is presented in section *5.2.3*. The more rigidly the structure is built up, the less important the term η_b becomes. Most often, the energy dissipation at the joints in the higher frequency range is negligible. Hence, it is generally assumed that the internal loss factors can be simplified :

$$\eta = \eta_s + \eta_{rad} \qquad (2.52)$$

When the damping in the connections becomes significant, then the basic SEA equations do not hold because the basic SEA equations are derived under the assumption of conservative couplings. Special techniques briefly addressed in section 2.12 could eventually be applied in this case.

In acoustic spaces, the damping is usually dependent on the surface absorption characteristics. Because the level of added damping is so strongly dependent on the details of the application of a damping or absorption treatment, measurements are usually essential to verify analytical calculations of damping levels.

2.8.2 Coupling loss factor.

The coupling loss factor governs the energy exchange between subsystems and is defined by the basic SEA equation :

$$P_{ij} = P_{i \to j} - P_{j \to i} = \omega \cdot \eta_{ij} \cdot E_i - \omega \cdot \eta_{ji} \cdot E_j \quad and \quad n_i \cdot \eta_{ij} = n_j \cdot \eta_{ji} \qquad (2.53)$$

The coupling loss factor can be identified experimentally (chapter *3*) or can be calculated using analytical or numerical techniques as explained in chapter *5* and *6*. The number of coupling loss factors of an SEA model increases as the square of the number of subsystems.

Damping loss factors are fairly well known outside the SEA field. This is however not the case for the coupling loss factors, which are uniquely associated with SEA. Fortunately it is possible to relate the SEA coupling loss factor to other parameters such as transmission coefficients and radiation efficiencies (see chapter *5* & *6*).

The number of different types of couplings between subsystems is too extensive to be presented in an exhaustive list. Nevertheless, it is worthwhile mentioning some of the frequently encountered connections with respect to coupling loss factor evaluation :

- Beam-beam couplings.
- Beam-plate couplings.
- Plate-plate couplings.
- Plate-acoustic cavity couplings.

Plate-acoustic cavity couplings have been examined for several years by building acousticians and the relation between radiation efficiencies and the corresponding

coupling loss factors is therefore quite well studied and understood. Chapter 5 addresses the computational implementation in this respect. Structure-structure interactions constitute the most difficult group of couplings to evaluate as the transmission of energy from one substructure to the other is very much dependent upon the geometrical details of the connection, especially at high frequencies. An accurate computational evaluation of structure-structure coupling loss factors can be very complicated such that the evaluation may require expensive computational models which are sometimes not justified in a preliminary design stage.

It should be emphasized in here that the coupling loss factor is not only dependent on the characteristics of the junction, but also on some properties, in particular the extent, of the subsystems involved. As a final point of interest, it should be pointed out that the coupling loss factor is in principle dependent upon the damping of the subsystems, as illustrated by equation (2.13). In practice however, the dependency of the damping can be assumed negligible small, especially for high modal overlap factors.

2.8.3 Modal density.

The modal density is defined as the number of modes per unit frequency (as a function of frequency in narrow bands or averaged in third octave bands). It is the asymptotic limit of the ratio of the number of natural frequencies per unit frequency. It often varies monotonically with frequency, but in some cases modes "clump" together to give local maxima.

The modal density is important for response prediction as it tells how many resonant modes are available to store energy and how many modes are transferring energy from one subsystem to the other and vice versa.

The number of modes in Δf is related to the modal density by :

$$N_i = \Delta f \cdot n_i \qquad (2.54)$$

Among the SEA parameters, the modal density is generally the easiest to determine, using either analytical or experimental procedures. Accurate analytical values of modal densities can be found in literature (FAHY [5]) for a variety of idealized subsystems such as beams, plates, shell, acoustic cavities etc. For more complicated geometry's a numerical solution, for example based on a finite element model can be used to determine the eigenvalues of a subsystem in a given frequency band. In this case, it is necessary to average the mode count over a number of particular geometrical configurations or boundary conditions in order to obtain an accurate estimate of the average mode count.

Before terminating this section on modal densities, let us consider the problem of a flat plate excited by a white noise load in the frequency range $\Delta\omega$. It has been shown (LYON [1]), that the relation between modal density and the real part of the mobility[`] can be expressed by :

[`] The mobility is defined as the ratio between the normal plate velocity and the excitation force. The real part of the mobility is called the conductance.

$$n = 4m\langle G(\omega)\rangle \tag{2.55}$$

Where m represents the mass of the subsystem and $\langle G(\omega)\rangle$ is the averaged real part of the mechanical mobility.

In the case of acoustical subsystems of volume V, equation (2.55) becomes :

$$n(\omega) = \frac{2V}{\rho c^2 \pi} \cdot \langle R(\omega)\rangle \tag{2.56}$$

$\langle R(\omega)\rangle$ represents the averaged input resistance (real part of the impedance = ratio of pressure to volume velocity).

The measurement should be averaged over a variety of boundary conditions and over several excitation locations. Therefore, we can view the mobility as a measure of the number of modes that are available to absorb energy from a noise source. In general, there is a tied relation between modal density, conductance and applied white noise load. This relationship makes it possible to calculate the power input and the conductance from the knowledge of modal density and applied white noise excitation forces. (See also chapter 3).

2.8.4 Modal Overlap.

The modal overlap factor is defined as the product of the average modal half-power bandwidth and the modal density (or the ratio between the modal half-power bandwidth and the modal frequency spacing). It may be thought of as the average number of modal resonance frequencies lying within a typical modal half power bandwidth. The modal overlap factor of subsystem i is given by :

$$M_i = \omega \eta_i n_i \tag{2.57}$$

It can be noted that for one-dimensional subsystems (beams, ducts etc.) described by a wave approach, the spatial energy density of a traveling wave is given by :

$$e^{-\eta\omega x/c_g} \quad or\ by \quad e^{-Mx/2L} \tag{2.58}$$

L denotes the length of the subsystem, c_g represents the group speed of the waves involved.

From equation (2.58), it follows that values of the modal overlap factor of the order of unity and larger correspond to essentially non-resonant systems[`], to which SEA does not apply because it assumes a reasonably uniform distribution of stored energy over the spatial extent of each subsystem. This fact makes one-dimensional systems peculiar test cases for SEA. On the other hand, two- and three-dimensional systems can have modal overlap values much greater than unity and be highly resonant, making it suitable to analyze using SEA.

Practically, it is assumed that systems with modal overlap factors far below one are not amenable to an SEA approach (See also FAHY [106]).

[`] Because a wave will be damped if it reaches the boundaries, i.e. $x=L$.

2.9 SEA variables.

2.9.1 Main variables.

In section 2.6, we have shown how the vibrational energy level of a subsystem in a frequency averaged sense can serve as the main variable of an SEA model. The use of energy quantities has the considerable advantage that acoustic and structural vibrations are both described by the same variable, hence making a vibro-acoustic analysis straightforward. Secondly, because the energy is space averaged across a subsystem, only one variable is needed to describe the state of vibration of a subsystem, making SEA ideal for complex and large systems.

Expressions for energy density in terms of commonly measured quantities for different types of vibrations are given in the following table :

System	*Type of motion*	*Energy*
Uniform fluid	Acoustic wave	$\langle p^2/\rho c^2 \rangle_x \cdot V$
Uniform bar	Longitudinal	$\langle \rho A V_x^2 \rangle_x \cdot L$
Uniform bar	Flexural	$\langle \rho A V_y^2 \rangle_x \cdot L$
Uniform bar	Torsional	$\langle \rho I_x W_x^2 \rangle_x \cdot L$
Uniform plate	Flexural	$\langle \rho A V_z^2 \rangle_x \cdot S$

Table 2.3 : Vibrational energy of some subsystems.

Where $\langle\ \rangle_x$ denotes spatial averaging, V_x and V_y represent longitudinal respectively transversal particle velocities, W_x denotes angular velocity. I_x and A are quantities related to the beam section. L,S and V stand for the length, area respectively the volume of a subsystem.

The second main SEA variable constitutes the power input into a subsystem. It is generally accepted that SEA results tend to be more accurate if the input is due to a rain-on-the-roof, white noise excitation, although this has not been *proven* for whatever type of subsystem to be correct. In the case of rain-on-the-roof excitation, the waves which are contained in a subsystem and which are impinging upon the junction are uncorrelated. Single point force, or plane acoustic wave excitation produces correlated motion. In general, the actual excitation of a subsystem will mostly differ from the rain-on-the-roof excitation, resulting in higher uncertainties and a larger variability of the SEA responses. In some cases, only the excitation *force* is known, the power input is not. In these cases, one can use the relation between modal density, input force and power input to calculate the power input. This topic will be addressed in section *3.7*, which is dealing with experimental identification of modal densities.

2.9.2 Secondary variables.

Frequently, the objective of a high frequency vibro-acoustic analysis is not to determine global energy levels or power inputs as such. Engineers are mainly interested in strains, stresses, sound pressure levels etc. Consequently, the energy of vibration should be

converted into dynamic variables of engineering interest, further referred to as secondary variables, in order to perform a fatigue life time estimation or in order to assess the acoustical comfort of the interior of a car. The relation between vibration levels in the form of energy and vibration levels in terms of the secondary variables is addressed by many researchers. HUNT [62] and UNGAR [63] were amongst the first to develop relationships between energy, particle velocity and dynamic strains in plates and beams. FAHY [64], STEARN [65] and NORTON [66] subsequently developed a theoretical analysis, based upon the concept of bending waves in a reverberant field, for the prediction of the spatial variation of the dynamic stress, dynamic strain and acceleration in structures subjected to multi-mode excitation. Theoretical analyses backed up by experimental evidence have allowed for the development of very simple relationships between mean square vibrational velocities and dynamic stresses and strains for homogeneous structures such as beams, plates and shells. NORTON [80] shows that for a variety of mechanical motions the mean square dynamic stress is directly related to the mean square particle velocity by the following simple relationship :

$$\frac{\sigma^2}{V^2} = 1.61 K c^2 \rho^2 \qquad (2.59)$$

Where σ represents the space and frequency averaged dynamic stress, V^2 is the spatial and frequency averaged squared particle velocity, $c = \sqrt{E/\rho}$ denotes the longitudinal wave speed and K is a constant depending upon the type of motion and the systems geometry. The Poisson's ratio is assumed to be *0.3*. The constant K varies over a small range near unity, except for situations involving stress concentrations. For estimation purposes, it is acceptable to set $K=1$ in regions where there is no stress concentration. From experimental results on cylindrical shells Norton suggests that K varies between *3* and *20* in regions where there are some stress concentrations (See NORTON [66]).

2.10 Problems suited to SEA.

Many vibrational problems of practical engineering concern, involve complex structures subjected to broadband excitation which can not be satisfactory treated by deterministic methods (Chapter 1). Fortunately, in many cases it is sufficient to estimate the dynamic response in relatively broad frequency bands. Experience showed that the reliability of SEA predictions increases (decreasing variability) with the *diversity* and with the *physical extent* of the subsystem. The latter being due to the fact that the mode count increases with size. Another factor apparently favoring SEA is the presence of a large number of physical transmission paths within the system, e.g. large modular buildings. Serial (chain-like) systems seem to be less suited, particularly if they comprise regular, linear arrays of nominally identical subsystems. The latter is illustrated below.

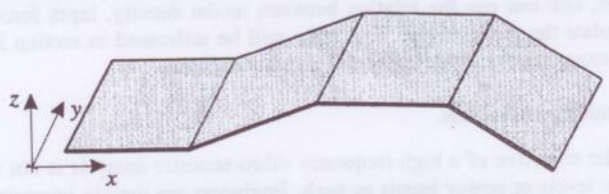

Figure 2.16 : Chain-like, regular connection of plates.

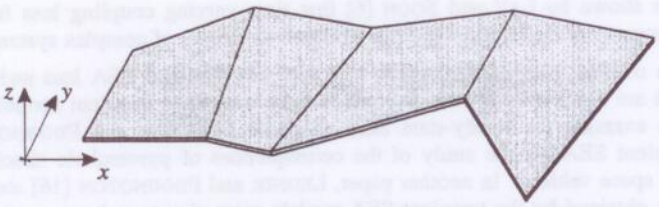

Figure 2.17 : Chain-like, irregular connection of plates.

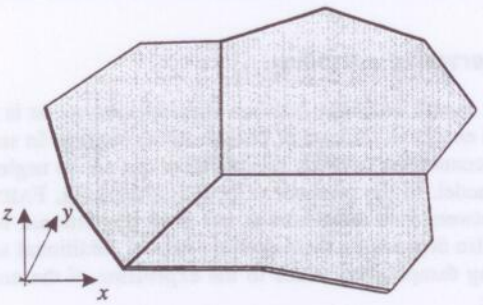

Figure 2.18 : Parallel like connection of plates.

SEA estimates, based on predictive SEA, are poor in the case of the first example. Irregular and parallel-like coupled subsystems give better results.

The reason for the poor predictions is the fact that predictive SEA is based on the evaluation of coupling loss factors between two *diffuse* wave fields. For the subsystems pictured in figure *2.14*, the junctions form a set of wavenumber filters and pass a restricted set of waves from one subsystem to the other. These waves do not form a diffuse field in each subsystem, but simply transmit very efficiently on their first arrival at the junction, no diffuse wave field is generated in the subsystems.

2.11 Non-stationary SEA.

SEA applications have been mainly limited to steady-state conditions notwithstanding the fact that SEA can definitely be applied to non-stationary problems. Transient SEA assumes time-varying energy responses and energy flows. MANNING and LEE [67] and POWELL and QUARTARANO [68] used modified SEA relations to predict time varying vibration envelopes. By adding an additional term to the energy balance equations - to account for time varying vibrational energy - a set of first order differential equations can be built. A transient SEA model is based on the assumption that the rate at which energy is transferred between two subsystems is proportional to the instantaneous energy difference. This leads to the following energy balance equations :

$$P_{i,in} = \dot{E}_i + \omega \cdot \sum_{j=1}^{n} \eta_{ij} \cdot E_i - \omega \cdot \sum_{j=1}^{n} \eta_{ji} \cdot E_j + \omega \cdot \eta_i \cdot E_i \qquad (2.60)$$

It has been shown by LAY and SOON [6] that time-varying coupling loss factors are needed to accurately model time-varying vibration envelopes of complex systems.

In the case of *time integrated* transient response, conventional SEA loss and coupling loss factors are applicable. It even follows that the integrated transient formulation can be used to examine the steady-state SEA parameters. LEDNIK and PINNINGTON [19] apply transient SEA for the study of the consequences of pyrotechnic shocks on the payload of space vehicles. In another paper, LEDNIK and PINNINGTON [16] showed that predictions obtained by the transient SEA models were shown to be very close to the actual energy values. Furthermore, the transient SEA results are found to be always conservative.

2.12 Non-conservative coupling.

SEA states that the energy exchange between coupled subsystems is proportional to the difference in modal energy in the case of conservative coupling. In some cases however, the damping at the connection between substructures can not be neglected and should be included into the model. In the presence of coupling damping, FAHY [35] showed that the energy flow between two resonators is not only proportional to the difference in modal energy but also depends on their absolute values. Additional terms caused by the presence of coupling damping are added to the expression of the energy flow between coupled oscillators :

$$P_{ij} = \alpha \cdot \left(\frac{E_i}{n_i} - \frac{E_j}{n_j} \right) + \beta \cdot \left(\frac{E_i}{n_i} + \frac{E_j}{n_j} \right) \qquad (2.61)$$

Furthermore, reciprocity ($n_i \eta_{ij} = n_j \eta_{ji}$) does not hold any longer. Nevertheless, when the theory concerning non-conservatively coupled oscillators is extended to multi-modal structures, FAHY [35] found that the influence of the coupling damping on the energy flow between the subsystems is negligible and that the coupling damping effectively increases the internal loss factors of the subsystems involved. Therefore, the classical energy balance equations for conservatively coupled subsystems can be used to represent non-conservatively coupled subsystems. Unfortunately, it is not possible to evaluate the exact contribution of the coupling damping that should be assigned to each substructure.

2.13 Non-resonant transmission.

It is generally found that subsystems which are not physically (or directly) coupled can exhibit a coupling loss factor not equal to zero. This means that the energy transferred from one subsystem to another subsystem may be transmitted without significantly contributing to the *reverberant* energy of the intervening subsystems. Consequently, this phenomenon is called *indirect* coupling characterized by a non-resonant transmission of energy from one subsystem to another non-adjacent subsystem.

A typical example deals with the transmission of sound accross flexible partitions (see figure *2.19*).

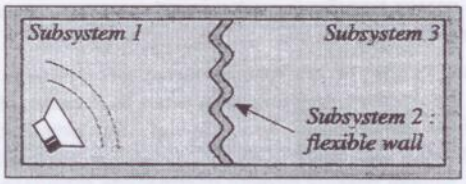

Figure 2.19 : Sound transmission through a flexible wall.

Although the acoustic cavities (subsystem *1* and subsystem *3*) are not directly coupled, a finite coupling loss factor between both cavities can arise because of the non-resonant transmission of energy from one cavity to the other.

At frequencies below the coincidence frequency[`] , it is shown that the transmission loss of a plate is predominantly not a function of the plate damping. In other words, the radiated noise below the coincidence frequency is not predominantly determined by the resonant modes of that frequency band. This situation is caused by the high radiation ratios associated with plate-acoustic cavities for off-resonant plate modes (modes with eigenfrequencies above the coincidence frequency) as compared to the low radiation ratios associated with a resonant mode below critical frequencies. Hence, one ends up with a situation where the plate response itself is dominated by the resonant behaviour (and hence inversily proportional to the damping) whereas the radiated power is independant of the plate damping. Formulations concerning this non-resonant transmission coefficient are given in chapter 5.

For frequencies above the coincidence frequency, one can ignore the non-resonant transmission because at these frequencies, the resonant path will always dominate since the resonant modes will in this situation have high radiation ratios associated with them.

Another example illustrating the non-resonant transmission of energy between two single plates which are not physically connected (plate *1* and plate *3*) is pictured in figure *2.20*.

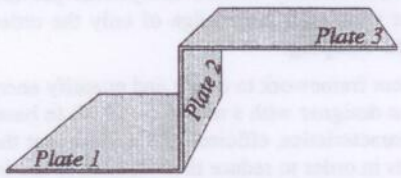

Figure 2.20 : Three coupled plates.

The transmission of energy from the bending wave field of plate *1* to the bending wave field of plate *2* is due to the energy transmission from bending in plate *1* to bending in plate *2* to bending in plate *3*. This transmission path is called the resonant transmission path of energy from plate *1* to plate *3*. On the other hand, if the in-plane wavelength of the intermediate plate is much larger than its dimension, then no modes can exist in this intermediate plate. Nonetheless, energy can be transferred from plate *1* to plate *3* through

[`] Frequency for which the bending wavelength of the plate equals the wavelength of the acoustic waves.

in-plane motion. This energy transfer is predominantly non-resonant and determined by the mass of the intermediate plate.

Comparison with the results of alternative forms of analysis and experimental observations indicate that indirect coupling must often be included if an SEA model is employed. It should be emphasized however that the presence of non-resonant transmission does not mean that energy can pass from one subsystem to another non-contiguous subsystem without passing through intermediate subsystems. It simply means that the SEA model does not represent all mechanism of energy transport if the non-resonant correction terms are not taken into account.

2.14 Advantages and disadvantages of SEA.

Chapter 2 concludes with an overview of some of the main benefits and drawbacks of SEA. Although the list does not cover all advantages nor all disadvantages, it is advisable to the engineer to consider carefully the following points.

2.14.1 Advantages of SEA.

- Since the dimensions of an SEA model have been decreased drastically due to the averaging with respect to location and frequency, changing the model and performing sensitivity analyses are very straightforward and cheap. Consequently SEA becomes a very useful tool in early design studies.
- Predictive SEA (based on computationally predicted SEA parameters) requires only a *few* gross parameters of a subsystem. For example, the modal density of a plate will be determined by *few* parameters such as thickness, overall dimensions and material characteristics.
- SEA is based upon conservation of energy and violations of this principle can be detected easily. Also, an assumption of equipartition of modal energy between directly excited and non-directly excited subsystems provides an estimate of the response of the latter with prior knowledge of only the order of magnitude of the coupling factor and the damping.
- SEA forms an excellent framework to detect and quantify energy transmission paths. Hence, it provides the designer with a model on which to base efficient strategies to alter the vibration characteristics, efficient in the sense that the engineer can change the transmission paths in order to reduce the vibration levels instead of applying less economic procedures such as applying damping materials in a very conservative way.

2.14.2 Disadvantages of SEA.

- At present, it is still difficult and certainly not well established how to estimate SEA confidence levels. For example, what about the response in the mid-frequency range, is the SEA model still valid, are the confidence levels not too wide ? The modal overlap factor seems to be very important in this respect. Wave transmission analysis for SEA purposes seems to be unreliable in cases where few resonant modes exist in a frequency band (low modal overlap).

- A judicious choice of the subsystems is critical. Yet, no real established methods are available to base the choice on. Therefore, building an accurate SEA model definitely requires experienced SEA engineers.
- Research is still going on dealing with narrow band excitation.
- No spatial information concerning the energy density of a subsystem can be obtained. EFFEA incorporates spatial information in an attempt to overcome this shortcoming.
- Tunneling phenomena problems are not straightened yet.
- SEA assumes a reverberant field in each subsystem in order to be able to apply the basic SEA equations relating energy flow and modal energy. However, in the cases for which waves are rather highly damped, as for example structural waves in aircraft fuselages, and sound waves in air cavities containing absorbent material, the reverberant characteristics of the vibrational field are not quite apparent and consequently the SEA equations become less applicable.
- The relation between the SEA parameters and the physical characteristics of the system are not always straightforward. For example, a coupling factor which is experimentally identified will be a function of the characteristics of the subsystems and of the properties of the junction, making a sensitivity analysis with respect to the physical properties of the structures not outspoken compared to the sensitivity analysis with respect to the SEA parameters. In other words, it is much more easy to evaluate the expression :

$$\frac{\partial E_i}{\partial \eta_{jk}} \tag{2.62}$$

then it is to evaluate

$$\frac{\partial E_i}{\partial x} \tag{2.63}$$

Where x represents a physical parameter of the problem. This is due to the fact that the relation between the coupling loss factor η_{jk} and x is not always exactly known. For example, for an experimentally identified model, one does actually not evaluate the relation between the SEA parameters and the physical parameters.

2.15 SEA computational aids.

Practically every SEA program which is commercially available these days exclusively incorporates predictive SEA. The implementation of experimental SEA is expected in the near future. Roughly, the existing programs contain three main parts :

- Calculation for the model parameters based on the characteristics (material properties, geometry) of the subsystems.
- Bookkeeping of the parameters. Basically, this module consists of a relevant database.

- The third module consists of the evaluation of responses, energy flows etc., basically involving simple mathematical manipulations on a matrix of coupling and internal factors.

A brief description of three principal, commercially available SEA programs is given below.

2.15.1 AUTOSEA

AUTOSEA is an Australian code (developed by Vibro Acoustic Sciences Ltd.) and is the most up-to-date code on the market. The program is a fully graphical, object oriented implementation of SEA and is available on Macintosh and recently also on Unix systems.

AUTOSEA requires definition of the main structural and acoustic wavefield subsystems. These are selected from AUTOSEA's *subsystem library*. Network connections for energy flow between subsystems is a simple graphical process, i.e. it consists of pointing and clicking the relevant icons. Coupling loss factors are calculated in the background from AUTOSEA's *library of coupling loss factor* formulations. The *power source library* provides models for power inputs. Measured operating data can be input here. AUTOSEA's *network window* is a 2D representation of all the subsystems. AUTOSEA assembles an SEA energy balance matrix which is solved to determine the system energy levels. A conversion from energy levels to an engineering unit can be performed for each subsystem. AUTOSEA can be used to investigate the effect of structural changes and the optimize the damping treatment. A special *damping database* is available.

One main advantage of AUTOSEA is the excellent graphical user interface which makes it possible to build an SEA model in a very efficient and very intuitive way. The library of input power sources, the library of different SEA subsystems and the library of damping values is considered as quite up to date. The interface to other programs and file types (NASTRAN, I-DEAS, IGES, spreadsheet files, ascii files) is likewise advantageous. Other advantages are its subjective visual/audio output capabilities. The latter makes it possible to carry out a structural modification of a structure (e.g. changing the thickness of a plate) and to immediately effectively hear the decrease or increase of the noise levels in the acoustic interior (e.g. a car).

The main disadvantage of AUTOSEA is the restricted, exhaustive list of types of couplings between subsystem. Its calculation method for transmission coefficients is mainly based on the formulas provided by CREMER et al. [79]). At present, new types of coupling are being introduced and the program is steadily increasing its capabilities.

2.15.2 VAPEPS : VibroAcoustic Payload Environment Prediction System.

VAPEPS is developed under the auspices of the NASA to provide the aerospace community with a consistent and reliable method for establishing vibro-acoustic design and test requirements for payload components. This is accomplished by :

- Supplying the aerospace community with a database containing what would be considered to be the best data sets and prediction schemes currently available.
- Through shared usage of VAPEPS by this community, updating or changing the prediction schemes as experience indicated that it would be appropriate.

Although VAPEPS is originally developed to serve as a modeling tool for the *aerospace industry*, including an aerospace oriented database (with respect to types of couplings, damping treatment, power sources and subsystems), it can be used outside the aerospace industry. The databases can eventually serve for this purpose. Nonetheless, the main part of VAPEPS users are aerospace oriented and naturally the program is most advantageous for them.

One of the main disadvantages of VAPEPS is the restricted list of couplings. As an example, the set of couplings between plates offered by VAPEPS only includes T, L and + junctions. No plates angles, plate off-set or additional plates can be included into the analysis. For many application in the shipbuilding, building and aerospace industry, the latter will not cause too many problems. If one is however up to analyzing structural couplings which are contained in cars, helicopters and many others more complex structures then VAPEPS not sufficient. In addition, VAPEPS does not support a graphical user interface. The commands read and store data on specially structured files.

2.15.3 SEAM

The SEAM software is developed by Cambridge Collaborative in the beginning of the *'80s*. Since that time, SEAM found its way into major shipyards, Navy research establishments, vehicle and aircraft manufacturers, mainly in the US. In addition to the solver, Cambridge Collaborative developed a pre- and postprocessor for the SEAM program. SEAMPRE and SEAMPST are text-based, while visiSEAM is a windows based graphical user interface. SEAM is available on UNIX workstations, PC compatibles and mainframe computers.

The calculation procedures for coupling loss factors are based on simple theories (based on CREMER et al. [79]).

2.15.4 SEAPACK.

SEAPACK is a general application SEA program which is developed at the division PMA of the department of mechanical engineering, K.U.Leuven. The program is based on Xmath (Matrixx), is menu driven and supports an OSF/MOTIF user interface. SEAPACK incorporates besides the three main modules which are integrated into AUTOSEA, SEAM and VAPEPS, an additional module : the feature to experimentally identify the SEA coupling loss factors, based on the theory presented in chapter *3*. A short description of the basic modules is given below.

- ***Preprocessing module.***

  This module mainly involves handling the SEAPACK databases (coupling loss factors, internal loss factors, modal densities, modal overlap factors, mode counts). The number of subsystems, the subsystem ID's, the number of frequency bands can be modified in here. Parameters can be viewed in matrix notation, plotted on the screen or printed.

- ***Analytical module.***

  This module incorporates predictive SEA. At present, the following types of couplings are included :

- ◊ Plate-plate couplings including an arbitrary number of plates, joined at an arbitrary angle and stiffened by a Timoshenko beam (chapter 5).
- ◊ Beam-beam couplings including an arbitrary number of beams, joined at an arbitrary angle. The general Timoshenko beams include thick bending terms, off-set shear axes, rigid connections with additional off-sets at the junction (chapter 5).
- ◊ Plate-acoustic cavity couplings. The evaluation of the coupling loss factors are based on radiation efficiencies (chapter 5).
- ◊ Acoustic volume - acoustic volume : based on non-resonant transmission through panels (chapter 5).
- ◊ Beam-beam couplings, including a detailed finite element model of the junction (chapter 6).

With respect to the calculation of modal densities, SEAPACK incorporates beams, plates and acoustic cavities. Internal loss factors for some materials are stored in a database. The database of internal loss factors can be extended to include loss factors which are obtained through experiments or which are obtained from external databases.

- ***Experimental module.***

The experimental identification procedures are based on the Power Injection Method (chapter 3). The data-acquisition is performed using the CADA-X software. A menu-driven user interface is written. The results of the measurements are input into SEAPACK in the form of ASCII files. From these data, SEAPACK calculates the relevant SEA parameters (coupling loss factors, internal loss factors, modal densities, modal overlap factors and the mode counts) and builds the corresponding SEA database of that problem. SEAPACK also includes the statistics of PIM as explained in chapter 4.

- ***Postprocessing module.***

This module allows to evaluate energy levels for given sources, to perform source localization, to predict energy flows and to perform sensitivity analyses. The latter is quite intuitively done by clicking on a specific coupling loss factor or internal loss factor, by changing its value (or dragging it). Automatically, a complete energy balance is performed and the latest energy levels are plotted on the screen.

Although SEAPACK does not offer the user interface which is requested these days by customers of software, and although SEAPACK does not offer all of the capabilities (e.g. in terms of databases of internal loss factors or in terms of databases of power sources) of the commercially available software, it incorporates some important features : the plate-plate coupling loss factors and beam-beam coupling loss factors are based on a general formulation which does not exclusively include simple connections. The experimental part of SEA the way it is implemented in SEAPACK can also be considered as advantageous compared to other programs.

2.16 Conclusion.

SEA has shown to be useful for diagnosing sound and vibration, based on response measurements of systems during *operational conditions*. The SEA model helps to interpret the results in energetic terms, i.e. energy flow etc. SEA gives quantitative predictions based on physical properties of the system. Hence, SEA can be used to evaluate the effectiveness of design modifications.

SEA can furthermore be applied in the *(preliminary) design stage* of a system to obtain estimates of the dynamic response even when not all details are specified. This is because preliminary SEA estimates can be made using the lumped characteristics of components : plate thickness, overall size, material characteristics, without requiring the details of components and attachments.

3. EXPERIMENTAL IDENTIFICATION OF SEA PARAMETERS BASED ON ENERGY INJECTION : METHODOLOGY AND IMPLEMENTATION.

3.1 Introduction.

For various complex structures, the coupling loss factors, internal loss factors and modal densities can not be determined sufficiently accurate purely by predictive computational procedures. The classical analytical procedures do not apply in the case of complex subsystems and connections. In other cases, it could be opportune to assess the main vibration transmission paths in structures during operating conditions in order to optimally carry out structural modifications. Often, these structures are severely complex and building a predictive SEA model based on a computational determination of the SEA parameters is not feasible. A relatively quick assessment of the SEA parameters is in these cases favored. In addition, for some structures the SEA parameters are to be identified for the purpose of verification of computational prediction techniques. Hence, in these cases it is beneficial to identify by means of response measurements the SEA parameters of a structure *in situ*.

LYON [1] has suggested that this may be done by measuring energy levels of the various subsystems of the structure for various arbitrary distributions of power input. If the number of measurement points is chosen sufficiently large, then the resulting linear system of energy balance equations may be inverted to yield the SEA parameters matrix. In *1975*, LYON states that the experimental identification of SEA parameters has received marginal attention and has granted a limited success due to the fact that small values of coupling loss factors sometimes turn out to be negative; the latter being physically unallowable. From the late *70's*, papers have been published dealing with the experimental identification of SEA parameters. A list of some contributions to this field of research is included in the reference.

In the beginning of the *80's*, BIES and HAMID [14] conducted in situ experiments to identify internal loss factors and coupling factors of two coupled plates. Good agreement

was obtained between the predicted and measured coupling loss factors and between the in situ measured loss factors and the loss factors obtained for each plate separately. A steady state energy injection procedure was applied. CLARKSON and POPE [31] developed indirect experimental methods to determine the modal density and internal loss factors for flat plates and cylinders. NORTON and GREENHALPH [7] identified the internal loss factors of a lightly damped pipeline system by both steady-state energy flow and burst random noise techniques. Still, at that time, experimental SEA has only been applied in rare occasions and for fairly simple structures.

From the end of the *80's* on, attempts were made to apply the experimental identification techniques on complex structures such as a car body. For example, the latter has been done in the framework of the EC sponsored BRITE project "Optimization of noise control measures in complex lightweight sheetmetal structures by using energy flow analysis" (see also WALSH et al. [9]). It turned out that the techniques which were applied in the framework of this project, namely non linear programming, with respect to the solution sequence and the measurement procedure were not satisfactory. Coupling loss factors significantly different from zero were obtained between not physically coupled subsystems. In addition, the experiments were very labor intensive. WU et al. [55] Employed experimental SEA for the determination of the SEA parameters of a diesel engine. Provided special precautions concerning the spatial averaging of the energies are taken, experimental verification showed that the four-subsystem SEA model can reasonably predict the vibrational behavior of the engine structure. Nonetheless, additional work has to be done more specifically with respect to the ill-conditioning of the measured energy matrix and with respect to the equivalent mass problem which is addressed later on in this chapter. Besides, not much has been done on the essential statistical and sensitivity aspects of experimental SEA.

To date, rare are the articles dealing with the application of the experimental SEA identification techniques on complex and large structures. A clarification and optimization of the experimental identification technique is unquestionably needed in order to be able to evaluate the SEA parameters more accurately and efficiently on large and complex structures.

3.2 The Power Injection Method (PIM).

The Power Injection Method, further referred to as PIM, is based on the measurement of the power input into the subsystems and of the vibrational kinetic energy as an estimate of the total vibrational, reverberent energy of the subsystem. No serious bias errors are introduced, as long as the response measurements in terms of squared velocities are weighted correctly by the partial contributions of the mass corresponding to each subsystem. It can in principle be shown (LYON [1]) that the measurement result is fundamentally unbiased at the natural frequencies of individual, well separated modes and for frequency band averaged results in the presence of many modes.

Roughly, two approaches are stated in literature and are outlined in here : steady state PIM based on power spectral densities and the application of decay techniques. PIM based on the measurement of the appropriate power spectral densities of the responses constitutes the most widely used technique to experimentally identify SEA parameters and this section will mainly focus on this technique. The decay technique can be

considered as complementary to steady state PIM via the utilization of energy correction coefficients and related updating techniques.

The application of FRF based techniques offers an interesting and appealing alternative for the power spectral density approach and is explained in section *3.5*.

PIM aims at identifying the SEA parameters by means of response measurements namely energy and power input measurements. From the mathematical viewpoint, this technique corresponds to the identification of the transformation matrix acting on the E vector to produce the P vector, i.e. :

$$\{P\} = \omega \cdot [\eta^o] \cdot \{E\} \tag{3.1}$$

The simplest and most obvious way of evaluating the transformation matrix is by evaluating the projection of the set of orthogonal unit vectors vectors of the E or of the P domain. For practical reasons, the images of the set of orthogonal unit vectors of the P domain will be determined. In PIM terms, the relevant equation is given by :

$$\{E\} = \frac{1}{\omega} \cdot [E^n] \cdot \{P\} \tag{3.2}$$

The transformation matrix $[E^n]/\omega$ of this algebraic equation can be determined by evaluating the images of the basis x-vector :

$$\{P_1\} = \{1 \quad 0 \quad \dots \quad 0\}^T \; ; \; \{P_2\} = \{0 \quad 1 \quad 0 \quad \cdots \quad 0\}^T \; ; \; etc. \tag{3.3}$$

The corresponding E-vector constitutes one single column of the transformation matrix $[E^n]/\omega$. Hence, by applying the orthonormal basis vectors of the P domain, and evaluating the response in the E domain, it is possible to build up the normalized energy matrix. This procedure is explained in detail in the following section.

3.2.1 Two-subsystem model.

To illustrate the principles of PIM, let's consider a two-subsystem SEA model.

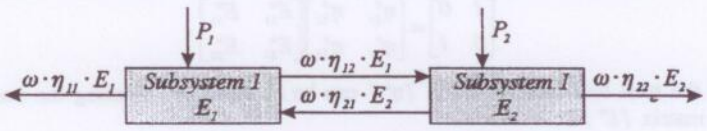

Figure 3.1 : Two-subsystem SEA model.

The basic SEA equations (disregarding for the moment the reciprocity relation) become :

$$\begin{Bmatrix} P_1 \\ P_2 \end{Bmatrix} = \omega \begin{bmatrix} \eta^o_{11} & \eta^o_{12} \\ \eta^o_{21} & \eta^o_{22} \end{bmatrix} \begin{Bmatrix} E_1 \\ E_2 \end{Bmatrix} \tag{3.4}$$

First, energy is injected (white noise excitation is used) into subsystem *1*. Hence, equation (3.4) becomes :

$$\begin{Bmatrix} P_1 \\ 0 \end{Bmatrix} = \omega \begin{bmatrix} \eta^{\circ}_{11} & \eta^{\circ}_{12} \\ \eta^{\circ}_{21} & \eta^{\circ}_{22} \end{bmatrix} \begin{Bmatrix} E_{11} \\ E_{21} \end{Bmatrix} \tag{3.5}$$

With :

- E_{ij} : Band and space averaged energy of vibration of subsystem i when only subsystem j is excited.
- P_j : Band averaged power input into subsystem j.

The way to calculate the energy levels and power input levels is addressed in section 3.4 in the case of structural and acoustic subsystems. In this section, the energy levels and power input levels are assumed to be known from measurements. Equation (3.5) can be normalized with respect to the power input by dividing the energies on the right hand side of equation (3.5) by the power input. A non-dimensional energy level can be obtained by multiplying by the angular frequency. Equation (3.5) becomes :

$$\begin{Bmatrix} 1 \\ 0 \end{Bmatrix} = \begin{bmatrix} \eta^{\circ}_{11} & \eta^{\circ}_{12} \\ \eta^{\circ}_{21} & \eta^{\circ}_{22} \end{bmatrix} \begin{Bmatrix} E^{n}_{11} \\ E^{n}_{21} \end{Bmatrix} \tag{3.6}$$

Where E^{n}_{ij} represents the normalized, frequency and space averaged energy of vibration of subsystem i when only j is excited, defined by :

$$E^{n}_{ij} = \frac{\omega \cdot E_{ij}}{P_j} \tag{3.7}$$

Similarly, if energy is injected into subsystem 2 and if the energy of vibration is normalized with respect to the power input, the basic SEA equations become :

$$\begin{Bmatrix} 0 \\ P_2 \end{Bmatrix} = \begin{bmatrix} \eta^{\circ}_{11} & \eta^{\circ}_{12} \\ \eta^{\circ}_{21} & \eta^{\circ}_{22} \end{bmatrix} \begin{Bmatrix} E_{12} \\ E_{22} \end{Bmatrix} \quad \Rightarrow \quad \begin{Bmatrix} 0 \\ 1 \end{Bmatrix} = \begin{bmatrix} \eta^{\circ}_{11} & \eta^{\circ}_{12} \\ \eta^{\circ}_{21} & \eta^{\circ}_{22} \end{bmatrix} \begin{Bmatrix} E^{n}_{12} \\ E^{n}_{22} \end{Bmatrix} \tag{3.8}$$

Combining equation (3.6) and (3.8) yields :

$$\begin{bmatrix} 1 & 0 \\ 0 & 1 \end{bmatrix} = \begin{bmatrix} \eta^{\circ}_{11} & \eta^{\circ}_{12} \\ \eta^{\circ}_{21} & \eta^{\circ}_{22} \end{bmatrix} \begin{bmatrix} E^{n}_{11} & E^{n}_{12} \\ E^{n}_{21} & E^{n}_{22} \end{bmatrix} \tag{3.9}$$

Hence, the total loss factors matrix $[\eta^{\circ}]$ can be obtained by inverting the normalized energy matrix $[E^{n}]$:

$$[\eta^{\circ}] = \begin{bmatrix} \eta^{\circ}_{11} & \eta^{\circ}_{12} \\ \eta^{\circ}_{21} & \eta^{\circ}_{22} \end{bmatrix} = \begin{bmatrix} E^{n}_{11} & E^{n}_{12} \\ E^{n}_{21} & E^{n}_{22} \end{bmatrix}^{-1} \tag{3.10}$$

The SEA coupling loss factors and internal loss factors are recovered by rearranging the terms of the total loss factor matrix $[\eta^{\circ}]$:

$$\begin{cases} \eta_{11} = \eta^{\circ}_{11} + \eta^{\circ}_{21} & \eta_{12} = -\eta^{\circ}_{21} \\ \eta_{21} = -\eta^{\circ}_{12} & \eta_{22} = \eta^{\circ}_{22} + \eta^{\circ}_{12} \end{cases} \tag{3.11}$$

It can be noted that the coupling loss factors and the internal loss factors are obtained without a knowledge of the modal densities. In other words, the reciprocity equation has not been used so far.

3.2.2 Multi-subsystem model.

In a similar way, the derivation of the PIM equations for a two-subsystem model can be extended to a multi-subsystem model.

- •First energy is injected into subsystem *1*. The power input and the energy level of each subsystem are measured, resulting in the following set of SEA equations (after normalization with respect to the injected energy and with respect to the angular frequency) :

$$\begin{Bmatrix} 1 \\ 0 \\ \vdots \\ 0 \end{Bmatrix} = [\eta^\circ] \cdot \begin{Bmatrix} E^n_{11} \\ E^n_{21} \\ \vdots \\ E^n_{n1} \end{Bmatrix} \tag{3.12}$$

- Next, energy is injected into subsystem *2*, the energy levels are measured and normalized :

$$\begin{Bmatrix} 0 \\ 1 \\ \vdots \\ 0 \end{Bmatrix} = [\eta^\circ] \cdot \begin{Bmatrix} E^n_{12} \\ E^n_{22} \\ \vdots \\ E^n_{n2} \end{Bmatrix} \tag{3.13}$$

- A similar procedure is followed for subsystem *3* to *n*.

Combining the *n* sets of *n* equations yields :

$$[I] = [\eta^\circ] \cdot [E^n] \tag{3.14}$$

The total loss factor matrix $[\eta^\circ]$ is given by the inverse of the measured energy matrix

To obtain the SEA parameter matrix $[\eta]$, the terms of $[\eta^\circ]$ have to be rearranged. The relation between η_{ij} and η°_{ik} is given by :

$$[\eta^\circ] = \begin{bmatrix} \sum_{k=1}^{n} \eta_{1k} & -\eta_{21} & \cdots & -\eta_{n1} \\ -\eta_{12} & \sum_{k=1}^{n} \eta_{2k} & \cdots & \vdots \\ \vdots & \vdots & \ddots & \vdots \\ -\eta_{1n} & \cdots & \cdots & \sum_{k=1}^{n} \eta_{nk} \end{bmatrix} \tag{3.15}$$

Therefore, the coupling loss factors and internal loss factors are given by the following formulas :

$$\begin{cases} \eta_{ij} = -\eta^{\circ}_{ji} & i \neq j \\ \eta_{ii} = \sum_{k=1}^{n} \eta^{\circ}_{ki} \end{cases} \tag{3.16}$$

3.2.3 Comparison to classical PIM.

Although the technique which is previously explained is very straightforward in its use, it does not represent the way that PIM has been applied in the past. For the classical PIM approach, equation (3.5) and (3.8) are not combined as outlined in section 3.2.2, but are rearranged in the case of a two-subsystem model in the following way (see also [2,3,4,55]) :

$$\omega \cdot \begin{bmatrix} E_{11} & E_{11} & -E_{21} & 0 \\ 0 & E_{11} & E_{21} & E_{21} \\ E_{12} & E_{12} & E_{22} & 0 \\ 0 & -E_{12} & E_{22} & E_{22} \end{bmatrix} \cdot \begin{Bmatrix} \eta_{11} \\ \eta_{12} \\ \eta_{21} \\ \eta_{22} \end{Bmatrix} = \begin{Bmatrix} P_1 \\ 0 \\ 0 \\ P_2 \end{Bmatrix} \tag{3.17}$$

For a two-subsystem model, the energy matrix on the left hand side of equation (3.17) is a fairly uncomplicated 4×4 matrix. However, a n-subsystem model yields a non-symmetrical, rather ill-conditioned (due to the large off-diagonal terms) $n^2 \times n^2$ normalized energy matrix. Appendix A presents the general form of the $n^2 \times n^2$ normalized energy matrix.

This approach can be justified by the fact that linear equations are usually written in the form $[A]\{x\}=\{b\}$, where $\{x\}$ represents the vector to be determined, i.e. the vector of SEA parameters.

For a small number of subsystems, equation (3.17) can be used with confidence. However, as the number of subsystems increases, the CPU time associated with calculating the SEA parameters increases since the dimension of the energy matrix equals $n^2 \times n^2$. The $n^2 \times n^2$ energy matrix also tends to be rather ill-conditioned due to large off-diagonal terms. In order to overcome numerical pitfalls it has been suggested to reorganize the basic equations. It has been shown by LALOR [3] that the internal loss factors can be eliminated from equation (3.17). Subsequently, n sets of generally well conditioned matrix equations of dimension n-1 are obtained. In the case of a n-subsystem model, it holds that :

$$\begin{Bmatrix} \eta_{1i} \\ \vdots \\ \eta_{ri} \\ \vdots \\ \eta_{ni} \end{Bmatrix} = \frac{P_i}{\omega \cdot E_{ii}} \cdot \begin{bmatrix} \frac{E_{11}}{E_{i1}} - \frac{E_{1i}}{E_{ii}} & \cdots & \cdots & \cdots & \frac{E_{n1}}{E_{i1}} - \frac{E_{ni}}{E_{ii}} \\ \vdots & \ddots & & \ddots & \vdots \\ & & \frac{E_{rr}}{E_{ir}} - \frac{E_{ri}}{E_{ii}} & & \\ \vdots & \ddots & & \ddots & \vdots \\ \frac{E_{1n}}{E_{in}} - \frac{E_{1i}}{E_{ii}} & \cdots & \cdots & \cdots & \frac{E_{nn}}{E_{in}} - \frac{E_{ni}}{E_{ii}} \end{bmatrix}^{-1} \cdot \begin{Bmatrix} 1 \\ 1 \\ \vdots \\ 1 \\ 1 \end{Bmatrix} \tag{3.18}$$

The internal loss factors are then obtained by a back-substitution of the coupling loss factors into the basic SEA equation.

$$\eta_{ii} = \frac{P_i}{\omega \cdot E_{ii}} - \sum_{j \neq i}^{n} \eta_{ij} + \sum_{j \neq i}^{n} \frac{E_{ji}}{E_{ii}} \cdot \eta_{ji} \qquad (3.19)$$

The matrix containing the energies in equation (3.18) is generally much better conditioned compared to the energy matrix of equation (3.17). This is because in the former case, the large terms occur on the leading diagonal. Equation (3.18) and (3.19) will yield accurate values of the internal loss and coupling factors provided of course that the measured power inputs and subsystem energies are measured sufficiently accurate.

It should be emphasized that although it is very straightforward to apply equation (3.9), as suggested in this dissertation, equation (3.17) is still often used to date.

To illustrate the ill-conditioning of the total energy matrix of equation (3.17) compared to the much more uncomplicated energy matrix of section 3.2.2, a mathematical simulation has been performed. A *nxn* matrix containing random numbers between *0.5* and *1.5* has been built. The leading diagonal has been multiplied by *10* to correspond to an admissible SEA energy matrix $[E^n]$. This *simulated* normalised energy matrix is thereupon transformed into the total energy matrix of equation (3.17). Finally, the ratio of the condition numbers between the classical energy matrix of equation (3.17) and the normalized energy matrix $[E^n]$ which is adopted in this dissertation is calculated as a function of the number of subsystems. The results are presented in figure *3.2*.

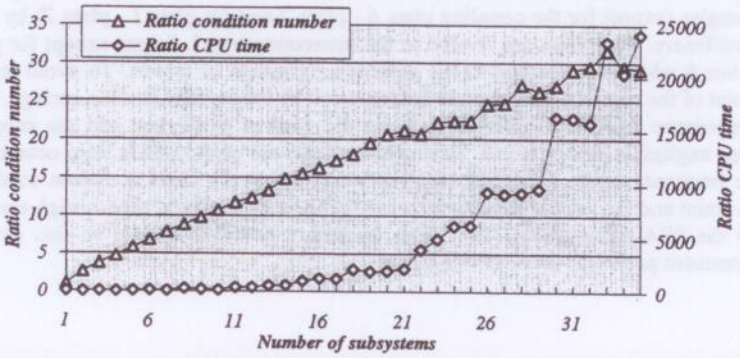

Figure 3.2 : Comparison between classical $n^2 \times n^2$ energy matrix and $n \times n$ normalised energy matrix.

Clearly the ratio of the condition numbers between the $n^2 \times n^2$ energy matrix and the normalised energy matrix adopted in this thesis is much larger than *1* and increases more or less linearly with the number of subsystems. In addition, the time to invert the energy matrix of equation (3.17) is compared to the time to invert the normalized energy matrix.

This simple simulation, using acceptable simulated SEA energy data indicates that ill-conditioning problems can arise when applying equation (3.17). It is therefore recommended to use the method proposed in section 3.2.2. Naturally, the transformation

---

n stands for the number of subsystems.

of the total energy matrix into *n* matrices of dimension *(n-1)x(n-1)* and the elimination of the internal loss factors is also a valid alternative and mathematically completely analogous. Nonetheless, no justification can be put forward to apply equation (3.18) instead of the inverse of the normalized energy matrix to calculate the SEA parameters.

3.3 Description of the test structure.

Before proceeding, it is found worthwhile to describe in here the test structure which has been fabricated to illustrate the techniques developed in the framework of the PIM research. The results presented hereafter are all obtained via experiments performed on the box structure described below.

For the investigation, *7* Aluminium flat plates of thickness *2 mm* are used, enclosing a cavity in between (figure 3.3). Hence, the SEA model comprises *8* subsystems. In order to increase the modal overlap and hence to guarantee to a larger extent the applicability of SEA, the vibrations of the plates (forming the mechanical subsystems of the SEA model) are slightly damped and the interior cavity (the acoustic subsystem of the SEA model) is treated by means of some sound absorbing material. The choice of the damping is based upon some experimental investigations which are performed in advance. The damping gives loss factors significantly higher than those of the undamped plates but not too high for the present purpose, i.e. the damping is chosen so that the internal losses for each plate dominate all other losses (losses to other subsystems). The plates are joined at right angles (expect for the coupling plate *6* - plate *7* and for plate *1* - plate *7*) by means of L-stiffeners. The plates are riveted to the interconnecting L-beams except for plate *5* and plate 6 which are attached to the stiffeners by means of screws. To avoid losses at the point of the support, the structure is suspended by means of *4* flexible springs. Due to the impedance mismatch achieved between the corners of the box and the supporting springs, negligible energy is lost. The measurements are performed in third octave bands in the frequency range *500-4500* Hz. The lower frequency band is chosen so that the mode count and the modal overlap factor in the lowest frequency band is high enough to fulfill the SEA assumptions. The upper frequency bound is chosen so that no major measurement problems occur in this range.

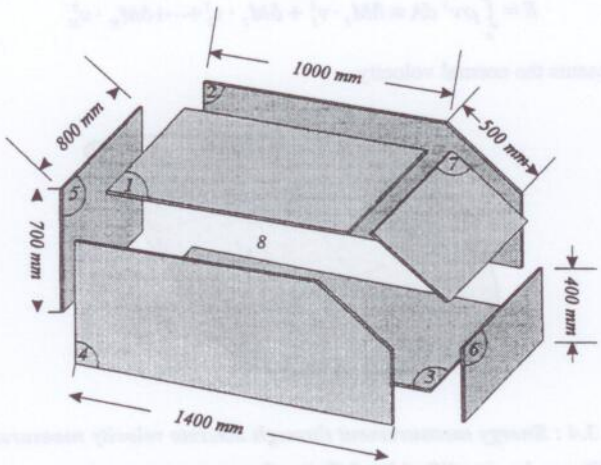

Figure 3.3 : Box structure.

The measurements are performed using a general purpose SEA software package called SEAPACK developed at the K.U.Leuven in the framework of this dissertation. SEAPACK allows to perform a complete acquisition and inverts the appropriate energy matrix. The acquisition part is based on the LMS CADA-X system, the evaluation of the SEA parameters and the prediction of energy levels and energy flows is written in a matrix handling program called Xmath.

3.4 Energy and power input measurements.

3.4.1 Energy measurements.

In order to be able to invert the normalised energy matrix, the energy levels and power input levels into the different subsystems have to be measured. This section is concerned with the measurement of the space and frequency averaged reverberent energy of vibration of acoustic and structural subsystems.

3.4.1.1 Structural energy measurements.

Since it is much easier to measure the kinetic energy of subsystems using accelerometers rather than to measure its potential energy using strain gauges, it is convenient to define vibrational energy in terms of kinetic energy exclusively.

Because of the relation between directly measurable response variables (such as velocity and acceleration) and energy, one can obtain the energy value by measuring the appropriate responses. For example, for structural subsystems the total reverberent averaged energy of vibration which is the sum of the kinetic and potential energy, is given by the sum of the squared particle velocities multiplied by the mass which can be attributed to that part of the subsystem where a response measurement has been made.

$$E = \int_A \rho v^2 \, dA \cong \delta M_1 \cdot v_1^2 + \delta M_2 \cdot v_2^2 + \cdots + \delta M_N \cdot v_N^2 \qquad (3.20)$$

Where v represents the normal velocity.

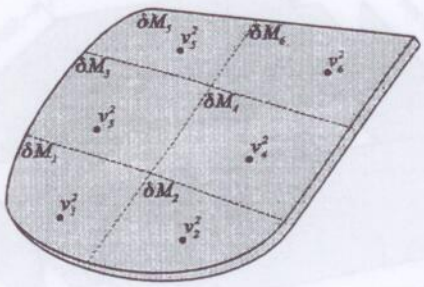

Figure 3.4 : Energy measurement through discrete velocity measurements.

Equation (3.20) can be simplified by defining the space averaged squared velocity of a subsystem :

$$< v^2 > \cong \frac{1}{N} \cdot \sum_{i=1}^{N} v_i^2 \qquad (3.21)$$

Averaging with respect to time yields :

$$< \overline{v}^2 > \cong \frac{1}{N} \cdot \frac{1}{T} \cdot \sum_{i=1}^{N} \int_0^T v_i^2(t) dt \qquad (3.22)$$

The subsystems time and space averaged reverberent energy of vibration can therefore be approximated by :

$$< \overline{E} > \cong \frac{M}{N} \cdot \frac{1}{T} \cdot \sum_{i=1}^{N} \int_0^T v_i^2(t) dt \qquad (3.23)$$

Where M equals the total mass of the subsystem. Note that equation (3.23) embodies an approximation because the energy is measured in only a finite number of points of the structure. The consequences of this approximation are addressed in section *3.5*.

For practical reasons, $< \overline{E} >$ will be replaced by E further on.

Making use of spectral notations, equation (3.23) can be rewritten as :

$$E \cong \frac{M}{N} \cdot \sum_{i=1}^{N} \int_0^{\infty} S_{i,vv}(\omega) d\omega \qquad (3.24)$$

Where $S_{i,vv}(\omega)$ represents the single sided spectral density of the velocity at location i.

In many occasions, accelerometers are used to measure the response. Hence, velocity should be transformed into acceleration:

$$E \cong M \cdot \frac{1}{N} \cdot \frac{1}{\omega^2} \cdot \sum_{i=1}^{N} \int_0^{\infty} S_{i,aa}(\omega) d\omega \qquad (3.25)$$

Where $S_{i,aa}(\omega)$ represents the single sided, space averaged spectral density of the acceleration of accelerometer i. Band levels (third octave bands) are considered further on and therefore :

$$E_{\omega_1,\omega_2} \cong M \cdot \frac{1}{N} \cdot \frac{1}{\omega^2} \cdot \sum_{i=1}^{N} \int_{\omega_1}^{\omega_2} S_{i,aa}(\omega) d\omega \qquad (3.26)$$

Equation (3.26) holds for general structural subsystems. The examples worked out in this thesis are concerned with the bending vibrational energy of plates.

It is worthwhile to mention in here that practically only flexural energy will be measured although indeed equation (3.26) holds for in-plane motion as well. Hence, experimental SEA will neglect the subsystems which contain in-plane energy. The latter constitutes one of the major disadvantages of PIM, especially for systems for which the in-plane energy becomes signficant. It is therefore quite meaningful for the PIM research to try to incorporate the in-plane wave fields into the model.

3.4.1.2 Acoustic energy measurements.

For acoustic cavities, the reverberent acoustic energy is measured by means of microphones randomly located in the reverberent acoustic field of the cavity. The space and time averaged energy of the reverberent field is given by :

$$< \overline{E} > \cong \frac{V}{\rho c^2} \cdot \frac{1}{N} \cdot \sum_{i=1}^{N} p_i^2(t) \qquad (3.27)$$

Where V represents the volume of the cavity.

Converting equation (3.27) into spectral notation results in :

$$< \overline{E} > \cong \frac{V}{\rho c^2} \cdot \frac{1}{N} \cdot \sum_{i=1}^{N} \int_0^{\infty} S_{i,pp}(\omega) d\omega \qquad (3.28)$$

Where $S_{i,pp}(\omega)$ represents the single sided spectral density of the pressure at location i.

In practical situations, third octave bands are used, therefore :

$$E_{\omega_1,\omega_2} \cong \frac{1}{N} \cdot \frac{V}{\rho c^2} \cdot \sum_{i=1}^{N} \int_{\omega_1}^{\omega_2} S_{i,pp}(\omega) d\omega \qquad (3.29)$$

Equation (3.29) holds for general cavities exhibiting a reverberent vibrational field. The microphones should not be positioned near the loudspeaker. Obviously, if the damping is too high, then formula (3.29) does not hold any longer as the pressure field becomes less reverberent.

3.4.2 Power input measurements.

The application of PIM requires accurately measured power inputs into *each* single subsystem, excited (classically) by a shaker, a horndriver-tube combination or a loudspeaker depending on the type of subsystem, i.e. plate or cavity.

3.4.2.1 Structural power input measurements.

The power input due to a point source is presented schematically in figure *3.5* :

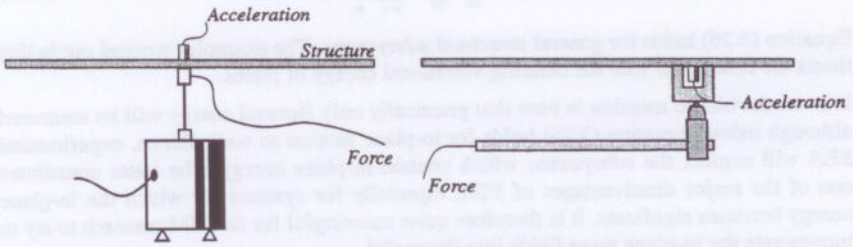

Figure 3.5 : Power input measurement set-up for shaker and hammer excitation.

The actual power input at any time equals :

$$f(t)\cdot v(t) \tag{3.30}$$

Where $f(t)$ represents the force measured at the excitation point of the structure and $v(t)$ represents the particle velocity of the excitation point. The time averaged power input is given by :

$$P_{in} = \frac{1}{T}\cdot\int_0^T f(t)\cdot v(t)\,dt \tag{3.31}$$

In spectral terms :

$$P_{in} = Re\left[\int_0^\infty S_{vf}(\omega)\,d\omega\right] \tag{3.32}$$

Where $S_{vf}(\omega)$ represents the single sided cross-spectrum of force and velocity at the excitation point. Because primarily accelerometers are used to measure accelerations, the velocities are transformed into accelerations :

$$P_{in} = \frac{1}{\omega}\cdot Im\left[\int_0^\infty S_{af}(\omega)\,d\omega\right] \tag{3.33}$$

or in band levels :

$$P_{\omega_1,\omega_2} = \frac{1}{\omega}\cdot Im\left[\int_{\omega_1}^{\omega_2} S_{af}(\omega)\,d\omega\right] \tag{3.34}$$

Clearly, power input measurements require the evaluation of the *imaginary* part of the cross spectrum $S_{af}(\omega)$. Hence, unlike the energy measurements for which phase information is not essential, an accurate knowledge of the phase between force and

acceleration at the excitation point is vital in the case of power input measurements. Every unwanted phase shift between the two signals could result in substantial bias errors, especially in the higher frequency range. The following graph shows the phase shift between force and acceleration at the excitation point of a *2 mm* damped Al plate of dimension *500x500* mm. Use is made of an accelerometer located on the opposite side of the force transducer (similarly to figure 3.5). A white noise source is applied in the range *0-7000* Hz.

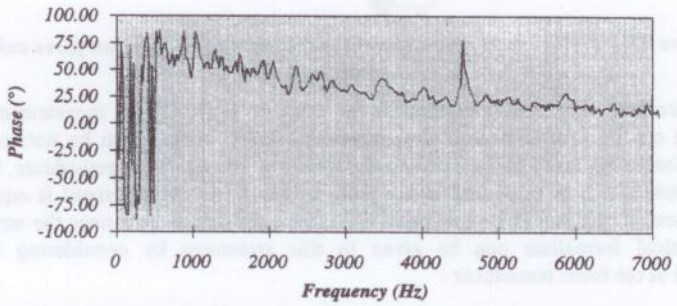

Figure 3.6 : Phase difference between force and acceleration at the input point.

Clearly, at higher frequencies, the phase difference between force and acceleration decreases. Hence, small bias errors (in terms of bias phase shifts between force and acceleration) could substantially affect the measured power input levels because the *imaginary* part of the cross-spectrum between force and acceleration can be considerably influenced by this bias error. An accurate power input value can only be obtained if a phase calibration is performed in advance to compensate for the bias phase shift between force and acceleration.

Practically, a force applied on a structure can never be measured exactly on the structure because of the finite dimensions of the force cell. At high frequencies, this additional mass can become important with respect to the force measured at the excitation point. However, it can be shown that it is *not* necessary to measure the force exactly at the excitation point of the structure. Eventually, one can measure the force a small distance away from the surface of the structure, as schematically illustrated in figure 3.7, hence including a small mass between the force cell and the structure. In this case, the shaker has to accelerate the mass which give rise to reactive energy. Because we are interested in active energy (and that's what we are measuring), no errors will occur.

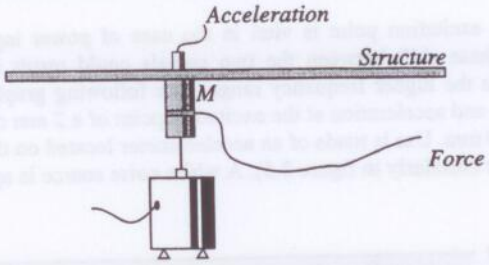

Figure 3.7 : Power input measurement; additional mass between force cell and structure.

A mass correction is not necessary in the case of power input measurements. This statement can be proven in two straightforward ways. First, it can be noticed that no energy dissipation takes place between the structure and the force transducer, hence the energy flow which is measured at the point of the force measurement is equal to the energy flow which would be measured by a force transducer just near the structure. A mathematical formalism can be given to this statement by considering the force measured at the force transducer :

$$F_{forcetransducer}(\omega) = F_{structure}(\omega) - M\,A(\omega) \qquad (3.35)$$

Where $F_{forcetransducer}(\omega)$ represents the force measured at the force transducer. $F_{structure}(\omega)$ denotes the force measured at the structure. A stands for the acceleration at the measurement points. The power input is proportional to the imaginary part of the cross-spectrum between force and acceleration. Hence, from equation (3.35) it follows that :

$$Im(F_{forcetransducer} \cdot A^*) = Im(F_{structure} \cdot A^*) - Im(M \cdot A \cdot A^*) \qquad (3.36)$$

Hence, it follows that :

$$Im(F_{forcetransducer} \cdot A^*) = Im(F_{structure} \cdot A^*) \quad or \quad P_{forcetransducer} = P_{structure} \qquad (3.37)$$

Where $P_{forcetransducer}$ represents the power input into the structure measured at the force transducer. $P_{structure}$ is the energy flow into the structure measured just near the structure itself.

Thus by taking a measurement device containing a mass between structure and force transducer, one can still obtain an accurate value of the power input as would be the case for force measurements directly on the structure, even though the amplitude of both force spectra is different. An illustrative measurement has been performed with a force transducer and an impedance head attached to the plate as shown in figure 3.8.

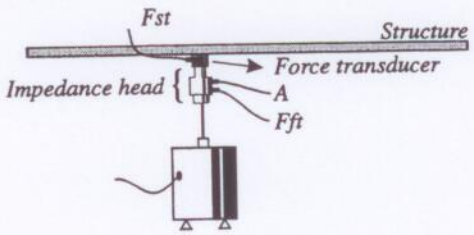

Figure 3.8 : Power input measurement; use of force cell and impedance head in tandem.

The acceleration measured at the impedance head serves as a reference. The amplitude of the complex power input of the impedance head and of the force transducer are shown in figure 3.9, revealing a substantial difference between both quantities. The active power input on the other hand agrees perfectly well as could be expected from the theoretical considerations established above. It should be mentioned though that the phase difference between the acceleration and the force of the impedance head has become smaller compared to the phase difference between the acceleration and the force of the force transducer. In the case of masses between the point of force measurements and the structure, the exciter will deliver more reactive energy corresponding to a phase difference between force and acceleration closer to 180° and consequently a bias phase shift between force and acceleration of the impedance head will be more crucial.

The only assumption made in this section is that no damping and no elastic deformation may occur in the part between force measurement of the impedance head and the force measurement of the single force transducer, because only in that case a rigid connection is obtained and only in that case the *imaginary* part between force and acceleration of both instruments will not change.

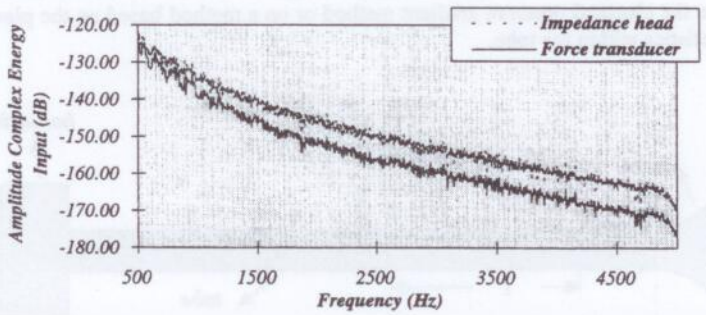

Figure 3.9 : Complex power input : comparison between impedance head and force transducer.

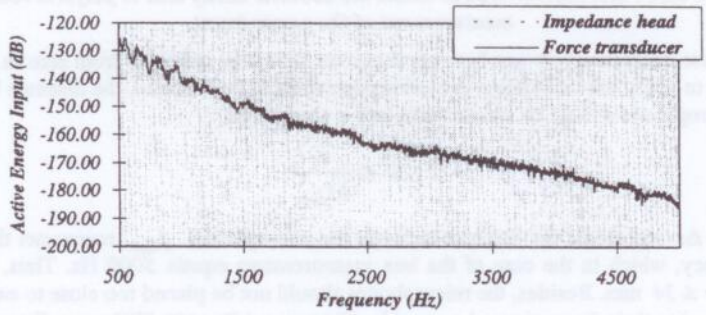

Figure 3.10 : Active power input : comparison between impedance head and force transducer.

3.4.2.2 Acoustic power input measurements..

In order to be applied, PIM requires the excitation of *all* subsystems and the measurement of the corresponding power input. Systems comprising acoustic cavities should therefore be acoustically excited besides the excitation of the structural subsystems. The problem of the measurement of the power input into acoustic SEA subsystems is not straightforward to answer. Not much has been done on the subject of real time, high frequency, acoustic power input measurements. For low frequency problems, YANG-SUB [81] describes a device for calibrated energy injection into a car passengers cavity. For high frequency problems, the latter device is not suitable. Therefore, a special horndriver-tube-horn device is constructed in the framework of this thesis to measure the power input into acoustic cavities.

3.4.2.2.1 Construction of the acoustic excitation device.

The acoustic source which is constructed consists of a horndriver-tube combination (figure 3.11). In the middle of the tube, two B&K quarter inch microphones are positioned to measure the acoustic intensity through the tube. The measurement can be based on the classical pressure gradient method or on a method based on the plane wave characteristics within the tube.

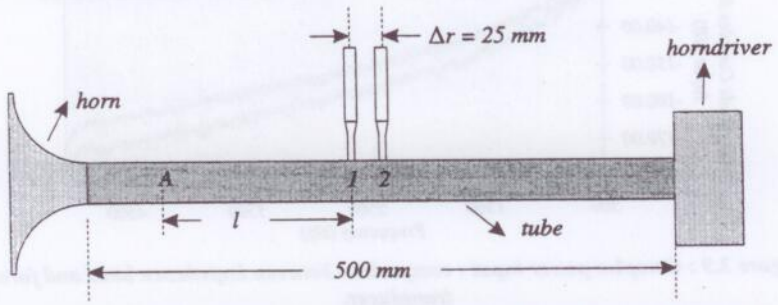

Figure 3.11 : Horndriver-tube to excite the acoustic cavity and to perform real-time measurement of the power input.

The phase difference between both microphones should be different from zero in order to be able to apply the calculation procedure described below. Hence, the distance between the microphones should be smaller than half a wavelength :

$$\Delta r \leq \frac{c}{2 f_{upper}} \qquad (3.38)$$

Where Δr represents the distance between the microphones. f_{upper} represents the upper frequency, which in the case of the box measurements equals *5000* Hz. Thus, it holds that $\Delta r \leq 34$ mm. Besides, the microphones should not be placed too close to each other compared to their dimensions. As an aside, CHUNG and BLASER [78] use a distance of *27* mm for a similar measurement device. The inner radius of the tube may not be too large

to avoid standing waves across the diameter of the tube. As a rule of thumb, the diameter should be larger than half a wavelength. For this reason, *30* mm has been taken as an acceptable value of the inner diameter of the tube. CHUNG and BLASER use a tube with a diameter of *51* mm to measure up to *4200* Hz. Finally, the length of the tube is taken large enough to remove edge effects at the end of the tubes. As a rule of thumb, the length of the tube should at least measure several diameters. *500* mm has been taken as the length of the tube of figure 3.11

Eventually, a horn can be mounted at the end of the tube to equalize to a certain extent the impedance mismatch between the acoustic waves in the tube and the cavity outside the tube. From the fluid dynamics point of view, the application of a horn is also advantaguous to diminish the energy loss at the end of the tube.

3.4.2.2.2 Evaluation of energy flow.

Classical intensity measurements are based upon the measurement of the cross-spectrum of two closely spaced microphones. To date, the measurement of the acoustic intensity has become routine and is summarized in an excellent reference by FAHY [82]. The pressure gradient technique is based on the approximation of the equation 39.

$$-\nabla p = \rho \frac{\partial u}{\partial t} \qquad (3.39)$$

With p representing pressure and u particle velocity.

In spectral terms, the intensity is approximated by :

$$I(f) = Im\left[\frac{S_{p_1 p_2}}{\omega \rho \Delta r}\right] df \qquad (3.40)$$

The distance between the two microphones Δr should be small enough in order to acceptably approximate equation (3.39). On the other hand, Δr may not be too small because in that case the gradient $\partial p / \partial r$ of equation (3.39) can not be sufficiently accurately approximated by $(p_2 - p_1)/\Delta r$. When using the quarter inch microphones located in the tube, the smallest conceivable difference between the microphones equals *25* mm ✎ and is found too high to apply equation (3.40) resulting in unacceptable errors with respect to the intensity. An alternative way to measure intensity is given by CHUNG and BLASER.

In the case of the tube, a plane wave pattern is generated, making it amenable to exact calculations. The intensity calculations are based upon the evaluation of the acoustic impedance at some point of the tube (point A). CHUNG and BLASER derived expressions of the acoustic impedance of the tube in terms of FRF's between the pressures of the two microphones :

$$Z = \frac{P_A}{V_A} = \rho c j \frac{H_{12} \sin(kl) - \sin(k(l - \Delta r))}{\cos(k(l - \Delta r)) - H_{12} \cos(kl)} \qquad (3.41)$$

✎ According to the construction of figure *3.11*.

Where $H_{12} = P_1 / P_2$ denotes the FRF between the pressures of the two microphones. k represents the wavenumber. l represents the distance between the first microphone and the location at which the impedance is calculated, i.e. location A on figure 3.11.

Without loss of generality, l can assumed to be 0, meaning that the impedance at the first microphone is considered further on. In this case, the ratio between the particle velocity and the pressure at the first microphone becomes :

$$Z_1 = \frac{P_1}{V_1} = \rho c j \frac{sin(k\Delta r)}{cos(k\Delta r) - H_{12}} \tag{3.42}$$

The acoustic intensity is calculated by the following equation :

$$I = \frac{1}{2} \cdot Re\left[V_1 P_1^*\right] \tag{3.43}$$

In terms of the FRF between the pressures of the two microphones and in terms of the autopower of the pressure of the first microphone, it holds that :

$$I = \frac{1}{2} \cdot Re\left[\frac{1}{Z_1} \cdot S_{p_1 p_1}(\omega)\right] \tag{3.44}$$

It can be shown that the expression of equation (3.44) converges to the expression of the gradient method of equation (3.40) for small values of Δr :

$$\lim_{\Delta r \to 0}\left(\frac{1}{2} \cdot Re\left[\frac{1}{Z_1} \cdot S_{p_1 p_1}(\omega)\right]\right) = \lim_{\Delta r \to 0}\left(\frac{S_{p_1 p_2(\omega)}}{\rho\, 4\pi\, f\, \Delta r}\right) \tag{3.45}$$

Figure 3.12 displays the intensity curves associated with the approximated gradient method and with the "exact" two-microphone method. The tube is located in the semi-anechoic room and the horndriver is excited by white noise.

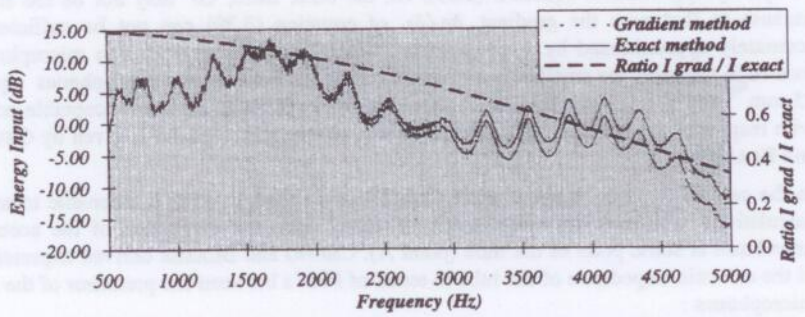

Figure 3.12 Power input into cavity : comparison between pressure gradient and exact method.

Clearly, the gradient method fails for the determination of the acoustic intensity in the higher frequency range. In the framework of this thesis, the exact two-microphone method is applied for all PIM measurements to evaluate on-line the power input.

3.4.3 FRF based techniques.

The employment of power-spectra to calculate the energy level and the power input level is very straightforward and became widespread (explained in paragraph *3.4.1-3.4.2*). The technique involves the use of a white noise excitation, i.e. the utilization of a *flat* force spectrum to achieve an acceptable weighting of all frequencies within a frequency band (flat volume velocity spectrum in the case of an acoustic cavity). The use of shakers to excite the structural subsystems is advised for wide frequency bands yet not compulsory. The power-spectrum approach embodies some disadvantages as explained below.

For hammer excitation, the force spectrum can hardly become flat in a wide frequency band, eventually resulting in an unwanted weighting of frequencies (from the power-spectrum point of view) within a frequency band. Similarly, in the case of shaker excitation, the force spectrum can exhibit unwanted peaks (and hence undesired weighting of the corresponding frequencies occurs) if no special measures are taken with respect to the connection shaker-structure. For example, the application of a stinger between shaker and structure can result in a manifest peak of the applied force spectrum at high frequencies corresponding to resonant behavior of the stinger. Figure 3.13 shows in this respect the force spectrum of the excitation in the case of the presence of a stinger between the force transducer and the exciter. Clearly, the influence of the stinger becomes very perceptible around *4300* Hz. By taking a different stinger, the peak exhibiting the dynamic behavior of the stinger will show up at different frequency. In any event, this situation should be avoided because of the weighting of certain frequencies.

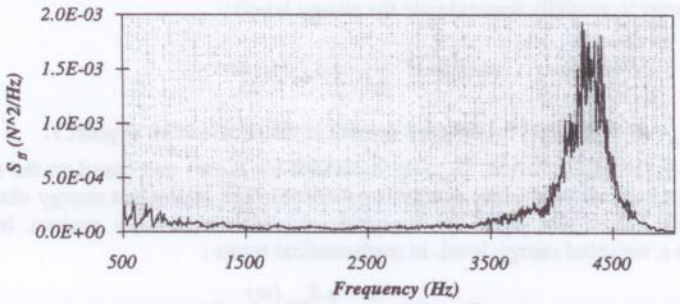

Figure 3.13 : Force spectrum in the case of shaker excitation and stinger connection.

Furthermore, the application of a white noise excitation in a *wide* frequency band can cause problems with respect to the measurement of the energy of vibration of remote subsystems (i.e. relatively distant from the driven subsystem (LIE WU [55])) at high frequencies due to the low signal to noise ratio..

Research has been undertaken to come up with a measurement procedure independent of the excitation device and of the type of the excitation signal. A solution of which has been found in the application of FRF's. The only requirement for this method is the accurate measurement of the FRF's between response at a sufficient number of locations of the structure and the driving force. By applying the appropriate equations, one is not

restricted any longer to apply white noise by means of a shaker or loudspeaker. Hammer excitation can be used with confidence in order to substantially reduce the time to perform a complete measurement. In the case of the FRF approach, pink noise or swept sine excitation can be applied to allow to put more energy into the system in the higher frequency bands if necessary.

The following picture intends to clarify the FRF concept:

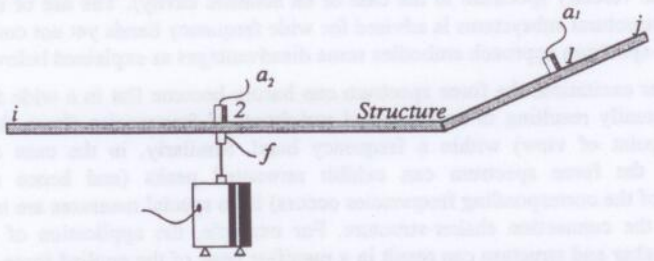

Figure 3.14 : Schematical representation of the FRF method.

A subsystem is excited and the FRF's between the acceleration at the response points *1* & *2* and the force at the excitation point are measured : $H_{a_1 f}(\omega)$ and $H_{a_2 f}(\omega)$. The calculation of the power input and of the energy level from the FRF's is explained below.

3.4.3.1 Energy measurement.

The band averaged energy level is given by (assuming for the moment only *1* accelerometer to spatially approximate the energy level) :

$$E \cong M \cdot \frac{1}{\omega^2} \cdot \int_{\omega_i}^{\omega_u} S_{a_1 a_1}(\omega)\, d\omega \qquad (3.46)$$

Where $S_{a_1 a_1}(\omega)$ represents the spectral density of the acceleration at point *1*.

To arrive at the FRF notation, $S_{a_1 a_1}(\omega)$ is divided by $S_{ff}(\omega)$ and based on the spectrum $S_{a_1 a_1}(\omega) / S_{ff}(\omega)$, an *equivalent* energy is calculated. The equivalent energy obtained by this approach does not equal the energy level which is actually present, but rather represents a weighted energy level. In mathematical terms :

$$E_{eq} \cong M \cdot \frac{1}{\omega^2} \cdot \int_{\omega_i}^{\omega_u} \frac{S_{a_1 a_1}(\omega)}{S_{ff}(\omega)} \cdot d\omega \qquad (3.47)$$

However, there is no fundamental rationale not to apply equation (3.47) because the division of the acceleration spectrum by the force spectrum of the excitation only represents some kind of weighting of the actual acceleration spectrum, i.e. the spectrum $S_{a_1 a_1}(\omega) / S_{ff}(\omega)$ represents the acceleration spectrum which would be present if a force spectrum $S_{ff}(\omega) = 1$ is applied.

Equation (3.47) can be written in terms of FRF's as :

$$E \cong M \cdot \frac{1}{\omega^2} \cdot \int_{\omega_i}^{\omega_u} \left| H_{a_1 f}(\omega) \right|^2 d\omega \qquad (3.48)$$

Where $H_{a_i f}(\omega)$ represents the FRF between acceleration at the response point *1* and the force at the excitation point. E_{eq} of equation (3.47) is replaced by E further on.

In conclusion and explicitly in FRF phraseology, it is shown that the energy of vibration is proportional to the square of the non-diagonal terms (indirect FRF's) of the FRF matrix, i.e. :

$$E_{ji} \approx \left|H_{ji}\right|^2 = \left|\frac{A_j}{F_i}\right|^2 \qquad i \neq j \tag{3.49}$$

3.4.3.2 *Power input measurement.*

By dividing the cross spectrum between force and acceleration at the excitation point $S_{a_i f}(\omega)$ by $S_{ff}(\omega)$, the equivalent power input into the structure can be expressed by :

$$P_{\omega_1,\omega_2} = \frac{1}{\omega} \cdot Im\left[\int_{\omega_1}^{\omega_2} \frac{S_{a_i f}(\omega)}{S_{ff}(\omega)} \cdot d\omega\right] \tag{3.50}$$

Which can be transformed in FRF notation :

$$P_{\omega_1,\omega_2} = \frac{1}{\omega} \cdot Im\left[\int_{\omega_1}^{\omega_2} H_{a_i f}(\omega) d\omega\right] \tag{3.51}$$

The equivalent power input obtained by applying the FRF approach does not equal the actual time averaged power input into the structure, but only equals the power input which would occur if a force spectrum $S_{ff}(\omega) = 1$ would be applied, in the same way the equivalent energy does not equal the actual energy.

Hence, it has been shown that the equivalent power input is proportional to the imaginary part of the diagonal terms (direct FRF's) of the FRF matrix, i.e. :

$$P_{in} \approx Im\left[H_{ii}\right] = Im\left[\frac{A_i}{F_i}\right] \tag{3.52}$$

3.4.3.3 *Conclusion.*

A FRF based calculation of equivalent energy levels and power input levels is worked out in this section. The corresponding energy and power input values do not correspond to the actual energy and power input values but are weighted against the force spectrum.

It is suggested to use the FRF approach in general because then the response can be considered as caused by an excitation force $S_{ff}(\omega) = 1$ and not caused by the actual force applied on the structure which could in some occasions be dominated by peaks caused by particularities of the excitation devices in such a way that the actual force does not represent white noise and unwanted weighting of some frequencies occurs (figure *3.13*). Furthermore, the FRF based approach allows to use whatever excitation device and signal, as long as the FRF's can be accurately obtained. Thus, besides white noise excitation using a shaker, one can think of hammer excitation, swept sine etc. Therefore,

in general one should use excitation devices capable of accurately measuring the FRF's in a specified frequency band.

To conclude this paragraph on FRF based techniques, an example is presented showing the difference between the FRF approach and the spectral density approach with respect to the difference of the normalized energy levels. Plate *4* of the box (figure *3.3*) is excited by a white noise point force. The energy level of the driven plate is taken out. The normalized energy value $E_{44}^{n} = \omega \cdot E_{44} / P_4$ is calculated by means of the FRF approach and by means of the classical spectral approach. The results are presented in figure *3.15* and reveal a general agreement between both approaches. All other normalized energy values of the normalized energy matrix were found to be similar for both approaches, hence there is no substantial difference in the case of the box structure between the FRF approach and the spectral approach which is classically applied.

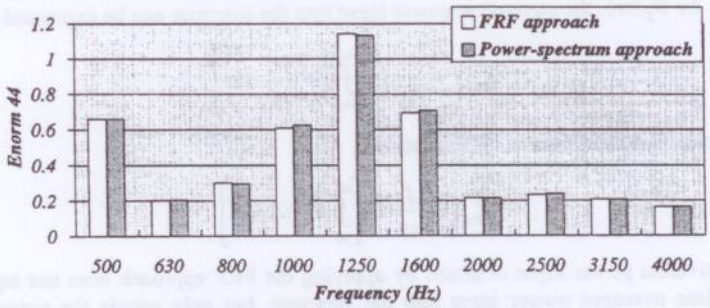

Figure 3.15 : Normalized energy value E_{44}

A second example shows the relative difference between the normalized energy E_{44}^{n} obtained by shaker excitation (white noise signal) and obtained by hammer excitation. In both cases, plate *4* is excited at the same locations. For the measurement, two types of hammers were used, i.e. soft and hard. Clearly, no significant differences between the shaker excitation and the hammer excitation are noticed. Hammer excitation can definitely be used for SEA purposes and can in some occasions help to reduce the measurement effort.

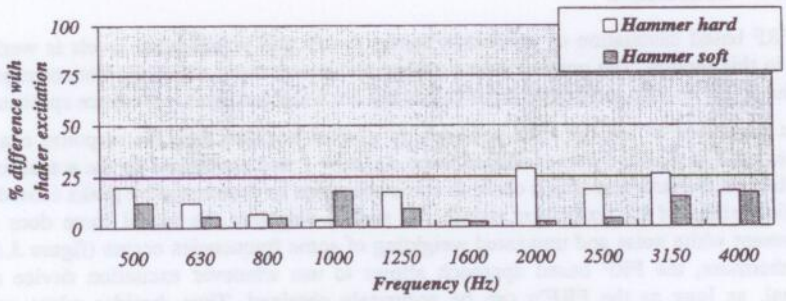

Figure 3.16 : Comparison hammer and shaker excitation.

3.5 Application of decay techniques and energy correction.

3.5.1 Energy correction.

As pointed out in section *3.4*, the vibrational energy of structures can not be measured directly. The evaluation of subsystem energies should be performed by means of related measurable variables such as acceleration and velocity. Whatever response variable is selected, the measured quantities should be transformed into subsystem energies of vibration by multiplying the squared velocity spectrum $< v^2 >$ by the mass of the subsystem M.

Mathematically :

$$E = 2 \cdot E_k \cong M \cdot < v^2 > \tag{3.53}$$

In reality however, the subsystem energy of vibration is given by :

$$E = 2 \cdot E_k = \int_V \rho v^2 \cdot dV \tag{3.54}$$

Where A represents the extent of the subsystem.

Hence, the energy which is obtained by using the approximation of equation (3.53) does in principle not equal the actual energy of a subsystem. LALOR [2] has suggested to adjust for this discrepancy by applying a correction factor on the mass of the subsystem, referred to as "equivalent mass". Hereafter the term *energy correction coefficient* instead of equivalent mass will be used because it is felt that this terminology is more appropriate to describe the correction of the approximation of equation (3.53) :

$$\int_A p v^2 \cdot dA = \alpha \cdot M \cdot < v^2 > \tag{3.55}$$

Where α represents the energy correction coefficient which can be determined by time decay measurements in the way as explained below.

3.5.2 Evaluation of energy correction coefficient.

3.5.2.1 Single subsystem SEA model.

The evaluation of the energy correction coefficient is based on decay measurements and is addressed below.

The basic transient SEA equation for a single subsystem SEA model is given by :

$$P = \dot{E} + \omega \cdot \eta \cdot E \tag{3.56}$$

Where the power input P and the energy level E are time dependent.

Assuming the system is being excited such that steady state conditions exist, it holds that $P = \overline{P}$, $E = \overline{E}$ and $\dot{E} = 0$. Where the overbar $\overline{\ }$ denotes time averaging.

It is assumed that at a certain time t_a, needed to arrive at steady state conditions, the power input is switched off, resulting in the following equation :

$$\dot{E} = -\omega \cdot \eta \cdot E \qquad (3.57)$$

A solution of which can readily be given by :

$$E = A \cdot e^{-\omega\eta(t-t_a)} \qquad (3.58)$$

The coefficient A is determined by the initial conditions ($t = t_a$), i.e. $A = \overline{E}$. The energy decay appears to be linear in a lin-log scale.

As an example, the energy decay of a damped Aluminium plate with dimensions *1170x750x1.5* mm has been determined. The plate is acoustically excited in the frequency range *1187.5-1312* Hz by burst random. An acoustic excitation has been used to remove the influence of the excitation device after the power input has been switched off. The latter is found to be necessary in the case of lightweight structures.

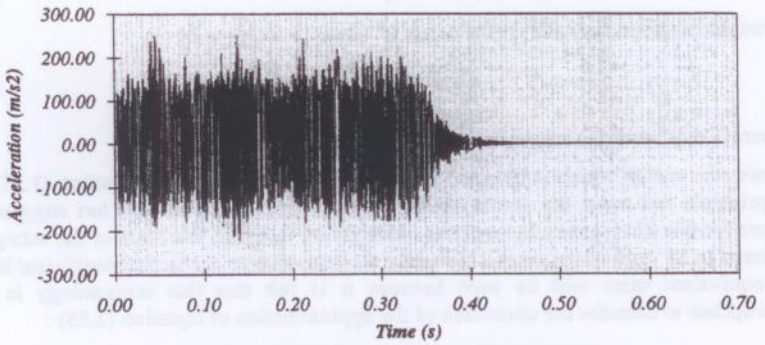

Figure 3.17 : Acceleration signal for decay measurements.

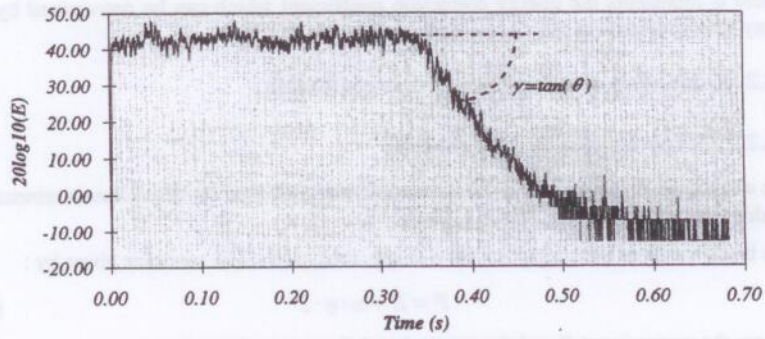

Figure 3.18 : Decay of energy in lin-log schale.

Figure 3.17 shows the acceleration as a function of time. At *t=0.34* s the power input is switched off and the acceleration decreases exponentially. The corresponding decay of the kinetic energy in a lin-log scale is shown in figure *3.18*.

Equation (3.58) can now be applied to identify the loss factor of the uncoupled subsystem. By taking the log_{10} of both sides of equation (3.58), it follows that :

$$10\log_{10}(E) = 10\log_{10}(\overline{E}) + \frac{10\omega\eta t_a}{ln(10)} - \frac{10\omega\eta t}{ln(10)} \qquad (3.59)$$

Hence, the decay γ of the curve of figure 3.18 is related to the loss factor through :

$$\gamma = \frac{\omega \cdot \eta \cdot 10}{ln(10)} \quad or \quad \eta = \frac{0.23\gamma}{\omega} \qquad (3.60)$$

The decay of the energy curve of figure 3.18 can be obtained by an appropriate fitting procedure. Equation (3.60) allows to evaluate the loss factor of an uncoupled subsystem as an alternative for the steady state PIM measurements.

As an example, this technique is compared to the steady state PIM in the case of the flat plate considered previously. An acoustic burst random excitation has been used for the time decay measurements. Shaker excitation is used for the steady state PIM measurements. Third octave bands between *500* Hz and *4000* Hz are retained. Figure *3.19* depicts the loss factor obtained by the steady state and by the decay method. Good agreement is obtained, thereby validating the basic transient SEA equation for a single subsystem model.

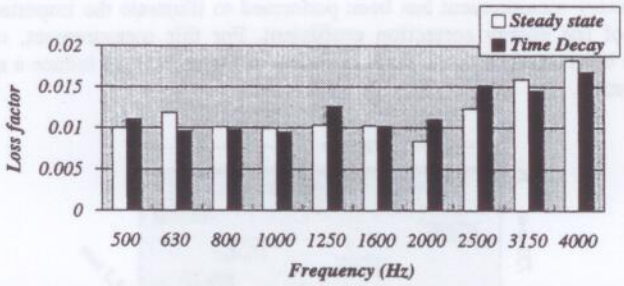

Figure 3.19 : Comparison of internal loss factors in the case of decay and steady state measurements.

In the framework of this thesis, transient measurements are performed and shown to be effective to update the steady state PIM measurements. More specifically time decay results can be applied to adjust for the approximation of equation (3.53) or in other words to evaluate the energy correction coefficient.

For steady state conditions it holds that :

$$\overline{P} = \omega \cdot \eta \cdot \overline{E} = \omega \cdot \alpha \cdot \eta \cdot M \cdot < v^2 > \qquad (3.61)$$

Where M represents the mass of the subsystem.

Substituting the loss factor of equation (3.60) into (3.61) results in :

$$\alpha = \frac{\overline{P}}{M < v^2 > 0.23\gamma} \qquad (3.62)$$

The energy correction coefficient has been evaluated in the case of the Aluminium rectangular plate considered above. The results are shown in figure *3.20*. Clearly, the energy correction coefficient does not significantly differ from 1, a result which could be expected because the mass is equally distributed along the plate and therefore the quantity $M < v^2 >$ will fairly well represent the actual reverberent energy of the plate.

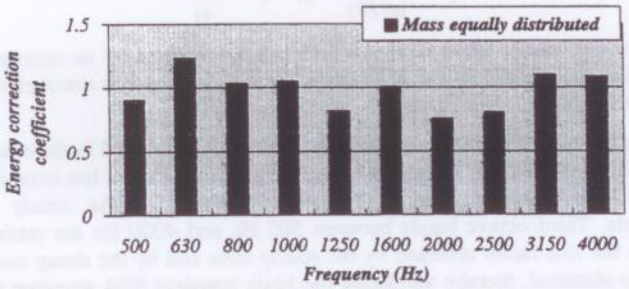

Figure 3.20 : Energy correction coefficient : mass equally distributed along the plate.

A supplementary measurement has been performed to illustrate the importance and the essentiality of the energy correction coefficient. For this measurement, concentrated masses have been attached to the plate as shown in figure *3.21*, to induce a non-uniform mass distribution.

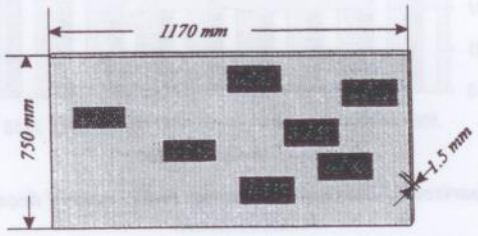

Figure 3.21 : Mass not equally distributed along the plate.

The loss factors obtained by decay measurements and by steady state PIM measurements are displayed in figure *3.22*. The corresponding energy correction coefficient is pictured in figure *3.23*, revealing higher values for the latter quantity compared to the plate for which the mass is equally distributed. Hence, it is advisable to employ a correction coefficient for steady state PIM measurements in the case of structures with a non-uniformly distributed mass. It should be mentioned however that the example is somehow extreme : the additional masses are of the same order of magnitude compared to the mass of the plate itself. This has been done to enforce a discrepancy between steady state and decay techniques.

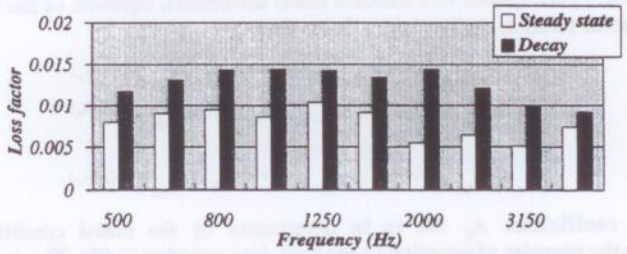

Figure 3.22 : Comparison of internal loss factors in the case of decay and steady state measurements (mass not equally distributed).

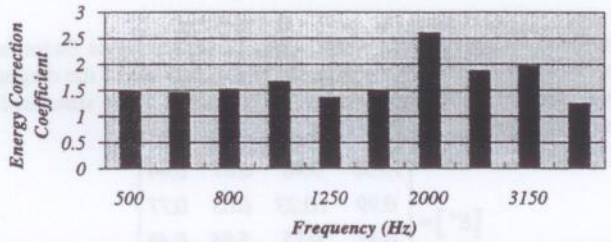

Figure 3.23 : Energy correction coefficient; mass not equally distributed.

Conclusion. It has been shown that loss factors of a single subsystem SEA model can be obtained by relevant time decay measurements. Comparison with steady state PIM measurements revealed the inconsistency between both approaches, caused by the approximation of equation (3.53), particularly for a non-uniform distribution of the mass, resulting in an energy correction coefficient which can not be neglected. Hence, the measured subsystem energy in steady state conditions should be adjusted and updated by the energy correction coefficient.

3.5.2.2 n-subsystem SEA model

The basic transient SEA equations for a n-subsystem SEA model can be written as :

$$\{P\} = \left\{\dot{E}\right\} + \omega \cdot \left[\eta^{\circ}\right] \cdot \{E\} \qquad (3.63)$$

Suppose the subsystems are being excited and steady state conditions are present, such that :

$$\{P\} = \{\overline{P}\};\ \{E\} = \{\overline{E}\} \text{ and } \{\dot{E}\} = \{0\} \qquad (3.64)$$

Self-evidently in this case, equation (3.63) becomes identical to the classical SEA steady state equations. It is assumed that at a certain time t_a, necessary to arrive at steady state conditions, the power input is switched off. Equation (3.63) becomes :

$$\left\{\dot{E}\right\} = -\omega \cdot \left[\eta^{\circ}\right] \cdot \{E\} \qquad (3.65)$$

Equation (3.65) corresponds to a standard linear differential equation of the first order of which a general solution can be written in the form :

$$\begin{cases} E_1 = A_{11}\, e^{-\lambda_1(t-t_a)} + A_{12}\, e^{-\lambda_2(t-t_a)} + \cdots + A_{1n}\, e^{-\lambda_n(t-t_a)} \\ E_2 = A_{21}\, e^{-\lambda_1(t-t_a)} + A_{22}\, e^{-\lambda_2(t-t_a)} + \cdots + A_{2n}\, e^{-\lambda_n(t-t_a)} \\ \vdots \\ E_n = A_{n1}\, e^{-\lambda_1(t-t_a)} + A_{n2}\, e^{-\lambda_2(t-t_a)} + \cdots + A_{nn}\, e^{-\lambda_n(t-t_a)} \end{cases} \qquad (3.66)$$

Where the coefficients A_{ij} are to be determined by the initial conditions and by substituting the energies of equation (3.66) back into equation (3.65). The coefficients λ_i symbolize the eigenvalues of the total loss factor matrix multiplied by ω. Note that in the case of a n-subsystem model for which $n \neq 1$, the energy variation of a subsystem does *not* exhibit a linear decay in a lin-log scale because the number of exponential terms is larger than *1*.

It can be mentioned in here that the eigenvalues of the total loss factor matrix can in most occasions be approximated by its diagonal terms, because of the diagonal dominant attribute of the normalized energy matrix. An example using simulated normalized energy data is given below :

$$[E^n] = \begin{bmatrix} 15.56 & 0.98 & 0.07 & 0.44 \\ 0.99 & 10.23 & 0.63 & 0.77 \\ 0.37 & 0.75 & 5.85 & 0.48 \\ 0.25 & 0.65 & 0.27 & 25.0 \end{bmatrix} \qquad (3.67)$$

$$[\eta^\circ] = \begin{bmatrix} 0.0647 & -0.0061 & -0.0001 & -0.0009 \\ -0.0060 & 0.0993 & -0.0105 & -0.0028 \\ -0.0033 & -0.0121 & 0.1724 & -0.0029 \\ -0.0005 & -0.0024 & -0.0016 & 0.0401 \end{bmatrix} \qquad (3.68)$$

The eigenvalues of the total loss factor matrix are :

$$\lambda_1 = 0.0636 \quad \lambda_2 = 0.0988 \quad \lambda_3 = 0.1741 \quad \lambda_4 = 0.0399 \qquad (3.69)$$

and hence the eigenvalues are in good agreement with the diagonal terms of the total loss factor matrix. In general, it can be stated that the diagonal terms of the total loss factor matrix constitute in most occasions a sufficient approximation of its eigenvalues as long as the normalized energy matrix is diagonal dominant.

If during steady state conditions, only subsystem i is excited, then in most occasions the energy level of subsystem i will be much higher than the energy levels of the other subsystems. Hence, after switching off the power input into subsystem i, the initial variation as a function of time will mainly be determined by the term of equation (3.66) comprising the total loss factor of subsystem i. It holds therefore (for practical reasons t_a is assumed to be 0)

$$E_{ii} \cong A_{ii}\, e^{-\omega \eta_{ii}^\circ t} + \sum_{j \neq i}^{n} A_{ij}\, e^{-\omega \eta_{ji}^\circ t} \cong A_{ii}\, e^{-\omega \eta_{ii}^\circ t} \qquad (3.70)$$

Or in log_{10} terms :

$$10log_{10}(E_{ii}) \cong 10log_{10}(A_{ii}) - \frac{10\omega\eta_{ii}^{o}t}{ln(10)} \qquad (3.71)$$

Where $A_{ji} << A_{ii}$ for $i \neq j$.

In the case of a coupled subsystem, the decay of the subsystem energy is not linear in a lin-log scale as a function of time during the total acquisition time, especially if the term A_{ii} is not dominant compared to A_{ij}. As an example, the energy decay of plate number 2 of the box is shown. The plate is excited by a burst random excitation in the frequency range *760-840* Hz. The plate is coupled to the box, which in this case is very lightly acoustically damped to show explicitly the coupling between the plate and the acoustic cavity at the end of the decay time. One curve shows the decay of the plate, the second curve shows the decay of the enclosure. For the uncoupled plate, (figure *3.18*), no influences of the terms $A_{ij}\,e^{-\eta t}$ are noticed because the plate is separated. In the case of the coupled plate however, roughly two decay characteristics are noticed (figure 3.24). For $t_1 < t < t_2$, the decay is determined by the damping of the plate. At a certain time $t = t_2$, the energy of vibration of plate *2* which has been dominated by the power input during steady state conditions, will have decreased notably. From $t = t_2$ on, the influence of the coupling between the acoustic volume and the plate can be noticed. Because the decay time of the acoustic volume is much higher than for the plate, the energy of the plate is determined by the energy flow from the acoustic volume to the plate and hence determined by the decay time of the acoustic volume. The latter example is given to illustrate a typical problem that can arise when dealing with interpretation of decay curves.

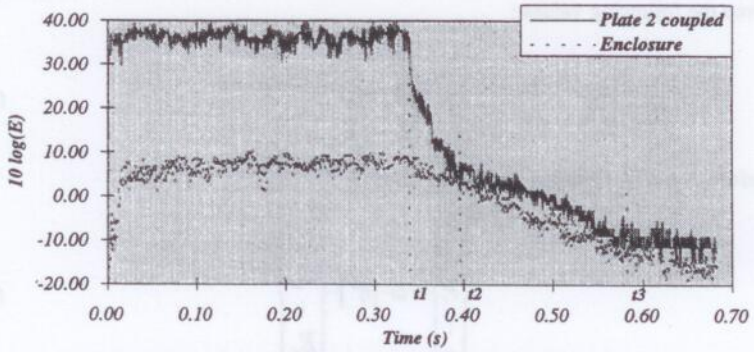

Figure 3.24 : Energy decay curves for plate and enclosure.

Rare are the occasions for which a perfect, identifiable linear decay is noticed. A lot of engineering expertise is essential to interpret the decay rates in terms of total loss factors.

What follows is a description of the identification process of the energy correction coefficient of a *n*-subsystem model.

The linear decay (in logarithmic terms) of the kinetic energy a short time after switching off the power input indicates that the energy is exponentially related to time by the expression of equation (3.72), i.e. :

$$E_{ii} \cong A_{ii} \cdot e^{-\lambda_i (t-t_a)} \tag{3.72}$$

Where A_{ii}, λ_i are constants to be determined by means of measurements.

Taking the logarithm of both sides of equation (3.72) yields :

$$ln(E_{ii}) = ln(A_{ii}) - \lambda_i (t-t_a) \tag{3.73}$$

Since at $t = t_a$ the energy level of subsystem i is given by $E_{ii} = \overline{E}_{ii}$, it is clear that $A_{ii} = E_{ii}$

In terms of *log10*, equation (3.73) can be written as :

$$10 \cdot log_{10}(E_{ii}) = 10 \cdot log_{10}(\overline{E}_{ii}) - (t-t_a) \cdot 10 \cdot \lambda_i / ln(10) \tag{3.74}$$

Equation (3.74) represents the initial linear decay curve of figure 3.24. If the decay rate in figure 3.24 is $\gamma_i = tan(\vartheta_i)$, then $\lambda_i = 0.23\gamma_i$.

Besides, differentiating equation (3.72) with respect to time yields :

$$\dot{E}_{ii} = -A_{ii} \lambda_i e^{-\lambda_i (t-t_a)} \tag{3.75}$$

Hence at $t = t_a$:

$$\dot{E}_{ii} = -A_{ii} \lambda_i = -0.23\gamma_i \overline{E}_{ii} \tag{3.76}$$

Now consider the state of energy around point A of figure. Immediately before A ($t < t_a$), steady state conditions exist and therefore the variables of equation (3.63) can be given the following values :

$$\begin{cases} P_i = \overline{P}_i \\ \dot{E}_{ij} = 0 \\ E_{ij} = \overline{E}_{ij} \end{cases} \tag{3.77}$$

Therefore, the SEA equation (3.63) becomes :

$$\begin{Bmatrix} 0 \\ \vdots \\ \overline{P}_i \\ \vdots \\ 0 \end{Bmatrix} = \omega \cdot [\eta^a] \cdot \begin{Bmatrix} \overline{E}_{1i} \\ \overline{E}_{2i} \\ \vdots \\ \overline{E}_{ni} \end{Bmatrix} \tag{3.78}$$

When the power is switched off at $t = t_a$, there will be a rapid rounding of the curve at point A into the decay slope at $t = t_a^+$. Since there will be a negligible change in the subsystems energy levels over this short period of time, the right hand side of equation (3.78) must remain effectively constant. On the other hand, the left hand side of equation (3.63) describes the energy decay, hence at $t = t_a^+$, equation (3.63) becomes :

$$\begin{Bmatrix} -\dot{E}_{1i} \\ \vdots \\ -\dot{E}_{ii} \\ \vdots \\ -\dot{E}_{ni} \end{Bmatrix} = \omega \cdot [\eta^{\circ}] \cdot \begin{Bmatrix} \overline{E}_{1i} \\ \overline{E}_{2i} \\ \vdots \\ \overline{E}_{ni} \end{Bmatrix} \tag{3.79}$$

Because the right hand side of equations (3.78) and(3.79) are similar, so should be the left hand side, therefore it follows that :

$$-\dot{E}_{ii} = \overline{P}_i \text{ and } \dot{E}_{ji} = 0 \ \forall j \neq i \tag{3.80}$$

Substituting $\dot{E}_{ii}$ into equations (3.76) yields :

$$\overline{P}_i = 0.23 \gamma_i \overline{E}_{ii} \tag{3.81}$$

Hence, the actual total energy of subsystem i when the power input into i equals $\overline{P}_i$ is given by :

$$\overline{E}_{ii} = \frac{\overline{P}_i}{0.23 \gamma_i} \tag{3.82}$$

On the other hand, it holds that :

$$\overline{E}_{ii} = \alpha_i \cdot M_i \cdot < \overline{v}_{ii}^2 > \tag{3.83}$$

Hence by combining equations (3.83) and (3.84), the energy correction coefficient of subsystem i readily follows :

$$\alpha_i = \frac{\overline{P}_i}{M_i \, 0.23 \gamma_i < \overline{v}_{ii}^2 >} \tag{3.84}$$

In a similar manner as for single subsystem SEA models, the correction coefficient α_i should be applied for subsystems for which the mass is not equally distributed.

3.5.3 Updating PIM measurements by using data of uncoupled subsystems.

One of the main advantages of the application of decay techniques is the possibility to rapidly and efficiently identify the total *internal* ✎ loss factor of structures and acoustic cavities. These results can then eventually be used to update the experimental data obtained during steady state PIM, more specifically to update the normalized energy values which can incorporate uncertainties.

For example, the energy level of a subsystem does not equal $M \cdot \langle v^2 \rangle$. Due to the approximation of equation (3.53), an uncertainty can arise. One way of evaluating the energy correction coefficient is given in the previous paragraph.

Another measured quantity which is amenable to be updated consists of the measured power input level into acoustic cavities. Sometimes, measuring the acoustic power input

---

✎ Only internal loss factors can be determined, no coupling loss factors.

is performed by placing a loudspeaker into the cavity. It is then assumed that the power output out of the loudspeaker when located in the cavity equals the power output out of the loudspeaker when located in a anechoic room. Hence, by calibrating the loudspeaker in the anechoic room using intensity measurements, one can recover the power input into a cavity. However, this approach can lead to errors with respect to the measured versus actual power input into the cavity.

This paragraph aims at updating the values of the normalised energy matrix (e.g. energy correction coefficient, power input into a cavity) in order to be closer to the actual values. The technique consists of efficiently applying prior knowledge of the systems parameters. For example, in some occasions, the loss factor of a subsystem is known (e.g. measured by decay techniques). This additional information is then used (i.e. substituted into the SEA equations) to update the measurements as explained below.

Suppose the internal loss factor of one of the subsystems of a general n-subsystem SEA model has been identified by means of decay techniques. Since one of the unknown parameters of the global model is known, it is possible to update the measurements with respect to a factor amenable to be updated such as the energy correction coefficient α_n. Mathematically, the previous statement can be translated into the following set of relevant PIM equations :

$$[I]=\begin{bmatrix} \eta^{o}_{11} & \eta^{o}_{12} & \cdots & \eta^{o}_{1n} \\ \eta^{o}_{21} & \eta^{o}_{22} & \ddots & \vdots \\ \vdots & \ddots & \ddots & \eta^{o}_{n-1n} \\ \eta^{o}_{n1} & \cdots & \eta^{o}_{nn-1} & \eta_{nn}+\sum_{j\neq n}^{n}\eta_{nj} \end{bmatrix} \cdot \begin{bmatrix} E^{n}_{11} & E^{n}_{12} & \cdots & E^{n}_{1n} \\ E^{n}_{21} & E^{n}_{22} & \ddots & \vdots \\ \vdots & \ddots & \ddots & E^{n}_{n-1n} \\ \alpha_n E^{n}_{n1} & \cdots & \alpha_n E^{n}_{nn-1} & \alpha_n E^{n}_{nn} \end{bmatrix} \quad (3.85)$$

The total loss factor matrix represents the matrix of unknown parameters except for the internal loss factor η_{nn} which is obtained by decay measurements. The coefficient which will be used in this example to update the normalised energy matrix constitutes the energy correction coefficient associated with subsystem n, namely α_n. From equation (3.85), it can be seen that the general form of the PIM equations has become non-linear and consequently more laborious to solve, compared to the classical linear PIM equations. A straightforward and effective procedure to solve equation is by using an elementary iteration technique :

An initial value of α_n is taken and the inverse of the normalized energy matrix is calculated to yield the total loss factor matrix associated with the first iteration : $[\eta^{o}_{1}]$. The n^{th} column of $[\eta^{o}_{1}]$ is summed to yield the initial value of the internal loss factor of the n^{th} subsystem : $\eta_{1,nn}$. The latter value is compared to the given loss loss factor η_{nn}. Depending on the difference between the initial internal loss factor and the given loss factor, a subsequent value of the energy correction coefficient is chosen and the procedure outlined above is repeated. After some iterations, the loss factor of the n^{th} subsystem, calculated by the iteration technique, will converge to the given loss factor and an energy correction coefficient is obtained. Although from the numerical viewpoint a less efficient method such as described above is used, the use of it can be justified by the fact that SEA models based on PIM are usually quite small and a limited number of DOF's is involved (for a car, a 50×50 matrix is involved). Eventually, more sophisticated numerical techniques which are generally available in matrix handling

programs can be applied to solve the non-linear set of equations (3.85). This dissertation does however not intend to concentrate on the numerical procedures to solve the non-linear set of equations (3.85).

The procedure outlined above is sufficiently effective in obtaining the total loss factor matrix in occasions for which some of the loss factors are known in advance. The procedure can be extended to incorporate more than one parameter to be updated and more than one given internal loss factor.

One interesting example deals with acoustic cavities for which it is sometimes hard to measure accurately the power input. Using the decay technique, one can determine the reverberation time and hence one can approximate the internal loss factor of the acoustic cavity. By means of the iteration procedure, it is possible to update the power input (one column of the normalized energy matrix) into the cavity when performing PIM measurements and hence to produce more accurate SEA parameters. Therefore, the application of decay measurements overcomes the problem of an accurate measurement of the acoustic power input during PIM.

The technique is illustrated by means of an example on the box structure. A basic measurement (further referred to as original measurement) is performed for which it holds that the acoustic power input is produced by a loudspeaker. The power output out of the loudspeaker is calibrated in a semi-anechoic room. The calibrated power output data is assumed to represent the power input into the acoustic cavity during the steady state PIM measurements. Clearly, the latter constitutes a major and crucial assumption because the power output out of the loudspeaker will not be equal to the power output out of the loudspeaker while in the cavity, because of the mismatching of the input impedance of the semi-anechoic room and the enclosure of the box. Hence, large errors can be expected. A second, reference measurement has been performed making use of a combination horndriver-tube to produce the acoustic energy as described in section *3.4.2.2*. The measurements and associated SEA model making use of the horndriver-tube combination serves as a reference model. From figure *3.25* it can be observed that a significant difference between the reference model and the original model exists with respect to the loss factor of the enclosure and with respect to the coupling loss factors between the structural subsystems and the enclosure i.e. η_{*8}, a difference which could be expected due to the use of an inferior power input measurement procedure in the case of the original model. The loss factor of the structural subsystems and the coupling loss factors between structural subsystems are more or less similar for both original and reference model. For the updated model, use is made of the "exact ✎ " loss factor of the enclosure, i.e. subsystem *8*. By applying the updating procedure explained above, with respect to the loss factor of the 8^{th} subsystem and with respect to the power input into the cavity, the original model turns into a largely improved (closer to the reference model) updated model. The loss factor of the cavity in case of the updated model is similar to the one for the reference model, being quite evident as the loss factor η_{88} of the enclosure serves as given parameter. However, in addition, the coupling loss factors between structural subsystems and the cavity of both reference model and updated model are in closer agreement compared to the one of the original model and the reference model. On

---

✎ The loss factor of the reference model is assumed to be exact in here.

the other hand, structural loss factors and coupling loss factors between structural subsystems remain more or less the same after updating, except for the loss factor η_{11} at *500* Hz

In conclusion it can be stated that the updating procedure explained above offers an interesting possibility to update the experimentally identified model with respect to uncertain measured quantities such as the acoustic power input into the cavity or the energy correction coefficient. It should nevertheless be emphasized that the information which is a priori used to update the measurements (like information on loss factors), should be correct in the first place. If for example, decay measurements are used to identify the net loss factor of a subsystem and one encounters problems with respect to the identification of the loss factors from the decay curves, resulting in uncertainties, then one should be aware of these uncertainties and realize that the parameters which are finally obtained by PIM (after updating) can never be more accurate compared to the parameters which are obtained from the decay curves.

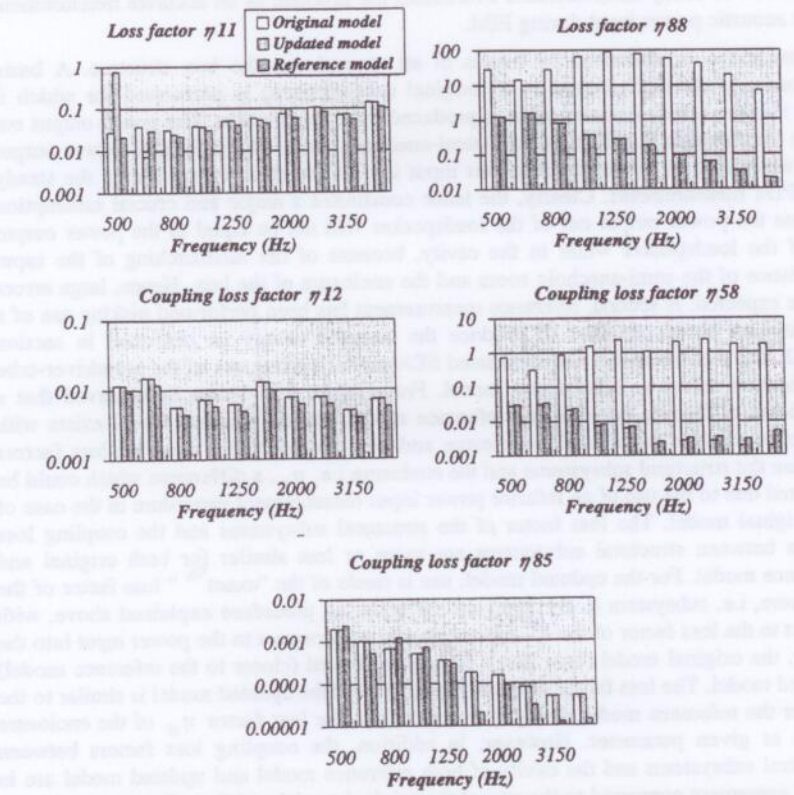

Figure 3.25 : SEA parameters for original, updated and reference model.

3.6 Measurement strategy.

One of the concerns of the engineer when applying PIM is related to the set-up of the PIM experiments in order to obtain accurate yet affordable estimates of the normalized energy matrix. Roughly, the following parameters are essential with respect to defining the test set-up : number of subsystems, number of available acquisition channels, number of excitation and response points to be taken into account. Several plausible measurement set-ups as a function of these parameters are conceivable and are described below.

It is frequently suggested in literature to use a fixed number of excitation and response points, i.e. *3* excitation and *5* response locations per subsystem, in order to obtain sufficiently accurate SEA parameters; see also BIES and HAMID [14]. Naturally, this statement does not hold for whatever type of structure. Some structures require more measurement points than others due to the larger variance of the energy density.

As pointed out in section *3.4.3*, PIM requires the measurement of the FRF's between the acceleration and the force at a sufficient number of response and excitation points. The squared amplitude of the non-diagonal terms of the FRF matrix is shown to be proportional to the *equivalent* reverberent energy of the subsystem. The diagonal terms of the FRF matrix are proportional to the equivalent power input into the subsystem. The previous statement can be translated into a mathematical formalism in the following way :

$$\begin{bmatrix} H_{11}(\omega) & H_{12}(\omega) & \cdots & H_{1N}(\omega) \\ H_{21}(\omega) & H_{22}(\omega) & \ddots & \vdots \\ \vdots & \ddots & \ddots & \vdots \\ H_{N1}(\omega) & \cdots & \cdots & H_{NN}(\omega) \end{bmatrix} \Rightarrow \begin{bmatrix} Im[H_{11}(\omega)] & |H_{12}(\omega)|^2 & \cdots & |H_{1N}(\omega)|^2 \\ |H_{21}(\omega)|^2 & Im[H_{22}(\omega)] & \ddots & \vdots \\ \vdots & \ddots & \ddots & \vdots \\ |H_{N1}(\omega)|^2 & \cdots & \cdots & Im[H_{NN}(\omega)] \end{bmatrix} \quad (3.86)$$

Where the FRF matrix of equation (3.86) is associated with one specific subsystem. The rows and columns represent excitation respectively response location of that specific subsystem.

Hence, to obtain an accurate value of the space averaged equivalent energy of vibration of a subsystem, one has to measure a sufficient number of non-diagonal terms of the FRF matrix. An averaged power input can be obtained by acquiring and averaging a sufficient number of diagonal terms of the FRF matrix.

3.6.1 Description of the test set-up.

This paragraph puts into perspective some relevant solutions concerning the measurement sequence of PIM. Because when applying PIM for a relatively large structure (e.g. 50 subsystem model in the case of a car), a vast amount of data is obtained through extensive and expensive measurements. For example, for a *50*-subsystem model and for *10* measurement points/subsystem (to perform the averaging), already $50 \times 50 \times 10 = 25000$ FRF's should be obtained.

3.6.1.1 First measurement strategy : Concentration of all instruments on one subsystem.

The first measurement set-up constitutes basically of the acquisition of a sufficient number of FRF's such that *all* response instruments are concentrated on *one* subsystem and that the excitation is applied at a sufficient number of excitation locations on one subsystem. An example for which five response instruments are located on one subsystem is given below. Three excitation locations are applied. The complete measurement procedure is explained in detail below.

- Subsystem *1* is excited at three excitation locations (*). Five response locations (o) are chosen on the first subsystem to measure the relevant FRF's. *3x5=15* FRF's are acquired in this case. E_{11} can be calculated.

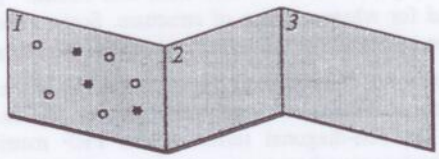

- Five response locations are chosen on the second subsystem. The FRF's are acquired for excitation of the first subsystem. E_{21} can be calculated.

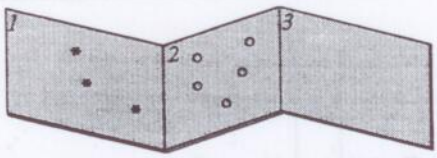

- This procedure is repeated for the response measurements of subsystems 3 to n.
- Subsystem 2 is excited, the response instruments are mounted on the first subsystem. E_{12} can be calculated.

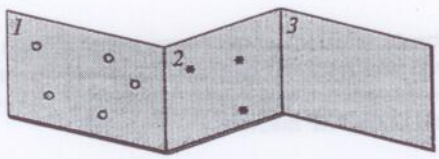

- Successively, the response instruments are mounted on the subsystem *2* to *n*.
- The same procedure is repeated for the excitation of subsystem *3* to *n*.

For the measurement procedure described above, changing the excitation location from one subsystem to the other takes place after changing the response subsystem. Eventually, an equivalent measurement set-up can be thought of such that first the response instruments are changed from one subsystem to the other after which the excitation points are changed from one subsystem to the other. Both approaches are in principle similar. For shaker excitation, it is most opportune to replace first the response instruments followed by changing the location of the shaker. In the case of hammer

excitation, it is most suitable to replace the response instruments from one subsystem to the other after all subsystems are excited.

The main disadvantage of this measurement procedure is that it implies the completion of the whole measurement cycle in order to obtain a normalized energy matrix ready to be inverted. In other words, the SEA parameters can only be obtained after the whole set of measurements is terminated. Therefore, it can eventually be found that too much measurement effort is spent on obtaining the desired accuracy (in terms of variance) of the SEA parameters. If on the other hand it holds that the number of excitation and response points is not sufficient to obtain the desired accuracy after the first measurement cycle, a second set of data has to be acquired involving the complete measurement procedure once again. A second important disadvantage of this test set-up is that due to the fact that all response instruments are located on one single subsystem, problems can arise when dealing with lightweight structures because of mass distortion. Third, if the excitation at the excitation points of a subsystem is applied *at the same time* (Multi Input shaker excitation) then the extent of the total direct vibration field near the points of excitation can become large, especially for lower frequencies. Nonetheless, the response instruments should be located in the reverberent field, which in this case can become small.

It can be noted that for the measurement procedure outlined above, it holds that :

- A total number of $N_e \cdot n^2$ acquisitions are performed.
- For every excited and measured subsystem, $N_e \cdot N_r$ non-diagonal FRF's are obtained, hence the averaging of the energies can be performed using $N_e \cdot N_r$ values.

Where N_e represents the number of excitation points per subsystem, N_r denotes the number of response points per subsystem and n stands for the number of subsystems.

In order to obtain a sufficient number of *diagonal* terms of the FRF matrix (power input), one can choose basically between two options :

- The power input measurements are performed after the complete acquisition of the non-diagonal terms of the FRF matrix. This approach is appropriate when using hammer excitation. Eventually, one can measure direct and indirect FRF's at the same time by exciting the structure according to the following figure :

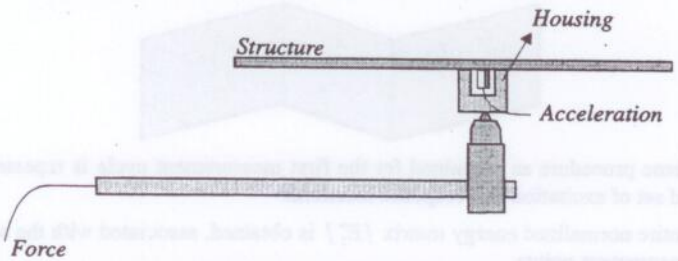

Figure 3.26 : Power input set-up for hammer excitation.

However, in this case, the housing of the accelerometer should be replaced and attached for every single excitation location which can take quite some time.

- The acquisition of the diagonal terms of the FRF matrix is done during the acquisition of the non-diagonal terms. Hence, for every excitation point, the driving FRF is measured. In the case of shaker excitation, this approach should be preferred.

3.6.1.2 Second measurement strategy : One response point and one excitation point on each subsystem.

The basis of the approach described below is that the energy levels are measured on *all* subsystems at the same time, while exciting each specific subsystem in turn at one location. The entire measurement procedure is explained in detail below.

First measurement cycle :

- On every subsystem one response point (o) and one excitation point (*) are chosen.

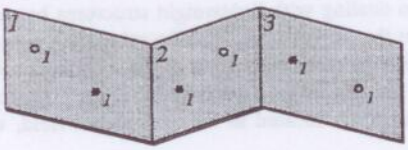

- Subsystem *1* is excited, the FRF's (non-diagonal and driving FRF) between all responses and the excitation force are measured.
- Next, the second subsystem is excited at its first excitation location, the driving FRF and the non-diagonal terms of the FRF matrix are measured.
- The same procedure is repeated for the excitation of subsystem *3* to *n*.
- The response spectra are converted into energies.
- The complete normalized energy matrix $[E_1^n]$, associated with the first measurement position can already be obtained and is ready to be inverted. The SEA parameters can be calculated according to equation (3.9).

Second measurement cycle :

- On every subsystem, another excitation location and another response location are chosen.

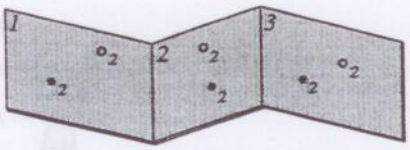

- The same procedure as explained for the first measurement cycle is repeated for the second set of excitation and response locations.
- The entire normalized energy matrix $[E_2^n]$ is obtained, associated with the second set of measurement points.

Two strategies concerning the averaging of the acquired data can be thought over :

Averaging type 1. The second set of excitation and response locations allows to acquire a second set of measured energy levels and corresponding power inputs. The averages of

the energy levels associated with the first and the second set of measurement points are calculated. Similarly, the averaged power inputs are calculated :

$$E_{ij} = \frac{E_{ij,1} + E_{ij,2}}{2} \quad \text{and} \quad P_j = \frac{P_{j,1} + P_{j,2}}{2} \tag{3.87}$$

Next, the normalized energy levels E_{ij}^n are calculated according to equation (3.7). Hence, by applying the averaging type *1* approach, the energy levels and power inputs are averaged in advance, i.e. before the calculation of the normalized energy values.

Averaging type 2. After the second set of measurements, the normalized energies associated with the second set of measurements are calculated by using the data of the second set of measurements exclusively :

$$E_{ij,2}^n = \frac{\omega \cdot E_{ij,2}}{P_{j,2}} \tag{3.88}$$

Subsequently, the averages of the normalized energies associated with both sets of measurement points are calculated :

$$E_{ij}^n = \frac{E_{ij,1}^n + E_{ij,2}^n}{2} \tag{3.89}$$

Hence for the second averaging approach, the averaging is performed with respect to the *normalized energy values*.

Independent of the averaging procedure, the SEA parameters can be obtained by means of equation (3.9). Experimental results however revealed no significant differences between both averaging approaches.

In the same way, after the second set of measurements, a third set of data can be acquired yielding a third set of SEA parameters. Thus, by performing subsequent sets of measurements, corresponding to a randomly chosen set of *single* excitation and *single* response locations on each subsystem, and by evaluating the SEA parameters after every measurement sequence it is possible to obtain *on-line* an estimate of the convergence of the SEA parameters as a function of the number of excitation and response locations.

It can be noted that for this measurement procedure, it holds that :

- A total number of $N \cdot n$ response instruments (e.g. accelerometers) is replaced.
- A total number of $N \cdot n$ excitations is applied.
- For every excited and measured subsystem, N non-diagonal and N driving FRF's are obtained, hence the averaging of the normalized energies can be performed by taking into account N values.

With N representing the number of measurement points.

Advantages :

- An on-line assessment of the convergence of the SEA parameters as a function of the number of measurement points is feasible, giving rise to the appearance of convergence curves. These curves make it possible to assess the convergence of the

SEA parameters as a function of the measurement effort. The measurement procedure applied in here incorporates the notable advantage that the labor intensive PIM measurements can be terminated when the parameters are sufficiently converged to their "exact" value. Consequently, the measurement effort can be kept to a minimum. One should not wait until the measurements are completely finished to obtain the SEA parameters. A convergence curve consisting of the coupling loss factor η_{12} of the box at *1000* Hz and at *4000* Hz is shown in figure 3.27.

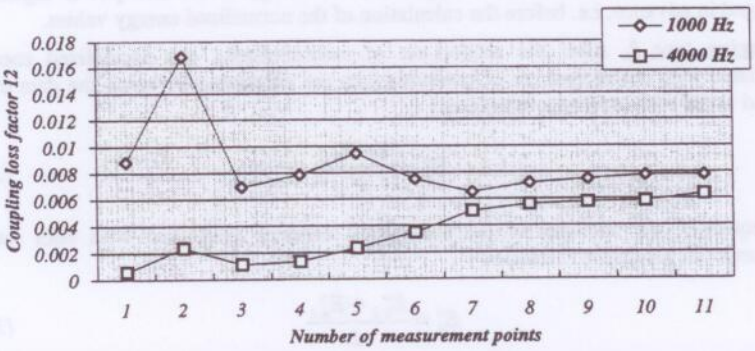

Figure 3.27 : Convergence of the SEA coupling loss factor as a function of the number of measurement points.

- Only one response instrument (for the basic configuration) is mounted on the structure, hence the mass distortion for lightweight structures can be kept low.

Disadvantages :

The number of acquisition channels should at least equal the number of subsystem plus one. If the number of available acquisition channels is too low, it is still possible to apply this measurement strategy and to assess the convergence curves, providing slight modifications. Instead of measuring the energy level of all subsystems at the same time, it is possible to split up the response measurements such that a limited number of subsystems is measured during the excitation of one subsystem. Next, the response instruments are replaced on the other subsystems and the responses are measured. Thus instead of obtaining one single column of the normalized energy matrix at once (corresponding to the excitation of a specific subsystem), two or more separate measurements are needed. One can still assess the convergence of the SEA parameters and perform the statistics in a similar way. Naturally, due to the fact that this technique implies *sequential* energy measurements, performing a complete set of measurements is much more labor intensive.

3.6.1.3 Third approach : hybrid form.

The measurement set-ups described above constitute in one way or another two extreme set-ups. For the first approach, *all* instruments are located on *one* subsystem. In the case of the second approach, *all* subsystems are equipped with *one* response instrument. It is however possible to conceive a hybrid form of these two methods in such a way that the excitations and the responses are respectively applied and measured at several points at

the same time and in such a way that *several* subsystems are equipped with response instruments. A corresponding test set-up is schematically pictured below (figure *3.28*) incorporating two different excitation locations (*) and three response locations (o) for each subsystem and for each measurement cycle. Hence, $2 \times 3 = 6$ non-diagonal FRF's are associated with one energy value for every single measurement cycle. For the hybrid approach, the convergence curves are modified such that every additional point on the curve corresponds to six additional FRF's taken into account for the averaging (for the second approach described in section 3.6.1.2, every point of the convergence curve corresponds to only one additional FRF).

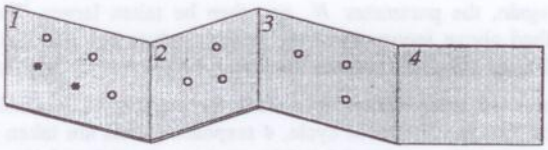

It will be supposed further on that the parameters N_e and N_r represent respectively the number of excitation and response locations associated with one subsystem. N_s denotes the number of subsystems on which response instruments are located during a specific measurement cycle. Hence, N_s equals *3*, N_e equals 2 and N_r equals 3 in the case of the set-up pictured above.

3.6.2 Comparison and cost estimation.

For an entire PIM measurement, several distinct actions have to be undertaken ranging from acquisition to postprocessing of the acquired data. The following table states a typical and rough estimate of the major costs and profits in the case of the three measurement procedures previously established.

	Cost		
	First approach	*Second approach*	*Hybrid*
Number of acquisitions	$N_s \cdot n^2$	$N \cdot n$	$N_s \cdot n \cdot round(n/N_s + 0.5)$
Number of channels to be available	$N_s + 1$	$n+1$	$N_s \cdot N_r + 1$
	Profit		
	First approach	*Second approach*	*Hybrid*
Number of measured FRF's/ subsystem	$N_e \cdot N_r$	N	$N_e \cdot N_r$

Table 3.1 : Cost of the measurement procedures.

Every one single PIM measurement should be examined from the measurement set-up point of view using table *3.1* as a general guideline. The first approach is characterized by the possibility to obtain a large number of FRF's (i.e. $N_e \cdot N_r$) per subsystem because all response instruments are located on one single subsystem and consequently the parameters N_e and N_r can become large. The second approach incorporates the possibility to assess the convergence of the parameters as a function of the number of excitation and response points taken into account. The number of FRF's per subsystem which can be obtained is however low. The hybrid approach combines the advantages of both approaches.

It is recommended in general to apply the hybrid approach to minimize the measurement effort and to obtain accurate results. For the first measurement cycle, the number of response points and the number of excitation points should be *relatively large* in order to acquire a relatively large number of FRF's per subsystem. If the desired accuracy has not been attained after the first measurement cycle, the measurement procedure based on the hybrid approach should be repeated once again. For the second measurement cycle however, the number of response and excitation points can be taken smaller compared to the first measurement cycle. The parameter N_s can therefore be taken larger (as long as $N_r \cdot N_s + 1 <$ the number of available acquisition channels). Similarly, a third measurement cycle can be performed for which the parameters N_e and N_r can be decreased once again, the parameter N_s can then be taken larger. The measurement procedure described above incorporates the notable advantage that the FRF's can be obtained in an efficient way. An example illustrates the previously established statement.

Suppose the number of subsystem n equals *50*, the number of available channels N_c equals *64*. For the first measurement cycle, *4* response points are taken in combination with *4* excitation points. From table 3.1 it follows that a feasible solution with respect to the parameter N_s equals *15*.

The main parameters N_e, N_r and N_s yield a cost (based on the number of acquisitions) of $4 \times 50 \times round(50/15) = 800$. A total number of $4 \times 4 = 16$ FRF's per subsystem is obtained in this way. If after the first measurement cycle, the number of FRF's is too low with respect to the expected accuracy, then a second set of data can be acquired. For the second measurement cycle, the number of response points and excitation points is lowered, resulting in the following measurement parameters :

$$N_e = 3,\ N_r = 3,\ N_s = 20 \qquad (3.90)$$

A total number of $3 \times 3 = 9$ FRF's per subsystem is obtained for the second measurement cycle with a total cost of $3 \times 50 \times round(50/20) = 450$ (in terms of the number of acquisitions).

Combining the first and the second measurement set-up, a total number of *25* FRF's is obtained. Whether or not the measurement can be terminated depends on the accuracy which is obtained after two measurement cycles. The accuracy can be assessed by means of the convergence curves (see *3.6.1.2*) or by using the confidence levels (see Chapter *4*). Eventually a third measurement cycle can be performed.

3.6.3 Conclusion.

Because SEA parameter identifications based on PIM are quite expensive in terms of measurement effort, especially for large systems, it is essential to efficiently perform the measurements. Section 3.6.1 stated some feasible set-ups characterized by the measurement parameters, i.e. the number of response locations, the number of excitation locations, the number of subsystems for which response spectra are simultaneously acquired. Although it is impossible to define these parameters in advance in general, it is suggested to perform some measurement cycles such that for *consecutive* measurements cycles the number of response points and the number of excitation points are lowered and the number of subsystems for which response spectra are acquired is increased. An acceptable initial value for the number of inputs and the number of outputs equals *3* or *4*. A small example illustrated the measurement procedure. Let's assume that a system

which comprises *50* subsystems (typical for an automotive vehicle), has to be identified; this results in a total number of *1250* acquisitions to obtain *25* FRF's per subsystem. Taking *5* minutes per acquisition, the *50* subsystem model is identified within an period of a the order of weeks. Nonetheless, every additional, substantial reduction of measurement effort is most welcome.

3.7 Modal density and modal overlap measurements.

One of the fundamental SEA parameters is the modal density which expresses the energy storage in a subsystem. In addition, the modal density is related to the modal overlap factor by :

$$M = \omega \cdot \eta \cdot n \qquad (3.91)$$

Where M represents the modal overlap, η stands for the internal loss factor and n represents the modal density.

Analytical expressions of modal densities are available for simple structures (see chapter *5*). The modal density is evaluated to check the reciprocity relation (See chapter *2*) and to evaluate the modal overlap factor which is crucial with respect to the applicability of the SEA model.

Experimental techniques have been reported in literature in case of complex structures for which no analytical results are available. In the framework of this thesis, a classical existing modal density evaluation procedure has been implemented. Two main experimental techniques are conceivable : *mode count technique* and *mobility techniques*.

The mode count technique is based on counting the peaks of relevant FRF's which are associated with a structure. RENNISON and BULL [83] applied the mode count technique to obtain modal densities of cylindrical pipes. Good agreement with theoretical results was obtained. Nonetheless, the mode count is not applicable for structures exhibiting a high modal overlap (high damping and/or high modal density). In addition, the mode count technique tends to be time consuming.

The point mobility technique is based on the relation between modal density and mobility (chapter *2*). The point mobility technique is advised when the modes are so closely packed or when the damping is so large that counting resonance peaks is not feasible. For the experimental method adopted in this thesis, use is made of the point mobility technique, derived by CREMER et al [79].

CLARKSON and POPE [8] report on the experimental identification - via the measurement of point mobilities - of modal densities of flat plates and cylinders and conclude that the method can be used for uniform structures. BROWN [13] investigates the experimental identification procedure in the case of lightly damped structures for which it is difficult to make successful measurements using classical experimental techniques. The author applied an alternative of the existing techniques, based on random excitation and extremely short data lengths. The technique is shown to give good results on lightly damped structures. KESWICK and NORTON [12] present an overview of modal density measurement techniques based on point impedance measurements with emphasis on lightly damped pipeline systems. Their results revealed good agreement between experiment and theory provided that specific experimental requirements are met.

According to CREMER et al. [79], the modal density is equal to the real part of the point mobility by :

$$n(\omega)=\frac{4m}{\Delta\omega}\cdot\int_{\omega_1}^{\omega_2}<Re[Y(\omega)]>d\omega \qquad (3.92)$$

Where $n(\omega)$ is the modal density evaluated over the frequency band $[\omega_1,\omega_2]$, m represents the total mass of the structure. $<Y>=<G+j\cdot C>=<S_{vf}(\omega)/S_{ff}(\omega)>$ denotes the point mobility averaged along the structure. It should be emphasized that the equations are approximations. CLARKSON [17] states that at least 5 measurement points are needed in order to obtain accurate results.

As an interesting aside, it can be noted that in the case of a flat plate, the modal density equals $A\sqrt{12\rho(1-\gamma^2)}/2t\sqrt{E}$. Hence by substituting the modal density into equation (3.94), it follows that the real part of the point mobility G is given by :

$$G=\frac{\sqrt{12\rho(1-\gamma^2)/E}}{8\rho t^2} \qquad (3.93)$$

This result corresponds to the point mobility of an infinite plate (CREMER and HECKL [79]), showing that averaged impedance functions of a finite plate are the same as those of the same system infinitely extended.

KESWICK and NORTON address the importance of a mass correction to be introduced for lightweight structures. The masses between the force transducer of the impedance head and the structure can corrupt the measurement of the force spectrum $S_{ff}(\omega)$. Note that the real part of the cross-spectrum $S_{vf}(\omega)$ will not be affected by this added mass as already pointed out in section *3.4.2.1.* The force spectrum applied to the structure is corrected in the following way :

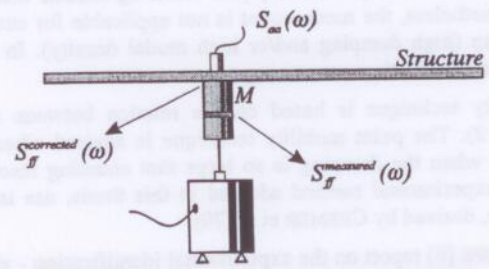

Figure 3.27 : Measurement set-up for modal density with an additional mass between force cell and structure.

From figure *3.27*, it follows that :

$$F^{corrected}=F^{measured}-M\cdot A. \qquad (3.94)$$

Hence for the corrected spectrum $S_{ff}^{corrected}(\omega)$ it holds that :

$$S_{ff}^{corrected}(\omega)=S_{ff}^{measured}(\omega)+M^2\cdot S_{aa}(\omega)-2M\,Re\left[S_{af}(\omega)\right] \qquad (3.95)$$

Hence the modal density is given by :

$$n(\omega) = \frac{4m}{\Delta\omega} \cdot < Re\left[\int_{\omega_1}^{\omega_2} \frac{S_{vf}(\omega)}{S_{ff}^{corrected}(\omega)} d\omega\right] > \qquad (3.96)$$

The procedure outlined above is implemented in the SEA program SEAPACK. A PIM measurement performed by SEAPACK calculates for every excitation point of a subsystem the relevant point mobilities and hence the modal densities of the subsystem. The modal overlap factors are obtained by applying equation (3.91). Figure *3.29* shows the modal overlap factor for the fifth plate of the box. All modal overlap factors are larger than *1*, hence fulfilling a necessary condition concerning the applicability of SEA.

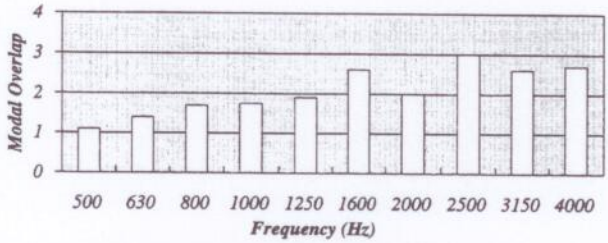

Figure 3.30 : Modal overlap of the plate.

3.8 Conclusion

Chapter *3* presents the methodology of the experimental identification of SEA parameters (PIM) and the way PIM is implemented in the SEA program SEAPACK. A straightforward identification procedure is applied, consisting of a set of input / output measurements (power input and energy level) of the subsystems. A normalized energy matrix is obtained, the inverse of which represents the total loss factor matrix.

Energy measurements and power input measurements are explained in the case of structural and acoustical subsystems. Structural energy measurements are based upon the measurement of acceleration response spectra at randomly chosen points of the subsystem. For acoustical subsystems, microphones are applied. Structural power input measurements are performed using an impedance head. Some important remarks regarding active and reactive power input are presented. For acoustical power input measurements, a special device, incorporating a horndriver, tube, horn and two quarter-inch microphones is constructed and calibrated. The formulas to calculate the acoustic intensities are based upon the plane wave characteristics of the acoustic waves in the tube. The acoustic power input measurement device works well in the high frequency range.

The need of an energy correction coefficient and the way to evaluate the energy correction coefficient of subsystems is addressed in section *3.5*. An extension of the application of decay techniques constitutes the updating of the measured normalized energy values. Based upon a prior knowledge of some of the parameters of the SEA model, it is possible to update the measurements; e.g. determine the energy correction coefficient or update the acoustical power inputs into a cavity during PIM.

The PIM method, the way it is implemented in here makes use of FRF's (direct and indirect FRF's) from which *equivalent* energies and power inputs can be calculated.

Finally, some notes are made regarding the measurement set-up. Especially for large structures (e.g. a car including 50 subsystems), the number of acquisitions is quite large, resulting in expensive measurement sequences. One should therefore carefully contemplate the measurement set-up, which is a function of the number of subsystems, the number of acquisition channels and the number of response and excitation points to be taken into account.

4. CONTRIBUTIONS TO STATISTICAL AND SENSITIVITY ASPECTS OF PIM.

4.1 Statistical Analysis of PIM.

As pointed out in chapter *3*, an accurate estimation of the SEA parameters implies reliably estimated normalized energy values. It is stated in literature that the expedient of sequentially driving the driven subsystem at a few points chosen at random is sufficient to adequately simulate statistical independence for SEA purposes. For response measurements, approximately five locations are taken to give adequate results. For the excitation, at least three locations should be taken. These numbers should only be considered as rough guideline or a rule of thumb. In practice, however, the accuracy of the SEA model will depend on the specific number of excitation and response points and is definitely not the equivalent for whatever structure.

There will always be a certain spread associated with the normalized energy levels due to the averaging of a *finite* number of normalized energy values. It is therefore meaningful to calculate the associated confidence levels and to comprehend how the confidence levels of the normalized energies can be translated into confidence levels associated with SEA parameters.

Standard conventional PIM measures the expected mean RMS value of the subsystem energy level and the power input level in the form of frequency spectra (most of third octave spectra). One of the topics of research of this thesis deals with the statistics associated with PIM. Formulas have been derived and methods are developed allowing one to evaluate the confidence levels of the SEA parameters and allowing one to obtain on-line data concerning the convergence of the SEA parameters as a function of the number of measurement points.

Because the populations which are dealt with in PIM are infinite (infinite number of potential excitation and response points), it is necessary to use a sample, and infer from it results pertaining the entire population, basically the mean value and the confidence

limits are of concern. The statistical problem we are dealing with in the case of PIM can be stated in the following way :

From the measurements, a sample of *normalized energy matrices* is obtained, each corresponding to a specific measurement point (excitation and response point) of the structure. From these data, estimates of the mean value and of the confidence levels of the *SEA* parameters and predictions should be calculated.

Paragraph *4.1.1* outlines the calculation of the statistics of the normalized energies. Paragraph *4.1.2* extends the statistics to the SEA parameters. Paragraph *4.1.3* addresses the statistical analysis of the SEA predictions.

4.1.1 Confidence levels of the normalized energies.

Before proceeding with the statistics of the normalized energy values, the following side remark is made concerning the distribution of the estimated mean of a variable in the case of a small sample size *N*.

If $\bar{x}$ is the estimated mean of a sample of size N taken from a normal population having the mean μ and the variance σ^2, then

$$t = \frac{\bar{x} - \mu}{\sigma / \sqrt{N}} \qquad (4.1)$$

is the value of a random variable having the t-distribution with the parameter *N-1*.

Note that further on the overbar $\bar{\ }$ denotes the estimated value of the relevant variable.

Just as the standard normal distribution, the *t*-distribution has the mean *0*, but its variance depends on the parameter *N*, called the number of degrees of freedom. The *t*-distribution approaches the standard normal distribution if $N \to \infty$.

For PIM, the sample size, i.e. the number of measurement points is quite small. Hence, the *t*-distribution should in principle be used instead of the normal distribution to evaluate the confidence levels of the estimated normalized energy values. For practical reasons however and because later on the confidence levels of the SEA parameters are in any event approximated by a linear Taylor approximation, it is found more convenient to determine the confidence levels of all SEA parameters and SEA predictions under the assumption of a normally distributed population. Hence, further on in this dissertation, *95%* confidence levels correspond to the confidence interval $[\bar{x} - 3s, \bar{x} + 3s]$.

Depending upon the type of averaging, particular statistical formulas regarding the normalized energies can be derived.

4.1.1.1 Averaging type 1.

In this case, the ij^{th} element of the normalized energy matrix is estimated by :

$$\bar{E}_{ij}^{n} = \frac{\sum_{k=1}^{N} E_{ij,k}}{\sum_{k=1}^{N} P_{j,k}} = \frac{\bar{E}_{ij}}{\bar{P}_{j}} \qquad (4.2)$$

Where $E_{ij,k}$ denotes the measured energy level of subsystem i at the response location k when subsystem j is excited. $P_{j,k}$ represents the power input into subsystem j at the excitation point k.

The variance of a normalized energy term E_{ij}^n is given by equation (4.3) :

$$s^2_{E^n_{ij}} = \left(\frac{\partial E^n_{ij}}{\partial E_{ij}}\right)^2 \cdot s^2_{E_{ij}} + \left(\frac{\partial E^n_{ij}}{\partial P_j}\right)^2 \cdot s^2_{P_j} \quad \textit{or indeed by} \quad : \quad s^2_{E^n_{ij}} = \frac{1}{\overline{P}_j^2} \cdot s^2_{E_{ij}} + \frac{\overline{E}_{ij}^2}{\overline{P}_j^4} \cdot s^2_{P_j} \qquad (4.3)$$

With :

$$s^2_{E_{ij}} = \frac{1}{N} \cdot \sum_{k=1}^{N} \frac{\left(E_{ij,k} - \overline{E}_{ij}\right)^2}{N-1} \quad \textit{and} \quad s^2_{P_j} = \frac{1}{N} \cdot \sum_{k=1}^{N} \frac{\left(P_{j,k} - \overline{P}_j\right)^2}{N-1} \qquad (4.4)$$

Where $s^2_{E_{ij}}$ and $s^2_{P_j}$ are representing the variance of the sample of the measured energy values respectively power input values.

4.1.1.2 Averaging type 2.

The mean value of the ij^{th} element of the normalized energy matrix is calculated by :

$$\overline{E}^n_{ij} = \frac{1}{N} \cdot \sum_{k=1}^{N} E^n_{ij,k} \qquad (4.5)$$

The sample variance of the normalized energy values E_{ij}^n is given by :

$$s^2_{E^n_{ij}} = \frac{1}{N} \cdot \sum_{k=1}^{N} \frac{\left(E^n_{ij,k} - \overline{E}^n_{ij}\right)^2}{N-1} \qquad (4.6)$$

By assuming a normal population of normalized energy levels, the confidence levels readily follow.

4.1.2 Confidence levels of the SEA parameters.

This paragraph is concerned with providing expressions for the variance and hence the confidence intervals of the SEA parameters as a function of the variance associated with the normalized energy values. The total loss factor matrix $[\eta^o]$ is estimated through the inverse of the normalized energy matrix $[E^n]$. By performing a first order Taylor expansion of the inverse of the normalized energy matrix in terms of the elements E^n_{lm}, the variance of the elements of the total loss factor matrix can be written in terms of variances of the elements of the normalized energy matrix :

$$s^2_{\eta^o_{ij}} \cong \sum_{l,m=1}^{n} \left(\frac{\partial \eta^o_{ij}}{\partial E^n_{lm}}\right)^2 \cdot s^2_{E^n_{lm}} \qquad (4.7)$$

It holds that (see appendix B) :

$$\frac{\partial \eta_{ij}^{\circ}}{\partial E_{lm}^{n}} = -\eta_{ii}^{\circ} \cdot \eta_{mj}^{\circ} \qquad (4.8)$$

By combining equation (4.7) and equation (4.8), the variance associated with η_{ij}° is given by :

$$s_{\eta_{ij}^{\circ}}^{2} \cong \sum_{l,m=1}^{n} \left(\overline{\eta}_{ii}^{\circ} \cdot \overline{\eta}_{mj}^{\circ}\right)^{2} \cdot s_{E_{lm}^{n}}^{2} \qquad (4.9)$$

The SEA coupling loss factor η_{ij} $(i \neq j)$ is given in terms of the elements of the total loss factor matrix through :

$$\eta_{ij} = -\eta_{ji}^{\circ} \qquad i \neq j \qquad (4.10)$$

Thus, the variance of the estimated SEA coupling loss factor η_{ij} can be written in terms of the variances of the normalized energy values E_{lm}^{n} :

$$s_{\eta_{ij}}^{2} \cong \sum_{l,m=1}^{n} \left(\overline{\eta}_{jl}^{\circ} \cdot \overline{\eta}_{mi}^{\circ}\right)^{2} \cdot s_{E_{lm}^{n}}^{2} \qquad i \neq j \qquad (4.11)$$

Note that equation (4.11) can be regarded as yielding the contribution of the variance of every single normalized energy E_{lm}^{n} to the variance of the SEA coupling loss factor η_{ij}. The major contribution will occur if $l=j$ and if $m=i$, in which case the contribution reduces to $(\overline{\eta}_{jj}^{\circ} \cdot \overline{\eta}_{ii}^{\circ})^{2}$. Where $\overline{\eta}_{ii}^{\circ}$ and $\overline{\eta}_{jj}^{\circ}$ represent the *dominant diagonal* terms of the total loss factor matrix.

In the case of the SEA internal loss factors :

$$s_{\eta_{ii}}^{2} \cong \sum_{l,m=1}^{n} \left(\frac{\partial \eta_{ii}}{\partial E_{lm}}\right)^{2} \cdot s_{E_{lm}^{n}}^{2} \qquad (4.12)$$

Besides it holds that :

$$\eta_{ii} = \sum_{k=1}^{n} \eta_{ki}^{\circ} \qquad (4.13)$$

Combining equations (4.8) and (4.13), it follows that :

$$\frac{\partial \eta_{ii}}{\partial E_{lm}^{n}} = \sum_{k=1}^{n} \frac{\partial \eta_{ki}^{\circ}}{\partial E_{lm}^{n}} = -\sum_{k=1}^{n} \eta_{ki}^{\circ} \cdot \eta_{mi}^{\circ} = -\eta_{mi}^{\circ} \cdot \eta_{ii} \qquad (4.14)$$

Therefore, equation (4.12) becomes :

$$s_{\eta_{ii}}^{2} \cong \sum_{l,m=1}^{n} \left(\overline{\eta}_{mi}^{\circ} \cdot \overline{\eta}_{ii}\right)^{2} \cdot s_{E_{lm}^{n}}^{2} \qquad (4.15)$$

Where $s_{E_{lm}^{n}}^{2}$ is given by equation (4.3) or by equation (4.6), depending upon the type of averaging.

The calculation of the confidence levels can be carried out after the data associated with each measurement point are acquired. One should then decide whether or not the required accuracy has been achieved and whether or not the PIM measurements can be

terminated. Furthermore, due to the fact that after every measurement position a complete set of normalized energy data is available for which the SEA parameters can be calculated, it is feasible to obtain an *on-line* overview of the convergence of the SEA parameters and their confidence levels as a function of the number of measurement points. These convergence curves offer the engineer all essential data needed to decide whether or not a PIM measurement can be terminated.

4.1.3 Statistical analysis of SEA predictions.

Once a SEA model has been identified, one has the possibility to apply the model in order to perform vibration prediction, source localization, sensitivity analysis, transmission paths analysis etc. Because PIM does not yield exact values of the SEA parameters but rather inferences of means and variances of the corresponding statistical distributions, it is worthwhile to statistically analyze the SEA predictions. The next paragraph establishes the statistics associated with the SEA predictions. In other words, the accuracy of the predicted vibration levels, predicted source levels, predicted energy flow levels, contributions of the sources is assessed by applying variance analysis.

4.1.3.1 Vibration level prediction.

It is assumed that the power inputs into the different subsystems are given and that all SEA parameters of the SEA model are identified. The mean energy level of each subsystem can be estimated by applying the basic SEA equation (4.16) :

$$\{\overline{E}\} = \frac{1}{\omega} \cdot [\overline{\eta}^{\circ}]^{-1} \cdot \{P\} \qquad (4.16)$$

Where $\{P\}$ represents the known power input vector, $[\overline{\eta}^{\circ}]$ represents the estimated total loss factor matrix.

The SEA parameters are experimentally identified, therefore it is more convenient to rewrite equation (4.16) in terms of normalized energy values :

$$\{\overline{E}\} = \frac{1}{\omega} \cdot [\overline{E}^{n}] \cdot \{P\} \quad or \quad \overline{E}_i = \frac{1}{\omega} \cdot \sum_{k=1}^{n} \overline{E}_{ik}^{n} \cdot P_k \qquad (4.17)$$

Where $[\overline{E}^{n}]$ represents the estimated normalized energy matrix obtained by PIM.

Consequently, the variance of the predicted energy level of subsystem i as a function of the variances of the normalized energy levels is given by :

$$s_{E_i}^2 = \frac{1}{\omega^2} \cdot \sum_{k=1}^{n} s_{E_{ik}^n}^2 \cdot P_k^2 \qquad (4.18)$$

4.1.3.2 Source localization.

On the basis of the knowledge of the SEA parameters and of the knowledge of the energy levels of the different subsystems, it is possible to perform a source localization. By applying equation (4.19), one can estimate the source levels and one can obtain the

locations in terms of subsystem id's where energy enters the structure during operating conditions :

$$\{\overline{P}\} = \omega \cdot [\overline{\eta}^{o}] \cdot \{E\} \quad or \quad \overline{P}_i = \omega \cdot \sum_{k=1}^{n} \overline{\eta}_{ik}^{o} \cdot E_k \tag{4.19}$$

$\{E\}$ represents the known energy level vector, $\{\overline{P}\}$ represents the predicted power input vector.

The variance of the estimated power input into subsystem i as a function of the variances of the normalized energies of vibration E_{lm}^{n} is approximated by :

$$s_{P_i}^2 \cong \sum_{l,m=1}^{n} \left(\frac{\partial P_i}{\partial E_{lm}^{n}} \right)^2 \cdot s_{E_{lm}^{n}}^2 \tag{4.20}$$

Equation (4.20) can be written in the following form :

$$s_{P_i}^2 \cong \sum_{l,m=1}^{n} \left(\overline{\eta}_{il}^{o} \cdot \overline{P}_m \right)^2 \cdot s_{E_{lm}^{n}}^2 \tag{4.21}$$

4.1.3.3 Contribution of sources.

The contribution of a specific source j to the vibration level of an individual subsystem i can be calculated by evaluating the response of subsystem i due to the excitation of one specific subsystem j. Equation (4.22) represents mathematically the contribution in an efficient way :

$$\overline{E}_{ij}^{c} = \frac{1}{\omega} \cdot \overline{E}_{ij}^{n} \cdot P_j \tag{4.22}$$

Where $\overline{E}_{ij}^{c}$ represents the estimated contribution of source j (excitation of subsystem j only) with respect to the energy level of subsystem i.

- In the case of given power inputs during operating conditions, the variance of the contribution E_{ij}^{c} is given by :

$$s_{E_{ij}^{c}}^2 = \frac{1}{\omega^2} \cdot s_{E_{ij}^{n}}^2 \cdot P_j^2 \tag{4.23}$$

- For given energy levels during operating conditions, the contribution of specific sources to the vibration level of an individual subsystem is given by :

$$\overline{E}_{ij}^{c} = \overline{E}_{ij}^{n} \cdot \sum_{k=1}^{N} \overline{\eta}_{jk}^{o} \cdot E_k \tag{4.24}$$

The variance of the contribution E_{ij}^{c} can be approximated in terms of variances of the normalized energy levels E_{lm}^{n} by :

$$s_{E_{ij}^{c}}^2 \cong \sum_{l,m=1}^{n} \left(\frac{\partial E_{ij}^{c}}{\partial E_{lm}^{n}} \right)^2 \cdot s_{E_{lm}^{n}}^2 \tag{4.25}$$

The derivative $\partial E_{ij}^{c} / \partial E_{lm}^{n}$ can be evaluated in the following way :

- If $l \neq i$ or $m \neq j$

$$\frac{\partial E_{ij}^{c}}{\partial E_{lm}^{n}} = \overline{E}_{ij}^{n} \cdot \sum_{k=1}^{n} \frac{\partial \eta_{jk}^{o}}{\partial E_{lm}^{n}} \cdot E_k = -\frac{1}{\omega} \cdot \overline{E}_{ij}^{n} \cdot \overline{\eta}_{ji}^{o} \cdot \overline{P}_m \tag{4.26}$$

- If $l = i$ and $m = j$

$$\frac{\partial E_{ij}^{c}}{\partial E_{ij}^{n}} = \sum_{k=1}^{n} \overline{\eta}_{jk}^{o} \cdot E_k + \overline{E}_{ij}^{n} \cdot \sum_{k=1}^{n} \frac{\partial \eta_{jk}^{o}}{\partial E_{ij}^{n}} \cdot E_k = \frac{1}{\omega} \cdot \left(1 - \overline{E}_{ij}^{n} \cdot \overline{\eta}_{ji}^{o}\right) \cdot \overline{P}_j \tag{4.27}$$

Hence, equation (4.25) becomes :

$$s_{E_{ij}^{c}}^{2} \cong \frac{1}{\omega^2} \cdot \overline{E}_{ij}^{n\,2} \sum_{l \neq i, m \neq j}^{n} \left(\overline{\eta}_{jl}^{o} \cdot \overline{P}_m\right)^2 \cdot s_{E_{lm}^{n}}^{2} + \frac{1}{\omega^2} \cdot \left(1 - \overline{E}_{ij}^{n} \cdot \overline{\eta}_{ji}^{o}\right)^2 \cdot \overline{P}_j^{2} \cdot s_{E_{ij}^{n}}^{2} \tag{4.28}$$

4.1.3.4 Energy flow prediction.

Energy flow prediction assumes given energy levels or given power input levels. A distinction should be made between both :

4.1.3.4.1 Given energy levels.

Because the energy levels are given, no variability is associated with the energy levels, and the energy flow can be estimated by :

$$\overline{P}_{ij} = \overline{\eta}_{ij} E_i \tag{4.29}$$

Where $\overline{P}_{ij}$ represents the predicted energy flow from subsystem i to subsystem j.

The variance of the energy flow $\overline{P}_{ij}$ is estimated through :

$$s_{P_{ij}}^{2} = s_{\eta_{ij}}^{2} E_i^2 \tag{4.30}$$

Where the variance of the SEA parameters is given by equation (4.11).

4.1.3.4.2 Given power input levels.

The mean energy flow from subsystem i to j is estimated through :

$$\overline{P}_{ij} = \frac{1}{\omega} \overline{\eta}_{ij} \sum_{k=1}^{n} \overline{E}_{ik}^{n} P_k \tag{4.31}$$

The variance associated with the energy flow can be approximated by a first order Taylor expansion of the energy flow in terms of the independent normalized energy values E_{lm}^{n} :

$$s_{P_{ij}}^{2} = \sum_{l \neq i, m \neq k}^{n} \left(\overline{E}_{ik}^{n} P_k \overline{\eta}_{jl}^{o} \eta_{mi}^{o}\right)^2 s_{E_{lm}^{n}}^{2} + \left(P_k \overline{\eta}_{ij} + \overline{E}_{ik}^{n} P_k \overline{\eta}_{ji}^{o} \eta_{ki}^{o}\right)^2 s_{E_{ik}^{n}}^{2} \tag{4.32}$$

From which confidence levels readily follow.

4.1.4 Example.

A representative measurement showing typical values of SEA parameters and their confidence levels is given below in the case of the box.

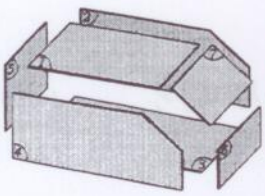

The measurement comprised ten measurement points[1]. The coupling loss factors η_{34}, η_{51} and the internal loss factors η_{33}, η_{66} and their *68%* confidence levels (corresponding to the interval $[\bar{x}-s, \bar{x}+s]$) are presented. The relative high value of the confidence levels indicate that a fairly large number of measurement points has to be taken in order to reach acceptable confidence levels. Even by taking ten measurement points, the standard deviation in relation to the mean is quite substantial.

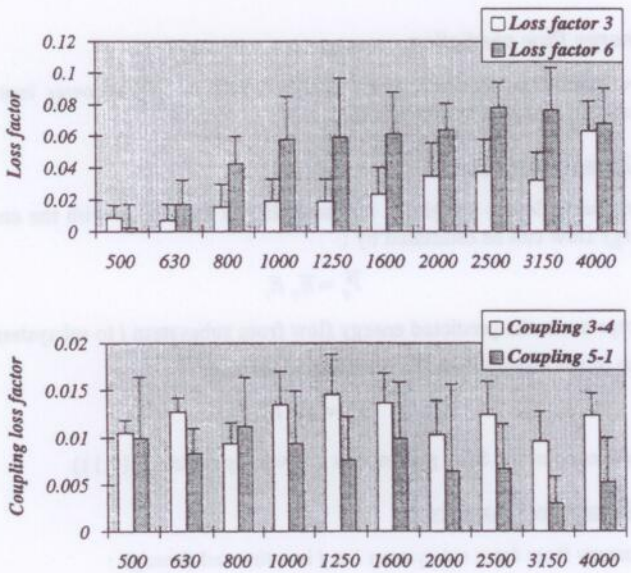

Figure 4.1 SEA internal - coupling loss factors and confidence levels.

The following example illustrates the aspect of the contribution of the sources. The box structure is excited by statistically independent white noise point forces at subsystems *5* and *7*. The power input spectrum is assumed flat. Both input spectra, i.e. associated with subsystem *5* and subsystem *7* are taken similar. The relative contributions and confidence levels of the sources with respect to the energy level of subsystem *2* are calculated using equation (4.22). The confidence levels indicate that by taking *10* measurement points in the case of the PIM measurements on the box, acceptable values concerning the contributions can be obtained.

---

[1] Ten excitation and ten response points.

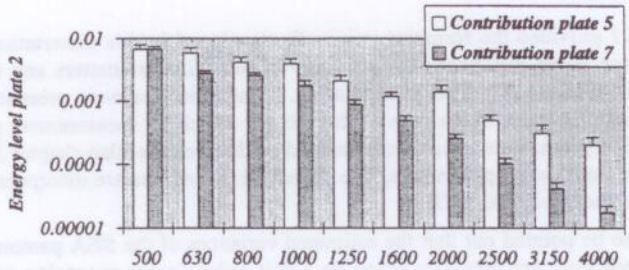

Figure 4.2 : Contributions of subsystem 5 and 7 with respect to the energy level of subsystem 2.

A final example in this respect aims at showing the difference between the two averaging approaches. Two SEA parameters of the box are retained, namely the internal loss factor of subsystem *3* and the coupling loss factor η_{12}. Mean values and 68% confidence levels are shown, revealing no significant differences between both approaches. Other SEA parameters show a similar trend. Because of the minor differences between both averaging approaches and because it is hard to state, based on physical grounds, that one specific averaging approach should be preferred, one can conclude that there is no best solution with respect to the averaging problem. The averaging type 1 has been implemented, serving as the standard averaging approach.

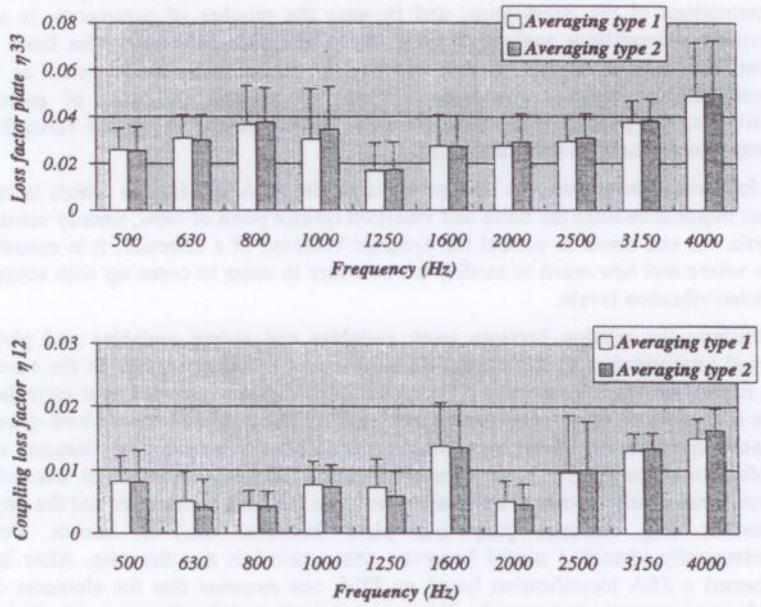

Figure 4.3 : Coupling loss factor η_{12} : a comparison of the averaging approach.

4.1.5 Conclusion.

Paragraph *4.1* provided the formulas, originally developed in this dissertation, to assess the confidence levels and hence the accuracy of the SEA parameters and of the SEA predictions in the case of a PIM identification. Some examples were presented showing typical confidence limits in the case of the box for which *10* measurement points were taken. All SEA predictions which are presented further on (See also chapter *5*) are based on the expressions developed in here. The statistical procedures are incorporated into the general SEA package SEAPACK.

It should also be pointed out that the estimated variances of the SEA parameters and of the SEA predictions are primarily based on a first order Taylor expansion and therefore constitute an approximation. However, no serious drawbacks are associated with this approximation as long as the number of measurement points is not too low.

4.2 Sensitivity analysis.

4.2.1 Introduction.

SEA provides a means of estimating the space and frequency averaged response of subsystems based on energy equilibrium. Because of the averaging involved, the multi-degree of freedom subsystem, e.g. when using finite elements, is replaced by a single degree of freedom energy response function. The penalty is that no information is available on the spatial distribution of the response variables within a subsystem. The main advantage on the other hand is that because SEA employs simple, idealized representations of the subsystems, and because the number of parameters is small, performing a sensitivity analysis is quite cheap and straightforward. The latter is in contrast to the huge amount of data involved in deterministic models such as finite element models, yielding the latter difficult to manage in terms of parameter sensitivities. The penalty of the more primitive SEA approach is that the variability of the response estimates is sometimes larger.

The following paragraph puts into perspective the SEA application which is of the utmost importance from the noise and vibration control point of view, namely sensitivity analysis. As one needs to control the dynamic behavior of a structure, it is essential to know *where* and *how much* to modify the structure in order to come up with accurately predicted vibration levels.

Establishing the relation between input variables and output variables and giving a physical interpretation to the parameters of a model is indispensable. In the case of a SEA model, the variables consist of the power input into subsystems (input variable) and of the energy levels of subsystems (output variable). The relation between both quantities is linear algebraic, i.e. given by a simple transformation matrix. The elements of the transformation matrix $[\eta^o]$ are composed of coupling loss factors and internal loss factors. Ideal would be case if the relation between the SEA parameters and the physical parameters (e.g. material properties, plate thickness etc.) is known. For an experimentally identified model however, this a priori is *not* the case. After having performed a SEA identification based on PIM, one *assumes* that the elements of the transformation matrix between the E (energy) domain and the P (power input) domain are related to physical properties of the structure. In other words, one *assumes* that the

element η^{v}_{ji} represents specifically the strength of the coupling between subsystem i and j and does not incorporate any other physical parameter of the system, except for the extent of subsystem i.

4.2.2 Basic equations.

For PIM, performing a sensitivity analysis with respect to the vibration level of subsystem i can mathematically be translated into the evaluation of the following derivative :

$$\alpha_{i,jk} = \frac{\partial E_i}{\partial \eta_{jk}} \tag{4.33}$$

In other words, equation (4.33) states the sensitivity of the energy level of a subsystem i for a given power input condition to a modification of the structure, i.e. the change of a SEA parameter η_{jk}. The parameter $\alpha_{i,jk}$ of equation (4.33) is further referred to as the sensitivity parameter $\alpha_{i,jk}$. First, a simple analytical expression of the sensitivity parameter is derived.

It holds that :

$$E_i = \frac{1}{\omega} \cdot \sum_{m=1}^{n} \eta^{o\ -1}_{im} \cdot P_m \quad or \quad E_i = \frac{1}{\omega} \cdot \sum_{m=1}^{n} E^{n}_{im} \cdot P_m \tag{4.34}$$

Therefore :

$$\alpha_{i,jk} = \frac{\partial E_i}{\partial \eta_{jk}} = -\frac{1}{\omega} \cdot \sum_{m,p,q=1}^{n} E^{n}_{ip} \cdot \frac{\partial \eta^{o}_{pq}}{\partial \eta_{jk}} \cdot E^{n}_{qm} \cdot P_m \tag{4.35}$$

It holds that :

$$\begin{cases} \eta^{o}_{kj} = -\eta_{jk} & k \neq j \\ \eta^{o}_{jj} = \sum_{l=1}^{n} \eta_{jl} \end{cases} \tag{4.36}$$

- If $k \neq j$, i.e. in the case of the sensitivity of coupling loss factors, equation (4.35) becomes :

$$\frac{\partial E_i}{\partial \eta_{jk}} = -\frac{1}{\omega} \cdot \sum_{m,p,q=1}^{n} E^{n}_{ip} \cdot \left(-\delta_{p,k} \cdot \delta_{q,j} + \delta_{p,j} \cdot \delta_{q,j}\right) \cdot E^{n}_{qm} \cdot P_m \tag{4.37}$$

or finally :

$$\alpha_{i,jk} = \frac{\partial E_i}{\partial \eta_{jk}} = \left(E^{n}_{ik} - E^{n}_{ij}\right) \cdot E_j \tag{4.38}$$

Hence, the change of the energy level of a subsystem i due to a change of the coupling loss factor η_{jk} is given by :

δ represents Kronecker delta : $\delta_{i,j} = 1$ if $i=j$ and $\delta_{i,j} = 0$ if $i \neq j$.

$$\Delta E_i = \Delta \eta_{jk} \cdot \left(E_{ik}^n - E_{ij}^n \right) \cdot E_j \tag{4.39}$$

- If $k = j$, i.e. in the case of the sensitivity of E_i to internal loss factors, equation (4.35) becomes :

$$\frac{\partial E_i}{\partial \eta_{jj}} = -\frac{1}{\omega} \cdot \sum_{m,p,q=1}^{n} E_{ip}^n \cdot \delta_{p,j} \cdot \delta_{q,j} \cdot E_{qm}^n \cdot P_m \tag{4.40}$$

Or finally :

$$\alpha_{i,jj} = \frac{\partial E_i}{\partial \eta_{jj}} = -E_{ij}^n \cdot E_j \tag{4.41}$$

Hence, the change of the energy level of a subsystem i due to a change of an internal loss factor is given by :

$$\Delta E_i = -\Delta \eta_{jj} \cdot E_{ij}^n \cdot E_j \tag{4.42}$$

4.2.3 Discussion.

Equations (4.38) and (4.41) are very straightforward and a physical interpretation can easily be given :

- First it can be observed that the sensitivity parameter with respect to coupling loss factors and internal loss factors is proportional to the energy level of subsystem j, i.e. proportional to the energy level of the subsystem for which the coupling loss factor or internal loss factor is being changed, namely η_{jj} and η_{jk}. The dependency on the energy level of subsystem j is quite reasonable because it holds that the effect of damping treatment or the effect of carrying out structural modifications to junctions is most outspoken for subsystems near the excitation, i.e. for which energy levels are usually highest.

  It should be noted though that the sensitivity parameter is dependent on the global power input condition because it holds that for the energy level E_j :

$$E_j = \frac{1}{\omega} \cdot \sum_{k=1}^{n} \eta_{jk}^{o\ -1} \cdot P_k \tag{4.43}$$

  Hence, performing a sensitivity analysis implies the knowledge of the power input levels or energy levels during operating conditions. For every power input condition, there exists a coupling loss factor and/or an internal loss factor which maximizes the sensitivity parameter, i.e. for which the energy level of subsystem i is most sensitive to.

- If the subsystems are coupled as illustrated in figure *4.4* (for convenience, the phrase parallel-like coupling is used), then modifying the coupling factor between subsystem j and k will not be very effective with respect to the noise reduction of the cavity (subsystem i), because the normalized energies E_{ij}^n and E_{ik}^n will be of the same order of magnitude and the difference between both will be small. In other words, the response of subsystem i by exciting subsystem k will probably be more or less equal to the response of subsystem i by exciting subsystem j. Therefore, the sensitivity

parameter $\alpha_{i,jk}$ of equation (4.38) will be quite low. Without a doubt, this result corresponds to our physical knowledge of the system.

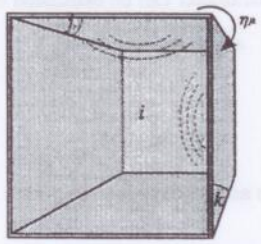

Figure 4.4 : Parallel like coupling of the subsystems.

- If on the other hand the subsystems are coupled as shown in figure *4.5* (the term serial-like coupling is used), it is likely that $E_{ik}^n >> E_{ij}^n$. In other words, the response of subsystem i by exciting subsystem k will probably be much larger than the response of subsystem i by exciting subsystem j. Hence, the sensitivity parameter $\alpha_{i,jk}$ will be larger compared to the parallel like coupling. Again, the result obtained by applying equation (4.38) corresponds to our physical understanding of the problem.

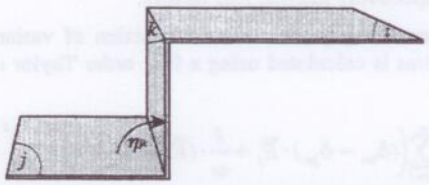

Figure 4.5 : Serial like coupling of the subsystems.

4.2.4 Statistical analysis of the sensitivity parameter.

The sensitivity parameter $\alpha_{i,jk}$ will exhibit an uncertainty due to the variation of the normalized energies E_{ij}^n measured during PIM. From the statistical viewpoint, the sensitivity parameter is basically treated the same way as the SEA parameters and the SEA predictions. Two cases should be discussed : given energy levels and given power input levels.

- ***Given energy levels.***

In this case, the sensitivity parameter $\alpha_{i,jk}$ for coupling loss factors and internal loss factors is estimated by equation (4.44) respectively equation (4.45) :

$$\overline{\alpha}_{i,jk} = \frac{\partial E_i}{\partial \eta_{jk}} = (\overline{E}_{ik}^n - \overline{E}_{ij}^n) \cdot E_j \qquad j \neq k \qquad (4.44)$$

and

$$\overline{\alpha}_{i,jj} = \frac{\partial E_i}{\partial \eta_{jj}} = -\overline{E}_{ij}^{n} \cdot E_j \qquad (4.45)$$

The variance of the sensitivity parameter can be estimated by :

$$s^2_{\alpha_{i,jk}} \cong E_j{}^2 \cdot (s^2_{E^n_{ik}} + s^2_{E^n_{ij}}) \qquad j \neq k \qquad (4.46)$$

and

$$s^2_{\alpha_{i,jj}} \cong E_j{}^2 \cdot s^2_{E^n_{ij}} \qquad (4.47)$$

for respectively coupling factors and internal loss factors

• ***Given power input levels.***

The sensitivity parameter $\alpha_{i,jk}$ for known power input levels $\{P\}$ is estimated by :

$$\overline{\alpha}_{i,jk} = \frac{\partial E_i}{\partial \eta_{jk}} = \frac{1}{\omega} \cdot (\overline{E}^n_{ik} - \overline{E}^n_{ij}) \cdot \sum_{p=1}^{n} \overline{E}^n_{jp} \cdot P_p \qquad (4.48)$$

$$\overline{\alpha}_{i,jj} = \frac{\partial E_i}{\partial \eta_{jj}} = -\frac{1}{\omega} \cdot \overline{E}^n_{ij} \cdot \sum_{p=1}^{n} \overline{E}^n_{jp} \cdot P_p \qquad (4.49)$$

for coupling factors respectively internal loss factors.

The variance of the sensitivity parameter as a function of variances of the estimated normalized energy values is calculated using a first order Taylor expansion in terms of E^n_{lm}. It holds that :

$$s^2_{\alpha_{i,jk}} \cong \sum_{m=1}^{n} \left((\delta_{km} - \delta_{jm}) \cdot \overline{E}_j + \frac{1}{\omega} \cdot (\overline{E}^n_{ik} - \overline{E}^n_{ij}) \cdot \delta_{ij} \cdot P_m \right)^2 \cdot s^2_{E^n_{ik}} + \sum_{m=1}^{n} \left(\delta_{ij} \cdot (\delta_{km} - \delta_{jm}) \cdot \overline{E}_j + \frac{1}{\omega} \cdot (\overline{E}^n_{ik} - \overline{E}^n_{ij}) \cdot P_m \right)^2 \cdot s^2_{E^n_{jm}} \qquad (4.50)$$

in the case of coupling factors and :

$$s^2_{\alpha_{i,j}} \cong \sum_{m=1}^{n} \left(\delta_{jm} \cdot \overline{E}_j + \frac{1}{\omega} \cdot \overline{E}^n_{ij} \cdot \delta_{ji} \cdot P_m \right)^2 \cdot s^2_{E^n_{im}} + \sum_{m=1}^{n} \left(\delta_{ij} \cdot \delta_{jm} \cdot \overline{E}_j + \frac{1}{\omega} \cdot \overline{E}^n_{ij} \cdot P_m \right)^2 \cdot s^2_{E^n_{jm}} \qquad (4.51)$$

in the case of internal loss factors.

4.2.5 Example.

The following example illustrates the applicability of the sensitivity equation derived in this section. The problem put forward in here deals with the sensitivity of the acoustic energy level of the interior of the box with respect to the damping of subsystem *5* when only subsystem *5* is excited. A flat third octave power input spectrum of *1* W/third octave is taken. First, the energy level of the interior is calculated for the basic configuration of the box. Next, the damping of the 5^{th} plate is decreased by *50%* (no physical change is introduced however, only a change of the relevant parameter of the SEA model is considered). The corresponding acoustic energy values calculated by using

the basic SEA equation $\{E\}=1/\omega\cdot[\eta^{\circ}]^{-1}\cdot\{P\}$ are compared to the predicted energy levels based on equation (4.41).

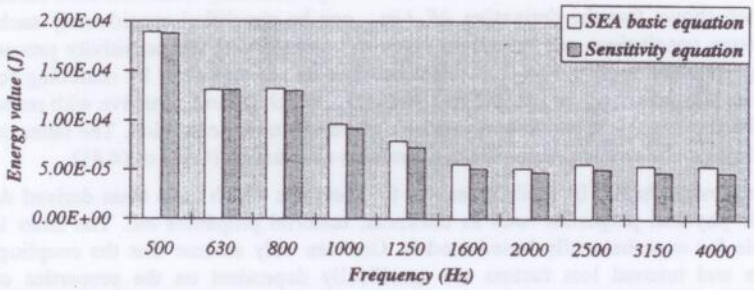

Figure 4.6 : Predicted acoustic energy levels of the box : a comparison between the SEA basic equation and the sensitivity equation.

The bars colored in white represent the energy level of the cavity calculated by using the basic SEA equation for which the loss factor of the 5^{th} plate is decreased by *50%* compared to the reference model. The gray shaded bars represent the energy level according to the sensitivity formula (4.41). Clearly no significant differences between both approaches are noticed, thereby validating the sensitivity equation.

Because the sensitivity formulas are based on a linear Taylor approximation, the SEA parameters may not change to a very large extent in order to apply the sensitivity equation with confidence. The following graph shows the predicted value of the acoustic energy of the interior of the box after decreasing the loss factor of the fifth plate by 90%.

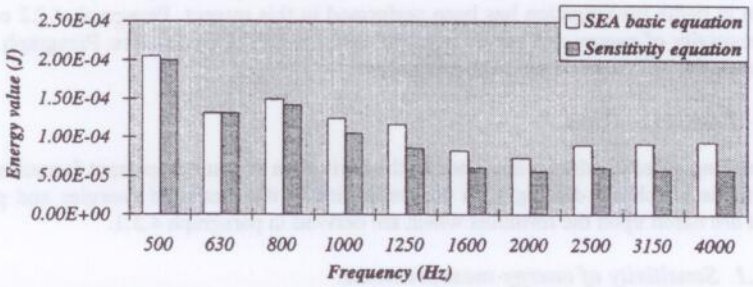

Figure 4.7 : Predicted acoustic energy levels of the box : a comparison between the SEA basic equation and the sensitivity equation for large parametrical changes.

Clearly, the difference between both calculation procedures has become more outspoken compared to figure *4.6*, yet not quite crucial.

4.2.6 Conclusion.

In section *4.2* formulas were derived with respect to sensitivities of subsystem energy levels to structural modifications in the case of experimentally identified SEA models. It has been shown that the derivative $\partial E_i / \partial \eta_{jk}$ can be simplified considerably such that interesting conclusions can be drawn from it. Implementing the sensitivity procedures and optimisation tools is straightforward and can be accomplished by searching for the coupling loss factor η_{jk} or internal loss factor η_{jj} which is most sensitive with respect to the vibration level of a subsystem i under a given excitation condition. The latter can be done through the maximization of the expression of equation (4.38) or (4.41).

It should nevertheless be made clear that the formulas which have been derived do not include physical properties such as thickness, material properties etc. The latter is not feasible for experimentally based models. One can only assume that the coupling loss factors and internal loss factors are specifically dependent on the properties of the junction and on the damping of the relevant subsystems but not on *all* properties of the structure.

4.3 Influence of measurement errors.

One of the important concerns when experimentally identifying SEA parameters by using PIM is related to the influence or to the sensitivity of measurement errors on the parameters and on the SEA predictions. From the PIM point of view, roughly two main types of measurement errors can arise :

- Errors associated with the measured subsystem *energy levels*.
- Errors associated with the measured *power input levels*.

In the past, it has been stated that errors on the measured power input levels are crucial. Yet no in depth investigation has been performed in this respect. Paragraph *4.3.2* covers the sensitivity of energy and power input values on the SEA parameters. Paragraph *4.3.3* addresses the influence on the SEA predictions.

4.3.1 Basic equations.

A foregoing point to address is related to the derivation of some important formulas. The paragraphs which are dealing with the sensitivity of the measured energies and power inputs are based upon the formulas which are derived in paragraph 4.3.1.

4.3.1.1 Sensitivity of energy measurements.

Suppose that the energy of vibration of subsystem i is systematically incorrectly measured during PIM, caused by for example a wrong mass multiplicator. Now, it holds that with respect to the normalized energy matrix, the i^{th} row of $[E^n]$ represents the measured energy level of subsystem i, normalized by the power input on which no error is assumed in here. Because of the error on the measured energy level, the i^{th} row can be assumed to be off by a factor α. Mathematically :

$$E_{ik}^{n,meas} = \alpha \cdot E_{ik}^{n,exact} \qquad \forall\, k:1 \rightarrow n \qquad (4.52)$$

To examine the influence of α on the SEA parameters, it is essential to calculate the following derivative :

$$\frac{\partial \eta^{\circ}_{jk}}{\partial \alpha} \tag{4.53}$$

This derivative can be calculated by expressing the relation between the total loss factor matrix and the normalized energy matrix :

$$\frac{\partial [\eta^{\circ}]}{\partial \alpha} = \frac{\partial [E^{n,meas}]^{-1}}{\partial \alpha} \tag{4.54}$$

Hence,

$$\frac{\partial \eta^{\circ}_{jk}}{\partial \alpha} = -\left[[E^{n,meas}]^{-1} \cdot \frac{\partial [E^{n,meas}]}{\partial \alpha} \cdot [E^{n,meas}]^{-1} \right]_{jk} \tag{4.55}$$

$$= -\frac{\eta^{\circ}_{ji}}{\alpha} \cdot \sum_{m=1}^{n} E^{n,meas}_{im} \eta^{\circ}_{mk} \tag{4.56}$$

Hence, finally :

$$\frac{\partial \eta^{\circ}_{jk}}{\partial \alpha} = -\frac{\eta^{\circ}_{ji}}{\alpha} \cdot \delta_{k,i} \tag{4.57}$$

Where $\delta_{k,i}$ represents the Kronecker symbol.

Hence, in the case of $k \neq i$, no influence of errors associated with the measured energies is noticed. Furthermore, it can be noticed that in the case of $k \neq i$ not only the derivative equals zero at the point of equilibrium, i.e. $\alpha=1$, but also for $\alpha \neq 1$.

Thus, even in the case of large errors (significantly away from the equilibrium point $\alpha = 1$) with respect to the measured energy level of subsystem i, η^{v}_{jk} is not influenced.

In the case of $k=i$ it holds that :

$$\frac{\Delta \eta^{\circ}_{ji}}{\eta^{\circ}_{ji}} = -\frac{\Delta \alpha}{\alpha} \tag{4.58}$$

Thus, the relative change of the total loss factor term η°_{ji} equals the relative error of the measured energy value of subsystem i.

4.3.1.2 Sensitivity of power input measurements.

Suppose that a systematic error occurred when measuring the power input into subsystem i, i.e. the power input of subsystem i is off by a factor α. Hence, the elements of the i^{th} column of the normalized energy matrix can be written as :

$$E^{n,meas}_{ki} = \frac{1}{\alpha} \cdot E^{n,exact}_{ki} \qquad \forall\, k:1 \rightarrow n \tag{4.59}$$

It holds that :

$$\frac{\partial \eta^{o}_{jk}}{\partial \alpha} = -\left[\left[E^{n,meas}\right]^{-1} \cdot \frac{\partial \left[E^{n,meas}\right]}{\partial \alpha} \cdot \left[E^{n,meas}\right]^{-1} \right]_{jk} \tag{4.60}$$

$$= \frac{1}{\alpha^2} \cdot \sum_{l=1}^{n} \eta^{o}_{jl} \cdot E^{n,exact}_{li} \cdot \eta^{o}_{ik} \tag{4.61}$$

Or finally :

$$\frac{\partial \eta^{o}_{jk}}{\partial \alpha} = \frac{\eta^{o}_{ik}}{\alpha} \cdot \delta_{j,i} \tag{4.62}$$

Similar remarks as the one stated in section *4.3.1.1* can be put forward in here. Equation (4.57) and (4.62) form the basic equations of this section as they yield the influence of errors associated with the measured energy levels and power input levels on the elements of the total loss factor matrix. It should be noted though that these equations do not cover all conceivable influences. It is perfectly conceivable to assess the sensitivity of only *one* element of the normalized energy matrix, instead of one row or column as postulated above. For all these cases, the same type of equations can be derived and will not be given here. It can be pointed out that due to the simplicity of the basic equations drawing conclusions will be fairly straightforward.

4.3.2 Sensitivity with respect to the SEA parameters.

4.3.2.1 Energy measurement errors.

If the measured energy of subsystem i is systematically off by a factor α, then the sensitivity with respect to the SEA parameter η_{kj} is given by :

$$\frac{\partial \eta_{kj}}{\partial \alpha} \tag{4.63}$$

In terms of elements of the total loss factor matrix $[\eta^{o}]$:

$$\begin{cases} \dfrac{\partial \eta_{kj}}{\partial \alpha} = -\dfrac{\partial \eta^{o}_{jk}}{\partial \alpha} & k \neq j \\ \dfrac{\partial \eta_{jj}}{\partial \alpha} = \displaystyle\sum_{l=1}^{n} \frac{\partial \eta^{o}_{lj}}{\partial \alpha} \end{cases} \tag{4.64}$$

Making use of the basic equation (4.57), equation (4.64) becomes :

$$\begin{cases} \dfrac{\partial \eta_{kj}}{\partial \alpha} = \dfrac{\eta^{o}_{ji}}{\alpha} \cdot \delta_{i,k} = -\dfrac{\eta_{ij}}{\alpha} \cdot \delta_{i,k} & k \neq j \\ \dfrac{\partial \eta_{jj}}{\partial \alpha} = -\dfrac{\delta_{i,j}}{\alpha} \displaystyle\sum_{l=1}^{n} \eta^{o}_{li} = -\frac{\delta_{i,j}}{\alpha} \cdot \eta_{ii} \end{cases} \tag{4.65}$$

Conclusion :

- A *coupling* loss factor η_{kj} will be influenced by an error on the measured energy of subsystem i only if $k=i$. In that case, it holds that :

$$\Delta\eta_{ij} = -\frac{\Delta\alpha}{\alpha}\cdot\eta_{ij} \tag{4.66}$$

- There will be an influence on the *internal* loss factor only if $j = i$. In that case it holds that :

$$\Delta\eta_{ii} = -\frac{\Delta\alpha}{\alpha}\cdot\eta_{ii} \tag{4.67}$$

  Hence, only the loss factor of the subsystem for which the measured energy during PIM is biased, will be affected.

The previous conclusions are schematically illustrated in the following figure :

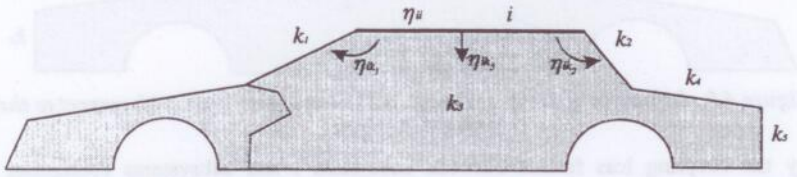

Figure 4.8 : Influence of errors on measured energy levels with respect to the SEA parameters.

Only the SEA coupling loss factors of subsystems contiguous to subsystem i will be affected, namely : $\eta_{ik_1}, \eta_{ik_2}, \eta_{ik_3}$. No influence will be noticed on $\eta_{k_1k_4}$, $\eta_{k_4k_5}$ nor on $\eta_{k_1j}, \eta_{k_2j}, \eta_{k_3j}$. In case of the internal loss factors, only the internal loss factor of subsystem i is sensitive to energy measurement errors of subsystem i during PIM.

4.3.2.2 Power input measurement errors.

If the measured power input into subsystem i is systematically off by a factor α, then the influence on the SEA parameters is given by :

$$\frac{\partial\eta_{kj}}{\partial\alpha} \tag{4.68}$$

Making use of equations (4.62), equation (4.68) becomes :

$$\begin{cases} \dfrac{\partial\eta_{kj}}{\partial\alpha} = -\dfrac{\eta^o_{ik}}{\alpha}\cdot\delta_{j,i} = \dfrac{\eta_{kj}}{\alpha}\cdot\delta_{j,i} & k \neq j \\ \dfrac{\partial\eta_{jj}}{\partial\alpha} = \displaystyle\sum_{l=1}^{n}\frac{\eta^o_{ij}}{\alpha}\cdot\delta_{l,i} = \frac{\eta^o_{ij}}{\alpha}\sum_{l=1}^{n}\delta_{l,i} = \frac{\eta^o_{ij}}{\alpha} \end{cases} \tag{4.69}$$

Conclusion :

- In the case of *coupling* loss factors η_{kj}, there will only be an influence if $j=i$.
- All *internal* loss factors η_{jj} will be influenced according to :

$$\Delta\eta_{jj} = \frac{\Delta\alpha}{\alpha} \cdot \eta_{ij}^{\circ} \qquad (4.70)$$

Hence, there is a fundamental difference with the sensitivity of energy measurements for which only the internal loss factor of subsystem i is influenced. Equation (4.70) will be maximized if $j=i$, i.e. in case of subsystems for which the power input is biased.

The conclusions are illustrated graphically below :

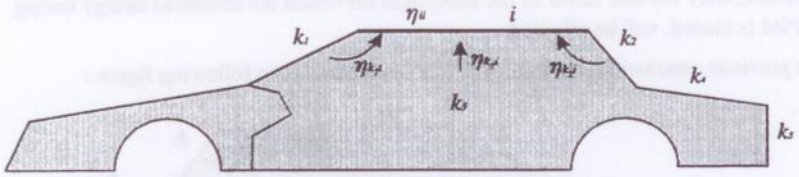

Figure 4.9 : Influence of errors on measured power input levels with respect to the SEA parameters.

Only the coupling loss factors between subsystem i and subsystems contiguous to subsystem i will be influenced, i.e. : $\eta_{k_1 i}, \eta_{k_2 i}, \eta_{k_3 i}$. No influence is noticed on $\eta_{ik_1}, \eta_{ik_2}, \eta_{ik_3}$. All internal loss factors are affected.

From equations (4.65) and (4.69), it becomes clear that the relative influence on the *coupling* loss factors due to an energy which is biased compared to the power input error is the same. *All* internal loss factors on the other hand are affected by measurement errors on the power input, while only the internal loss factor of subsystem i is influenced in the case of errors on the measured energies of subsystem i.

Remark.

In the same way, the sensitivity with respect to the SEA predictions can be assessed and is given by appendix C.

4.3.3 Application oriented PIM measurements.

An interesting feature of the sensitivity topic described above constitutes "application oriented PIM measurements", a topic which will be briefly addressed by means of an vibro-acoustic modelling example.

Many vibro-acoustic problems in the higher frequency range comprise in one way or another the evaluation of structure-borne sound. An automotive vehicle is a typical example in this respect. A principal objective of SEA is to reveal substantial transmission paths from the point of excitation into the interior, followed by effective measures to control and reduce the sound in the interior. SEA offers the opportunity to identify transmission paths and to study the contribution of sources with respect to the sound pressure level in the interior once the SEA parameters have been identified and once the power input into the structure is known. To identify the SEA parameters, all subsystems should theoretically be excited. The energy levels and power input levels should be measured in order to build a normalized energy matrix which can be inverted. Certain normalized energy terms could eventually be neglected as explained in section *4.4*.

For some applications however, it is not necessary to obtain from PIM a very accurate value of the power input for some subsystems. For example, in the case of a car which is excited during operating conditions at certain locations of the body structure, one is mainly interested in the transmission of energy from the point of excitation of the car body into the interior and not in the inverse i.e. in the energy transmission from the interior to the body structure. In these cases, only a rough estimation of the acoustical power input into the interior during PIM is needed as will be shown below. The critical SEA predictions are not crucially affected by roughly estimating the acoustical power input. A simple rough estimate is sufficient in order to be able to invert the normalized energy matrix.

The relevant formulas are derived in appendix C. It is concluded in there that although all internal loss factors and the SEA coupling loss factors from the surrounding subsystem into the cavity are influenced if an error on the acoustical power input is presumed, the influence on the predicted energy level of the cavity (equation (C.5)) is not substantial as shown below :

$$\Delta E_i = -\frac{\Delta\alpha \cdot E_{ii}^{n.meas} \cdot P_i}{\alpha \cdot \omega} \qquad (4.71)$$

Where the subsystem i represents the acoustic cavity. Because the operating conditions are characterized by an absence of power input into the cavity ($P_i = 0$ because for example in the case of cars energy enters the structure via the body structure), it holds that $\Delta E_i = 0$ (from equation (4.71)) and hence, no influence of the factor α is noticed on the predicted energy level of the cavity.

From the previous thoughts and based on the general formulas and conclusions of section *4.3.3*, one can conclude that the critical SEA predictions are not influenced by an error on the acoustic power input measured during PIM in the case of structures for which energy is mainly flowing from the body into the acoustic cavity. Therefore, one can eventually perform the acoustic power input measurements with simple loudspeakers. Moreover, it could sometimes be perfectly possible to disregard the acoustic cavity with respect to the excitation problem, such that the global SEA model does not contain an acoustic cavity. Hence, the inverse problem will be solved without incorporating the contribution of the cavity. Naturally, in order to be able to perform predictions with respect to the acoustic energy level of the cavity, one should measure the energetic response of the cavity while exciting the structural subsystem, yet without exciting the cavity.

On the other hand, if the transmission loss of enclosures is to be evaluated based on SEA, then accurate acoustic power input measurements are definitely needed, inasmuch as the energy flow from the cavity to the surrounding structure is critical.

Conclusion.

Paragraph 4.3.3 states that the excitation of an acoustic cavity during PIM can in some occasions be disregarded, especially if one is purely up to a vibration prediction during operating conditions of the structure (equation (4.71)). Paragraph 4.3.3 does certainly not state that acoustical excitation of a cavity is unessential for whatever structure : all depends on the final destination or application of the model. Even though there is no

influence on the predicted vibration level of the cavity, there is definitely an influence on all internal loss factors and on the coupling loss factors from the structural components to the cavity. Hence, if one is up to assessing an accurate value of the loss factor, then the measurement of the acoustical power input can become important. If on the other hand, only a prediction of the acoustical energy level during operating conditions is foreseen, then one can eventually obtain sufficiently accurate results without evaluating the acoustical power input in an accurate way.

4.3.4 Example.

The following example illustrates the consequences of measurement errors on SEA parameters. More specifically, the influence of the measured acoustic power input during PIM in the case of the box is assessed. First, a reference calculation is performed based on the actual measured energy and power input data. Subsequently, the measured power input into the acoustic cavity is multiplied by a factor of ten in the entire frequency range, whereupon the SEA parameters are calculated. According to the theory outlined above, no influence may be noticed on the structure-to-structure coupling loss factors. Figure *4.10* displays the coupling loss factor for the coupling plate *5* - plate *1*. Clearly, no influence of the measured acoustic power input is noticed. The same conclusions can be drawn with respect to all other structure-to-structure coupling loss factors.

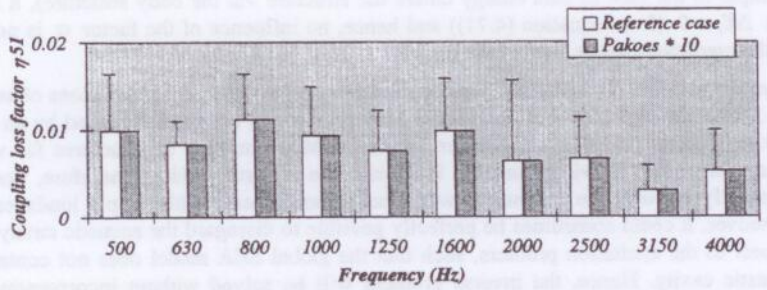

Figure 4.10 : Influence of errors on the measured acoustic power input levels with respect to structure-structure coupling loss factors.

According to equation (4.70), all internal loss factors are sensitive to power input measurements. As a representative example, the internal loss factor of plate *2* is presented, showing the influence of power input measurements. Seemingly, especially in the lower frequency bands (*500* Hz and *630* Hz), the influence of the measured acoustical power input is quite substantial. From figure *4.11*, it becomes clear that in the case of an overestimation of the measured acoustical power input, the SEA internal loss factors of the second plate will be underestimated, in accordance to the underestimation predicted by equation (4.70). The internal loss factors in the bands *500* Hz and *630* Hz even become negative for largely overestimated acoustical power inputs values, hence revealing the importance of accurate acoustical power input measurements when it comes to an accurate identification of internal loss factors.

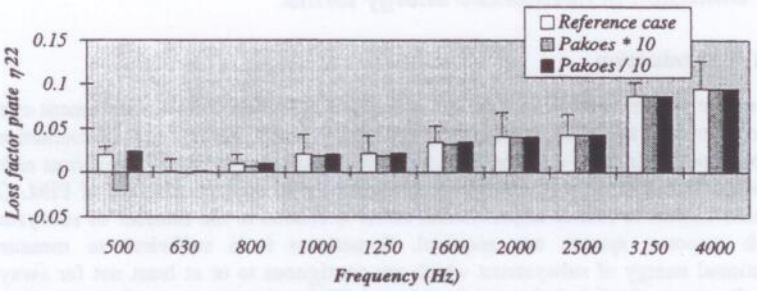

Figure 4.11 : Influence of errors on the measured acoustic power input levels with respect to internal loss factors.

Simple acoustic excitation devices such as a conical loudspeaker when placed in the cavity during the PIM measurements inherently lead to substantial errors with respect to all internal loss factors. One particular appealing solution to overcome this problem is by identifying the internal loss factor of the cavity by means of decay techniques, followed by an updating of the SEA model as explained and exemplified in section *3.5*.

4.3.5 Conclusion.

Section *4.3* revealed some interesting equations concerning the influence of measurement errors on the SEA parameters and the SEA predictions. The measurement errors which are considered are twofold :

- Energy measurement errors : bias error on the measured energy of subsystem *i* during PIM.
- Power input measurement errors : bias errors on the measured power input into subsystem *i* during PIM.

These two types of sensitivities can be translated mathematically by including a bias factor α into row *i* respectively column *i* of the normalized energy matrix. It should be made clear though that sensitivities of a single element of the normalized energy matrix can also be introduced and mathematically treated very well. However, it is not the aim of this section to give for every single measurement error the influence on the SEA parameters nor on the SEA predictions. The importance of this section should not be seen in the light of applying the equations as such, but rather to give the engineer a clear insight in sensitivities and in the consequences of measurement errors which can occur during PIM. For example, it is important to realize that an experimentally SEA model can still be used if some of the PIM measurements could not be performed very accurately.

Therefore, it is recommended that if one performs PIM measurements to take a closer look at the conclusions of the previous paragraphs in order to have a clear insight into the sensitivities of the SEA model with respect to measurement errors.

4.4 Omission of normalized energy terms.

4.4.1 Introduction.

One of the weaknesses of PIM is that it requires relatively long measurement cycles in order to obtain the SEA parameters, especially when the number of excitation and response points is large and the SEA subsystems are many. Every significant reduction of measurement effort will contribute substantially to the optimisation of PIM. One of the possibilities to reduce experimental effort is related to the number of subsystem for which response spectra are acquired. Sometimes it is sufficient to measure the vibrational energy of subsystems which are contiguous to or at least not far away from the subsystem which is being excited during PIM and hence to neglect the vibrational energy of the subsystems away from the excited subsystem. This conception is illustrated schematically in figure *4.12*.

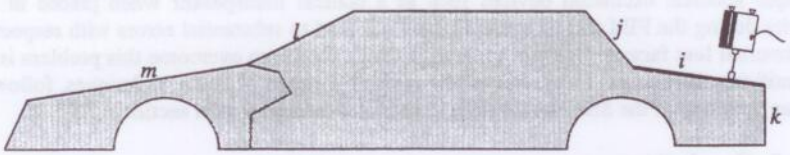

Figure 4.12 : Schematical representation of distant subsystems.

In the case of the structure pictured in figure *4.12*, the energy which enters the structure via *i*, propagates towards the nearby subsystems (subsystems *j&k*) and propagates towards the remote subsystems, namely subsystems *l,m* etc. The energy which is contained in the latter subsystems has frequently decreased significantly and therefore one could think of omitting the energy contribution of the subsystems *l,m* etc. and accordingly put their value in the normalized energy matrix to zero. The latter will naturally result in a significant reduction of the measurement effort : less subsystems should be taken into account for PIM response measurements. The consequences, drawbacks and advantages of this approach are addressed in this paragraph.

4.4.2 Influence on SEA parameters.

First, it is investigated from a purely "physically acceptable" viewpoint what would happen if elements of the normalized energy matrix are set to zero. In advance, a general theorem is given :

If a structure is excited and it is found that $E_j \neq 0$ and $E_k = 0$ than it should follow that $\eta_{jk} = 0$, under the presumption that all SEA parameters are positive, i.e. physically acceptable.

This statement can be proven fairly easy by considering the energy flows and energy balance of the system. If a subsystem *j* exhibits an energy level $E_j \neq 0$, then energy will flow to subsystem *k* according to the basic SEA energy flow relationship :

$$P_{j \to k} = \eta_{jk} \cdot E_j \qquad (4.72)$$

Hence, if there is an energy flow from *j* to *k*, there consequently should be an energy level $E_k \neq 0$. Thus, if it holds that $E_k = 0$ as presumed, it should follow that $\eta_{jk} = 0$.

This theorem will now be applied for the problem dealt with in this paragraph.

Suppose subsystem *1* is excited during the PIM measurements and suppose the energy contributions of subsystems *i* to *n* are neglected for reasons of reducing the measurement effort. In that case, the following set of coupling loss factors are zero according to the theorem previously established.

$$\eta_{1l} = 0 \qquad l: i \rightarrow n \qquad (4.73)$$

The previous statement is illustrated by means of an example (figure *4.13*).

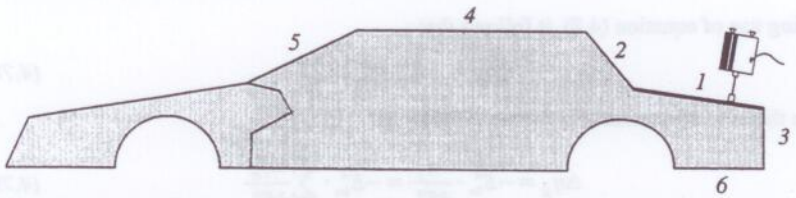

Figure 4.13 : Schematical representation of the omission of the energy levels of subsystem 4 5 and 6.

Suppose subsystem *1* is excited during PIM and the responses of subsystems *4,5* and *6* are neglected. From the previous statement, it holds that $\eta_{14} = \eta_{15} = \eta_{16} = \eta_{24} = \eta_{36} = 0$. The fact that the coupling factors η_{14}, η_{15} and η_{16} equal zero is not a concern because they correspond to uncoupled subsystems. However, the fact that the coupling loss factors η_{24} and η_{36} equal zero is totally irrelevant because the pair of subsystems *2-4* and *3-6* are contiguous.

As stated on the previous page, the above discussion on the consequences of neglecting normalized energy terms is given from a purely physically acceptable viewpoint, meaning that the conclusions could only be drawn under the assumption of a physically admissible energy balance.

It turns out that from the *mathematical* viewpoint, it does not hold that if one neglects one or more normalized energy terms, then the corresponding coupling loss factors become zero, as stated in the theorem given above. For example, setting E^n_{51} (omitting response measurement of subsystem *5* while *1* is excited) to zero will not result in η_{15} being zero. Instead, the element η_{15} becomes negative (see further on). Neglecting energy terms violates the physics of the SEA model.

What follows is a mathematical background of the disregard of elements of the normalized energy matrix. The influence of setting E^n_{lm} to zero on the SEA parameters can be evaluated through the following derivative :

$$\frac{\partial \eta_{jk}}{\partial E^n_{lm}} \qquad (4.74)$$

or by :

$$\delta\eta_{jk} = \delta E^n_{lm} \cdot \frac{\partial \eta_{jk}}{\partial E^n_{lm}} \qquad (4.75)$$

The expression of equation (4.75) should be evaluated for $\delta E^n_{lm} = -E^n_{lm}$, corresponding to setting E^n_{lm} to *0*. Equation (4.75) can be rewritten as :

$$\Delta\eta_{jk} \cong -E^n_{lm} \cdot \frac{\partial \eta_{jk}}{\partial E^n_{lm}} \tag{4.76}$$

- In the case of the SEA coupling factors ($j \neq k$) it holds that :

$$\Delta\eta_{jk} \cong E^n_{lm} \cdot \frac{\partial \eta^o_{kj}}{\partial E^n_{lm}} \tag{4.77}$$

Making use of equation (4.8), it follows that :

$$\Delta\eta_{jk} = -E^n_{lm} \cdot \eta^o_{kl} \cdot \eta^o_{mj} \tag{4.78}$$

- In the case of internal loss factors it holds that :

$$\Delta\eta_{jj} = -E^n_{lm} \cdot \frac{\partial \eta_{jj}}{\partial E^n_{lm}} = -E^n_{lm} \cdot \sum_{k=1}^{n} \frac{\partial \eta^o_{kj}}{\partial E^n_{lm}} \tag{4.79}$$

Making use of equation (4.8), it follows that :

$$\Delta\eta_{jj} = E^n_{lm} \cdot \sum_{k=1}^{n} \eta^o_{kl} \cdot \eta^o_{mj} \tag{4.80}$$

Or finally :

$$\Delta\eta_{jj} = E^n_{lm} \cdot \eta_{ll} \cdot \eta^o_{mj} \tag{4.81}$$

In the case of coupling loss factors, it can be concluded from equation (4.78) that :

- Mainly the coupling factor η_{ml} will be affected, in which case it holds that $k=l$ and $j=m$ and $\Delta\eta_{ml} = -E^n_{lm} \cdot \eta^o_{ll} \cdot \eta^o_{mm}$. Where η^o_{ll} and η^o_{mm} represent the diagonal dominant terms of the total loss factor matrix.
- The shift of the coupling loss factors η_{*l} and η_{m*} ($* \neq m$ *and* $* \neq l$) will be of second order.
- The alteration of the other SEA coupling loss factors will be of third order.

These conclusions can only be drawn under the assumption that the normalized energy matrix is diagonal dominant.

The previous statements are illustrated by means of a statistical simulation. The elements of a 4×4 normalized energy matrix are taken from a uniformly distributed population in a range *0.5 - 1.5*. The diagonal terms are taken from a uniformly distributed population with values in the range *5 - 15*, corresponding to the diagonal dominant characteristic of the normalized energy matrix. The normalized energy matrix $[E^n]$ and its inverse $[\eta^o]_a$ are given below :

$$[E^n]=\begin{bmatrix} 15.56 & 0.98 & 0.07 & 0.44 \\ 0.99 & 10.23 & 0.63 & 0.77 \\ 0.37 & 0.75 & 5.85 & 0.48 \\ 0.25 & 0.65 & 0.27 & 25.00 \end{bmatrix} \tag{4.82}$$

$$[\eta^o]_a=\begin{bmatrix} 0.0647 & -0.0061 & -0.0001 & -0.0009 \\ -0.0060 & 0.0993 & -0.0105 & -0.0028 \\ -0.0033 & -0.0121 & 0.1724 & -0.0029 \\ -0.0005 & -0.0024 & -0.0016 & 0.0401 \end{bmatrix} \tag{4.83}$$

Next, E^n_{32} has been set to zero and the inverse $[\eta^o]_b$ is taken once again :

$$[\eta^o]_b=\begin{bmatrix} 0.0647 & -0.0061 & -0.0001 & -0.0009 \\ -0.0060 & 0.0985 & -0.0104 & -0.0027 \\ -0.0041 & 0.0006 & 0.1711 & -0.0032 \\ -0.0004 & -0.0025 & -0.0016 & 0.0401 \end{bmatrix} \tag{4.84}$$

Comparing $[\eta^o]_a$ and $[\eta^o]_b$ clearly reveals no significant differences between the elements η^v_{ij} ; $i = 1,2,4$ *and* $j = 1,3,4$ of both total loss factor matrices $[\eta^o]_a$ and $[\eta^o]_b$. The shift of the parameters $\eta^o_{3\bullet}$ and $\eta^o_{\bullet 2}$ is of second order and the change of the parameter η^o_{32} is quite significant : from *-0.0121* to *0.0006*. The change which is predicted based on equation (4.78) amounts $\Delta\eta^v_{32} = E^n_{32} \cdot \eta^v_{a.33} \cdot \eta^v_{a.22} = 0.0128$, which agrees fairly well with the actual change of the total loss factor η^o_{32}. Interesting is the fact that η^o_{32} becomes positive and hence the SEA parameter η_{23} becomes negative. In fact, it has been found, by performing a large number of likewise statistical simulations, that for the occasions for which the normalized energy matrix is diagonal dominant, the total loss factor element η^o_{lm} corresponding to the normalized energy element E^n_{lm} which has been set to zero, becomes positive and hence the SEA coupling loss factor η_{ml} becomes negative.

Discussion.

- From equation (4.78), it is found that the change of the SEA coupling loss factor η_{ml} will be negative, because the total loss factors and the normalized energies are both positive. The SEA coupling loss factor η_{ml} becomes negative in the case of a diagonal dominant normalized energy matrix when putting $E^n_{l,m}$ to zero.
- The change of the SEA parameters $\eta_{\bullet l}$ and $\eta_{m\bullet}$ will be positive (the total and coupling loss factors assumed positive). Therefore, the coupling loss factors $\eta_{\bullet l}$ and $\eta_{m\bullet}$ will be *overestimated* by putting $E^n_{l,m}$ to zero.
- The internal loss factors are *underestimated*. The underestimation of the internal loss factors is proportional to the normalized energy which has been neglected, i.e. E^n_{lm}. Therefore, to diminish the effect of neglecting energy terms, one should take care to set the lowest normalized energy values to zero. This remark is quite evident because it was a priori the intention to set energy terms to zero (or in other words skip PIM response measurement) which are small.

- The influence of setting more than one normalized energy value to zero is additive : the more normalized energy values are set to zero, the more a specific loss factor will be overestimated.

$$\Delta\eta_{jk} = -\sum_{l,m=1}^{n} E_{lm}^{n} \cdot \eta_{kl}^{o} \cdot \eta_{mj}^{o} \qquad (4.85)$$

Conclusion.

The consequences of neglecting energy terms in order to reduce the measurement effort has been addressed from the SEA parameter point of view. The main outcome is that it is indeed worthwhile to set normalized energy values to zero and hence skip PIM response measurements providing the energy values E_{lm}^{n} being low. However, the latter does not mean that the subsystems which are "reasonably distant" from the subsystem being excited should be overlooked in PIM because "reasonably distant" does not necessarily imply low normalized energy values. If a subsystem is "distant" from the subsystem being excited and if this subsystem is in addition large, then the energy value can still be significant in order not to be neglected. Therefore, neglecting normalized energy terms requires an a priori considerable insight into the dynamic behavior of the structure and a lot of experience in order to obtain accurate results. The next paragraphs put into perspective the consequences of neglecting energy terms with respect to the SEA predictions.

4.4.3 Influence on SEA predictions.

4.4.3.1 Energy prediction.

Suppose that the SEA parameters of a structure have been identified according to the standard method explained in chapter 3. Some normalized energy terms E_{lm}^{n} are set to zero. Further assume that the system is being excited such that the power input during operating conditions is known. The energy level of subsystem j is estimated by :

$$E_j = \frac{1}{\omega} \cdot \sum_{k=1}^{n} E_{jk}^{n} \cdot P_k \qquad (4.86)$$

Hence, if the normalized energy term E_{lm}^{n} is set to zero, then only the predicted energy level of subsystem l will be influenced according to :

$$\Delta E_l = -\frac{1}{\omega} \cdot E_{lm}^{n} \cdot P_m \quad \text{and} \quad \Delta E_k = 0 \qquad k \neq l \qquad (4.87)$$

Thus, in the case of an power input given by :

$$\{P\} = \{0 \ \cdots \ 0 \ \ P_m \ \ 0 \ \cdots \ 0\}^T \qquad (4.88)$$

no energy level is noticed in subsystem l even though the coupling loss factors η_{*l} are not zero. Physically this is quite unacceptable : if one excites whatever subsystem and one of the subsystems j exhibits a zero energy, then one could reasonably conclude that this specific subsystem j is not connected at all to the rest of the system. The latter only holds from a physically acceptable viewpoint, i.e. all SEA parameters are positive !!. In reality however, this is not so because one of the SEA parameters have become negative

($\eta_{ml} < 0$) by putting the corresponding normalized energy value E^n_{lm} to zero, as shown before. This explains why a subsystem can exhibit an energy level equal to zero while the system is being excited.

Conclusion.

It is not possible to predict the energy level of a subsystem l due to the excitation of subsystem m, if the corresponding element of the normalized energy matrix E^n_{lm} has been set to zero. Therefore, one can state that the energy level of subsystem l and the power input into subsystem m are decoupled.

Consequently, one should be very careful to interpret SEA vibration prediction results if some elements of the normalized energy matrix are neglected because of the occurrence of the decoupling between *measured subsystems* and *excited subsystems* according to the elements of the normalized energy matrix which have been set to zero.

4.4.3.2 Source prediction.

It is assumed that the energies of vibration of the subsystems are known and that the SEA model is identified. The power input values are given by :

$$P_j = \omega \cdot \sum_{k=1}^{n} \eta^{\circ}_{jk} \cdot E_k \qquad (4.89)$$

Mathematically, the influence of neglecting the element E^n_{lm} of the normalized energy matrix with respect to the predicted power input level of subsystem i can be expressed by :

$$\Delta P_j \cong -E^n_{lm} \cdot \omega \cdot \sum_{k=1}^{n} \frac{\partial \eta^{\circ}_{jk}}{\partial E^n_{lm}} \cdot E_k \qquad (4.90)$$

Or in simplified form :

$$\Delta P_j \cong E^n_{lm} \cdot \eta^{\circ}_{jl} \cdot P_m \qquad (4.91)$$

If the power input into subsystem m during operating conditions equals zero, then $\Delta P_j = 0$ or in other words no influence is noticed on the predicted power input levels. Clearly, equation (4.91) will be maximized if j=l. Hence, mainly the predicted power input into subsystem l will be influenced by setting the normalized energy element E^n_{lm} to zero. The error on the predicted power input level of subsystem l is one order of magnitude higher compared to the predicted power input levels of the other subsystems under the assumption that the coupling loss factors are one order lower than the internal loss factors which is physically quite acceptable.

In reality, skipping measurements will not be restricted to only one element E^n_{lm}. The influence of setting more than one normalized energy element to zero is additive, the equations are straightforward and the conclusions are similar.

Conclusion.

Paragraph *4.4.3.2* revealed the influence of neglecting normalized energy terms with respect to the prediction of source levels. It has been proven that the influence of putting

the normalized energy terms E_{lm}^{n} to zero is mainly crucial with respect to the estimation of the source level of subsystem *l*. Furthermore, because of the decoupling between the energy levels of subsystem *l* and power input into subsystem *m*, one can not assess the contribution of the sources of *m* on the energy level of subsystem *l*. In other words, the energy of *l* is assumed to come from subsystems other than subsystem *m*.

4.4.3.3 Other SEA applications.

Similar equations can be derived concerning the influence of skipping PIM measurements on energy flow prediction, energy dissipation prediction etc. The equations can be derived via the application of the basic equation (4.8) and are basically quite straightforward, the reason for which we will not go into detail deriving them in this dissertation.

4.4.4 Example.

The validity of the problem dealt with in this section is revealed by means of measurement results on the box. The SEA parameters obtained by a reference, classical identification (comprising the entire normalized energy matrix) are compared to the SEA parameters obtained by neglecting all normalized energy terms of subsystems which are not directly coupled. Practically, a coupling matrix *[C]* is built for which it holds that a zero at location *ij* represents the absence of a direct coupling between subsystems *i* and *j*. An element *ij* being one denotes the presence of direct coupling between subsystems *i* and *j*. In the case of the box, the following coupling matrix is built :

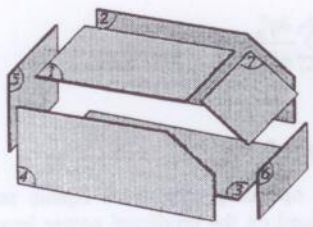

$$\Rightarrow [C]=\begin{bmatrix} 1 & 1 & 0 & 1 & 1 & 0 & 1 & 1 \\ 1 & 1 & 1 & 0 & 1 & 1 & 1 & 1 \\ 0 & 1 & 1 & 1 & 1 & 1 & 0 & 1 \\ 1 & 0 & 1 & 1 & 1 & 1 & 1 & 1 \\ 1 & 1 & 1 & 1 & 1 & 0 & 0 & 1 \\ 0 & 1 & 1 & 1 & 0 & 1 & 1 & 1 \\ 1 & 1 & 0 & 1 & 0 & 1 & 1 & 1 \\ 1 & 1 & 1 & 1 & 1 & 1 & 1 & 1 \end{bmatrix} \qquad (4.92)$$

The coupling matrix *[C]* is element-by-element multiplied by the normalized energy matrix, followed by the identification procedure of the SEA parameters as explained in chapter *3*. The SEA parameters of the reference calculation (reference model) are compared to the results of the calculation for which the uncoupled energy terms are set to *0* (reduced model). Only two representative parameters of the whole set of SEA parameters is retained, namely the loss factor of plate *1* and the coupling loss factor between plate *7* and *6*. All other parameters evidence a similar behavior and will not be presented in here.

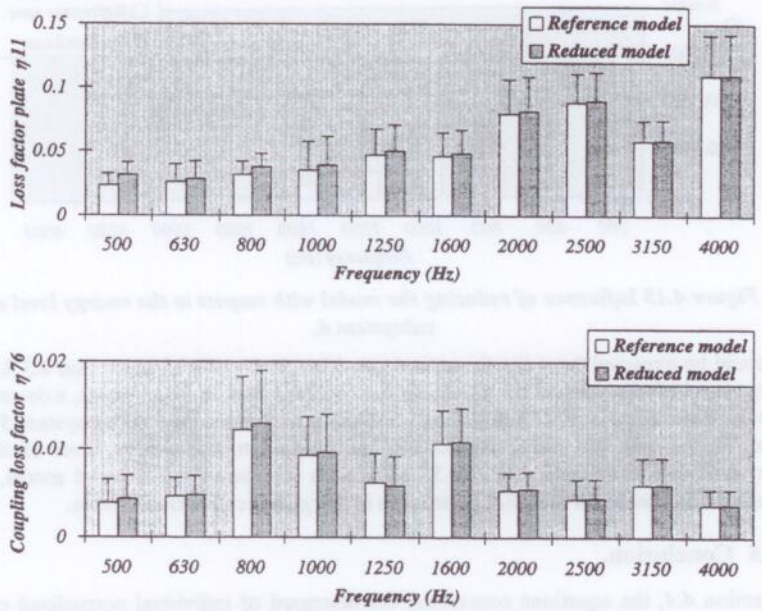

Figure 4.14 : Influence of reducing the model with respect to the coupling loss factor η_{76}.

Clearly, only minor differences between both models can be observed, thereby validating the formulas derived in this section.

A final example in this respect illustrates the decoupling between the energy level and power input level of individual subsystems if specific terms of the normalized energy matrix are neglected. The example considered in here assumes a given power input level into subsystem *5* (a flat power input spectrum *1* W/third octave band is considered). The energy level of the remote subsystem *6* is calculated by means of the reference SEA model and by means of the SEA model for which the normalized energy values of decoupled subsystems are neglected. The energy level of subsystem 6 of both models (reference and reduced) is shown below.

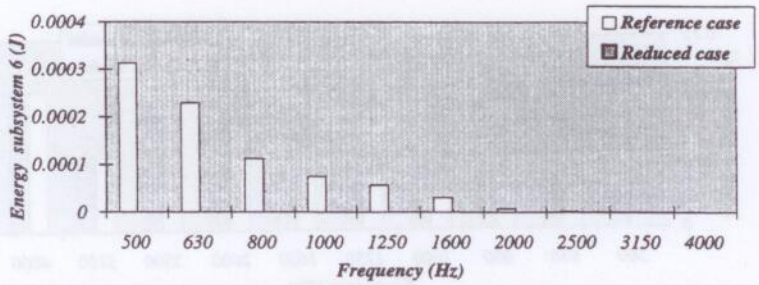

Figure 4.15 Influence of reducing the model with respect to the energy level of subsystem 6.

As could be expected from the theoretical considerations outlined in section *4.3.3.1,* the energy level of subsystem *6* for the reduced model equals *0*. In other words, a decoupling between the energy level of subsystem *6* and the power input level of subsystem *5* takes place. Hence, one can never predict the contribution to the energy level of the 6^{th} subsystem due to excitation of the 5^{th} subsystem in case of the reduced model, even though the influence on the SEA parameters is marginal as illustrated above.

4.4.5 Conclusion.

In section *4.4*, the equations concerning the disregard of individual normalized energy terms were derived and influences were discussed. In many occasions, the SEA parameters will not exhibit substantial changes, at least if one takes care of the fact that only small normalized energy terms are neglected and that only energy levels are disregarded of distant subsystems compared to the subsystem being excited.

The influence on SEA predictions was examined, revealing some important issues. Decoupling is revealed between the response subsystem l and the excited subsystem m when E_{lm}^{n} is set to zero. In addition, it has been shown that the coupling loss factors η_{ml} associated with the normalized energy elements becomes negative, explaining the decoupling. The decoupling phenomenon in mind, it is in some occasions not worthwhile to neglect normalized energy terms for remote subsystems. For example, for a car in which case one is up to assessing the contributions of the different power inputs to the energy level of the interior, one may never neglect the energy contribution during PIM of the interior while exciting a structural component even though the interior is not directly coupled to the subsystem being excited. Because if this energy term is neglected, then one can never assess the contribution of the corresponding power input into that specific subsystem.

Because of the various influences on SEA parameters and on SEA predictions, it can *not in general* be decided whether or not to eliminate normalized energy elements. The latter requires experienced engineers, having a clear insight into the physics of the model and into the consequences of the disregard of normalized energy values on the SEA predictions. Eventually, results based on previous measurements can serve as a guideline to the enigma of skipping response measurements.

4.5 Identification of internal loss factors.

Internal loss factors can be evaluated without evaluating coupling loss factors or even without making hypotheses concerning the energy flow. This can be shown by considering the energy balance of the total system when energy is injected into each subsystem *in turn*. The power input to any one subsystem must be equal to the total energy dissipated in all subsystems, i.e.

$$\begin{cases} P_1 = \omega \cdot \left(\eta_{11} E_{11} + \eta_{22} E_{21} + \cdots + \eta_{nn} E_{n1} \right) \\ P_2 = \omega \cdot \left(\eta_{11} E_{12} + \eta_{22} E_{22} + \cdots + \eta_{nn} E_{n2} \right) \\ \vdots \\ P_n = \omega \cdot \left(\eta_{11} E_{1n} + \eta_{22} E_{2n} + \cdots + \eta_{nn} E_{nn} \right) \end{cases} \tag{4.93}$$

And hence,

$$\begin{Bmatrix} \eta_{11} \\ \vdots \\ \eta_{nn} \end{Bmatrix} = \frac{1}{\omega} \cdot \begin{bmatrix} E_{11} & E_{21} & \cdots & E_{n1} \\ E_{12} & E_{22} & \ddots & \vdots \\ \vdots & \ddots & \ddots & \vdots \\ E_{1n} & \cdots & \cdots & E_{nn} \end{bmatrix}^{-1} \cdot \begin{Bmatrix} P_1 \\ P_2 \\ \vdots \\ P_n \end{Bmatrix} \tag{4.94}$$

It should be noted that the internal loss factors are calculated from equation (*4.94*) without having to make assumptions concerning the way energy is flowing between subsystems. Hence, even if the fundamental SEA assumption concerning energy flow does not hold, still it would be possible to estimate internal loss factors. For classical PIM, the internal loss factors were obtained by inverting the normalized energy matrix and by summing up the terms of one column. Mathematically, this is similar to calculating the expression of equation (4.93). However, equation (4.93) was derived without making assumptions on energy flow. Consequently, internal loss factors obtained by classical PIM are not dependent on the actual expression of the energy flow between subsystems.

4.6 Identification of single SEA parameters.

4.6.1 Theoretical considerations.

One of the disadvantages of PIM when applying it to large complex structures is that every single subsystem should be excited in turn and that the response should be measured in terms of acceleration, velocity or pressure, even if one is interested in only one specific coupling loss factor. The latter could for example be necessary to validate a structural modification. If a structural modification has been carried out with respect to the connection of two subsystems k and j and one is up to validating the modification of the corresponding coupling loss factors η_{jk} and η_{kj} then a quick assessment of that specific coupling loss factor is desired. In the classical way, a complete PIM measurement is needed in order to be able to invert the normalized energy matrix. An alternative solution is provided by STIMPSON and LALOR [15] who states that a very rough approximation of SEA parameters can be obtained by :

$$\eta_{jk} \cong \frac{E^n_{kj}}{E^n_{jj} \cdot E^n_{kk}} \quad and \quad \eta_{jj} \cong \frac{1}{E^n_{jj}} \tag{4.95}$$

This paragraph intents to extend equation (4.95) in order to calculate a specific SEA parameter more accurately yet without performing the complete set of PIM measurements. It will be shown that the lack of information of some subsystems does in some occasions not represent a major obstacle since with a limited subset of normalized energy data it is still possible to approximately calculate the SEA parameters. The basis of the method proposed in here deals with the assessment of the contribution of each subsystem to a specific SEA parameter η_{jk}.

As stated in section *4.1.2*, the coupling loss factors η_{jk} and internal loss factors η_{jj} do not depend on each normalized energy element to the same extent. In the case of coupling loss factors η_{jk} ($j \neq k$), the influence of a single normalized energy term is given mathematically by the following equation :

$$\frac{\partial \eta_{jk}}{\partial E^n_{lm}} = \eta^o_{kl} \cdot \eta^o_{mj} \tag{4.96}$$

Therefore, the contribution of a single E^n_{lm} term with respect to the SEA parameter η_{jk} can be approximated by :

$$\Delta \eta_{jk} \cong E^n_{lm} \cdot \eta^o_{kl} \cdot \eta^o_{mj} \tag{4.97}$$

Expression (4.97) will be dominated for the terms for which $m=j$ and $l=k$ because the total loss factor matrix is diagonal dominant.

Eventually, it is possible to roughly approximate coupling loss factors η_{jk} η_{kj} and internal loss factor η_{jj} and η_{kk} by only considering the contribution of the dominant subsystems j and k only. In that case, one can simply concentrate on the relevant 2×2 submatrix of the normalized energy matrix containing the contribution of subsystems j and k as schematically shown below.

$$[E^n] = \begin{bmatrix} & \downarrow j & \downarrow k & \\ & E^n_{jj} & E^n_{jk} & \\ & E^n_{kj} & E^n_{kk} & \end{bmatrix} \Longrightarrow [E^n_{subset}] = \begin{bmatrix} E^n_{jj} & E^n_{jk} \\ E^n_{kj} & E^n_{kk} \end{bmatrix} \tag{4.98}$$

Figure 4.16 : Approximation of SEA parameters by using a sub-set of the normalized energy matrix.

If the normalized energy matrix is diagonal dominant, one can approximate every element of it's inverse by the following expression :

$$\begin{cases} \eta_{jj}^{\circ} \cong \dfrac{1}{E_{jj}^{n}} & \eta_{kk}^{\circ} \cong \dfrac{1}{E_{kk}^{n}} \\ \eta_{kj}^{\circ} \cong -\dfrac{E_{kj}^{n}}{E_{jj}^{n} E_{kk}^{n}} & \eta_{jk}^{\circ} \cong -\dfrac{E_{jk}^{n}}{E_{jj}^{n} E_{kk}^{n}} \end{cases} \qquad (4.99)$$

The formulas stated above are a first amelioration of equation (4.95).

Hence, the approximate evaluation of the coupling loss factors η_{jk} and η_{kj} requires the measurement of four elements of the normalized energy matrix, instead of the evaluation of the complete normalized energy matrix. Equation (4.99) enables coupling loss factors between two coupled subsystems to be calculated from measurements on those two subsystems only, regardless of the contributions of the other subsystems. It should be noted however that equation (4.99) holds approximately.

The previous procedure can be generalized to include measurements (or indeed contributions) of more than two subsystems in order to more accurately determine specific SEA parameters. By performing measurements on for example three single subsystems, one can approximate a specific coupling loss factor more accurately because the contributions in equation (4.97) with respect to the additional subsystem are also included. This can eventually be extended to include *4,5 to n* subsystems, in order to take into account the contributions of these specific subsystems with respect to a specific SEA parameter.

The aim of this section is to extend the subset of normalized energy data by evaluating the influence of each subsystem p with respect to a specific SEA parameter.

It holds that one should add the contributions of the p^{th} row and p^{th} column of the normalized energy matrix $[E^n]$ in order to obtain the contribution of subsystem p.

The global contribution of the p^{th} column of $[E^n]$ with respect to η_{jk} equals (from equation (4.97)):

$$\sum_{l=1}^{n} E_{lp}^{n} \cdot \eta_{kl}^{\circ} \cdot \eta_{pj}^{\circ} = \eta_{pj}^{\circ} \cdot \sum_{l=1}^{n} E_{lp}^{n} \cdot \eta_{kl}^{\circ} = \eta_{pj}^{\circ} \cdot \delta_{p,k} \qquad (4.100)$$

The global contribution of the p^{th} row of $[E^n]$ equals :

$$\sum_{m=1}^{n} E_{pm}^{n} \cdot \eta_{kp}^{\circ} \cdot \eta_{mj}^{\circ} = \eta_{kp}^{\circ} \cdot \sum_{m=1}^{n} E_{pm}^{n} \cdot \eta_{mj}^{\circ} = \eta_{kp}^{\circ} \cdot \delta_{p,j} \qquad (4.101)$$

Because in equation (4.99) and (4.101), a complete column respectively row is accounted for, one should subtract the contribution of the term E_{pp}^{n} inasmuch as this term is accounted for two times[✎]. Thus, the global contribution to a coupling loss factor η_{jk} of a subsystem p is approximated by :

$$\eta_{jk,p} \cong \eta_{kp}^{\circ} \cdot \delta_{p,j} + \eta_{pj}^{\circ} \cdot \delta_{p,k} - E_{pp}^{n} \cdot \eta_{kp}^{\circ} \cdot \eta_{pj}^{\circ} \qquad (4.102)$$

✎ Sum of the p^{th} row + sum of the p^{th} column - term (p,p).

For practical reasons, only the subsystems for which $j \neq p$ and $k \neq p$ will be retained because one is mainly interested in the partial contributions of subsystem remote from j or k, i.e. contribution which can eventually be neglected.

Hence, in this case the contribution of subsystem p with respect to η_{jk} reduces to :

$$-E_{pp}^{n} \cdot \eta_{kp}^{o} \cdot \eta_{pj}^{o} \qquad (4.103)$$

From equation (4.103), it becomes clear that the contribution will be determined by the coupling loss factors η_{pk} and η_{jp}. Hence, in the case of remote (compared to subsystems j and k) subsystems, η_{pk} and η_{jp} will always be small (they should in principle be zero if p & k and j & p are decoupled) and no serious errors will arise when neglecting the contribution of subsystem p. A clarifying example is given below.

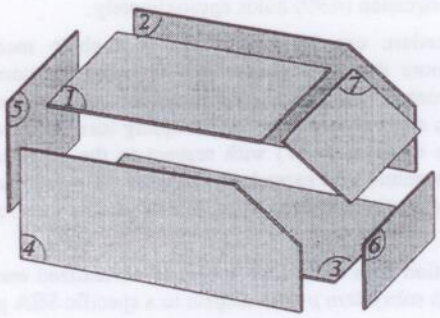

Figure 4.17: Box structure.

In the case of the box, it holds that to identify for example η_{51}, it is not necessary to excite nor to measure (and hence complete disregard) subsystem *6*, because subsystem *6* is not coupled with subsystem *1* nor *5*. Consequently, η_{61} and η_{65} are very small, so is the contribution of the 6^{th} subsystem with respect to the coupling loss factor η_{51}. On the other hand, subsystem *4* is coupled with *5* and with *1*. Hence, the contribution to η_{51} of the 4^{th} subsystem should not be neglected.

Formula (4.103) is validated by means of statistically simulated data. A 4×4 normalized energy matrix with the non-diagonal terms uniformly distributed between *0.5* and *1.5* and with the diagonal terms uniformly distributed between *5* and *15* is constructed and is given below :

$$[E^{n}] = \begin{bmatrix} 11.8677 & 1.0269 & 1.2012 & 0.5475 \\ 1.0890 & 5.9196 & 1.4103 & 1.2361 \\ 1.4304 & 1.1539 & 12.6220 & 0.8282 \\ 1.3462 & 0.9160 & 0.7625 & 11.3264 \end{bmatrix} \qquad (4.104)$$

The contribution of the 4^{th} subsystem with respect to the coupling loss factor η_{21} is examined. The coupling loss factor η_{21} by taking into account all four subsystems is given by : $\eta_{21} = 0.0134$. The coupling loss factor η_{21} by neglecting the 4^{th} subsystem is given by (inverting a 3×3 normalized energy matrix) : $\eta_{21} = 0.0137$. The contribution of the 4th subsystem is therefore quantified by $0.0134 - 0.0137 = -2.93e-4$.

According to equation (4.103) on the other hand, the relative contribution of the 4^{th} subsystem equals :

$$-E^{n}_{44} \cdot \eta^{\circ}_{14} \cdot \eta^{\circ}_{42} = -2.99e-4 \qquad (4.105)$$

which is in good agreement with the difference between the coupling loss factor η_{21} obtained by considering all subsystems and the coupling loss factor η_{21} obtained by neglecting the contribution of the 4^{th} subsystem, i.e. *2.93e-4*.

The previous formulas have been derived in the case of coupling loss factors. Similar equations and conclusions can be constructed respectively drawn for internal loss factors.

4.6.2 Example.

The convergence of a single SEA parameter as function of the subsystems which are taken into account is illustrated below in the case of the box. The coupling loss factor η_{15} of the box for *1000* Hz, *2000* Hz and *4000* Hz is retained. The minimum number of subsystems to be taken into account equals two, i.e. subsystem *5* and subsystem *1*.

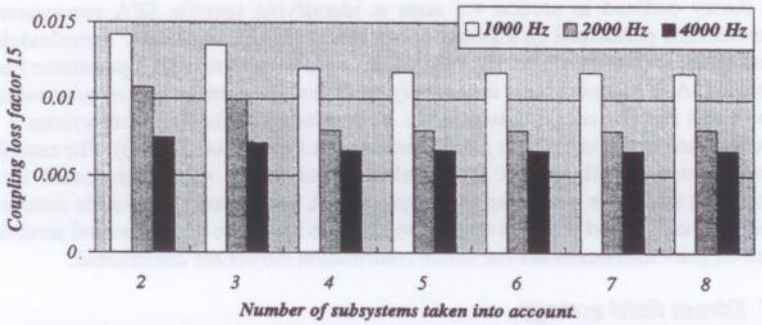

Figure 4.18 : Influence of the number of subsystems taken into account during PIM with respect to the coupling loss factor η_{15}.

Figure *4.18* clearly shows the convergence of the SEA parameter η_{15} as a function of the number of subsystems taken into account. For the box structure and for the coupling loss factor η_{15}, it holds that subsystems *2* and *4* are connected to subsystem *1* and to subsystem *5*.

A useful tool to efficiently identify specific SEA parameters encompasses the contribution curves of figure *4.19*. Figure *4.19* clearly illustrates that the coupling loss factor η_{15} can be approximated within an accuracy of $\pm 95\%$ if only subsystems *1,5,2* and *4* are taken into account for the PIM measurement.

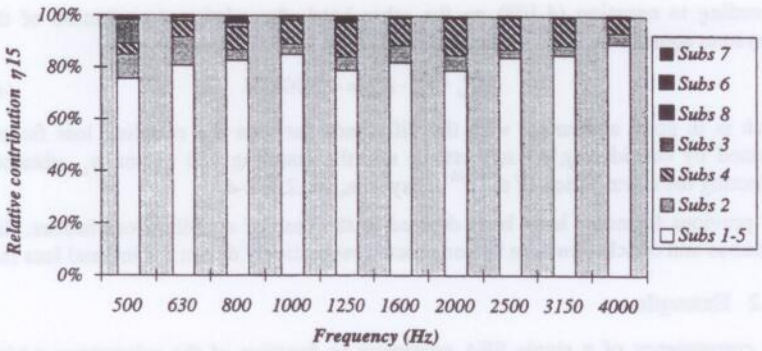

Figure 4.19 : Contributions of subsystems with respect to the coupling loss factor η_{15}

4.6.3 Conclusion.

The theory outlined in section *4.6* aims at identifying specific SEA parameters from measurements performed on a subset of the global set of energy data. A methodology to assess the contribution of specific subsystems with respect to a SEA parameter has been addressed. As a rule of thumb, it generally holds that the contribution of subsystems with respect to a specific coupling loss factor η_{jk} is substantial for these subsystems p which are connected to the subsystem j and to subsystem k (equation (4.103)). The contribution of subsystems p with respect to an internal loss factor η_{jj} is substantial for these subsystems which are connected to subsystem j. A substantial reduction in measurement effort can be obtained if one is up to assessing the influence of a structural modification based on prior measurements for which contribution curves are constructed.

4.7 Direct field energy.

As mentioned in chapter two, the subsystems energy of vibration which is comprised in the basic SEA equations constitutes exclusively reverberent energy. However, point excitation which is generally used for PIM generates an outspoken direct field nearby the point of excitation. In order not to include the kinetic energy of the direct field into the energies obtained during a PIM measurement, it is essential to have a knowledge of the extent of the direct field. Paragraph *4.7* aims at presenting rules based on analytical formulas to evaluate the extent of the direct field. An experiment conducted on the box validates the formulas presented in here.

- ***Beams in flexure.***

  In the case of an infinitely extended beam excited by a point force, it holds that :

$$U(x) = C \cdot \left(e^{-jkx} + e^{kx}\right) \qquad (4.106)$$

  Where U represents the particle displacement in the transversal direction, C represents a constant, x denotes the distance from the point of excitation. k represents the wave number of the wave solution of the dynamic equation of motion of a beam in flexure (See also chapter *5*).

Hence, the parameter which is indicative for the direct field in the case of beams is given by :

$$\lambda = \frac{2\pi}{k} = \frac{2\pi}{\sqrt[4]{\frac{\omega^2 \rho A}{EI}}} \qquad (4.107)$$

ρ, E, A, I represent respectively the material density, Young's modulus, section of the beam and second moment of area.

- ***Plates in flexure.***

In the case of an infinitely extended plate excited by a point force, it holds that the displacement field is given by (CREMER et al. [79]) :

$$U(r) = C \cdot H_o^{(2)}(kr) \qquad (4.108)$$

Where U represents the particle velocity perpendicular to the plate, r represents the distance from the excitation point and $H_o^{(4)}$ represents the Hanckel function of the second kind.

Hence, the length characterizing the near field of the vibrational pattern of a plate excited by a point force is given by :

$$\lambda = \frac{2\pi}{k} = \frac{2\pi}{\sqrt[4]{\frac{\omega^2 \rho 12(1-\nu^2)}{Et^2}}} \qquad (4.109)$$

An experiment showing the significance of the nearby energy with respect to the reverberent energy is conducted. Subsystem *4* of the box is excited in the middle and is scanned by means of a laser vibrometer. The vibrometer incorporates scanning mirrors to permit controlled deflection of the laser beam and therefore the measurement position across the structure.

For a prior measurement, only the velocity spectra in a square of *200* mm x *200* mm around the excitation point are acquired : area indicated dark gray on figure *4.20*.

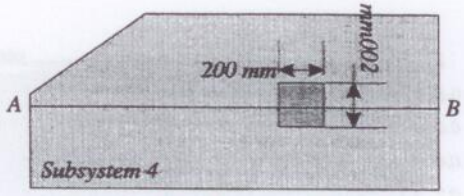

Figure 4.20 : Side panel of the box.

The distance between contiguous measurement points amounts *10* mm, yielding a total number of *21* x *21* measurement points. The *500* Hz and *3150* Hz third octave velocity spectra weighted with the spectrum of the input force are presented in here. The quantities displayed in the figures below comprise the squared magnitude of the FRF

between the velocity at the response point and the force at the excitation point. The values of figure *4.21* are normalized with respect to the maximum velocity value.

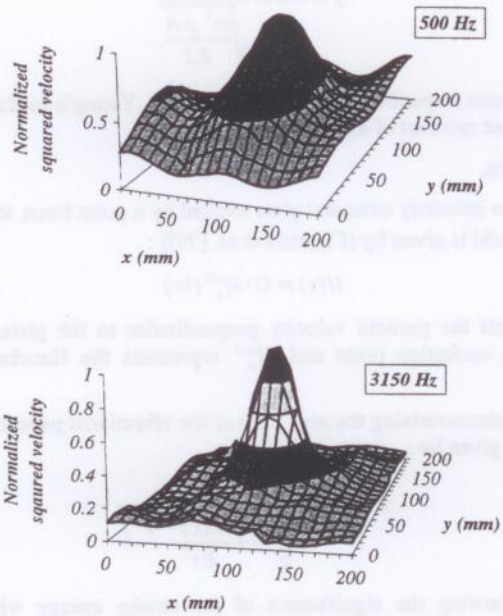

Figure 4.21 : Velocity distribution of the side panel.

A second measurement is performed in order to obtain the FRF's between velocity and input force along the line A-B (figure *4.20*). The normalized amplitude of the FRF is presented in figure *4.22* in the case of the third octave bands around *500* Hz and *3150* Hz. On both figures, the length characterizing the near field calculated by means of equation (4.121) is displayed and is shown to be in good agreement with the experiments.

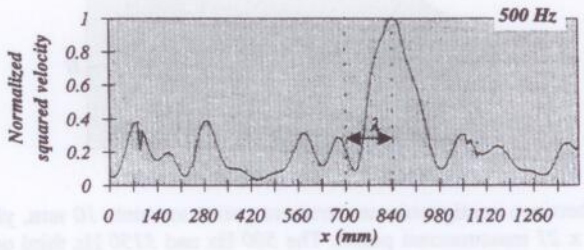

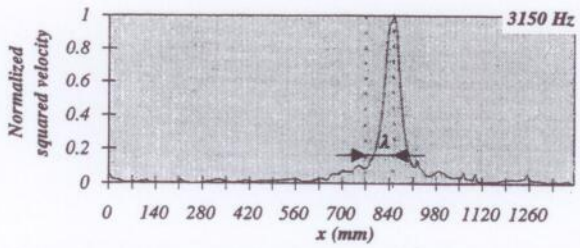

Figure 4.22 : Velocity distribution of the side panel.

4.8 Conclusion.

Chapter *4* covers some important statistical and sensitivity aspects of PIM. With respect to the statistics, formulations have been developed to predict the mean and the confidence levels of the SEA parameters and of the SEA predictions.

Chapter *4* also presents the formulas with respect to the sensitivity of a SEA parameter on the energy levels of a specific subsystem. The equations involved are very straightforward and an optimization can be performed in a cheap and quick way. In addition, these sensitivity equations are analyzed in a statistical sense as well.

Paragraph *4.3* covers the influence of measurement errors (energy levels and power input levels) on the SEA parameters and on the SEA predictions. An important extension of the theory involved, concerns the omission of normalized energy terms. In the past, it has been suggested (without studying the mathematics involved) to neglect the response measurement of subsystems which are relatively far away of the subsystem being excited. Paragraph *4.4* addresses the mathematics of neglecting response measurements. It is shown that with respect to the SEA parameters, it is possible to omit the responses of distant subsystems and hence to reduce the measurement effort substantially. Nevertheless, due to the appearance of decoupling between subsystems, one should be aware that it is impossible to predict the energy levels of a subsystem while exciting another subsystem if the corresponding normalized energy value is not taken into account (and hence neglected) during PIM.

Finally, it is shown that if a specific SEA parameter is requested, then one can make use of approximate solutions. The approximations are based upon the inverse of a sub-set of the global normalized energy matrix. By taking more subsystems into account during PIM, a specific SEA parameter can be identified more accurately. Interesting to calculate are the contribution plots of figure *4.19*. These plots show the contribution of a subsystem with respect to a specific coupling or internal loss factor. By evaluating these plots, one can more or less quantify the errors one is making when neglecting the contribution of distant subsystems, leading to an optimization (at least in terms of measurement time) of PIM.

5. COMPUTATIONAL IDENTIFICATION OF SEA PARAMETERS.

5.1 Introduction.

Often, it is necessary to perform vibration predictions in the (early) design stage of structures or it can be opportune to assess the energy flow within existing structures. This may be to provide data with respect to the validation or to the optimisation of the dynamical comfort of structures or to anticipate fatigue problems. In the fairly early design stage, one has to perform the vibration prediction in the face of a relatively large uncertainty due to the fact that only major structural properties are known. Structural details such as details of the connection between subsystems and details of the fastenings are usually not known at this stage.

At a later stage of the design or when a product already came available to customers, a much more detailed analysis can be performed and a design improvement of a product can be pursued as much more information regarding the structural integrity is available. Appropriate prediction techniques should therefore be capable of incorporating this detailed information and hence should give rise to a fine-tuning of the predicted dynamical characteristics of the structure. Chapter *6* describes a promising method in this respect, based on the employment of finite element models to evaluate coupling characteristics.

Chapter *5* covers the computational evaluation of SEA parameters in a classical sense (with emphasis on the SEA coupling loss factor), constituting the foundation of predictive SEA modelling. It should be pointed out though that the techniques which are presented in the following two chapters with respect to the evaluation of SEA parameters are not intended to verify the basic SEA theory. Rather, the methods described below are based in one way or another on solving classical, more deterministic-like dynamic problems (such as the problem dealing with the evaluation of transmission coefficients of junctions). In other words, we are assumed to accept the basic SEA equations and assumptions as presented in chapter *2* and are mainly interested in the evaluation of the SEA parameters in a computational way.

It should become clear that although the classical methods - based on the state of the art knowledge - as presented in this chapter offer the possibility to analyse quite some structures and connections in the design stage in a sufficiently accurate way, they nevertheless sometimes lack the possibility to include essential geometrical information, whenever this information is available. Therefore, the computational methods described in chapter *5* should preferably be used in the *early design* stage. To create a supplementary variety of subsystems and connections for which the SEA parameters can be evaluated, use has been made of numerical techniques which are described and discussed in chapter *6*.

Section *5.2* covers the predictive evaluation of the SEA internal loss factor. The damping mechanism which are briefly mentioned in section *2.8*, are recapitulated and it is shown how the loss factors can be calculated for some important cases. Section *5.3* discusses the predictive evaluation of modal densities. Existing techniques are mentioned concisely, no new techniques have been developed in this thesis. The next and moreover the main part of chapter *5* describes the evaluation of coupling loss factors, forming the basis of the predictive SEA work.

5.2 Loss factor evaluation.

Damping phenomena which occur in structures can roughly be subdivided into three main groups :

- *Structural damping* which is a function of the properties of the material.
- Damping due to the *built-up characteristics* of structures.
- *Acoustic radiation* : loss from the surface into the fluidum which surrounds it.

These three main damping mechanism are independent and the associated internal loss factors can be added linearly :

$$\eta = \eta_{structural} + \eta_{radiation} + \eta_{built-up} \qquad (5.1)$$

In some occasions, one of the terms can be dominant. For example, if substructures are rigidly connected together, then the damping associated with the energy dissipation at it's subsystem interfaces can be neglected. For lightweight structures with high acoustic radiation efficiencies, the acoustic radiation loss factor can become dominant.

What follows is a brief description of the evaluation procedures concerning the different types of internal loss factors, the way they are implemented in the SEA program SEAPACK. No in depth research has been devoted to the damping problem, i.e. existing techniques are implemented according to the way they are covered in literature.

5.2.1 Structural damping.

5.2.1.1 Material damping.

Table *5.1* presents typical values of loss factors for a range of some frequently encountered materials (after NORTON [80]).

Material	*Loss factor*
Aluminium	*0.0001*
Steel	*0.0001-0.0006*
Copper	*0.002*
Cast iron	*0.001*
PVC	*0.3*
Glass	*0.001*
Brick, concrete	*0.015*
Plaster	*0.005*
Plywood	*0.015*
Sand	*0.02-0.2*
Tin	*0.002*

Table 5.1 : Typical loss factors of some relevant materials.

Because of the complexity which is involved in the damping mechanism in *metals* (including grain boundary motion, molecular site transition and dislocation oscillations), it is not feasible to develop simple parametric functions taking into account all essential types of influences. Accordingly, the best we can do is to refer to material references in which typical values of material loss factors are tabulated. Frequently however, the losses due to material damping of structures which are primarily made of aluminium or steel are smaller compared to the losses due to the add-ons and to the losses due to the built-up. In these cases, it can be assumed that the material damping can be neglected compared to the damping generated by joints and to the damping produced by the add-on damping materials.

Structures built of other materials such as *elastomers* exhibit larger loss factor values. *Polymers* have a loss factor range comparable to the one of metals but are ten times softer, meaning that polymers have the same ratio between the imaginary part of the E modulus and the real part, but a different real part. Elastomeric materials are much softer than metals and the loss factors are much higher : ranging from *0.1* to about *5*. These materials are often used for add-on damping treatments of structures.

It should be emphasized in here that in some occasions it can be necessary to take into account the frequency dependency of the loss factor.

Figure *5.1* displays in this respect the loss factors and corresponding elastic moduli for some classes of important materials (after LYON [1]).

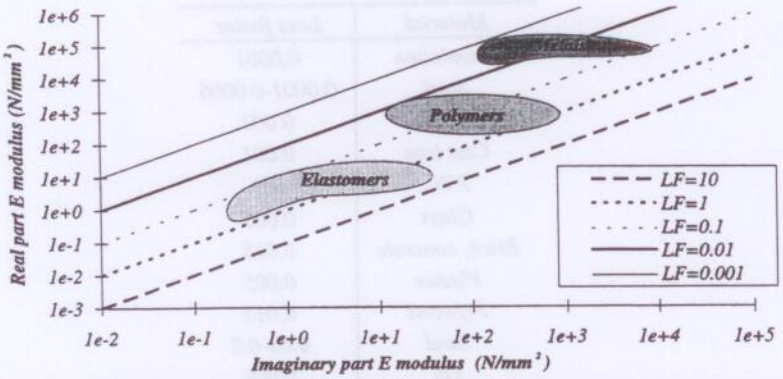

Figure 5.1 : Material loss factors. A comparison between metals, polymers and elastomers.

5.2.1.2 Damping of add-ons.

Since the vibration level tends to be inversely proportional to the internal loss factor[✎], it follows that for a single subsystem, a loss factor reduction of a factor of ten reduces the vibration level by *10* dB. Because changes of the loss factor by a factor of ten can most often not be achieved by the damping of the basic material only, one must resort to add-on damping material. The most widely used types of add-ons are :

- *Free layers* applied by spraying, troweling or in the form of tiles.
- *Constrained layers*. The damping material is constrained between two layers of the basic material. In this case, energy is dissipated mainly through shear effects of the interlayer. The difference between a free and a constrained layer is pictured in figure *5.2*.

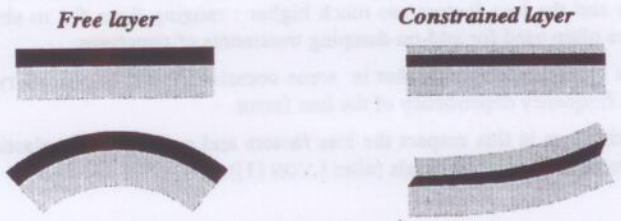

Figure 5.2 : Two main types of add-on damping treatment.

- *Spaced damping*. In this case, a spacing structure is applied between the actual structure and the damping layer (either free or constrained).

✎ Mathematically : $\{E\} = 1/\omega[\eta]^{-1}\{P\}$

- *A resonant damper* which is tuned to a specific mode (not important for SEA purposes).

The damping factor of free or constrained layers can be calculated by simple formulas, based upon the damping values of the different components, if available. Constrained layers are preferred if less weight for a given damping has to be achieved. The penalty for this performance is the narrow frequency range of performance. The reader is referred to NASHIF et al. [85] for an excellent in-depth discussion on the performance of damping treatments.

5.2.2 Damping of built-up structures.

Many structures used in mechanical industry (in particular in the aircraft and aerospace industry) are made up of metal sheets, ribs, stringers, riveted joints etc. In these cases, it is reasonably well established that increased damping *can* be due to the built-up of the structure. Joints between structural parts made up of stiffeners and rivets constitute a typical example.

Although the designer has very little control over this type of damping, there are some theories available to calculate the energy dissipation associated with the damping mechanism involved. The related theories can be based on surface slip and plastic deformation of the overlapping surfaces or on viscous flow in the region between the metal surfaces along the riveted joints.

Certainly, there remain other mechanism of damping of built-up structures which are important for several areas of dynamic modelling. Nonetheless, it is not the intention to put in this thesis an exhaustive list of the corresponding theories. The reader is referred to the state of the art literature.

5.2.3 Acoustic radiation.

As pointed out before, the total internal loss factor of structural subsystems incorporates acoustic radiation. The acoustic radiation loss factor will be substantial (compared to the other loss factors) for lightweight structures in cases for which there is very little material damping and very little damping at the joints. A classical way to calculate acoustic radiation loss factors is by means of the radiation ratio. The radiation ratio is defined by the sound power radiated by the structure into half space (i.e. one side of the structure) divided by the sound power radiated by a large piston with the same surface area and vibrating with the same space averaged RMS velocity of the structure. Hence, the radiation ratio describes the efficiency with which the structure radiates sound compared to a piston source. The radiated sound power equals :

$$P_{rad} = \sigma \rho_o A c \langle v^2 \rangle \qquad (5.2)$$

Where ρ_o is the air density, A represents the surface area, c is the sound velocity and $< v^2 >$ represents the spatially averaged squared velocity.

Or in spatially averaged energy terms (E) :

$$P_{rad} = \frac{\sigma \rho_o c}{\rho_s} E \qquad (5.3)$$

Where ρ_s denotes the material density of the structure.

Besides, the radiated sound power according to SEA theory equals :

$$P_{rad} = \omega \eta_{rad} E \qquad (5.4)$$

Hence, by combining equation (5.3) and (5.4), it follows that :

$$\eta_{rad} = \frac{\rho_o c \sigma}{\omega \rho_s} \qquad (5.5)$$

The radiation ratio can be either larger or less than one. Hence it is more appropriate to use the term *ratio* rather then the term *efficiency* which is sometimes used in literature. Generally, σ is small at low frequencies, so is the acoustic radiation loss factor. If ω increases, σ increases to unity at a rate faster than ω and hence, provided that the structural material density is small, the acoustic radiation loss factor can dominate other losses. For very high frequencies, the radiation ratio become one. The denominator of equation (5.5) still increases and hence the acoustic radiation loss factor decreases once again.

Quite some research has been performed in the past with respect to the problem of the evaluation of radiation ratios and radiation loss factors. CLARKSON and BROWN [86] compared the loss factor of flat plates in vacuum with the corresponding quantity measured in air, clearly manifesting the presence of the acoustic radiation loss factor. As a final item in this respect, figure *5.3* displays a design curve (after VER and HOLMER [87]) for radiation ratios in the case of broadband mechanical excitation of flat plates the way it is implemented in the SEA program SEAPACK.

In figure *5.3*, the parameter λ_c represents the critical wavelength of the plate, P denotes the perimeter of the structure, S is the radiating surface area and f_c represents the critical frequency given by :

$$f_c = \frac{c^2}{1.8 c_L t} \qquad (5.6)$$

c_L stands for the longitudinal wave speed in the plate; t denotes the thickness and c represents the speed of sound.

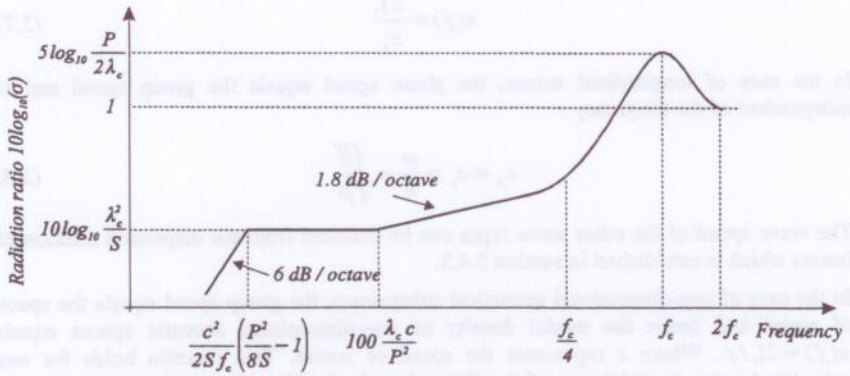

Figure 5.3 : Design curve representing radiation ratios of flat plates.

Another interesting paper concerning the evaluation of acoustic radiation ratios is written by LEPPINGTON et al. [84]. Their results confirm that σ has different asymptotic forms in different regions of the plate wavenumber space. Results are given for each region, together with transition formulae near the various connecting boundaries.

5.3 Modal density evaluation.

Generally, the modal density is amongst the SEA parameter which is the easiest to determine in a computational way. Formulas have been derived for plates, beams, cylinders and cavities and many more other relevant structures made of simple isotropic materials or eventually more complex anisotropic materials. Especially in the very high frequency range in which the vibration pattern is characterized by a low wavenumber compared to the dimensions of a subsystem, the modal density can be determined according to straightforward formulas.

This section describes briefly the evaluation procedures for some important subsystems (acoustic and structural). Meaningful to mention is that the techniques are fairly similar for a large variety of subsystems such that the method outlined in section 5.3 can therefore be extended to more complex subsystems.

5.3.1 Modal density of one-dimensional subsystems.

Altough one-dimensional structures are quite simple with respect to the modal density prediction, the actual dynamics (wave patterns) can be rather complex. For example, a beam can exhibit coupled torsional, bending and longitudinal motion. Each wave type has a different group speed. Nonetheless, the modal density of a one-dimensional system of length L and associated with waves exhibiting a group speed c_g [*] is similar for *all* wave types :

[*] speed with which energy is transported = $\partial\omega/\partial k$

$$n(f) = \frac{2L}{c_g} \tag{5.7}$$

In the case of longitudinal waves, the phase speed equals the group speed and is independent of the frequency :

$$c_p = c_g = \frac{\omega}{k} = \sqrt{\frac{E}{\rho}} \tag{5.8}$$

The wave speed of the other wave types can be deduced from the dispersion relation of beams which is established in section 5.4.3.

In the case of one-dimensional acoustical subsystems, the group speed equals the speed of sound and hence the modal density of one-dimensional acoustic spaces equals $n(f) = 2L/c$. Where c represents the speed of sound. This formula holds for any cylindrical space in which one of the dimensions is significantly larger compared to the other two dimension and for situation for which the wavelength of the sound is greater than the cross dimension.

5.3.2 Modal density of two-dimensional subsystems.

This paragraph establishes the modal density formulas in the case of two-dimensional subsystems. First, we may make the assumption that at frequencies far away from the fundamental frequency of the structure, the number of natural frequencies of the subsystem in a frequency band is not strongly dependent on it's boundary condition. Hence, we can chose a simple boundary condition, i.e. free-free. Secondly, at frequencies away from the fundamental one, we may assume that the modal density is not very dependent on its planform shape. Hence, a simple rectangular planform of size $A = a \times b$ is choosen. The mode shapes can be calculated resulting in the following expression for the displacement pattern :

$$U(x,y) = A \cdot \sin\left(\frac{m\pi x}{a}\right) \cdot \sin\left(\frac{n\pi y}{b}\right) \tag{5.9}$$

Where m and n are positive integers, indicating the mode number. The frequency equation can be written in terms of wavenumbers as :

$$k^2 = k_x^2 + k_y^2 \tag{5.10}$$

Where $k = \omega / c_p$, $k_x = m\pi / a$ and $k_y = n\pi / b$. c_p denotes the phase speed.

The plate modes are represented in the k_x and k_y wavenumber space by the crossing points of a rectangular lattice (figure *5.4*).

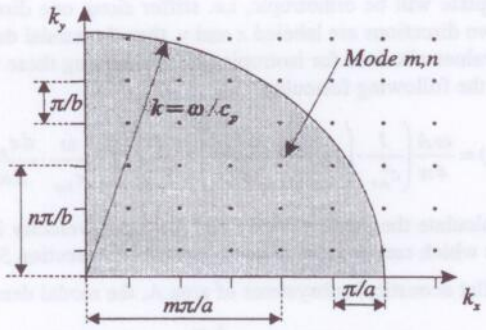

Figure 5.4 : k_x k_y wavenumber diagram.

For all modes exhibiting an eigenfrequency below ω, it holds that each crossing point should lie within a quarter circle of radius :

$$k = \frac{\omega}{c_p} \tag{5.11}$$

and thus to first order, the number of points representing modes within the quarter circle is given by the ratio between the area of the quarter circle and the rectangular area which can be attributed to each mode point :

$$N(\omega) = \frac{\pi k^2 / 4}{\pi^2 / ab} \tag{5.12}$$

Where $N(\omega)$ represents the number of modes in the range $[0\text{-}\omega]$.

Hence, the modal density $n(\omega)$ is given by :

$$n(\omega) = \frac{\partial N(\omega)}{\partial \omega} = \frac{ab\omega}{2\pi c_p c_g} \quad or\ by \quad n(\omega) = \frac{A\omega}{2\pi c_p c_g} \tag{5.13}$$

c_p and c_g represent respectively the phase velocity and the group velocity defined by :

$$c_p = \frac{\omega}{k} \quad and \quad c_g = \frac{\partial \omega}{\partial k} \tag{5.14}$$

Physically, the group velocity is the velocity with which energy is transported. The phase velocity is the velocity of a wave crest, sometimes referred to as carrier wave speed. For non-dispersive waves, the phase speed and group speed are equal. For dispersive systems, such as bending waves in plates and beams, the phase and group speed are not similar and are both functions of frequency. This topic will be addressed more in detail in section 5.4.3. Equation (5.13) is valid for all types of waves that can exist in a flat plate : out of plane, in-plane longitudinal, in-plane shear waves.

The modal density of a thin flat plate in the case of flexural motion is constant whereas in the case of in-plane wavetypes, the modal density is proportional to ω.

In some cases, the plate will be orthotropic, i.e. stiffer along one direction compared to the other. If these two directions are labeled x and y, then the modal density is an average value between the values obtained for isotropic plates exhbiting these two stiffnesses and is approximated by the following formula :

$$n(\omega) = \frac{\omega A}{4\pi}\left(\frac{1}{c_{p,x}^2}\cdot\left(1-\frac{\omega}{c_{p,x}}\cdot\frac{dc_{p,x}}{d\omega}\right)+\frac{1}{c_{p,y}^2}\cdot\left(1-\frac{\omega}{c_{p,y}}\cdot\frac{dc_{p,y}}{d\omega}\right)\right) \qquad (5.15)$$

The procedure to calculate the phase velocity and the group velocity in the case of some relevant wave types which can occur in plates is described in section 5.4.4.

In the case of thin, flat acoustical subsystems of area A, the modal density is given by :

$$n(\omega) = \frac{A\,\omega}{2\pi c^2} \qquad (5.16)$$

According to NORTON [80], equation (5.16) can be adjusted to incorporate edge effects, resulting in :

$$n(\omega) = \frac{A\,\omega}{2\pi c^2}+\frac{P}{2\pi c} \qquad (5.17)$$

5.3.3 Modal density of three-dimensional subsystems.

In the case of three-dimensional spaces, a similar procedure as the one explained for two-dimensional subsystems can be applied, resulting in the following expression for the modal density :

$$n(\omega) = \frac{\omega^2 V}{2\pi^2 c_p^2 c_s} \qquad (5.18)$$

Where V represents the volume of the subsystem. Practically, equation (5.18) will only be applied in the case of *acoustical* subsystems because three-dimensional *structural* subsystems are actually not encountered in practice.

According to MAA [102], equation (5.18) can be adjusted to incorporate the influence of the edges, resulting in :

$$n(\omega) = \frac{\omega^2 V}{2\pi^2 c^3}+\frac{\omega A}{8\pi c^2}+\frac{P}{8c} \qquad (5.19)$$

Where A represents the surrounding surface area and P is the total edge length.

The formulas given above are sufficiently adequate for general acoustical subsystems. In the very high frequency range, the exact shape and the presence of significant shape irregularities becomes less critical in order to apply equation (5.19).

5.4 Coupling loss factors evaluation.

5.4.1 Introduction.

Section 5.4 addresses the evaluation of SEA coupling loss factors, a parameter uniquely used within the SEA framework (modal densities and loss factors are also used outside SEA). Because of the variety of complex structures and connections, it is not possible to tabulate an exhaustive list of SEA coupling loss factors covering all potential cases of interest. Nevertheless, the main existing commercially available SEA softwares (AUTOSEA, SEAM and VAPEPS) present a very restricted list of simple couplings for which the parameters can be calculated, using closed formulas. For example, in the case of the beam-beam junctions incorporated in AUTOSEA, the different types of couplings are displayed in figure *5.5*. It should be mentioned though that recent versions of SEA programs *do* incorporate more complex junctions. It can be expected that the field of application of predictive SEA, insofar as commercially available programs are concerned, will be broadened and that the library of couplings will be extended.

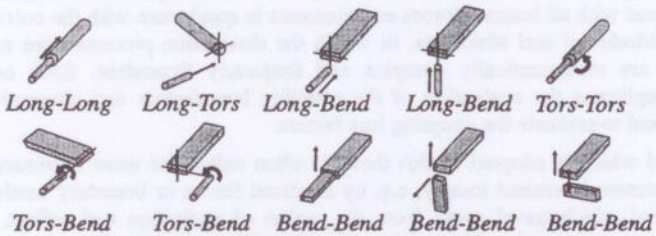

Figure 5.5 : Beam-beam couplings of AUTOSEA.

The basic idea of the wave approach to identify coupling loss factors is that waves are partially reflected and partially transmitted across a junction, quantified by the so-called transmission coefficient. From the transmission coefficients, one can infer the coupling loss factors under certain assumptions. The foremost problem with respect to the identification of coupling loss factors deals with obtaining accurate values of transmission coefficients for all kinds of junctions and wave types.

Three principal structural couplings will be considered in here✎ : beam-beam, plate-plate and beam-plate couplings. For these three types of structural couplings, the present state of the research will be commented and it will be mentioned how this thesis contributes to this field of the research.

In advance, it may be noted that many methods and formulas which are presented in chapter *5* are found in the state of the art literature. However, the way that this topic is addressed in literature is found to be quite fragmentary. In many cases, the classical methods to calculate transmission coefficients of junctions are definitely not refined. Therefore, the main aim of *this* chapter is to gather the essential ingredients dealing with the identification of transmission coefficients and to present the prediction procedures in a general, comprehensible and concise way. At some stages of the research, additional

---

✎ Naturally, this list is not exhaustive.

modifications were carried out in order to extend the range of application of the existing methods. As such, chapter *5* also provides an excellent basis for the application of the numerical techniques, based on wave-absorbing elements. The latter technique forms the major, most substantial contribution to predictive SEA, worked out in this dissertation.

5.4.2 The wave model.

The application of the modal model as outlined briefly in chapter 2 is often not practicable, especially since the individual modal coupling coefficients can exceptionally be quantified for complex subsystems. The evaluation of SEA coupling loss factors from the identification of modal interaction coefficients between modes of two subsystems has rarely been addressed and is unquestionably no the most suitable method. The wave approach on the other hand is.

Modes represent special combinations of travelling waves which interfere to form characteristic spatial distributions of field variables with corresponding characteristic frequencies. In dissipation free media with boundaries which neither dissipate nor transmit energy, the modes are mathematically real, with all points moving in phase or anti-phase and with all internal forces and moments in quadrature with the corresponding velocities. Modes of real structures, in which the dissipation processes are not ideally distributed are mathematically complex and frequency dependent. Such complexity greatly complicates the evaluation of the coupling loss factors and alternative means must be found to estimate the coupling loss factors.

The method which is adopted in this thesis is often called the *wave approach of SEA*. When a structure is excited locally, e.g. by localised forces or boundary motion, waves are generated which travel away from the region of excitation and reflect, transmit, diffract and are scattered at boundaries and other discontinuities. The waves transport vibrational energy which is partly dissipated during propagation by dissipative mechanism and partly transmitted into contiguous subsystems at the interface. If the boundary losses are not too high, then the waves will repeatedly reflect from the boundaries to form a reverberant field. This field may be considered to consist of a superposition of plane waves. In frequency bands in which only one or two modes are resonant and for which it holds that the FRF's manifest individual peaks, these plane waves will travel predominantly in discrete directions associated with the mode shapes and must be considered to be phase coherent. Figure *5.6* displays the nodal lines and the associated wave fronts in the case of the (3,2) mode of a free-free plate.

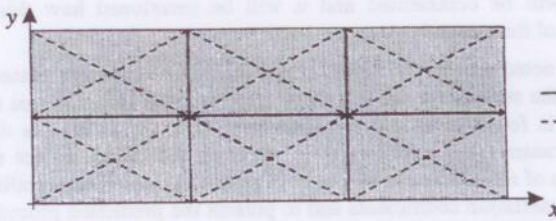

Figure 5.6 : Wave and modal representation of a vibration pattern within a plate.

If many modes resonate within a band and if these modes have close natural frequencies in terms of modal overlap ($M>1$), then the individual wave components may be considered to be incoherent, and in uniform isotropic media, may also be considered to travel with equal probability in all directions. The latter constitutes the ideal diffuse field. Each individual wave transports energy at a rate expressed by a vectorial intensity which equals the product of time averaged energy density and group velocity. In fact this relation provides the link between SEA and the wave methods. This link will be explicitely addressed in the case of the specific couplings considered in this chapter.

In summary, it can be stated that for the wave approach, the vibrations are considered in terms of elastic waves which propagate through the structure and are partly reflected and partly transmitted at the junction : the attenuation of structure-borne sound. Hence, of prime concern is the evaluation of the wave transmission properties of various discontinuities likely to be present in a structure. The transformation of transmission coefficients into SEA coupling loss factors is the final phase of the predictive evaluation of SEA coupling loss factors.

The evaluation of the transmission coefficient is central in chapter *5* and will be outlined for several types of junctions.

5.4.3 Beam-beam junction.

This paragraph outlines the calculation of transmission coefficients and SEA coupling loss factors for beam-beam junctions. Although formulas are generally available in literature concerning simple beam-beam junctions (e.g. right angled, T junctions etc.), this is not the case for general complex beam junctions for which coupling between several types of motion within a beam can occur, for which an arbitrary number of beams can couple together and for which several other substantial details of the junction are important. The method described in here includes the latter items.

5.4.3.1 Dynamic beam equations.

The beam-beam junctions which are considered in paragraph *5.4* comprise beams for which it holds that shear and centroid axis are not coincident, for which rotational effects of the beam section is taken into account and for which shear deformation is included (Timoshenko beam). Since the dynamic equations are the basis of the computational identification of transmission coefficient, they will be briefly focused on.

Because the SEA parameters are not dependent on the coordinate system, it is worthwhile to take an appropriate coordinate system, i.e. in which the equations of motion are somewhat simplified. Therefore, a rectangular coordinate system is chosen such that the beam centroid axis is coincident with the x axis and such that the principal axes of inertia of a section are parallel to the y and z axes (figure *5.7*) :

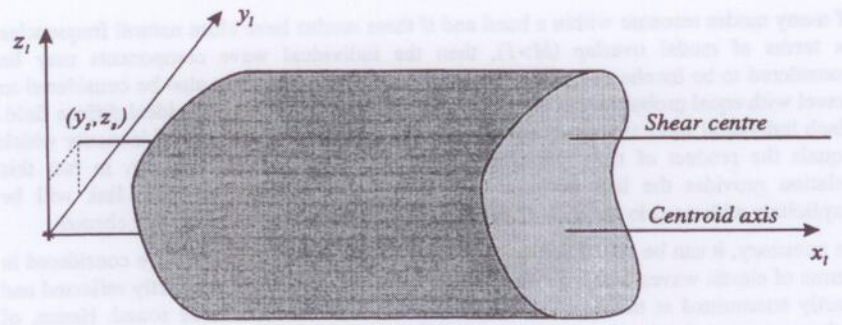

Figure 5.7 : Schematic representation of a beam section and the corresponding coordinate system.

(y_s, z_s) represent the coordinates of the shear centre.

For simplicity, the beam is supposed to be isotropic, in the sense that longitudinal motion is decoupled from bending motion. However, this restriction can in principle be omitted in order to include more general beam motions. The global beam motion which is considered in here incorporates :

- Longitudinal motion.
- Bending motion coupled with torsional motion.
- Torsional motion coupled with bending motion.

More general beam sections could eventually include retarding forces in the beam (caused by surrounding media), Poisson ratio of the materials (Mindlin-Herrmann theory), lateral inertia effects (Lowe theory). The latter phenomena will not be considered in here as they are not essential in most applications and since they would complicate the equations too much without contributing substantially.

Because the beam is assumed to be isotropic, longitudinal motion is decoupled from bending and torsional motion, therefore Hooks law and Newtons law for longitudinal motion (figure *5.8*) can be written as :

$$\begin{cases} f_x = EA \cdot \dfrac{\partial u_x}{\partial x} \\ \rho A \cdot \dfrac{\partial^2 u_x}{\partial t^2} = \dfrac{\partial f_x}{\partial x} \end{cases} \qquad (5.20)$$

With :

f_x : internal force in the x direction applied at the centroid axis; u_x : displacement of the centroid in the x direction; ρ represents the material density, A is the section of the beam and E denotes the modulus of elasticity.

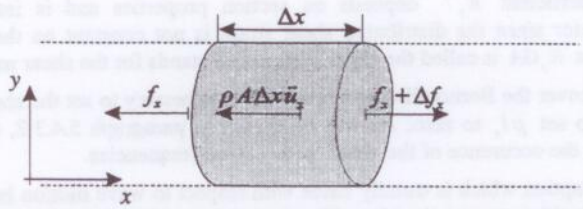

Figure 5.8 : Internal forces and displacements for longitudinal motion.

For bending motion in the *x-y* plane (figure *5.9*), there are four rather than two basic equations of motion. Hooks and Newtons laws take the following form in the case of a Bernouilli-Euler beam and in the case of coincident centroid and shear axis :

$$\begin{cases} \vartheta_z = \dfrac{\partial u_y}{\partial x} \\ m_z = EI_z \cdot \dfrac{\partial \vartheta_z}{\partial x} \\ \rho A \cdot \dfrac{\partial^2 u_y}{\partial t^2} = \dfrac{\partial f_y}{\partial x} \\ f_y = -\dfrac{\partial m_z}{\partial x} \end{cases} \qquad (5.21)$$

With :

f_y : internal shear force in the *y*-direction applied at the centroid; m_z : internal moment about the *z* axis applied at the centroid; u_y : displacement of the centroid in the *y*-direction; ϑ_z : rotation of a cross section about the *z*-axis; I_z : second moment of area about the *z*-axis

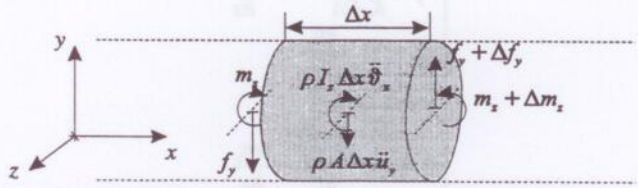

Figure 5.9 : Internal forces and displacements for flexural motion.

If the rotatory inertia is not included in the analysis (Bernouilli-Euler beam theory), then unrealistic velocities occur at high frequencies. While the magnitude of ρI_z may be small at lower frequencies, at higher frequencies, the contribution of ϑ_z (rotatory inertia) which is neglected in the Bernouilli-Euler theory is significant. Another assumption made in the Bernouilli-Euler theory is that shear deformation is not taken into account, although a shear force f_y is present. Both assumptions are relaxed in the Timoshenko beam theory.

The shear coefficient K_y[*] depends on section properties and is introduced as a correction factor since the distributed shear strain is not constant on the section. The group constant $K_y GA$ is called the shear stiffness. G stands for the shear modulus.

In order to recover the Bernouilli-Euler theory, it is necessary to set the shear stiffness to infinity and to set ρI_z to zero. As will be shown in paragraph 5.4.3.2, a Timoshenko beam leads to the occurence of the shear mode cut-on frequencies.

Another assumption which is usually made with respect to wave motion in beams is that shear and centroid axes are coincident. The shear axis is defined such that for a beam in a cantilever configuration, any static force applied on and perpendicular to the shear axis will result in a zero rotational deflection.

In order to take account of the off-set shear axis, it is simply necessary to exclude from f_y that part associated with torsion. Thus, for bending in the x-y plane, we have :

$$\begin{cases} \vartheta_z + \dfrac{f_y}{K_y GA} = \dfrac{\partial(u_y - z_s \vartheta_x)}{\partial x} \\ m_z = EI_z \cdot \dfrac{\partial \vartheta_z}{\partial x} \\ \rho A \cdot \dfrac{\partial^2 u_y}{\partial t^2} = \dfrac{\partial f_y}{\partial x} \\ f_y = \rho I_z \cdot \dfrac{\partial^2 \vartheta_z}{\partial t^2} - \dfrac{\partial m_z}{\partial x} \end{cases} \qquad (5.22)$$

A similar set of four equations can be obtained for bending in the x-z plane, with appropriate changes of signs according to the choice of the coordinate system and to the choice of the variables (internal forces and displacements).

$$\begin{cases} \vartheta_y - \dfrac{f_z}{K_z GA} = \dfrac{\partial(u_z + y_s \vartheta_x)}{\partial x} \\ m_y = EI_y \cdot \dfrac{\partial \vartheta_y}{\partial x} \\ \rho A \cdot \dfrac{\partial^2 u_z}{\partial t^2} = \dfrac{\partial f_z}{\partial x} \\ f_z = \rho I_y \cdot \dfrac{\partial^2 \vartheta_y}{\partial t^2} - \dfrac{\partial m_y}{\partial x} \end{cases} \qquad (5.23)$$

For torsional motion and in the case of coinciding shear axis and centroid axis the equations are conceptually similar to those of longitudinal motion. If shear axis and centroid axis are not coincident, appropriate changes should be made to the terms of equation (5.20).

If m_x is the moment about the centroid axis, then the moment developed about the shear axis equals $m_x + z_s f_y - y_s f_z$. The latter moment is reacted by the torsional stiffness GJ, hence Hooks and Newtons laws become :

---

[*] 5/6 for square sections.

$$\begin{cases} m_x + z_s f_y - y_s f_z = GJ \cdot \dfrac{\partial \vartheta_x}{\partial x} \\ \rho I_x \cdot \dfrac{\partial^2 \vartheta_x}{\partial t^2} = \dfrac{\partial m_x}{\partial x} \end{cases} \tag{5.24}$$

With I_x the second moment of area about the centroid axis (polar moment), ϑ_x the rotation about the centroid (or rotation about the shear axis, which indeed is the same).

The equations (5.20), (5.23), (5.24) can be combined to recover the following set of twelve, coupled equations of motion of a beam, including thick bending terms and off-set shear axis :

$$\begin{gathered} f_x = EA \cdot \partial u_x / \partial x \\ \vartheta_z + f_y / K_y GA = \partial (u_y - z_s \vartheta_x) / \partial x \\ \vartheta_y - f_z / K_z GA = \partial (u_z + y_s \vartheta_x) / \partial x \\ m_x + z_s f_y - y_s f_z = GJ \cdot \partial \vartheta_x / \partial x \\ m_y = EI_y \cdot \partial \vartheta_y / \partial x \\ m_z = EI_z \cdot \partial \vartheta_z / \partial x \\ \rho A \cdot \partial^2 u_x / \partial t^2 = \partial f_x / \partial x \\ \rho A \cdot \partial^2 u_y / \partial t^2 = \partial f_y / \partial x \\ \rho A \cdot \partial^2 u_z / \partial t^2 = \partial f_z / \partial x \\ \rho I_x \cdot \partial^2 \vartheta_x / \partial t^2 = \partial m_x / \partial x \\ f_z = \rho I_y \cdot \partial^2 \vartheta_y / \partial t^2 - \partial m_y / \partial x \\ f_y = \rho I_z \cdot \partial^2 \vartheta_z / \partial t^2 - \partial m_z / \partial x \end{gathered} \tag{5.25}$$

Eventually additional terms arise if supplementary phenomena, which are not accounted for in this thesis, would also be inluded in the analysis.

5.4.3.2 *Wave solution.*

The general wave solution of equations (5.25) is applied and discussed. Without loss of generality, we may look for solutions for which all twelve basic variables[`] incorporate the wave factor : $e^{j(\omega t - kx)}$. Where k represents the wavenumber, ω is the angular frequency.

Hence, each variable y can be replaced by it's wave representation : $Y \cdot e^{j(\omega t - kx)}$. After substituting this wave solution into equations (5.25) and after eliminating the wave terms $e^{j(\omega t - kx)}$ in the left and right hand side of equations (5.25), one obtains :

[`] The variables are : $\{u_x, u_y, u_z, \vartheta_x, \vartheta_y, \vartheta_z, f_x, f_y, f_z, m_x, m_y, m_z\}$

$$
\begin{aligned}
F_x &= -jkEA\cdot U_x \\
\Theta_z + 1/K_y GA\cdot F_y &= -jk\cdot(U_y - z_s\Theta_x) \\
\Theta_y - 1/K_z GA\cdot F_z &= -jk\cdot(U_z + y_s\Theta_x) \\
M_x + z_s F_y - y_s F_z &= -jkGJ\cdot\Theta_x \\
M_y &= -jkEI_y\cdot\Theta_y \\
M_z &= -jkEI_z\cdot\Theta_z \\
-\omega^2\rho A\cdot U_x &= -jk\cdot F_x \\
-\omega^2\rho A\cdot U_y &= -jk\cdot F_y \\
-\omega^2\rho A\cdot U_z &= -jk\cdot F_z \\
-\rho\omega^2 I_x\cdot\Theta_x &= -jk\cdot M_x \\
F_z &= -\omega^2\rho I_y\cdot\Theta_y + jk\cdot M_y \\
F_y &= -\omega^2\rho I_z\cdot\Theta_z + jk\cdot M_z
\end{aligned}
\qquad (5.26)
$$

The time variables are grouped to form :

$$\{q\}^T = \{u_x \quad u_y \quad u_z \quad \vartheta_x \quad \vartheta_y \quad \vartheta_z \quad f_x \quad f_y \quad f_z \quad m_x \quad m_y \quad m_z\} \qquad (5.27)$$

The corresponding frequency dependent variables are grouped into :

$$\{Q\}^T = \{U_x \quad U_y \quad U_z \quad \Theta_x \quad \Theta_y \quad \Theta_z \quad F_x \quad F_y \quad F_z \quad M_x \quad M_y \quad M_z\} \qquad (5.28)$$

Hence, equation (5.26) results in the following matrix equation :

$$[A]\cdot\{Q\} = k\cdot\{Q\} \qquad (5.29)$$

The algebraic form of matrix $[A]$ is given in appendix D :

Equation (5.29) is a standard eigenvalue problem which can be solved to yield twelve eigenvalues (or indeed wavenumbers) k_i and twelve eigenvectors $\{\Psi_i\}$. Each eigenvalue corresponds to a specific wave type.

The solution of the eigenvalue problem (in terms of eigenvalues) comprises the relation between the wavenumber and the frequency : $k = k(\omega)$, called the spectrum or dispersion relation. For simple beam sections, the dispersion relation can be written in the form of a closed formula. The latter is however not the case for a general beam section for which the spectrum relation appears to be in a transcendental form. The analysis of the dispersion relation provides a comprehensible insight into the wave motion. A real wavenumber corresponds to a propagating wave, an imaginary wavenumber corresponds to an evanescent (exponential decaying) wave.

The twelve eigenvalues k_i are such that for frequencies below the shear mode cut-on frequencies[*], four lie on the positive real axis, four lie on the negative real axis, two lie on the positive imaginary axis and two lie on the negative imaginary axis. All twelve wavenumbers and associated waves are plotted on the Argand diagram (wavenumber in the complex plane).

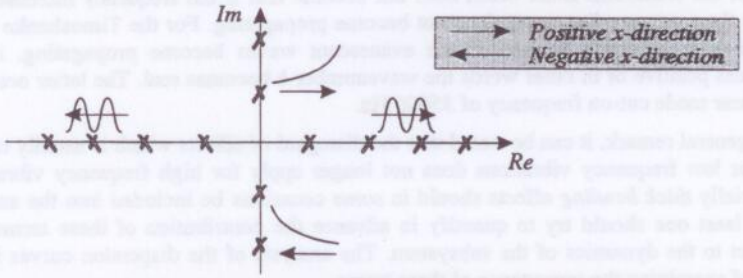

Figure 5.10 : Representation of waves in the complex wavenumber plane.

On the real axis lie the propagating waves. Four in each direction : one longitudinal, one bending in the *x-y* plane, one bending in the *x-z* plane and one torsional wave (bending and torsion can be coupled if the centroid and the shear axis are not coupled). The evanescent waves in the *x-y* plane and the evanescent waves in the *x-z* plane do not become necessarely shear mode waves at the same frequency; i.e. there will be *two* shear mode cut-on frequencies (*one* related to bending in the x-y plane and *one* related to bending in the x-z plane) and hence five or six propagating waves can be noticed

If the frequency tends to become higher than the shear mode cut-on freqencies, the imaginary wavenumbers become real. Hence, in this case, eleven or twelve propagating waves can be present on the beam. Below the shear mode cut-on frequency, only eight propagating waves are noticed and four evanescent waves. The phenomenon of shear mode cut-on only occurs because of the presence of *thick bending* terms. For Bernouilli-Euler beams, there would always be eight propagating waves and four evanescent waves.

The occurrence of the shear mode cut-on frequency is illustrated by means of a numerical example. A beam of which the essential properties are listed in the following table is considered.

Beam property	*Value*
Shear coefficient K_y	*0.833*
Beam section A	*2500* mm^2
Modulus of elasticity E	*70000* N/mm^2
Second moment of area Iz	*500000* mm^4
Material density ρ	*2700* kg/mm^3

Table 5.2 : General properties of a beam section.

[*] Frequencies for which the exponential decaying waves become propagating.

The dispersion relation (in terms of k^2 versus ω) for the evanescent wave in the positive x-direction in the x-y plane is plotted in figure *5.11*. Two cases are retained : the dispersion relation for a Bernouilli-Euler beam (omitting K_y and rotational inertia) and the dispersion relation for a Timoshenko beam.

From figure *5.11*, it is clear that the wavenumber of the evanescent bending wave in the case of the Bernouilli-Euler beam does not become real if the frequency increases and hence the corresponding wave does not become propagating. For the Timoshenko beam and beyond a certain frequency, the evanescent waves become propagating, i.e. k^2 becomes positive or in other words the wavenumber k becomes real. The latter occurs at the shear mode cut-on frequency of *35000* Hz.

As a general remark, it can be stated that the disregard of effects which is usually carried out for low frequency vibrations does not longer apply for high frequency vibrations. Especially *thick bending* effects should in some occasions be included into the analysis or at least one should try to quantify in advance the contribution of these terms with respect to the dynamics of the subsystem. The analysis of the dispersion curves is one way of examining the importance of these terms.

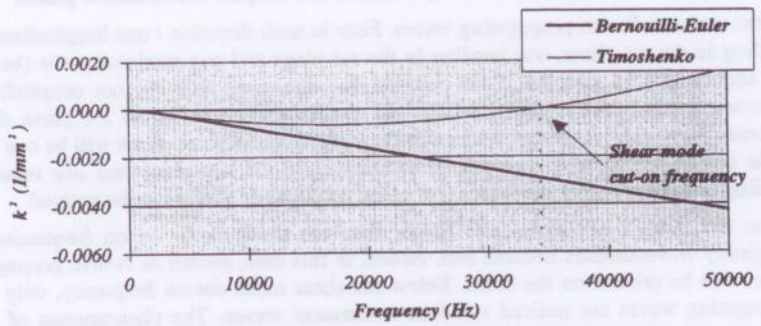

Figure 5.11 : Dispersion relation in terms of k^2 versus ω

Section 5.4.3.2 is concluded by introducing the general wave solution of a beam which is - from the mathematical viewpoint - a weighted summation of the twelve eigenvectors. The vector of basic variables $\{q\}$, can be written as :

$$\{q(x,t)\} = \sum_{i=1}^{12} a_i \cdot \{\Psi_i\} \cdot e^{j(\omega t - k_i x)} \qquad (5.30)$$

The complex quantity a_i will be referred to as the general wave coordinate of the wave denoted i[*]. Equation (5.30) can be written in matrix form as :

$$\{q(x,t)\} = [\Psi] \cdot [D(x,t)] \cdot \{a\} \qquad (5.31)$$

---

[*] The duality *modal model* versus *wave modal* can be seen in the light of the terms "*generalised modal coordinates*" versus "*generalised wave coordinates*", representing the relative importance of a specific mode i respectively a specific wave i.

$[D]$ is a diagonal matrix, it's diagonal terms are given by : $D_{ii} = e^{j(\omega t - k_i x)}$. $[\Psi]$ is a 12×12 matrix for which each column i represents the eigenvector $\{\Psi_i\}$. By eliminating the time dependent terms in equation (5.31), one obtains :

$$\{Q(x)\} = [\Psi] \cdot [D(x)] \cdot \{a\} \tag{5.32}$$

For convenience and without loss of generality, the terms e^{-jkx} contained in the matrix $[D]$ will not be considered further on because these terms only incorporate phase information of the wave with respect to a location along the beam. For the beam junction problem, we are not interested in the wave pattern along the beam but in the generalised wave coordinate at the point where the beams intersect. Therefore, it will be assumed that :

$$\{Q\} = [\Psi] \cdot \{a\} \tag{5.33}$$

at a certain location along the beam. The phase information of the waves at that location is contained in the generalised wave coordinate $\{a\}$.

At this stage, the general wave solution or in other words the vibration pattern of a beam in wave terms has been established. The next phase in the process of calculating the transmission coefficients of beam junctions is the evaluation of the semi-infinite beam stiffnesses, a topic which is addressed in the next paragraph.

5.4.3.3 *Semi-inifinite beam stiffness.*

A semi-infinite beam stiffness is defined through the algebraic relation between the internal forces and particle displacements of a cross-section of a beam under the assumption that only propagating waves in a *specific* direction are present. The semi-infinite beam stiffnesses are denoted $[K_\infty^+]$ and $[K_\infty^-]$ for respectively positive and negative going waves and are defined by the relation :

$$\{F^+\} = [K_\infty^+] \cdot \{U^+\} \quad \textit{respectively} \quad \{F^-\} = [K_\infty^-] \cdot \{U^-\} \tag{5.34}$$

Where $\{F^+\}$ and $\{U^+\}$ represent respectively the internal force in a beam section and the particle displacement of that same section in the case of the presence of exclusively positive going waves.

The matrix $[\Psi]$ containing the eigenvectors of the wave field is partitioned in such a way that the first six columns (eigenvectors) are associated with positive going waves (positive x-direction) and the remaining six columns (eigenvectors) are associated with negative going waves (negative x-direction). The latter can be done through the sign of the eigenvalues k_i. A positive sign (real or imaginary) denotes a positive going wave. The corresponding 6×1 generalised wave coordinates are denoted $\{a^+\}$ and $\{a^-\}$ for respectively positive and negative going waves.

Equation (5.33) becomes :

$$\{Q\} = \begin{Bmatrix} U \\ F \end{Bmatrix} = \begin{bmatrix} \Psi_{11} & \Psi_{12} \\ \Psi_{21} & \Psi_{22} \end{bmatrix} \cdot \begin{Bmatrix} a^+ \\ a^- \end{Bmatrix} \tag{5.35}$$

If only positive waves are taken into account, then $\{a^-\}=0$ and the displacements and internal forces can be written as :

$$\{U^+\}=[\Psi_{11}]\cdot\{a^+\} \quad \{F^+\}=[\Psi_{21}]\cdot\{a^+\} \tag{5.36}$$

By eliminating $\{a^+\}$, one can obtain a relation between internal forces and displacements associated with positive going waves :

$$\{F^+\}=[\Psi_{21}]\cdot[\Psi_{11}]^{-1}\cdot\{U^+\} \tag{5.37}$$

Hence, the 6×6 wave dynamic stiffness of the beam for positive going waves is given by :

$$[K_\infty^+]=[\Psi_{21}]\cdot[\Psi_{11}]^{-1} \tag{5.38}$$

Similarly, the 6×6 semi-infinite beam stiffness for negative going waves is given by :

$$[K_\infty^-]=[\Psi_{22}]\cdot[\Psi_{12}]^{-1} \tag{5.39}$$

Hence, for *every* propagating wave and for every combination of propagating waves in the positive or in the negative direction, the relation between the internal forces and particle displacements is given through equation (5.37). The relation previously established will be applied in the next section to express the compatibility and equilibrium at the junction.

This section concludes by pointing out the way to calculate the generalised wave coordinates of the positive and negative going waves if a specific vibration field on the beams is given.

The relative contributions of each wave are given through the generalised wave coordinates $\{a\}$:

$$\{a\}=[\Psi]^{-1}\cdot\{Q\} \tag{5.40}$$

Hence, in the case of positive going waves, the displacements and forces which can be attributed to the wave field are given by :

$$\{U^+\}=[\Psi_{11}]\cdot\{a^+\} \quad \{F^+\}=[\Psi_{21}]\cdot\{a^+\} \tag{5.41}$$

In the case of negative going waves :

$$\{U^-\}=[\Psi_{12}]\cdot\{a^-\} \quad \{F^-\}=[\Psi_{22}]\cdot\{a^-\} \tag{5.42}$$

5.4.3.4 Coordinate transformation.

In section 5.4.3.5, the compatibility and equilibrium condition at the point where the beams intersect are expressed. The displacements and the corresponding internal forces of the beams should therefore be considered in a *global* coordinate system. The forces and displacements which are considered in the previous section however are associated with a local - with respect to the beam - coordinate system. The transformation from a local beam coordinate system to a global coordinate system is carried out via the Euler angles (figure *5.12*). The index *g* in figure *5.12* denotes the global coordinate system. The index *l* denotes the local coordinate system.

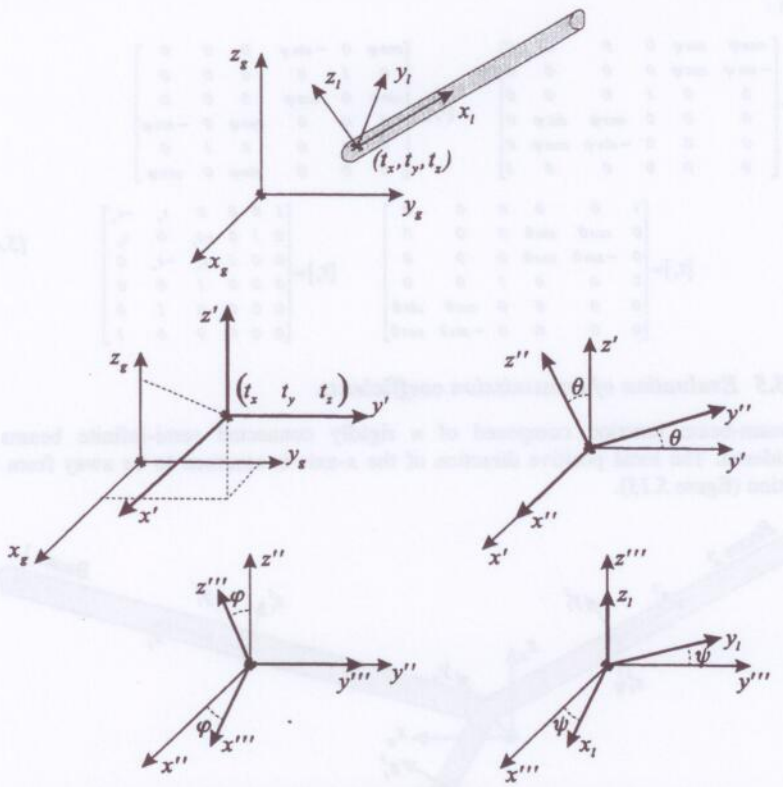

Figure 5.12 : Transformation from local to global coordinate system.

It can readily be shown that a transformation matrix can be defined such that with respect to the displacements :

$$\{u\}_l = [T_u] \cdot \{u\}_g \tag{5.43}$$

and with respect to the forces :

$$\{f\}_g = [T_f] \cdot \{f\}_l \tag{5.44}$$

The transformation of the stiffness matrix from the local to the global coordinate system, is given by :

$$[K]_g = [T_f] \cdot [K]_l \cdot [T_u] \tag{5.45}$$

The transformation matrices $[T_u]$ and $[T_f]$ are given below :

$$[T_u] = [T_\psi] \cdot [T_\varphi] \cdot [T_\theta] \cdot [T_s] \quad \textit{and} \quad [T_f] = [T_s]^T \cdot [T_\theta] \cdot [T_\varphi]^T \cdot [T_\psi]^T \tag{5.46}$$

With :

$$[T_\psi]=\begin{bmatrix} \cos\psi & \sin\psi & 0 & 0 & 0 & 0 \\ -\sin\psi & \cos\psi & 0 & 0 & 0 & 0 \\ 0 & 0 & 1 & 0 & 0 & 0 \\ 0 & 0 & 0 & \cos\psi & \sin\psi & 0 \\ 0 & 0 & 0 & -\sin\psi & \cos\psi & 0 \\ 0 & 0 & 0 & 0 & 0 & 1 \end{bmatrix} \quad [T_\varphi]=\begin{bmatrix} \cos\varphi & 0 & -\sin\varphi & 0 & 0 & 0 \\ 0 & 1 & 0 & 0 & 0 & 0 \\ \sin\varphi & 0 & \cos\varphi & 0 & 0 & 0 \\ 0 & 0 & 0 & \cos\psi & 0 & -\sin\varphi \\ 0 & 0 & 0 & 0 & 1 & 0 \\ 0 & 0 & 0 & \sin\varphi & 0 & \cos\varphi \end{bmatrix}$$

$$[T_\theta]=\begin{bmatrix} 1 & 0 & 0 & 0 & 0 & 0 \\ 0 & \cos\theta & \sin\theta & 0 & 0 & 0 \\ 0 & -\sin\theta & \cos\theta & 0 & 0 & 0 \\ 0 & 0 & 0 & 1 & 0 & 0 \\ 0 & 0 & 0 & 0 & \cos\theta & \sin\theta \\ 0 & 0 & 0 & 0 & -\sin\theta & \cos\theta \end{bmatrix} \quad [T_t]=\begin{bmatrix} 1 & 0 & 0 & 0 & t_z & -t_y \\ 0 & 1 & 0 & -t_z & 0 & t_x \\ 0 & 0 & 1 & t_y & -t_x & 0 \\ 0 & 0 & 0 & 1 & 0 & 0 \\ 0 & 0 & 0 & 0 & 1 & 0 \\ 0 & 0 & 0 & 0 & 0 & 1 \end{bmatrix} \qquad (5.47)$$

5.4.3.5 Evaluation of transmission coefficients.

A beam-beam junction composed of n rigidly connected semi-infinite beams is considered. The local positive direction of the x-axis is assumed to be away from the junction (figure *5.13*).

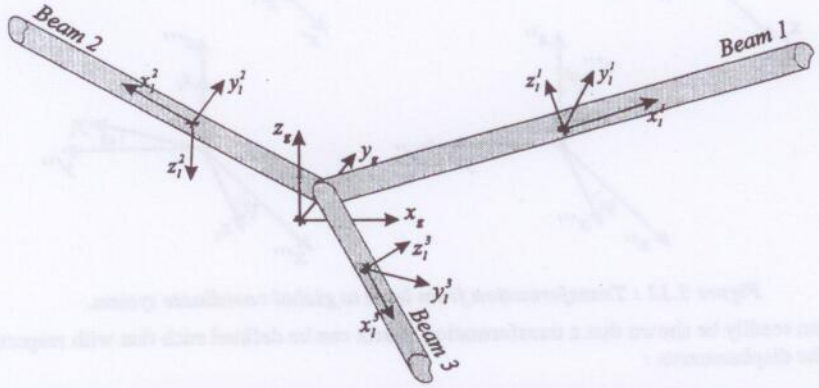

Figure 5.13 : Three beam junction and the corresponding coordinate systems.

In case of frequencies below the shear mode cut-on frequencies, each beam can transmit energy via four different wave types : longitudinal, bending in the x-y plane, bending in the x-z plane, torsion (eventually coupled with the bending waves) and hence the order of the transmission matrix will be four times the number of beams. Beyond the shear mode cut-on frequencies, the evanescent waves become shear waves and five or six propagating waves are noticed, resulting in a dimension of the transmission matrix of five or six times the number of beams.

In order to calculate the transmission coefficients of the junction, one has to impose a certain energy input into one of the beams (input beam) in such a way that a specific wave gets excited. The input wave propagates towards the junction and will be partially transmitted and partially reflected, producing the so-called outgoing (reflected and

transmitted) waves. Each of the outgoing waves is carrying a certain energy flow. The ratio between the energy flow associated with outgoing waves and the energy flow associated with input wave is called the transmission coefficient. The matrix which is built-up of transmission coefficients is called the transmission matrix of the junction.

The first step in the evaluation process of a transmission matrix deals with expressing the equilibrium and compatibility condition at the junction, making it possible to determine the relation between the particle displacements of the outgoing waves and the displacements of the input waves.

5.4.3.5.1 Equilibrium condition.

The equilibrium condition implies that the sum of all forces of all beams acting upon the junction equals zero :

$$\sum_{i=1}^{n}\{F_i\}=0 \qquad (5.48)$$

With $\{F_i\}$ representing the 6×1 internal force vector of beam i in the global coordinate system. Each force vector $\{F_i\}$ can in essence be decomposed into a force vector associated with positive going waves in beam i and a force vector associated with negative going waves in beam i :

$$\{F_i\}=\{F_i^+\}+\{F_i^-\} \qquad (5.49)$$

The equilibrium equation can be written in terms of particle displacements by applying the formulas of the semi-infinite stiffnesses as derived in paragraph 5.4.3.3. Equation (5.48) becomes :

$$\sum_{i=1}^{n}[K_{i\infty}^+]\cdot\{U_i^+\}+\sum_{i=1}^{n}[K_{i\infty}^-]\cdot\{U_i^-\}=0 \qquad (5.50)$$

Where $\{U_i^-\}$ and $\{U_i^+\}$ represent the 6×1 displacement vectors of beam i at the junction point for respectively incidence and outgoing waves.

5.4.3.5.2 Compatibility condition.

Because the beams are assumed to join in *one* point and the connection is assumed to be rigid, it holds that the particle displacements of all beams at the junction point are equal :

$$\{U_1\}=\{U_2\}=\cdots=\{U_n\} \qquad (5.51)$$

$\{U_i\}$ represents the 6×1 displacement vector at the junction point of beam i, in a global coordinate system.

By decomposing the particle displacement $\{U_i\}$ into particle displacements associated with input waves $\{U_i^-\}$ and particle displacements associated with the outgoing waves $\{U_i^+\}$, equation (5.51) becomes :

$$\begin{cases} U_1^+ + U_1^- = U_2^+ + U_2^- \\ U_2^+ + U_2^- = U_3^+ + U_3^- \\ \vdots \\ U_{n-1}^+ + U_{n-1}^- = U_n^+ + U_n^- \end{cases} \tag{5.52}$$

5.4.3.5.3 Assembling equilibrium and compatibility equations.

The equilibrium and compatibility equations (5.50) and (5.52) of the junction can be combined to yield :

$$\begin{bmatrix} I & -I & 0 & 0 & \cdots & 0 \\ 0 & I & -I & 0 & \cdots & 0 \\ 0 & 0 & \ddots & \ddots & \cdots & 0 \\ \vdots & \vdots & \ddots & \ddots & \ddots & \vdots \\ 0 & 0 & \cdots & 0 & I & -I \\ K_{1m}^+ & K_{2m}^+ & K_{3m}^+ & \cdots & \cdots & K_{nm}^+ \end{bmatrix} \cdot \begin{Bmatrix} U_1^+ \\ U_2^+ \\ \vdots \\ U_n^+ \end{Bmatrix} = - \begin{bmatrix} I & -I & 0 & 0 & \cdots & 0 \\ 0 & I & -I & 0 & \cdots & 0 \\ 0 & 0 & \ddots & \ddots & \cdots & 0 \\ \vdots & \vdots & \ddots & \ddots & \ddots & \vdots \\ 0 & 0 & \cdots & 0 & I & -I \\ K_{1m}^- & K_{2m}^- & K_{3m}^- & \cdots & \cdots & K_{nm}^- \end{bmatrix} \cdot \begin{Bmatrix} U_1^- \\ U_2^- \\ \vdots \\ U_n^- \end{Bmatrix} \tag{5.53}$$

Or in simplified form :

$$[K^+] \cdot \{U^+\} = [K^-] \cdot \{U^-\} \tag{5.54}$$

Where $\{U^+\}^T = \{U_1^+ \quad U_2^+ \quad \cdots \quad U_n^+\}$ represents the $6n \times 1$ vector containing the displacements (in a global coordinate system) of all positive going waves of all beams.

By applying the coordinate transformation formulas (5.43), one can readily infer the relation between the local displacements of the positive waves and the local displacements associated with the negative going waves. All displacements are combined into *one* $6n \times 1$ vector :

$$\{U^+\}_l = [A] \cdot \{U^-\}_l \tag{5.55}$$

With :

$$[A] = [T_u] \cdot [K^+]^{-1} \cdot [K^-] \cdot [T_u]^{-1} \tag{5.56}$$

The relation between the generalised wave coordinates of the incidence waves and the generalised wave coordinates of the outgoing waves can be established by applying equations (5.41) and (5.42) :

$$\{a^+\} = [\Psi_1] \cdot [A] \cdot [\Psi_2]^{-1} \cdot \{a^-\} \tag{5.57}$$

Or :

$$\{a^+\} = [B] \cdot \{a^-\} \tag{5.58}$$

Where $[B]$ is a $6n \times 6n$ matrix. $[\Psi_1]$ and $[\Psi_2]$ represent appropriate $6n \times 6n$ matrices built up of the matrices $[\Psi_{11}]$ and $[\Psi_{12}]$.

Every single element B_{ij} yield the generalised coordinate of a specific wave i if a specific wave j is excited, according to $a_j^- = 1$ and $a_l^- = 0\ ;\ l \neq j$. *[B]* does however not yet represent the transmission matrix : to calculate the transmission matrix of a junction, the relation between the generalised wave coordinates *{a}* and the corresponding energy flow variable should first be established as described below.

Consider a specific beam i. The energy flow (scalar) associated with the positive going waves in beam i equals :

$$E_i^+ = \frac{1}{2} \cdot Re\left[\{F_i^+\}^T \{V_i^+\}^*\right] \tag{5.59}$$

or in terms of particle displacements :

$$E_i^+ = \frac{1}{2} \cdot \omega \cdot Im\left[\{F_i^+\}^T \{U_i^+\}^*\right] \tag{5.60}$$

Where $\{F_i^+\}$ and $\{U_i^+\}$ represent the 6×1 internal force vector respectively particle displacement vector associated the positive going waves in beam i in a local coordinate system. In terms of wave coordinates (application of equation (5.41)), it holds that :

$$E_i^+ = Im\left(\{a_i^+\}^T \cdot [C_i] \cdot \{a_i^+\}^*\right) \tag{5.61}$$

Where $[C_i] = \omega / 2 \cdot [\Psi_{i,21}]^T \cdot [\Psi_{i,11}]^*$.

Hence, in physical terms : the imaginary part of every single element $C_{i,kk}$ represents the energy flow within beam i associated with a positive wave k with generalised wave coordinates $a_{i,k}^+ = 1$ and $a_{i,l}^+ = 0\ ;\ l \neq k$. For a wave with a generalised coordinate $a_{i,k}^+ \neq 1$ and $a_{i,l}^+ = 0$, the associated energy flow is given by : $a_{i,k}^{+*} \cdot Im(C_{i,kk})$

Similarly, the relation between the energy flow and the generalised wave coordinates for every single beam i can be established in the case of negative going waves :

$$E_i^- = Im\left(\{a_i^-\}^T \cdot [D_i] \cdot \{a_i^-\}\right) \tag{5.62}$$

Where $[D_i] = \omega / 2 \cdot [\Psi_{i,22}]^T \cdot [\Psi_{i,12}]^*$

Hence, for a negative going wave exhibiting a generalised coordinate $a_{i,k}^- = 1$ and $a_{i,l}^- = 0\ ;\ l \neq k$, the energy flow within beam i is given by : $a_{i,k}^{-*} \cdot Im(D_{i,kk})$

At this stage, all ingredients are present to be able to calculate the transmission coefficients. This can be done in the following way :

An input wave in beam i exhibiting generalised wave coordinates : $a_{i,k}^- = 1$ and $a_{i,l}^- = 0\ ;\ l \neq k$ is considered and the generalised wave coordinates of the outgoing waves are calculated by applying equation (5.58) :

$$\{a^+\} = [B] \cdot \{a^-\} \tag{5.63}$$

The energy flow associated with the input wave equals $Im(D_{kk})$ (equation (5.62)). The energy flow associated with a specific outgoing wave j can be calculated using equation (5.61). Hence, each element of the transmission matrix is given by the appropriate combination of the terms of the matrices *[C]*, *[D]* and *[B]*.

$$\tau_{jk} = \frac{Im(C_{jj}) \cdot a_{jk}^{+2}}{Im(D_{kk})} \qquad (5.64)$$

5.4.3.6 *Blocking mass.*

This paragraph addresses the use of a blocking mass at the junction as represented in figure *5.14*

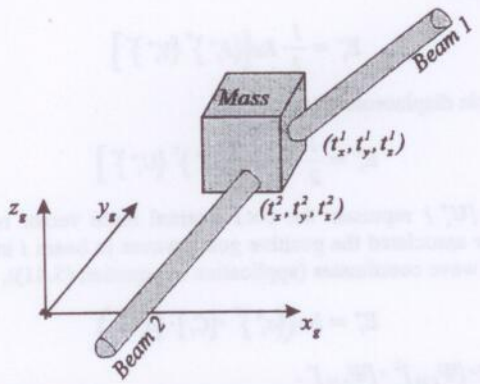

Figure 5.14 : Blocking mass contained in the junction.

In this case, the sum of the beam forces acting at the center of gravity of the rigid mass is compensated by the force of inertia of the mass :

$$\sum_{i=1}^{n} \{F_i\} = \omega^2 \cdot [M] \cdot \{U_j\} \qquad (5.64)$$

Where *[M]* represent the 6×6 mass matrix of the rigid mass.

The compatibility condition of equation has not changed and therefore, equation (5.53) is modified in the following way to include the use of a rigid mass :

$$\begin{bmatrix} I & -I & 0 & 0 & \cdots & 0 \\ 0 & I & -I & 0 & \cdots & 0 \\ 0 & 0 & \ddots & \ddots & \cdots & 0 \\ \vdots & \vdots & \ddots & \ddots & \ddots & \vdots \\ 0 & 0 & \cdots & 0 & I & -I \\ K_{j_1}^{+} & K_{j_2}^{+} & K_{j_3}^{+} & \cdots & \cdots & K_{j_n}^{+} - \omega^2 M \end{bmatrix} \cdot \begin{Bmatrix} U_1^{+} \\ U_2^{+} \\ \vdots \\ U_n^{+} \end{Bmatrix} = - \begin{bmatrix} I & -I & 0 & 0 & \cdots & 0 \\ 0 & I & -I & 0 & \cdots & 0 \\ 0 & 0 & \ddots & \ddots & \cdots & 0 \\ \vdots & \vdots & \ddots & \ddots & \ddots & \vdots \\ 0 & 0 & \cdots & 0 & I & -I \\ K_{j_1}^{-} & K_{j_2}^{-} & K_{j_3}^{-} & \cdots & \cdots & K_{j_n}^{-} - \omega^2 M \end{bmatrix} \cdot \begin{Bmatrix} U_1^{-} \\ U_2^{-} \\ \vdots \\ U_n^{-} \end{Bmatrix} \qquad (5.66)$$

From here on, the procedure to calculate the transmission matrix is completely analogous to the procedure outlined in section 5.4.3.5.3.

5.4.3.7 Evaluation of SEA Coupling Loss Factors.

The aim of this paragraph is to stress the relation between SEA coupling loss factors and transmission coefficients in the case of beam networks. From the SEA point of view, each wave in each beam can be associated with one specific SEA subsystem. Hence, if the network contains n beams, the SEA model will have four times n subsystems (eventually five or six times n depending on the shear mode cut-on frequencies).

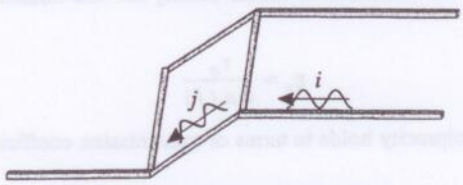

Figure 5.15 : SEA beam network.

Let subsystem i have a vibrational energy E_i (spatial and frequency averaged). The group velocity of the corresponding wave is represented by $c_{i,g}$ and the length of subsystem i is given by L_i.

It is assumed that the energy flowing in subsystem i is given by P_i^+ and P_i^- respectively in the positive and negative x-direction. One of the major assumptions which should now be made is that these energy flows P_i^+ & P_i^- are incoherent, in order to be added. The following relation between the energy flows P_i^+ & P_i^- and vibration energy E_i can now be established.

$$E_i = L_i \cdot \frac{P_i^+ + P_i^-}{c_{i,g}} \qquad (5.67)$$

The wave which is carrying an energy flow P_i^- (subsystem i) will impinge upon the junction and transmit energy into subsystem j. By definition (SEA hypothesis), the energy flow from subsystem i to j is given by :

$$P_{i \to j} = \omega \cdot \eta_{ij} \cdot E_i \qquad (5.68)$$

Besides, by definition of transmission coefficients, the energy flow from subsystem i to subsystem j is given by :

$$P_{i \to j} = \tau_{ij} \cdot P_i^- \qquad (5.69)$$

In addition, we will assume that the energy flows P_i^+ and P_i^- are equal. Consequently, it holds that :

$$P_i^+ = P_i^- = P_i \quad \textit{and hence} \quad E_i = \frac{2P_i}{c_{i,g}} \qquad (5.70)$$

The previous assumption is equivalent to the ideal diffuse field when dealing with acoustic volumes. Strictly, it implies zero energy flow throughout the network. However, the assumption can be justified by the fact that equation (5.67) contains the *sum* (and not

the *difference* between two more or less equal values). Besides, this assumption corresponds to the weak coupling assumption made in SEA.

Combining equation (5.68)- (5.70), it follows that :

$$\eta_{ij} = \frac{\tau_{ij}\, c_{i,g}}{2\omega L_i} \tag{5.71}$$

Or by making use of the definition of modal density for one-dimensional subsystems : $n_i(f) = L_i / \pi c_{i,g}$

$$\eta_{ij} = \frac{\tau_{ij}}{\omega n_i(f)} \tag{5.72}$$

Furthermore, since reciprocity holds in terms of transmission coefficients : $\tau_{ij} = \tau_{ji}$ one obtains :

$$n_i \cdot \eta_{ij} = n_j \cdot \eta_{ji} \tag{5.73}$$

resulting in the SEA reciprocity relation.

5.4.4 Plate-plate junction.

5.4.4.1 Introduction.

In the process of analysing structure-borne noise, one is often faced with problems associated with the passage of vibrational energy through plate joints. Examples in this respect include ships, buildings, helicopters, cars. CREMER [92] was amongst the first to investigate the transmission characteristics of a corner junction including inclined incidence angles of the waves. KIHLMAN [93] extended the analysis to that of a cross-junction but, like Cremer, neglected in-plane vibrations on the source plate and coplanar plate. This assumption is correct for the symmetrical structures considered by Kihlman but is not so for corners, T-junctions and other non-symmetrical plate couplings. RECCHART and RICHTER [94] discussed the use of the reciprocity relation to calculate transmission coefficients for incidence travelling waves other than out of plane bending waves. HWANG and PI [95] extended these relations based on thin plate theory to calculate the coupling between bending and in-plane waves of two plates. GRAVEN and GIBBS [26] gave a description of sound transmission at a cross junction composed of thin plates, including mode coupling. Bending, longitudinal and transverse shear waves are coupled and are assumed to be generated on each plate. As in actual practice, one usually encounters more complicated structural joints such as T-joints and right-angled cross joints between plates of *different thickness*, a parametric survey on the effect of essential junction parameters on the transmission coefficients at a T-junction is given. LYON and TRATCH [18] investigated the influence of the in-plane vibrations with respect to the noise levels in ships, taking right-angled plates with different thicknesses. They concluded that at high frequencies, the effect of in-plane vibrations can in some occasions become essential. GIBBS [43] described a method to analyse sound waves generated at a series of T-junctions composed of thin plates as a result of a wave incident on one of the plates. Transmission characteristics are studied in detail including in-plane

longitudinal, transverse shear and bending waves and it is found that the transmission coefficient is strongly dependent on the incidence angle, indicating that *normal* incidence characteristics do not offer a satisfactory representation of wave transmission in the case of plate junctions and therefore, oblique wave incidence should be included into the analysis. MCCOLLUM and CUSHIERI [36] evaluated the energy transmission through a junction composed of two plates in an L-shaped configuration. Their solution includes shear and rotatory inertia and in-plane wave effects. The paper concluded that in terms of vibrational energy flow through a junction (L shaped in their case), the effects of shear and rotatory inertia and the effects of in-plane waves are important, especially at high frequencies. Yet, most of the publications on the evaluation of transmission coefficients deal with thin plates for which the effect of thick bending terms is neglected. If the shear effect, which constitutes the most important thick bending contribution, is ignored, then vibration solutions for such plates are unconservatively large (See LIEW et al. [69]). Research on incorporating shear deformation effects in plates has yielded many theories which range from the pioneering first order of REISSNER [96] and MINDLIN [54] and the modified Mindlin type plate theories of BERGAN and WANG [97] to higher order theories (displacements are expanded in powers of the thickness coordinate) as for example proposed by NELSON and LORCH [98]. In here, the classical Mindlin thick plate theory is adopted.

MEES and VERMEIR [38] studied the bending wave transmission between semi-infinite thin plates connected by a hinge or by an elastic interlayer. The wave transmission across the interlayer is calculated analytically, the stiffening effect of the interlayer is simulated with a finite element model. Several critical parameters of the interlayer were investigated such as : off-set mounting of the plate, modulus of elasticity, Poisson's ratio, the loss factor and the shape of the interlayer. LANGLEY and HERON [23] calculated the wave transmission coefficients of structural joints which consist of an arbitrary number of *thin* plates which are either coupled through a beam or directly coupled along a line.

The analysis presented in this section aims at merging some important items, which have been investigated separately in the past, in order to perform an accurate evaluation of the transmission characteristics and of the associated coupling loss factors of plate junctions at high frequencies. As such, this section provides the procedures to calculate the transmission coefficients of flat plate junctions composed of an arbitrary number of plates, including thick bending terms (MINDLIN [54]), coupled together along a line (CREMER et al. [79], HERON [23]). The angles of the plates are arbitrary, an off-set of each plate at the junction line can be included (figure *5.16*).

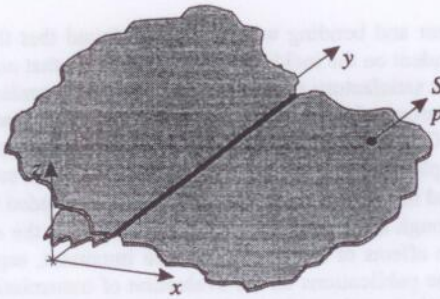

Figure 5.16 : Schematic representation of a plate-plate coupling.

Out of plane and in-plane waves are accounted for. The analysis is restricted to isotropic plates although the method can be extended to non-isotropic plates in a conceptually similar way. As much as possible, the entire procedure to calculate the transmission coefficients of plate junctions is resembling to the procedure to calculate the transmission coefficients of beam junctions. First, the derivation of the relevant dynamic equations of motion of plates is presented, followed by the extraction of a plane wave solution. Next, the semi-infinite stiffnesses of the waves are calculated. Subsequently, by expressing compatibility and equilibrium at the junction line, a relation between the particle displacements of the outgoing waves and the particle displacements of the incidence waves can be established. Finally, the transmission coefficients are computed.

In advance, one important point should be mentioned dealing with the difference between plate-plate and beam-beam junctions. Whereas for beam-beam junctions, waves can only travel in two directions (positive x and negative x-direction), this is not the case for plate junctions for which plane waves can impinge upon a junction under an infinite number of directions. Therefore, one additional parameter arises in the case of plate couplings : the incidence angle φ of the plane wave (see figure *5.17*).

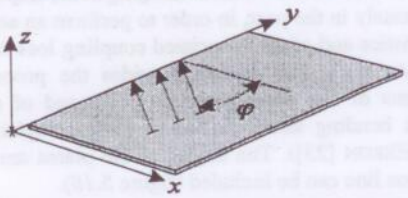

Figure 5.17 : Plane waves on a plate : representation the coordinate system and of the incidence angle.

Consequently, the transmission coefficients will be a function of the incidence angle, i.e. $\tau = \tau(\varphi)$.

As a final point, it can be noted that the local coordinate system of the plate is chosen such that waves are flowing in the x-y plane and are impinging upon the y-axis which constitutes the junction line.

5.4.4.2 Out of plane motion.

5.4.4.2.1 Dynamic plate equations.

The equations of motion governing the normal deflection of thin plates yields a phase velocity - for waves travelling in a certain direction - which is inversely proportional to the wavelength and thus tends to infinity for very short wavelengths. This is entirely analogous to the classical Bernouilli-Euler beams. In order to remedy this shortcoming, Timoshenko included the effects of rotatory inertia and transverse shear into the beam equations giving rise to the Timoshenko beam which gives better results at higher frequencies or shorter wavelengths. By an comparable procedure, it is possible to obtain an equation of motion for the flexural vibrations of thick elastic plates, taking into account the effects of rotatory inertia and transverse shear. MINDLIN [54] has shown how the corresponding two-dimensional flexural equations of motion of a plate can be derived directly from the three-dimensional equations of elasticity. The equations governing the thick bending motion of plates are called the Mindlin or occasionally the Timoshenko-Mindlin plate equations.

If the displacements in the direction perpendicular to the undeformed middle surface is denoted u_z and by assuming that plane sections originally perpendicular to the undeformed middle surface remain plane after deformation but not necessarely perpendicular to the deformed middle surface, then the equations governing the out of plane motion of the plate, including thick bending terms, is given by (MINDLIN [54]):

$$\left(D\nabla^2 - \frac{\rho h^3}{12}\cdot\frac{\partial^2}{\partial t^2}\right)\cdot\left(\nabla^2 - \frac{\rho}{\kappa^2 G}\cdot\frac{\partial^2}{\partial t^2}\right)u_z + \rho h\cdot\frac{\partial^2 u_z}{\partial t^2} = \left(1 - \frac{D}{\kappa^2 G h}\cdot\nabla^2 + \frac{\rho h^2}{12\kappa^2 G}\cdot\frac{\partial^2}{\partial t^2}\right)q(x,y,t) \qquad (5.74)$$

Where $D = Eh^3/12(1-\nu^2)$ represents the bending stiffness of the plate, ν denotes Poisson's ratio and $q(x,y,t)$ represents the applied load on the plate. The term $\kappa^2 G$ accounts for the fact that the transverse shear strain is not truly independent of the thickness coordinate. Furthermore, by adjusting the value of this constant, the limiting value of the phase velocity can be made to coincide with the Rayleigh wave speed which is the limiting value of the phase speed as predicted by three-dimensional elasticity theory. According to Mindlin, for the vibration analysis of isotropic moderately thick plates, the first order Reissner-Mindlin theory will usually suffice. Although in this theory, a constant shear stress distribution through the thickness is assumed, it can give reasonably accurate solutions when used in conjunction with an acceptable shear correction factor κ on the shear modulus as illustrated by SRINIVAS and RAO and PRASAD [99]. The commonly used values for κ are 5/6 (derived by Reissner). Mindlin takes $\kappa = \pi^2/12$ and NANNI [100] showed that the shear correction factor κ can be expressed in terms of Poisson ratio ν, according to : $\kappa = 20(1+\nu)/(24+25\nu+\nu^2)$.

The rotatory influence is contained in the terms :

$$\frac{\rho h^3}{12}\cdot\frac{\partial^2}{\partial t^2} \quad \text{and} \quad \frac{\rho h^2}{12\kappa^2 G}\cdot\frac{\partial^2}{\partial t^2} \qquad (5.75)$$

In absence of loads, the equation governing the normal deflection of a thick plate reduces to :

$$\left(D\nabla^2 - \frac{\rho h^3}{12}\cdot\frac{\partial^2}{\partial t^2}\right)\cdot\left(\nabla^2 - \frac{\rho}{\kappa^2 G}\cdot\frac{\partial^2}{\partial t^2}\right)u_z + \rho h\cdot\frac{\partial^2 u_z}{\partial t^2} = 0 \qquad (5.76)$$

The equations relating the rotations ϑ_x and ϑ_y (figure *5.18*) of a cross section to the normal diplacement u_z is given by :

$$\begin{cases} \dfrac{D}{2}\cdot\left((1-\nu)\cdot\nabla^2\vartheta_x + (1+\nu)\cdot\dfrac{\partial}{\partial x}\left(\dfrac{\partial\vartheta_x}{\partial x} + \nu\dfrac{\partial\vartheta_y}{\partial y}\right)\right) + \kappa^2 Gh\left(\dfrac{\partial u_z}{\partial x} - \vartheta_x\right) = \dfrac{\rho h^3}{12}\cdot\dfrac{\partial^2\vartheta_x}{\partial t^2} \\ \kappa^2 Gh\left(\nabla^2 u_z - \dfrac{\partial\vartheta_x}{\partial x} - \dfrac{\partial\vartheta_y}{\partial y}\right) = \rho h\dfrac{\partial^2 u_z}{\partial t^2} \end{cases} \qquad (5.77)$$

The resultant, relevant bending moment, twisting moment and transverse shear force on a plane perpendicular to the x-axis and per unit length in terms of the displacement u_z and the rotation variables ϑ_x and ϑ_y are given by :

$$\begin{aligned} m_y &= D\cdot\left(\frac{\partial\vartheta_y}{\partial x} + \nu\frac{\partial\vartheta_x}{\partial y}\right) \\ m_x &= \frac{Gh^3}{12}\cdot\left(\frac{\partial\vartheta_y}{\partial y} + \frac{\partial\vartheta_x}{\partial x}\right) \\ f_z &= \kappa^2 Gh\cdot\left(\frac{\partial u_z}{\partial x} + \vartheta_x\right) \end{aligned} \qquad (5.78)$$

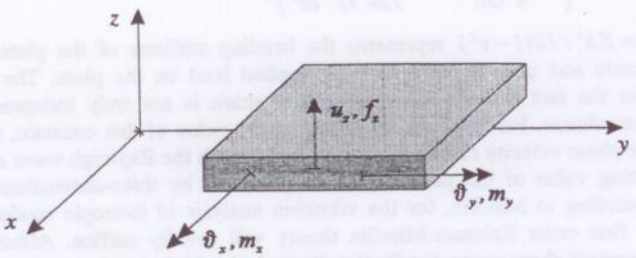

Figure 5.18 : Out of plane forces and displacements.

Note that in the light of the calculations which will be performed at a later stage, only the relevant variables, namely $u_z, \vartheta_x, \vartheta_y, f_z, m_x, m_y$, are retained and are named correspondingly. It should be mentioned however that the *classical* designation of the internal plate forces and moments is different. In literature (See also Mindlin [54]), the variables denoted $M_x, M_{xy}, Q_x, \psi_x \psi_y$ are replaced in here by $m_y, m_x, f_z, -\vartheta_y\ \vartheta_x$. This has been done because it is felt that the notation adopted in here gives rise to more clarity when applied to our specific problem, i.e. out of plane motion wave propagation.

5.4.4.2.2 Plane wave solution.

Because only *plane* waves travelling in the *x-y* plane and impinging upon the junction (*y* −axis) are considered, all variables *z(x,y,t)* can be replaced by $Z \cdot e^{j(\omega t - k_x x - k_y y)}$. Thus, derivatives can be replaced by algebraic multiplicators :

$$\frac{\partial}{\partial x} \Rightarrow -jk_x \quad \frac{\partial}{\partial y} \Rightarrow -jk_y \quad \frac{\partial}{\partial t} \Rightarrow j\omega \tag{5.79}$$

In terms of differential operators which have properties analogous to those of algebraic quantities, it holds that the operator polynomial in ∇ of equation (5.76) can be written as :

$$\left(D\nabla^2 + \frac{\rho h^3 \omega^2}{12}\right) \cdot \left(\nabla^2 + \frac{\rho \omega^2}{\kappa^2 G}\right) \cdot U_z - \rho h \omega^2 \cdot U_z = 0 \tag{5.80}$$

Or in simplified form :

$$(\nabla^4 + A \cdot \nabla^2 + B) \cdot U_z = 0 \tag{5.81}$$

The characteristic equation which has four roots becomes (replacing ∇^2 by $k_x^2 + k_y^2$) :

$$(k_x^2 + k_y^2 - A_1) \cdot (k_x^2 + k_y^2 - A_2) = 0 \tag{5.82}$$

Where :

$$A_{1,2} = -\frac{\rho \omega^2}{2\kappa^2 G} - \frac{\rho h^3 \omega^2}{24 D} \pm \sqrt{\left(\frac{\rho \omega^2}{\kappa^2 G} - \frac{\rho h^3 \omega^2}{12 D}\right)^2 + \frac{4 \rho h \omega^2}{D}} \tag{5.83}$$

represent the two real roots of equation (5.82).

Hence, the dispersion relation for out of plane, plane waves on thick plates is given by :

$$\begin{cases} k_x^2 + k_y^2 - A_1 = 0 \\ k_x^2 + k_y^2 - A_2 = 0 \end{cases} \tag{5.84}$$

Because the dispersion relation determines the different wave types (propagating or evanescent), a discussion is required.

For our purposes, a given *propagating* plane wave is impinging upon the junction line (*y* −axis) which is infinitely long. Therefore, without loss of generality, we can assume that the wavenumber k_y of the incidence wave is real and without loss of generality, the wavenumber k_y is taken positive (i.e. wave flowing in the positiv *y*-direction). All other waves (reflected and transmitted) will exhibit the same wavenumber k_y because of the compatibility conditions at the junction line (tracing wavenumber k_y). In other words, from the *y*-direction point of view, *all* waves (incidence, reflected and transmitted) are propagating, no one evanescent term is present in the *y*-direction.

For the calculation of the transmission coefficients, one has to impose a specific incidence wave which is impinging upon the junction. Hence, the incidence angle of the incidence wave (See also figure *5.17*) is known. Because the wavenumber k_y is directly related to the incidence angle through :

$$k_y \propto sin(\varphi) \tag{5.85}$$

one can also assume a given wavenumber k_y instead of a given incidence angle φ of the incidence wave. An incidence angle ranging from 0 to $\pi/2$ is analogous to a given wavenumber k_y ranging from 0 to a certain number (see further on). Hence, if further on it is mentioned that k_y is given, then the latter denotes automatically that the incidence angle of the incidence wave is given.

The dispersion relation with respect to the wavenumber k_x is given by (from equation (5.84)) :

$$k_x = \pm\sqrt{A_{1,2} - k_y^2} \tag{5.86}$$

According to the standard form of the quadratic equation (5.81), it holds that :

$$sign(A_1 + A_2) = sign(A) = 1 \quad and \quad sign(A_1 \cdot A_2) = sign(B) \tag{5.87}$$

Hence, the sign of B of equation (5.86) will determine the relative sign of the roots $A_{1,2}$ and hence will determine the wavenumber k_x and consequently the characteristics of the wave.

The following cases can be distinguished :

- $B > 0$ or $\omega > \omega_c = \sqrt{12\kappa^2 G/\rho h^2}$.

A_1 and A_2 are both positive. Without loss of generality, it will be assumed that $A_1 < A_2$. Three different cases can be looked upon :

- ❑ $k_y^2 < A_1 < A_2$.

  In this case, equation (5.86) yields four real roots of which two are positive and two are negative.

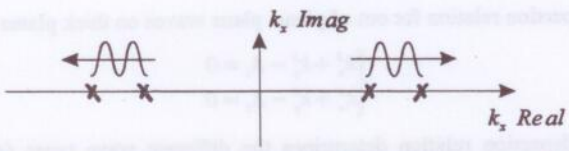

Figure 5.19 : Representation of waves in the complex wavenumber plane.

- ❑ $A_1 < k_y^2 < A_2$.

  Equation (5.86) yields two real roots (one positive and one negative) and two imaginary roots (one positive and one negative). The corresponding waves are represented in figure *5.20.*

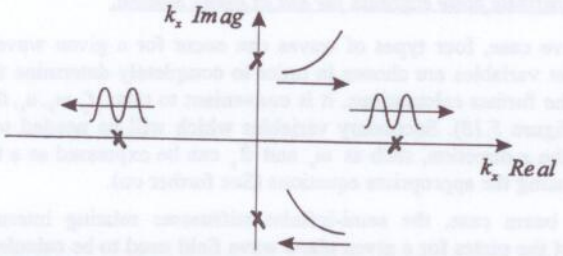

Figure 5.20 : Representation of waves in the complex wavenumber plane

- $A_1 < A_2 < k_y^2$

Only imaginary roots can occur meaning that all associated four waves are evanescent (figure *5.21*).

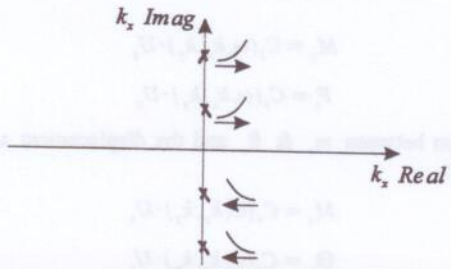

Figure 5.21 : Representation of waves in the complex wavenumber plane

- $B < 0$ or $\omega < \omega_c = \sqrt{12\kappa^2 G/\rho h^2}$.

In this case, the roots A_1 and A_2 exhibit a different sign. Let's assume $A_1 < 0$ and $A_2 > 0$. Remark that for thin bending : $A_2 = -A_1$. Two different cases need to be examined.

- $k_y^2 < A_2$

Equation (5.86) yields two real roots and two imaginary roots, corresponding to figure *5.20*.

- $k_y^2 > A_2$

Two positive and two negative imaginary roots are found. This situation is similar to the one of figure *5.21*.

From the discussion of the dispersion relation, it became clear that for higher frequencies, i.e. above the shear mode cut-on frequency : $\omega > \omega_c = \sqrt{12\kappa^2 G/\rho h^2}$, the coefficient B of equation (5.81) can become positive and the evanescent flexural waves become propagating shear waves, in a similar way as for the Timoshenko beam.

5.4.4.2.3 Semi-infinite plate stiffness for out of plane motion.

In the plane wave case, four types of waves can occur for a given wavenumber k_y[`]. Four independent variables are chosen in order to completely determine the wave field. In the light of the further calculations, it is conveniant to take $f_z, m_y, u_z, \vartheta_y$ as the basic variables (See figure *5.18*). Secondary variables which will be needed to calculate the energy flow in the x-direction, such as m_x and ϑ_x can be expressed as a function of the basic variables using the appropriate equations (See further on).

Similar to the beam case, the semi-infinite stiffnesses relating internal forces and displacements of the plates for a given plane wave field need to be calculated. First, four eigenvectors $\{U_z, \Theta_y, F_z, M_y\}$, associated with four possible wavenumbers k_x (eigenvalues) are sought for. By eliminating Θ_x in equation 5.77, it follows that :

$$\Theta_y = C_1(\omega, k_x, k_y) \cdot U_z \tag{5.88}$$

The forces M_y and F_z can be expressed in terms of U_z using equation (5.77) and (5.78), resulting in :

$$M_y = C_2(\omega, k_x, k_y) \cdot U_z \tag{5.89}$$

$$F_z = C_3(\omega, k_x, k_y) \cdot U_z \tag{5.90}$$

Further on, the relation between m_x & ϑ_x and the displacement u_z can be calculated using equation (5.78) :

$$M_x = C_4(\omega, k_x, k_y) \cdot U_z \tag{5.91}$$

$$\Theta_x = C_5(\omega, k_x, k_y) \cdot U_z \tag{5.92}$$

In summary, for a given wavenumber k_y (given incidence angle of the incidence wave), four wavenumbers k_x can be calculated (equation (5.86)) and accordingly four different relations between U_z, Θ_y, F_z, M_y can be established (equations (5.89-92)), giving rise to four *eigenvectors*. It will be assumed that these eigenvectors represent the columns of the matrix $[\Psi]$. Hence, it follows that (analogous to the beam case) :

$$\{Q\} = \begin{Bmatrix} U_z \\ \Theta_y \\ F_z \\ M_y \end{Bmatrix} = [\Psi] \cdot \begin{Bmatrix} a_1 \\ a_2 \\ a_3 \\ a_4 \end{Bmatrix} \tag{5.93}$$

The eigenvectors are grouped such that the first two eigenvectors are associated with positive[``] going waves (propagating or evanescent) and the last two eigenvectors are associated with negative going waves (propagating or evanescent) :

[`] or indeed for a given incidence angle of the incidence wave.

[``] If a wave is supposed to be positive or negative going, propagating or evanescent then the latter is always with respect to the x-axis. With respect to the y-axis, it is assumed that *all* waves are *propagating* in the *positive* y-direction because the incidence wave is *propagating* in the y-direction.

$$\{Q\} = [\Psi] \cdot \begin{Bmatrix} a^+ \\ a^- \end{Bmatrix} \tag{5.94}$$

The wave dynamic stiffness of the plate, relating the internal forces $\{F_z \quad M_y\}$ to the displacements $\{U_z \quad \Theta_y\}$, in the case of plane waves with a given wavenumber k_y can now be obtained in the following way :

- In the case of positive going waves, it holds that $\{a^-\} = 0$ and hence equation (5.94) becomes :

$$\begin{Bmatrix} U_z^+ \\ \Theta_y^+ \end{Bmatrix} = [\Psi_{11}] \cdot \{a^+\} \quad and \quad \begin{Bmatrix} F_z^+ \\ M_y^+ \end{Bmatrix} = [\Psi_{21}] \cdot \{a^+\} \tag{5.95}$$

By eliminating the generalised wave coordinates $\{a^+\}$, the following expression is obtained for the relation between forces and associated displacements in the case of plane waves in the positive x-direction.

$$\begin{Bmatrix} F_z^+ \\ M_y^+ \end{Bmatrix} = [\Psi_{21}] \cdot [\Psi_{11}]^{-1} \begin{Bmatrix} U_z^+ \\ \Theta_y^+ \end{Bmatrix} \quad or \quad \begin{Bmatrix} F_z^+ \\ M_y^+ \end{Bmatrix} = [K_\infty^+] \begin{Bmatrix} U_z^+ \\ \Theta_y^+ \end{Bmatrix} \tag{5.96}$$

Where $[K_\infty^+]$ represents the wave dynamic stiffness matrix associated with positive going plane waves and with out of plane motion.

- Similarly, the relation between forces and displacement for negative going waves can be obtained and is given by :

$$\begin{Bmatrix} F_z^- \\ M_y^- \end{Bmatrix} = [\Psi_{22}] \cdot [\Psi_{12}]^{-1} \begin{Bmatrix} U_z^- \\ \Theta_y^- \end{Bmatrix} \quad or \quad \begin{Bmatrix} F_z^- \\ M_y^- \end{Bmatrix} = [K_\infty^-] \begin{Bmatrix} U_z^- \\ \Theta_y^- \end{Bmatrix} \tag{5.97}$$

5.4.4.3 *In-plane motion.*

5.4.4.3.1 *Dynamic plate equations.*

For a linear isotropic plate, the equations of motion governing the in-plane motion are given by :

$$\begin{cases} \dfrac{\partial^2 u_x}{\partial x^2} + \dfrac{1-\nu}{2} \cdot \dfrac{\partial^2 u_x}{\partial y^2} + \dfrac{1+\nu}{2} \cdot \dfrac{\partial^2 u_y}{\partial x \partial y} = \dfrac{\rho(1-\nu^2)}{E} \cdot \dfrac{\partial^2 u_x}{\partial t^2} \\ \dfrac{\partial^2 u_y}{\partial y^2} + \dfrac{1-\nu}{2} \cdot \dfrac{\partial^2 u_y}{\partial x^2} + \dfrac{1+\nu}{2} \cdot \dfrac{\partial^2 u_x}{\partial x \partial y} = \dfrac{\rho(1-\nu^2)}{E} \cdot \dfrac{\partial^2 u_y}{\partial t^2} \end{cases} \tag{5.98}$$

The relevant forces (See figure 5.22) on a plane perpendicular to the x-axis per unit length in terms of the displacements are given by :

$$\begin{cases} f_x = \dfrac{Eh}{1-\nu^2} \cdot \left(\dfrac{\partial u_x}{\partial x} + \nu \dfrac{\partial u_y}{\partial y} \right) \\ f_y = \dfrac{Eh}{2(1+\nu)} \cdot \left(\dfrac{\partial u_y}{\partial x} + \dfrac{\partial u_x}{\partial y} \right) \end{cases} \tag{5.99}$$

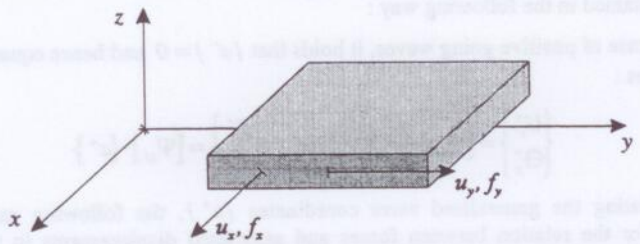

Figure 5.22 : Relevant forces and displacements for in-plane motion.

5.4.4.3.2 Plane wave solution.

Plane waves will be considered further on and therefore all variables z can be replaced by $Z \cdot e^{j(\omega t - k_x x - k_y y)}$. Derivatives can be replaced by algebraic multiplicators.

Equation (5.98) therefore becomes :

$$\begin{cases} k_x^2 \cdot U_x + \dfrac{1-\nu}{2} \cdot k_y^2 \cdot U_x + \dfrac{1+\nu}{2} \cdot k_y k_x \cdot U_y = \dfrac{\rho(1-\nu^2)}{E} \cdot \omega^2 \cdot U_x \\ k_y^2 \cdot U_y + \dfrac{1-\nu}{2} \cdot k_x^2 \cdot U_y + \dfrac{1+\nu}{2} \cdot k_y k_x \cdot U_x = \dfrac{\rho(1-\nu^2)}{E} \cdot \omega^2 \cdot U_y \end{cases} \tag{5.100}$$

The displacements U_x and U_y can be eliminated from equation (5.100), resulting in an algebraic equation relating the wavenumbers k_x and k_y to the frequency ω (dispersion relation) :

$$\left(k_x^2 + \frac{1-\nu}{2} \cdot k_y^2 - \frac{\rho(1-\nu)}{E} \cdot \omega^2 \right) \cdot \left(k_y^2 + \frac{1-\nu}{2} \cdot k_x^2 - \frac{\rho(1-\nu)}{E} \cdot \omega^2 \right) = \frac{(1+\nu)^2}{4} \cdot k_x^2 k_y^2 \tag{5.101}$$

Equation (5.101) represents an algebraic equation for which the wavenumber k_x and k_y are interchangeable and which can be rewritten in the following form :

$$(k_x^2 + k_y^2 - A_1) \cdot (k_x^2 + k_y^2 - A_2) = 0 \tag{5.102}$$

The roots A_1 and A_2 are given by :

$$A_1 = \frac{\rho\omega^2(1-\nu^2)}{E} \quad \text{and} \quad A_2 = \frac{2\rho\omega^2(1+\nu)}{E} \tag{5.103}$$

Note that it always holds that $A_1 < A_2$. The solutions A_1 and A_2 represent the squared wavenumbers corresponding to respectively longitudinal and shear waves[*] . The latter can be shown by considering the ratio between the wavenumbers k_x and k_y and the ratio between the particle displacements U_x and U_y.

In the case of the root A_1, it holds that :

$$cot\, g(\varphi) = \frac{k_x}{k_y} = \frac{U_x}{U_y} \qquad (5.104)$$

Equation (5.104) corresponds to an in-plane quasi-longitudinal wave because the direction of the wave (determined by k_x / k_y) is similar to the direction of the particle displacements (see figure *5.23*)

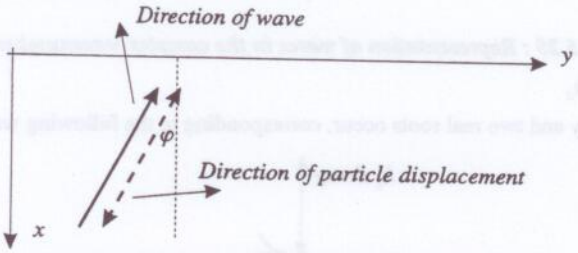

Figure 5.23 : Longitudinal plane wave in a plate.

In the case of the root A_2, it holds that :

$$\frac{k_x}{k_y} = -\frac{U_y}{U_x} \qquad (5.105)$$

Equation (5.105) corresponds to an in-plane shear wave. The direction of the wave and of the particle displacements are indicated in figure *5.24*.

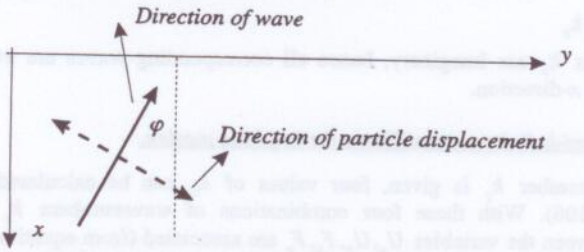

Figure 5.24 : In-plane shear wave in a plate.

For our purposes, the wavenumber k_y is given and is assumed to be real and positive. The type of wave will therefore be determined by the wavenumber k_x. For a given k_y, the wavenumber k_x can exhibit four values:

---

[*] Therefore, A_1 and A_2 will be replaced by k_L^2 and k_S^2.

$$k_x = \pm\sqrt{k_L^2 - k_y^2} \text{ or } k_x = \pm\sqrt{k_S^2 - k_y^2} \quad (5.106)$$

The following cases can be considered :

- $k_y < k_L < k_S$

In this case, equation (5.106) yields four real roots, two of the roots are positive and two are negative, resulting in the following wave types :

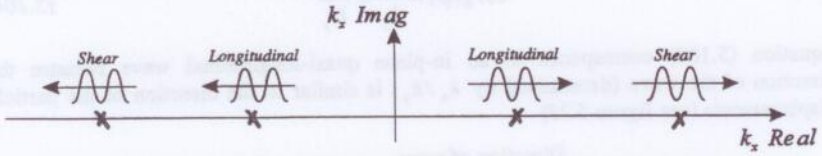

Figure 5.25 : Representation of waves in the complex wavenumber plane.

- $k_L < k_y < k_S$

Two imaginary and two real roots occur, corresponding to the following waves :

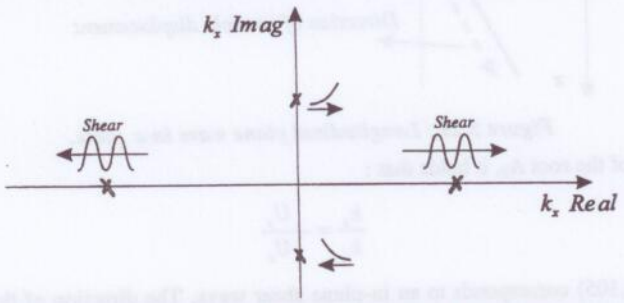

Figure 5.26 : Representation of waves in the complex wavenumber plane.

- $k_S < k_L < k_y$

All four roots k_x are imaginary, hence all corresponding waves are evanescent with respect to the *x*-direction.

5.4.4.3.3 Semi-infinite plate stiffness for in-plane motion.

If the wavenumber k_y is given, four values of k_x can be calculated, according to equation (5.106). With these four combinations of wavenumbers k_x and k_y, four relations between the variables U_x, U_y, F_x, F_y are associated (from equation (5.99-5.100)). Hence, four eigenvectors (4×1) $\{\Psi_i\}$ can now be constructed. Two eigenvectors are corresponding to longitudinal waves and two eigenvectors are corresponding to shear waves :

Longitudinal waves *Shear waves*

$$\begin{Bmatrix} k_x \\ k_y \\ -\dfrac{jEh}{1-\nu^2}\cdot(k_L^2-(1-\nu)k_y^2) \\ -\dfrac{jEh}{1+\nu}\cdot k_x k_y \end{Bmatrix} \quad and \quad \begin{Bmatrix} k_y \\ -k_x \\ -\dfrac{jEh}{1+\nu}\cdot k_x k_y \\ \dfrac{jEh}{2(1+\nu)}\cdot(k_L^2-(1-\nu)k_y^2) \end{Bmatrix} \qquad (5.107)$$

Let the 4×4 matrix $[\Psi]$ be composed of the set of four eigenvectors, such that the first two columns (two eigenvectors) correspond to positive going waves, the other two eigenvectors are associated with negative going waves (with respect to the x-direction).

In the case of the presence of a wave field composed of in-plane, plane waves with a given wavenumber k_y being positive and real, every single vector $\{U_x, U_y, F_x, F_y\}$ can be written in terms of the eigenvectors :

$$\begin{Bmatrix} U_x \\ U_y \\ F_x \\ F_y \end{Bmatrix} = [\Psi]\cdot\begin{Bmatrix} a^+ \\ a^- \end{Bmatrix} = [\Psi]\cdot\begin{Bmatrix} a_1 \\ a_2 \\ a_3 \\ a_4 \end{Bmatrix} \qquad (5.108)$$

Where the 4×1 vector $\{a\}=\{a^+ \;\; a^-\}^T$ represents the vector of generalised wave coordinates.

Finally, the wave dynamic stiffness matrices associated with positive and with negative going waves can now readily be calculated.

In the case of positive going waves the generalised wave coordinates $\{a^-\}$ can be set to zero. Hence, it holds that :

$$\begin{Bmatrix} U_x^+ \\ U_y^+ \end{Bmatrix} = [\Psi_{11}]\cdot\{a^+\} \quad and \quad \begin{Bmatrix} F_x^+ \\ F_y^+ \end{Bmatrix} = [\Psi_{21}]\cdot\{a^+\} \qquad (5.109)$$

By eliminating the generalised coordinates $\{a^+\}$, the relation between the internal forces and displacement is given by :

$$\begin{Bmatrix} F_x^+ \\ F_y^+ \end{Bmatrix} = [\Psi_{21}]\cdot[\Psi_{11}]^{-1}\cdot\begin{Bmatrix} U_x^+ \\ U_y^+ \end{Bmatrix} \quad or \quad \begin{Bmatrix} F_x^+ \\ F_y^+ \end{Bmatrix} = [K_\infty^+]\cdot\begin{Bmatrix} U_x^+ \\ U_y^+ \end{Bmatrix} \qquad (5.110)$$

Where $[K_\infty^+]$ represents the 4×4 wave dynamic stiffness matrix associated with positive going in-plane waves with a given wavenumber k_y, the latter being positive and real.

Similarly, the wave dynamic stiffness matrix of the negative going waves can be obtained :

$$[K_\infty^+] = [\Psi_{22}]\cdot[\Psi_{12}]^{-1} \qquad (5.111)$$

5.4.4.4 Combined out of plane and in-plane motion.

By combining equations (5.96-97-110), the global wave dynamic stiffness matrix, relating the relevant internal forces $\{F_x \;\; F_y \;\; F_z \;\; M_y\}$ to the displacements $\{U_x \;\; U_y \;\; U_z \;\; \Theta_y\}$ in the case of a combined in-plane and out of plane motion is given by :

$$\begin{Bmatrix} F_x^+ \\ F_y^+ \\ F_z^+ \\ M_y^+ \end{Bmatrix} = \begin{bmatrix} K_\infty^{+,in-plane} & 0 \\ 0 & K_\infty^{+,out\ offplane} \end{bmatrix} \cdot \begin{Bmatrix} U_x^+ \\ U_y^+ \\ U_z^+ \\ \Theta_y^+ \end{Bmatrix} and \begin{Bmatrix} F_x^- \\ F_y^- \\ F_z^- \\ M_y^- \end{Bmatrix} = \begin{bmatrix} K_\infty^{-,in-plane} & 0 \\ 0 & K_\infty^{-,out\ offplane} \end{bmatrix} \cdot \begin{Bmatrix} U_x^- \\ U_y^- \\ U_z^- \\ \Theta_y^- \end{Bmatrix} \tag{5.112}$$

for respectively positive and negative going waves (with respect to the x-direction).

Besides, every vector of basic variables - which is associated with a plane wave field with a given k_y - , namely :

$$\{Q\} = \{U \;\; F\}^T = \{U_x \;\; U_y \;\; U_z \;\; \Theta_y \;\; F_x \;\; F_y \;\; F_z \;\; M_y\}^T \tag{5.113}$$

can be written in terms of generalised wave coordinates (weighted sum of eigenvectors) by combining equation (5.95) and equation (5.109) for respectively out of plane and in-plane motion and by taking the appropriate elements of the $[\Psi]$ matrices.

$$\{U^+\} = [\Psi_1] \cdot \{a^+\} \; and \; \{F^+\} = [\Psi_2] \cdot \{a^+\} \tag{5.114}$$

Similar equations hold for negative going waves :

$$\{U^-\} = [\Psi_3] \cdot \{a^-\} \; and \; \{F^-\} = [\Psi_4] \cdot \{a^-\} \tag{5.115}$$

Where $[\Psi_i]$ represents a 4×4 matrix which is made up of the appropriate matrices.

The variables M_x and Θ_x can also be included into the analysis through the equations (5.91-92). It therefore holds that :

$$\{Q'\} = \{U' \;\; F'\}^T = \{U_x \;\; U_y \;\; U_z \;\; \Theta_x \;\; \Theta_y \;\; F_x \;\; F_y \;\; F_z \;\; M_x \;\; M_y\}^T \tag{5.116}$$

In addition :

$$\{U'^+\} = [\Psi'_1] \cdot \{a^+\} \; and \; \{F'^+\} = [\Psi'_2] \cdot \{a^+\} \tag{5.117}$$

and :

$$\{U'^-\} = [\Psi'_3] \cdot \{a^-\} \; and \; \{F'^-\} = [\Psi'_4] \cdot \{a^-\} \tag{5.118}$$

5.4.4.5 Coordinate transformation.

Because the middle surface of the plates are not coinciding with the global x-y plane, it is necessary to establish the coordinate transformation from the local (plate) coordinate system to the global coordinate system.

Suppose the angle of a plate i is given by θ_i . The junction line is assumed to have an off-set x_i, z_i (figure 5.27)

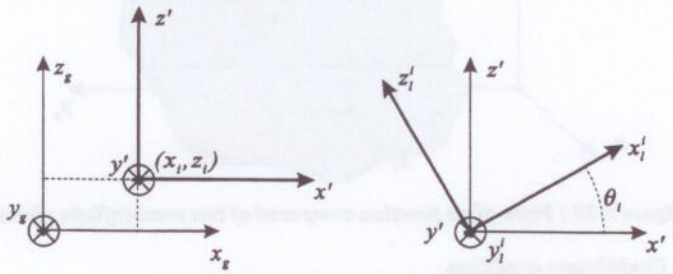

Figure 5.27 : Coordinate transformation.

The relation between local and global forces is given by :

$$\begin{Bmatrix} F_x \\ F_y \\ F_z \\ M_y \end{Bmatrix}_g = \begin{bmatrix} 1 & 0 & 0 & 0 \\ 0 & 1 & 0 & 0 \\ 0 & 0 & 1 & 0 \\ z_i & 0 & -x_i & 1 \end{bmatrix} \cdot \begin{bmatrix} \cos\theta_i & 0 & -\sin\theta_i & 0 \\ 0 & 1 & 0 & 0 \\ \sin\theta_i & 0 & \cos\theta_i & 0 \\ 0 & 0 & 0 & 1 \end{bmatrix} \cdot \begin{Bmatrix} F_x \\ F_y \\ F_z \\ M_y \end{Bmatrix}_l \qquad (5.119)$$

The relation between local and global displacements is given by :

$$\begin{Bmatrix} U_x \\ U_y \\ U_z \\ \Theta_y \end{Bmatrix}_l = \begin{bmatrix} \cos\theta_i & 0 & -\sin\theta_i & 0 \\ 0 & 1 & 0 & 0 \\ \sin\theta_i & 0 & \cos\theta_i & 0 \\ 0 & 0 & 0 & 1 \end{bmatrix} \cdot \begin{bmatrix} 1 & 0 & 0 & z_i \\ 0 & 1 & 0 & 0 \\ 0 & 0 & 1 & -x_i \\ 0 & 0 & 0 & 1 \end{bmatrix} \cdot \begin{Bmatrix} U_x \\ U_y \\ U_z \\ \Theta_y \end{Bmatrix}_g \qquad (5.120)$$

Or in simplified form :

$$\{F\}_g = [T_f] \cdot \{F\}_l \text{ and } \{U\}_l = [T_u] \cdot \{U\}_g \qquad (5.121)$$

In terms of stiffness matrices, the relation between the local and the global stiffness matrix is given by :

$$[K]_g = [T_f] \cdot [K]_l \cdot [T_u] \qquad (5.122)$$

5.4.4.6 Evaluation of transmission coefficients.

This section addresses the calculation of the transmission matrix by expressing equilibrium and compatibility at the junction. The procedure which is adopted in here is conceptually similar to the one outlined in the corresponding paragraph in the case of beam-beam junctions.

Consider a set of n semi-infinite plates, rigidly coupled together (figure 5.28). Eventually, a plate i can incorporate an off-set x_i, z_i

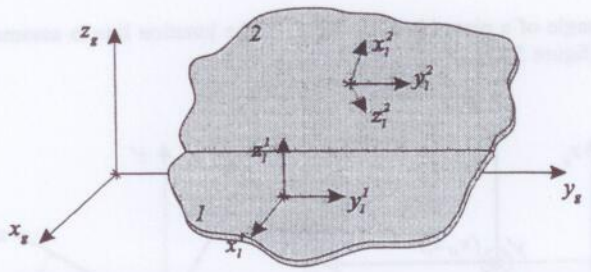

Figure 5.28 : Plate-plate junction composed of two semi-infinite plates.

5.4.4.6.1 Equilibrium condition.

The sum of all the forces acting upon the junction (global *y*-axis) should equal zero :

$$\sum_{i=1}^{n}\{F_i\}=0 \tag{5.123}$$

Where $\{F_i\}=\{F_{i,x} \quad F_{i,y} \quad F_{i,z} \quad M_{i,y}\}^T$ represents the relevant force vector associated with the i^{th} plate in a global coordinate system. Every force vector of every plate can be decomposed into forces associated with negative going waves and forces associated with positive going waves (with respect to the *x*-direction). Therefore :

$$\{F_i\}=\{F_i^+\}+\{F_i^-\} \tag{5.124}$$

Note that all forces are related to a global coordinate system. By applying the wave dynamic stiffness matrix, the equilibrium equation can be written as :

$$\sum_{i=1}^{n}[K_{wi}^+]\cdot\{U_i^+\}+\sum_{i=1}^{n}[K_{wi}^-]\cdot\{U_i^-\}=0 \tag{5.125}$$

Where $\{U_i^+\}$ and $\{U_i^-\}$ represent the displacement vectors of plate *i* at the junction line, associated respectively with positive and negative going plane waves.

5.4.4.6.2 Compatibility condition.

The connection between the plates is assumed to be rigid. It therefore holds that for the displacement of the plates in a global coordinate system at the junction line :

$$\{U_1\}=\{U_2\}=\cdots=\{U_n\} \tag{5.126}$$

Or by decomposing the displacement vector into positive and negative going waves, one can obtain the following set of equations :

$$\begin{cases} U_1^+ + U_1^- = U_2^+ + U_2^- \\ U_2^+ + U_2^- = U_3^+ + U_3^- \\ \vdots \\ U_{n-1}^+ + U_{n-1}^- = U_n^+ + U_n^- \end{cases} \tag{5.127}$$

5.4.4.6.3 Assemling equilibrium and compatibility equations.

By combining the equilibrium equation (5.125) and compatibility equation (5.127), the relation between the displacements associated with the positive going waves can be written in terms of the displacements associated with the negative going waves :

$$\begin{bmatrix} I & -I & 0 & 0 & \cdots & 0 \\ 0 & I & -I & 0 & \cdots & 0 \\ 0 & 0 & \ddots & \ddots & \cdots & 0 \\ \vdots & \vdots & \ddots & \ddots & \ddots & \vdots \\ 0 & 0 & \cdots & 0 & I & -I \\ K_{1m}^{+} & K_{2m}^{+} & K_{3m}^{+} & \cdots & \cdots & K_{nm}^{+} \end{bmatrix} \cdot \begin{Bmatrix} U_1^{+} \\ U_2^{+} \\ \vdots \\ U_n^{+} \end{Bmatrix} = - \begin{bmatrix} I & -I & 0 & 0 & \cdots & 0 \\ 0 & I & -I & 0 & \cdots & 0 \\ 0 & 0 & \ddots & \ddots & \cdots & 0 \\ \vdots & \vdots & \ddots & \ddots & \ddots & \vdots \\ 0 & 0 & \cdots & 0 & I & -I \\ K_{1m}^{-} & K_{2m}^{-} & K_{3m}^{-} & \cdots & \cdots & K_{nm}^{-} \end{bmatrix} \cdot \begin{Bmatrix} U_1^{-} \\ U_2^{-} \\ \vdots \\ U_n^{-} \end{Bmatrix} \qquad (5.128)$$

Or in simplified form :

$$[K^{+}] \cdot \{U^{+}\} = [K^{-}] \cdot \{U^{-}\} \qquad (5.129)$$

The global displacements contained in equation (5.129) should now be transformed into local displacements using equation (5.120). Hence, the relation between the displacements associated with the outgoing waves and the incidence waves is given by :

$$\{U^{+}\}_l = [A] \cdot \{U^{-}\}_l \qquad (5.130)$$

For reasons of clarity, the subscript l - denoting the local coordinate system - is removed further on.

Using equations (5.115-118), the displacements for every plate i can be transformed into generalised wave coordinates :

$$\{U_i^{+}\} = [\Psi_{i,1}] \cdot \{a_i^{+}\} \quad and \quad \{U_i^{-}\} = [\Psi_{i,3}] \cdot \{a_i^{-}\} \qquad (5.131)$$

Where $\{a_i\}$ represents the vector of generalised wave coodinates of plate i : every element of $\{a_i\}$ represents the contribution of a specific wave to the global plane wave field of plate i for a given wavenumber k_y.

Thus, by combining all wave coordinates into one vector, equation (5.130) becomes :

$$\{a^{+}\} = [\Psi]^{-1} \cdot [A] \cdot [\Psi] \cdot \{a^{-}\} \quad or \quad \{a^{+}\} = [B] \cdot \{a^{-}\} \qquad (5.132)$$

Through equation (5.132), a relation has been established between the generalised wave coordinates of the incidence waves and the generalised wave coordinates of the outgoing waves. Every single element B_{ij} of the matrix $[B]$ represents the generalised wave coordinate a_i^{+} of a specific outgoing wave if an incidence wave (exhibiting wave coordinates $a_j^{-} = 1; a_l^{-} = 0 \; l \neq j$) is impinging upon the junction.

Finally, the energy flow associated with the positive going waves and the energy flow associated with the negative going waves should be established.

The energy flow in the x-direction can be calculated by summing up the contributions of the relevant forces and associated particle velocities. The relevant forces are pictured in figure *5.29* and equals :

$$E_i^+ = 1/2 \cdot \omega \cdot Im\left[\left\{F_{i,x}^+ \quad F_{i,y}^+ \quad F_{i,z}^+ \quad M_{i,x}^+ \quad M_{i,y}^+\right\} \cdot \left\{U_{i,x}^+ \quad U_{i,y}^+ \quad U_{i,z}^+ \quad \Theta_{i,x}^+ \quad \Theta_{i,y}^+\right\}^*\right] \tag{5.133}$$

or in terms of generalised wave coordinates :

$$E_i^+ = Im\left[\left\{a_i^+\right\}^T \cdot \left[A_i\right] \cdot \left\{a_i^+\right\}^*\right] \tag{5.134}$$

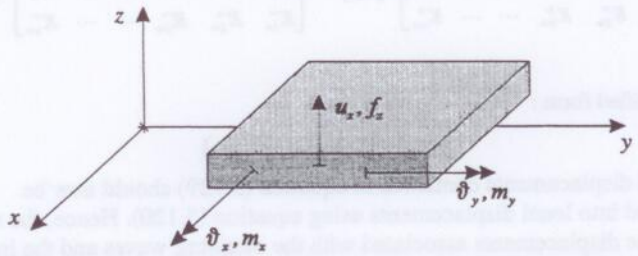

Figure 5.29 : Relevant forces associated with out of plane motion.

Hence, the imaginary part of every single diagonal element $A_{i,kk}$ of $[A_i]$ represents the energy flow of the wave denoted k in plate i exhibiting generalised wave coordinates : $a_{i,k}^- = 1; a_{i,l}^- = 0\ (l \neq k)$.

A similar equation can be derived in the case of the energy flow associated with the negative going waves :

$$E_i^- = Im\left[\left\{a_i^-\right\}^T \cdot \left[B_i\right] \cdot \left\{a_i^-\right\}^*\right] \tag{5.135}$$

Hence, the imaginary part of every single diagonal term $B_{i,kk}$ represents the energy flow of the corresponding wave denoted k propagating in the negative x-direction (incidence wave), exhibiting a generalised wave coordinate $a_{i,k}^- = 1\ ;\ a_{i,l}^- = 0\ (l \neq k)$.

From here on, all ingredients to calculate the transmission coefficients are present :

- For every incidence wave exhibiting a known generalised wave coordinate, the generalised wave coordinate of every outgoing wave can be calculated using equation (5.132).
- The energy flow associated with a specific wave is obtained using equation (5.134) and (5.135) for positive respectively negative going waves.

Hence, each element of the transmission matrix is given by the appropriate combination of elements of the matrices *[B], [C]* and *[D]*.

5.4.4.7 Evaluation of SEA Coupling Loss Factors.

Whereas four, five or six wave types can be present on a beam, a plate can contain three or four independent types of plane wave. Each wave type corresponds to a SEA subsystem.

The transmission coefficients which are calculated in the previous paragraphs are a function of the angle between the incidence wave direction and the normal to the line junction. For SEA purposes, an ideal diffuse incidence wave field will be assumed meaning that the energy flow in a certain point of the input plate is the same in all directions. Suppose the coupling loss factor between subsystem i and j (namely η_{ij}) has to be calculated. Let's assume that the total vibrational energy of subsystem i equals E_i (spatial and frequency averaged). Hence, the energy density equals :

$$e_i = \frac{E_i}{A_i} \tag{5.136}$$

Where A_i represents the area of subsystem i. The energy density per unit angle, i.e. the energy density which can be attributed to the waves travelling in a unit angle equals :

$$e_i(\varphi) = \frac{E_i}{2\pi A_i} \tag{5.137}$$

Converting energy density into intensity can be performed by multiplying the energy density by the group speed of the waves :

$$I_i(\varphi) = \frac{E_i c_{i,g}}{2\pi A_i} \tag{5.138}$$

The structural energy flow in a direction parallel to the x-axis per unit angle wave, of a wave exhibiting an incidence angle φ equals :

$$I_{i,x}(\varphi) = \frac{L E_i c_{i,g}}{2\pi A_i} \cdot cos(\varphi) \tag{5.139}$$

Where L denotes the length of the connection line.

The energy flow from i to j can now be calculated by integrating over the incidence angles of the incidence waves :

$$P_{i \to j} = 2 \int_0^{\pi/2} \frac{L E_i c_{i,g}}{2\pi A_i} \cdot cos(\varphi) \cdot \tau_{ij}(\varphi) \cdot d\varphi \tag{5.140}$$

Or in a simplified form :

$$P_{i \to j} = \frac{L E_i c_{i,g} < \tau_{ij} >}{\pi A_i} \tag{5.141}$$

Hence, the coupling factor η_{ij} is given by :

$$\eta_{ij} = \frac{c_{i,g}\, L < \tau_{ij} >}{\pi\, A_i\, \omega} \qquad (5.142)$$

Or in terms of modal densities (applying equation (5.13)) :

$$\eta_{ij} = \frac{L < \tau_{ij} >}{2\pi^2\, c_{i,p}\, n_i(\omega)} \qquad (5.143)$$

5.4.5 Beam - plate junctions.

Whereas the plate-plate junctions have been quite extensively reported in literature during the last decade, this is not the case for plate-beam couplings (figure *5.32*). LYON [1] reported in *'75* that few cases had been found for beams which connect to plates. Recent research on this topic is published by STEEL and CRAIK [103].

The results are sparse, even nowadays. The method used for calculating the transmission coefficients in the case of beam-plate junctions is basically similar to the method used for beam-beam and plate-plate junctions. First, the wave dynamic stiffness matrix of the beam and the driving point stiffness of an infinite plate should be calculated. Next, by expressing compatibility and equilibrium at the junction, a relation between the displacement field associated with the outgoing waves and the displacement field associated with the incidence waves can be established. The transmission matrix readily follows.

5.4.5.1 Wave dynamic stiffness matrix of a plate.

The calculation procedure of the wave dynamic stiffness matrix of the beam has been outlined in detail in paragraph 5.4.3 and will not be given here. Only driving point stiffnesses of a homogenous, isotropic plate are of concern in this paragraph.

5.4.5.1.1 Force perpendicular to the plate.

The formulas which are adopted in this thesis and which are implemented in the SEA program SEAPACK concern dynamic point stiffnesses of plates as derived by CREMER et al.[79].

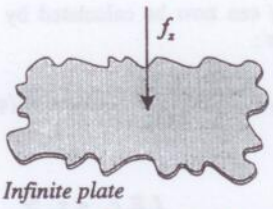

Figure 5.30 : Infinite plate excited by a point force.

The most efficient method for deriving point stiffnesses of a plate consists of solving the suitable differential equations of the plate, subjected to appropriate boundary conditions.

In the case of a normal point force acting on a plate, these boundary conditions take the form :

- The displacements must be axially symmetric.
- At the excitation point, the angular displacement, i.e. the first derivative of the lateral displacement must vanish.
- At the excitation point, the sum of the shear forces must equal the exciting force.
- The Sommerfield radiation condition must be fulfilled, meaning that the displacements at large distances from the excitation point must behave like a decaying wave.

These boundary conditions only apply for perpendicular point forces on the plate. With every type of force is a specific set of boundary conditions associated. Using these boundary conditions and using the appropriate differential equation, one can deduce some kernel solutions associated with the wave field produced by the exciting force. In the case of a point force perpendicular to the plate, Hankel functions constitute the kernel solutions. Cremer showed that the expression for the driving point stiffness is given by :

$$K_{\infty} = 8\,j\omega\sqrt{\frac{E t^4 \rho}{12(1-\nu^2)}} \qquad (5.144)$$

Where t denotes the thickness of the plate.

The expression concerning the particle displacement perpendicular to the plate implies that the shear stresses tend towards infinity as the radius tends towards zero. Such stresses are physically unrealistic. One must therefore assume that the exiting force acts over an area whose dimensions are small compared to the bending wavelength, but not so small as to result in shear deformations in the excitation region.

Equation (5.144) has been derived for thin bending motion. In the case of important thick bending effects, rotatory inertia and shear effects must be included in the derivation of the bending wave equation.

CREMER et al.[79] showed that one may state that for point excitation of a plate, consideration of shear deformation and rotatory inertia result in a near field exhibiting a spring like character. The effect of these added terms on the transmitted force is negligible as long as $kt << 1$, that is as long as the bending wavelength is at least six times the thickness of the plate. Even for $kt \approx 1$, the result differs by only about 2.5% from that obtained from the simpler, thin bending form. However, for high frequencies ($kt >> 1$), the difference increases rapidly. The exact form of the driving point stiffness in the case of thick bending becomes :

$$\frac{1}{K_{\infty}} = \left[\frac{j\omega \ln\infty}{8\pi\kappa^2 G h} + \frac{\sqrt{12(1-\nu^2)}}{8\sqrt{\rho h^4 E}} \cdot \frac{1+\left(\frac{k^2h^2}{24}\right)^2 \frac{2E}{\kappa^2 G(1-\nu^2)}\left(\frac{E}{\kappa^2 G(1-\nu^2)}-1\right)}{\sqrt{1+\left(\frac{k^2h^2}{24}\right)^2\left(\frac{E}{\kappa^2 G(1-\nu^2)}-1\right)^2}} \right] \qquad (5.145)$$

5.4.5.1.2 Moment acting upon the plate.

When a beam is connected to a plate, it is likely that moment forces are acting on the plate. To calculate the transmission coefficients in an accurate way, including the exchange of energy via bending moments, it is necessary to obtain reliable values concerning the driving moment stiffness of the plate, defined by :

$$\frac{M_x}{\Theta_x} \qquad (5.146)$$

Where M_x represents the moment acting on the plate. Θ_x represents the rotation at the driving point. Figure *5.31* pictures the plate and the excitation.

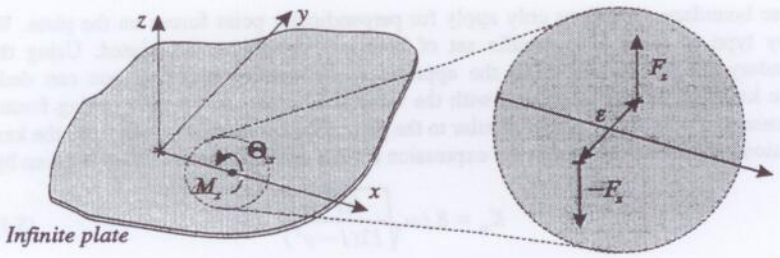

Figure 5.31 : Infinite plate excited by a moment.

The approach which consist of considering the plate to be excited by two oppositely directed point forces applied at two neighboring points, should preferably be employed. The exciting moment is given by : $F_z \cdot \varepsilon$, the resulting force vanishes. By doing this, one can make use of the solutions derived for the single force case. An asymptotic limit, for which the distance between the neighboring points approaches zero, can be taken, resulting in the following expression for moment stiffnesses :

$$K_\infty = \frac{4Eh^3 j}{3(1-\nu^2)} \cdot \frac{1}{1+\frac{4j}{\pi} \cdot ln\left(\frac{1.1}{k\varepsilon}\right)} \qquad (5.147)$$

From equation (5.147), it is found that the real part of the corresponding admittance (Moment per angular velocity) is proportional to frequency. Thus for plates (and also for beams), energy transmission due to moments is more significant at high frequencies. As in the case of excitation of a thick plate by a point force, one encounters a near field, which becomes infinitely large ($\varepsilon \to 0$) in the limit.

5.4.5.1.3 In-plane motion.

In-plane forces will not be considered in this dissertation. Usually, the input impedance for in-plane excitation is much higher then the one for out of plane excitation and the contribution to the energy transmission can be neglected. It should however be mentioned that for very high frequencies, the in-plane contributions become more and more important (similar to the plate-plate couplings), making it worthwhile to extend the beam-plate coupling to incorporate in-plane motion.

The calculation of the appropriate in-plane driving impedances is however not straightforward. Whereas for out of plane point excitation of a plate, the displacement and velocities remain finite, this is not the case of in-plane point excitation. In-plane point forces will result in an infinite displacement of the point of excitation and hence will result in a dynamic stiffness being zero. Therefore, the in-plane force which is applied to the plate should be distributed along a finite area. The main problem is related to the area along which the force is distributed.

5.4.5.1.4 Summary of additional formulas.

Some other formulas which can be important for the calculation of SEA coupling loss factors in the case of beam-plate couplings, are given by CREMER et al.[79] :

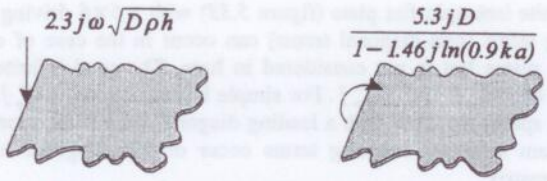

Figure 5.32 : Input dynamic stiffnesses for semi-infinite plates.

It should be noted that due the fact that the plate equations which are adopted in here do not include a rotational degree of freedom around the axis perpendicular to the plate, the corresponding plate stiffness can not be evaluated. Besides, the stiffnesses associated with the in-plane point forces are not considered as well. Hence, the compatibility and equilibrium condition at the junction do *not* take into account the associated types of motion and hence only three *local* degrees of freedom will be contained in the compatibility and equilbrium equation compared to the six degrees of freedom which are taken into account for beam-beam couplings.

5.4.5.2 Coordinate transformation.

The driving point stiffnesses, the displacements and the forces which are derived in the previous paragraph are primarily considered in the local coordinate system, i.e. associated with the plate or the beam. The transformation matrices, relating the local coordinate system and the global coordinate system are given in section 5.4.3.4. All six degrees of freedom can be taken into consideration for the transformation from local to global coordinate systems and vice versa. The fact that the forces and displacements in only *three* directions (local plate coordinate system) can be taken into account with respect to equilibrium and compatibility is contained in the stiffness matrix which has some diagonal terms equal to zero. In other words, the 6×6 driving point stiffness matrix of the plate is singular and is given by :

$$[K_\infty]=\begin{bmatrix} 0 & 0 & 0 & 0 & 0 & 0 \\ 0 & 0 & 0 & 0 & 0 & 0 \\ 0 & 0 & K_z & 0 & 0 & 0 \\ 0 & 0 & 0 & K_{\theta_x} & 0 & 0 \\ 0 & 0 & 0 & 0 & K_{\theta_y} & 0 \\ 0 & 0 & 0 & 0 & 0 & 0 \end{bmatrix} \qquad (5.148)$$

The fact that the stiffness matrix presented above is singular does however not give rise to problems with respect to compatibility and equilibrium.

5.4.5.3 *Evaluation of transmission coefficients.*

Consider an infinite isotropic flat plate (figure *5.33*) with a 6×6 driving point stiffness matrix. Coupling terms (non-diagonal terms) can occur in the case of orthotropic and fully anisotropic plates but is not considered in here. The semi-infinite stiffnesses of beam i are given by $[K_{im}^{+}]$ and $[K_{im}^{-}]$. For simple beam sections, $[K_{im}^{+}]$ and $[K_{im}^{-}]$ are barely populated sparse matrices with a leading diagonal (in a local coordinate system). For complex beam sections, coupling terms occur on non-diagonal locations in the infinite stiffness matrix.

The procedure to calculate the transmission coefficients is conceptually similar to the one for beam-beam junctions.

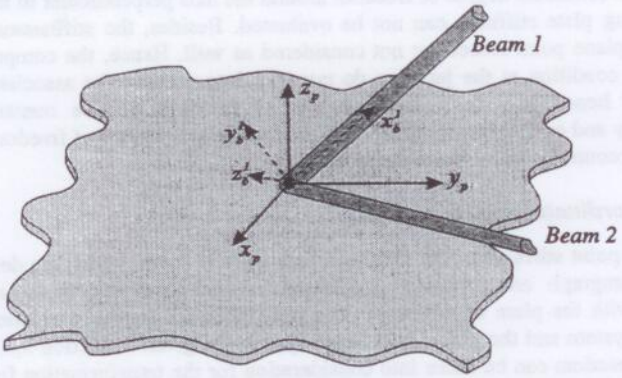

Figure 5.33 : Schematic representation of a plate-beam coupling.

Consider a specific wave in beam i impinging upon the junction. Part of the energy of the incidence wave will be transmitted into the plate, resulting in a superposition of different wave fields. The beam i will carry the incidence and the outgoing waves. The other beams will only carry outgoing waves. By expressing equilibrium and compatibility at the junction, one can obtain a relation between the displacements of the outgoing waves and of the incidence waves associated with the beam and with the plate. This procedure is conceptually similar to the one outlined for beam-beam junctions. After transforming the displacements of the beams and of the plate into generalised wave coordinates, a

relation between the wave coordinates of the outgoing waves and of the incidence waves can be established. The transmission matrix readily follows.

5.4.5.4 *Structural-acoustic coupling.*

The coupling loss factor between a structure and an acoustic cavity is extensively covered in literature. The procedure is based on the radiation ratio of the structure interacting with an infinite space. This is an acceptable approximation if the wavelength of the sound field is a third or less compared to a typical dimension of the cavity. It is evident that the acoustic radiation loss factor for a structure becomes a coupling loss factor when the structure couples to an acoustic volume. The coupling loss factor between the structure *i* and the cavity *j* is given by :

$$\eta_{ij} = \frac{\rho_o c \sigma}{\omega \rho_s} \qquad (5.149)$$

From the reciprocity relationship, the coupling loss factor between the volume *j* and the structure *i* is :

$$\eta_{ji} = \frac{\rho_o c \sigma n_i}{\omega \rho_s n_j} \qquad (5.150)$$

Where n_i is the modal density of the structure and n_j is the modal density of the cavity. Hence, the problem concerning the evaluation of structural-acoustic coupling loss factors reduces to evaluation of radiation efficiencies, in the same way the coupling loss factor evaluation between structure reduces to the evaluation of transmission coefficients.

In this respect is also mentioned the coupling loss factor calculation between two acoustic cavities separated by a wall.

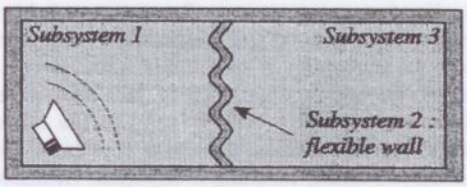

Figure 2.34 : Coupling between two panels separated by a flexible wall.

Concerning sound energy flow through walls, the dominant sound transmission is non-resonant, or in other words mass controlled at frequencies below the critical frequency. The coupling loss factor for non-resonant mass-law transmission through a panel from a source room *1* into the receiving room *3* is given by :

$$\eta_{13} = \frac{c A}{4 \omega V_1} \cdot \tau_{13} \qquad (5.151)$$

Where *c* is the speed of sound, *A* is the surface area of the panel, V_1 is the volume of the source room and τ_{13} is the sound intensity transmission coefficient from the source room

through the panel to the receiving room. According to LEPPINGTON [101], τ_{13} is given by :

$$\tau_{13} = \frac{4\varepsilon^2}{(1-\mu^{-4})^2} \cdot \left(\frac{1}{2} \cdot \log_e(1+k^2 A) + 0.16 - U(S) + \frac{V(\mu)}{4 \cdot \mu^6} \right) \quad (5.152)$$

Where :

$$V(\mu) = (2\mu^2 - 1) \cdot (\mu^2 + 1)^2 \cdot \log_e(\mu^2 - 1) + (2\mu^2 + 1) \cdot (\mu^2 - 1)^2 \cdot \log_e(\mu^2 + 1) - 4\mu^2 - 8\mu^6 \cdot \log_e(\mu) \quad (5.153)$$

And :

$$U(S) = \frac{1+S^2}{2\pi S} \cdot \log_e(1+S^2) - \left[\frac{1}{2} + \frac{S}{\pi} \right] \cdot \log_e(S) - \frac{1}{\pi} \cdot \log_e(2) - \frac{2}{\pi} \int_S^1 \frac{\tan^{-1}(t)}{t} dt \quad (5.154)$$

S denotes the aspect ratio of the partition, ε represents the fluid loading parameter given by $\rho c / m\omega$. m stands for the mass per unit area of the plate, c is the speed of sound and ρ is the density of the air.

5.5 Some examples.

5.5.1 Beam-beam junction.

5.5.1.1 On the importance of coupling between different types of wave motion.

For many problems which are dealt with to date concerning structure-borne sound and in practically every commercially available SEA software packages, the role of the coupling between different types of wave fields is neglected. In other words, for the calculation of the coupling factors between two *flexural* wave fields in the case of beam-beam junctions, the contribution of the longitudinal and torsional impedance is neglected. Even though the amplitudes of longitudinal vibrations (in terms of velocity or displacement) are small, the higher impedance of such motion means that vibratory energy is effectively carried from one discontinuity to the other where it is partly converted into flexural energy. In addition, the higher impedance also means that the in-plane motion is less damped possibly resulting in important vibration transmission paths.

The next example presents some transmission coefficients of a right angled junction (pictured in figure *5.35*) for which additional properties are stated in table *5.3*.

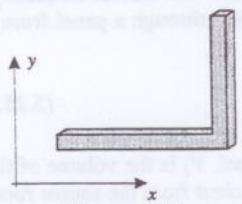

Figure 5.35

Beam property	*Value*
Shear coefficient	*0.833*
Beam section	*10×10 mm²*
Material	*Rigid PVC*

Table 5.3 : Properties of the analysis

A comparison is made between the situation for which no coupling between flexural and longitudinal motion is taken into account and the situation for which a full coupled analysis - the way it is implemented in this thesis - is performed. Two representative transmission coefficients are retained :

- Transmission coefficient associated with bending energy in beam *1* and bending energy in beam *2*.
- Transmission coefficient associated with bending energy in beam *1* and longitudinal energy in beam *2*.

Both transmission coefficients are calculated in the case of full coupled and in the case of decoupled bending-longitudinal motion.

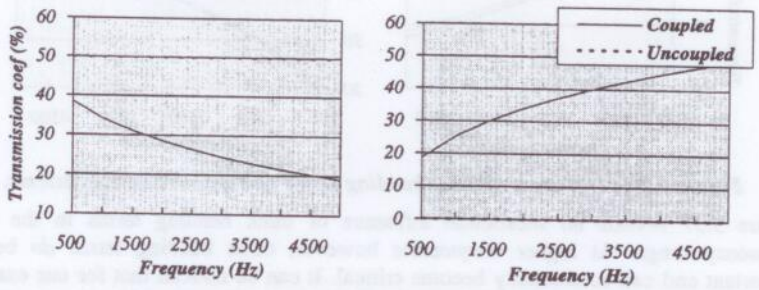

Figure 5.36 : Left side : bending to bending transmission coefficient. Right side : bending to longitudinal transmission coefficient.

Figure *5.36* shows a "high" bending transmission coefficient at low frequencies. At high frequencies, in-plane transmission can become important, as the transmission coefficient relating bending energy in beam *1* and longitudinal energy in beam *2* increases substantially with frequency. The latter variable can however not be calculated in the case of an uncoupled analysis.

This example illustrated concisely the importance of including all wave fields when it comes to accurately predicting transmission coefficients in the higher frequency range.

5.5.1.2 Thick bending effects.

The next example aims at illustrating the influence of thick bending effects in the higher frequency range. The correction terms dealing with thick bending are :

- Rotatory inertia of a beam section.
- Transverse shear.

Including both terms result in a *finite* wave velocity and should give rise to satisfactory results for short wavelength and high modes of vibration.

The effects of the thick bending terms are quantified by means of some relevant transmission coefficients of a two beam junction.

The junction which is considered in this paragraph is pictured in figure *5.35*. The transmission coefficients which are retained in here are similar to the one of the previous paragraph. These transmission coefficients are evaluated for the following cases :

- Including all thick bending terms.
- Neglecting rotatory inertia of a beam section.
- Neglecting shear terms.

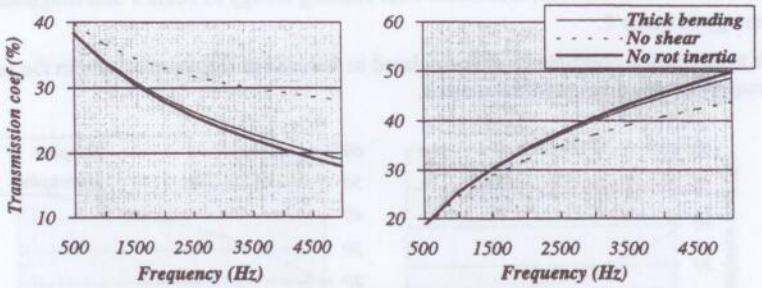

Figure 5.37 : Influence of thick bending terms of transmission coefficients.

Figure *5.37* reveals no substantial influence of thick bending terms in the lower frequency range. At higher frequencies however, thick bending terms *do* become important and can occasionally become critical. It can be noticed that for our example, shear deformation accounts most for the thick bending influence.

Remark.

As an aside, it is worthwhile emphasizing that the criterion which has been applied to judge the importance of effects such as decoupling of wave fields, thick bending etc., namely based on the actual value of the transmission coefficient exclusively is not the only relevant factor because even though the transmission coefficient between two wave fields (associated with two subsystems *i* and *j*) is high or low, the latter does not necessarely imply that energy is predominantly respectively marginally flowing from subsystem *i* to *j*. The energy which flows from subsystem *i* to *j* *also* depends on the susceptibility of vibrational energy of subsystem *j*, quantified by the modal density. If the modal density of the receiving subsystem is low then it is conceivable that the energy flowing from subsystem i to j is not very substantial even though the transmission coefficient could be high.

5.5.2 Plate-plate junction.

5.5.2.1 Transmission coefficient as a function of incidence angle.

The evaluation of the transmission coefficient between wave fields lacks the incidence angle (or wave angle) as an input variable. Due to the large variation of the transmission

coefficient in terms of incidence angles, it is necessary to calculate the transmission coefficient for a large number of incidence angle in order to infer an acceptable value of the averaged (with respect to the incidence angle) transmission coefficient. Taking the *Normal* incidence transmission coefficient would result in substantial errors.

As an example of the influence of the wave angles on the transmission coefficient, a structure composed of two right angled, semi-infinite coupled plates is taken. Additional properties are stated in table *5.4*.

Plate properties	*Value*
Frequency	*10000 Hz*
Thickness plate 1 & 2	*10 mm*
Material	*Rigid PVC*

Table 5.4 : Properties of the analysis.

For reasons of simplicity, thin plate theory has been used to calculate the transmission coefficients.

Figure *5.38* pictures the transmission coefficient relating the in-plane *longitudinal* wave field in plate *1* to all output (reflected and transmitted) wave fields. The indices *l*, *s*, *b* stand for the longitudinal in-plane, the shear in-plane respectively the bending out of plane wave fields[*].

Clearly, "smooth" curves are obtained. As an aside, it can be noticed that for an incidence angle equal to *90 deg*, all energy is reflected, i.e. the transmission coefficient $\tau_{l1\,l1}$ equals *100 %*.

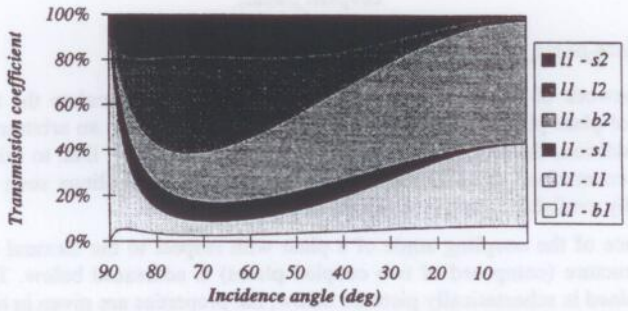

Figure 5.38 : Transmission coefficients for longitudinal input waves of two right angled coupled plates.

Figure *5.39* pictures the transmission coefficient relating bending energy input into plate *1* to each output wave field. In this case, the transmission coefficients exhibit an abrupt

[*] For example : $\tau_{l1\,-\,b2}$ stands for the transmission coefficient with respect to longitudinal energy in plate *1* (input) and bending energy in plate *2* (output).

drop or increase caused by the fact that from specific incidence angles on, the bending input wave field can couple with the longitudinal or shear wave fields.

For example, let's consider the transmission coefficient relating bending energy in plate *1* to in-plane shear energy in plate *2* (see upper curve of figure *5.38*). Above *40 deg*, no coupling between both wave fields is noticed. Below an incidence angle of *40 deg*, a substantial coupling is noticed. The fact that above *40 deg* the bending wave field can *not* couple to the in-plane shear can be explained by the relative value of the wavenumber k_y which is imposed by the input wave field (bending), in relation to the wavenumber of an in-plane shear wave in plate *2*. At an incidence angle of *40 deg*, the wavelength noticed at the junction line equals the wavelength of an in-plane shear wave. Hence, only from that angle on, an in-plane shear wave can couple with an out of plane bending input wave.

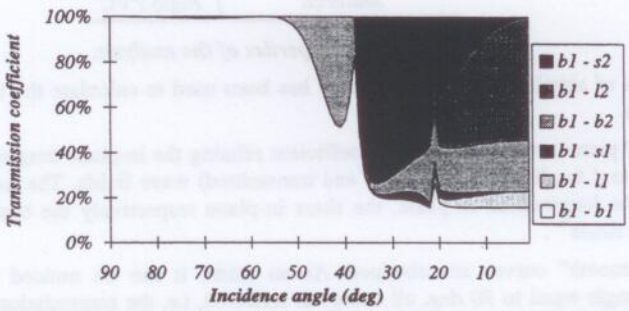

Figure 5.39 : Transmission coefficient for bending input waves of two right angled coupled plates.

5.5.2.2 Plate-plate junction joined at arbitrary angles.

In the framework of this thesis, a program is developed to calculate the transmission coefficient of plate-plate junctions including the feature to couple an arbitrary number of plates. In addition, the coupling angles of the plates is arbitrary. Due to this flexibility, one is not constrained to an exhaustive list of plate-plate couplings such as found in commercially available software packages to date.

The influence of the coupling angle of a plate with respect to the flexural energy flow within a structure (composed of two coupled plates) is addressed below. The structure being examined is schematically pictured below, the properties are given in table *5.5*.

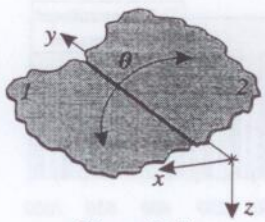

Figure 5.40

Property	Value
Frequency	10000 Hz
Thickness plate	10 mm
Material	Rigid PVC

Table 5.5

The transmission coefficients and subsequently the coupling loss factors are calculated including incidence angles ranging from *0* to *90 deg*. The internal loss factors are experimentally obtained by means of PIM. Figure *5.41* displays the transmission coefficient relating bending energy in plate *1* to bending energy in plate *2* as a function of the incidence angle of the input wave and in terms of the coupling angle of the second plate.

For our example, energy is injected into the first plate (flat spectrum : 1W / third octave band). The energy level of the second plate is calculated as a function of the coupling angle θ of the second plate. The horizontal line denotes the energy level which is contained in plate *2* if the junction is considered right angled and hence represents the approximation which is generally made when dealing with plate-plate junctions.

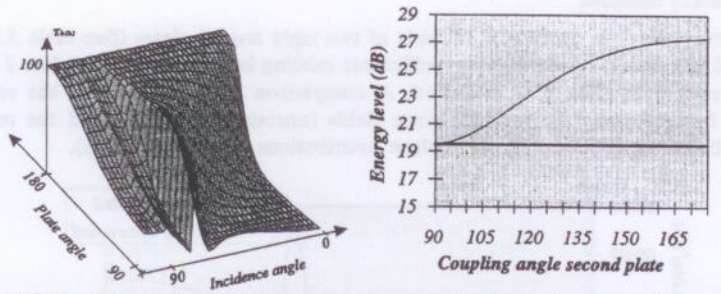

Figure 5.41 : Transmission coefficient and energy level as a function of the coupling angle.

A final example validates the computational procedures implemented in here. A structure composed of two Aluminium plates (thickness *1 mm*) is considered. The coupling angle θ equals *135 deg*. Energy is injected into the first plate. The energy level in the frequency bands *100-1000* Hz are picture on the left side of figure *5.42* in the case of plate *1* and on the right side in the case of plate *2*. Experiment and prediction agree well.

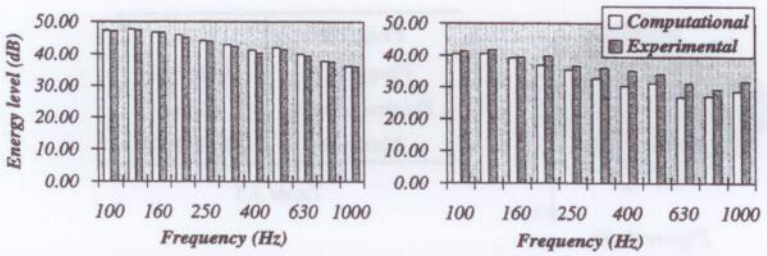

Figure 5.42 : Comparison between experimentally and computationally predicted energy levels.

5.5.2.3 Plate-plate junctions : contribution of in-plane motion.

The next example in this respect aims at showing the necessity to incorporate all types of wave fields which can exist in the plate, i.e. bending out of plane, shear in-plane and longitudinal in-plane, when it comes to assessing the energy flow in plate type structures in an accurate way. Often, the in-plane shear and longitudinal contribution with respect to the energy flow between subsystems is neglected. In the higher frequency range however, these effects do become increasingly important. Although it is not possible to establish a general rule of thumb to assess the importance of in-plane motion with respect to energy flow, it is suggested to include the in-plane motion when performing high frequency analyses.

The structure which is considered consists of two right angled plates (See table *5.5* for additional properties). Transmission coefficients relating bending energy in plate *1* with bending energy in plate *2* is evaluated. A comparison is made between the results obtained by neglecting the in-plane wave fields (uncoupled solution) and the results obtained by taking into account the in-plane contributions (coupled solution).

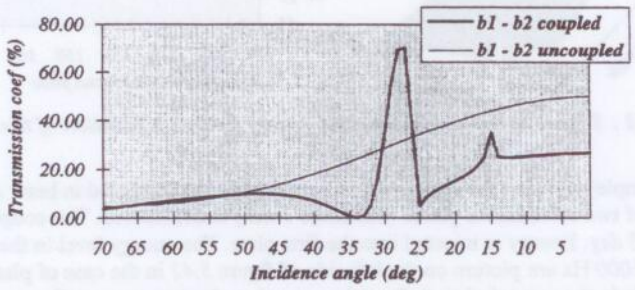

Figure 5.43 : Bending to bending transmission coefficient of a right angled junction.

5.6 Conclusion.

The evaluation of the SEA parameters through computational techniques is addressed in chapter *5*. This so-called predictive SEA can be used in the (early) design stage of structures, even if only few gross structural parameters are known. A continuous refinement of the SEA model can be achieved if more details with regards to the structural integrity are known.

Paragraph *5.2* covers the evaluation of the internal loss factors of subsystems due to material damping, damping through layers, acoustic radiation and damping due to assembling characteristics. No new techniques have been developed in this respect. Only some relevant formulations are presented the way these formulations are implemented in the SEA program SEAPACK.

Paragraph *5.3* addresses the evaluation of modal densities of subsystems. Some general formulas covering the calculation of modal densities of one- two- and three-dimensional subsystems (made up of isotropic materials) are presented. In general, it can be stated that the evaluation of modal densities is relatively straightforward, no major difficulties arise.

Paragraph 5.4 covers the evaluation of coupling loss factors. This parameter constitutes the foremost difficult parameter to calculate, especially if the junction is not simple (e.g. right angled). Paragraph *5.4* aims at bringing together and synthesizing different features of the junctions which are essential for the coupling loss factor evaluation. As such, a general procedure is presented to evaluate the coupling loss factor of non-specific junctions (including an arbitrary number of beams or plates, including arbitrary connection angles, including thick bending terms etc.). A high degree of similarity has been achieved in the calculation procedure for beam-beam, plate-plate and beam-plate junctions. This procedure is based upon extracting wave dynamic stiffnesses, upon expressing equilibrium and compatibility at the junction and assembling the relevant matrices in order to relate the generalized wave coordinates of the incoming and outgoing waves. Chapter *5* contributes to this field of the research because it generalizes the evaluation procedures to a profound extent in an original way and allows one to further extend the method in order to incorporate more features (such as stiffening beams, elastic layers at the junction) in a comprehensive way.

Two main types of couplings are extensively addressed within the framework of this dissertation : beam-beam and plate-plate couplings[*] . For these two types of couplings, an arbitrary number of Timoshenko beams (or thick plates in the case of plate-plate couplings), joined at an arbitrary angle, including an additional off-set of each beam or plate at the junction line can be taken into account. A total of six wave types for the beams (and four wave types in the case of plates) are included. The general form of the transmission matrix equals $4n \times 4n$ for a beam-beam junction and $3n \times 3n$ for a general plate-plate junction. For the latter junction, an additional variable, namely the incidence angle of the waves is taken into account and can be selected as an additional parameter in SEAPACK.

---

[*] Plate-beam couplings are just concisely mentioned.

Although one has not arrive at the situation for which it is possible to analyze all types of conceivable complex junctions which are dealt with in industrial relevant structures, the couplings which are covered in chapter *5 do* incorporate a major benefit compared to the types of couplings which are presented by commercially available software packages at present.

6. THE UTILIZATION OF FINITE ELEMENT MODELS FOR THE EVALUATION OF TRANSMISSION COEFFICIENTS OF COMPLEX JUNCTIONS.

6.1 Introduction.

One of the foremost drawbacks of the state-of-the-art computational techniques as described in chapter *5* with respect to the evaluation of coupling loss factors and transmission coefficients deals with the impossibility to take into account vital structural details which become more and more critical (from the vibration transmission characteristics viewpoint) for high frequencies. For this reason, it is meaningful to establish pertinent methods capable of evaluating the transmission characteristics in an accurate way, other than the inept existing computational methods. The finite element wave approach which is originally developed in the framework of this dissertation aims at the evaluation of complex junctions (theoretically of arbitrary geometrical complexity) through the application of local finite element models of the junction with wave absorbing boundary conditions. The finite element wave approach allows to fully optimize the vibration transmission characteristics of a junction.

A typical, relevant example in this respect deals with the energy transmission between two right angled coupled beams for which the junction incorporates a round off (this example is discussed more in detail in section *6.5.4*).

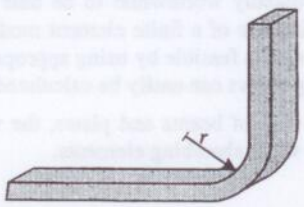

Figure 6.1 : Two right angled beams incorporating a round off.

At low frequencies, (this is at frequencies for which the wavelength is large compared to the radius of the round off), the procedures explained in chapter *6* can be used to evaluate the transmission characteristics of the junction. If, on the other hand, the frequency increases and if the wavelength tends to equal the radius of the round off, then the former methods do not yield adequate results in terms of vibration transmission characteristics. Although for this specific example of two beams incorporating a round-off, one can deduce without too many problems the governing equations and one can obtain from these equations the exact solution, this is not the case for a general complex junction.

Another typical example constitutes the connection between the *A*-pillar and the roof of the car (See figure *6.2*). This junction is generally considered as quite critical with respect to vibration transmission within an automotive vehicle since a substantial amount of vibrational energy is passing from the *A*-pillar towards the roof where it is radiated into the interior. Optimization of the junction with respect to vibration transmission, including all wave types in the *A*-pillar and in the roof of the car is therefore considered as most valuable.

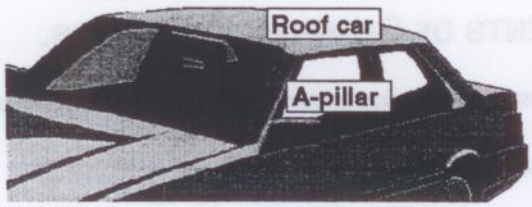

Figure 6.2 : Connection between A-pillar and roof of a car.

The approach explained in chapter *5* is not capable of incorporating all essential geometrical details in order to accurately predict the transmission coefficients. The approach developed in here (further referred to as the finite element wave approach) is based on the finite element method and is able to take into account every essential geometrical detail of the junction. It will be shown that by using the finite element wave approach, it is sufficient to build an appropriate finite element model of the junction. At the boundaries of the finite element model, suitable boundary conditions are applied and a consistent dynamic analysis on the finite element model is performed in order to obtain the transmission coefficients. Note that *exclusively the junction itself* will be modeled, not the entire structure. Hence, a substantial reduction in computational cost can be achieved compared to classical finite element models of the global structure.

The evaluation of transmission coefficients comprises the evaluation of the energy flow associated with the outgoing waves and the energy flow associated with the incidence waves. Therefore it is undoubtedly worthwhile to be able to simulate these traveling waves on the structure, making use of a finite element model. It will be shown that the simulation of propagating waves is feasible by using appropriate boundary conditions. In addition, the associated energy flows can easily be calculated.

Paragraph *6.2* shows, in the case of beams and plates, the way to generate propagating waves by using the so-called wave absorbing elements.

6.2 Simulation of propagating waves using wave-absorbing elements.

6.2.1 Waves on beams.

The aim of this paragraph is to outline a procedure for simulating propagating waves on beams. The basic idea is quite straightforward. If a specific wave is propagating along a structure, then a unique relationship can be established between the internal forces and the associated displacements, a relationship which is further referred to as the semi-infinite stiffness[✎] of the beam. In a more vulgarized terminology, one can state that a wave actually *sees* the semi-infinite stiffness whilst it is propagating along the beam. Therefore, if the ends of the beams are made up of semi-infinite stiffness, then the waves which impinge upon the boundary, notice the same stiffness compared to the stiffness whilst propagating within the beam. Therefore the waves will be completely absorbed. No reflections will arise.

This concept is illustrated by means of a rod on which a force is applied in the middle. First, the rod is clamped at both ends and a direct frequency response calculation is performed (figure *6.3*). The steady state condition is obtained by using a direct frequency response analysis :

$$\{U_x\} = \left([K] - \omega^2 [M]\right) \cdot \{F_x\} \qquad (6.1)$$

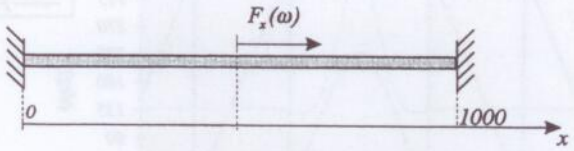

Figure 6.3 : Rod clamped at both ends.

Without taking notice of the specific properties of the analysis, the spatial displacements pattern at a certain frequency looks like :

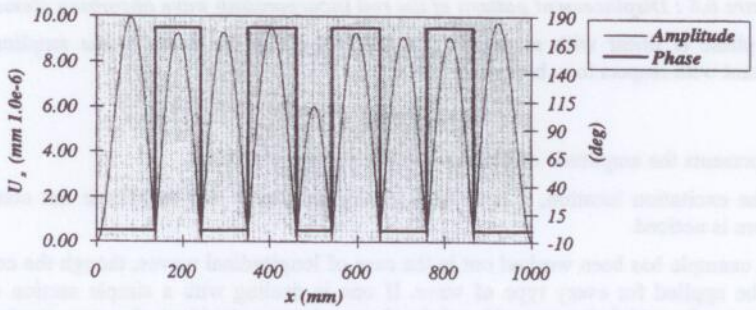

Figure 6.4 : Displacement pattern of the rod with clamped boundary condition.

✎ Also referred to as characteristic stiffness.

The steady state situation can be considered as a superposition of two traveling waves : one positive going wave and one negative going wave. These waves are continuously reflected at the boundaries, thereby generating a modal displacement field. In the absence of damping, the phase equals *0°* or *180°*. The global amplitude pattern combines harmonic and exponential terms.

It is however conceivable to construct a boundary condition such that traveling waves are completely absorbed at the end of the beam. This boundary condition is made up of a classical damping element with a value equal to the semi-infinite stiffness of the - in this case - longitudinal wave in the beam.

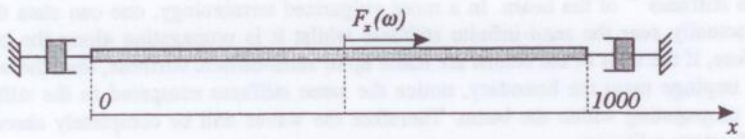

Figure 6.5 : Rod incorporating wave absorbing elements.

In this case, the displacement results of the direct frequency response analysis take the form of a propagating wave for which the displacement pattern at one frequency looks like :

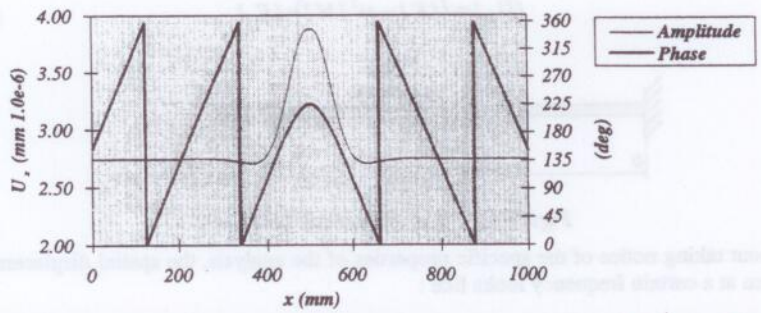

Figure 6.6 : Displacement pattern of the rod incorporating wave absorbing elements.

The phase is linear with respect to the distance along the beam x, the amplitude is constant with respect to x, hence :

$$U_x(x,t) = A \cdot e^{-j(\omega t \pm kx)} \qquad (6.2)$$

A represents the amplitude of the wave and kx denotes the phase.

At the excitation location, a near field (phase non linear and amplitude not constant) pattern is noticed.

This example has been worked out in the case of longitudinal waves, though the concept can be applied for every type of wave. If one is dealing with a simple section of the beam, i.e. for which the centroid and the shear axis are coincident, then two single wave absorbing elements (damping elements) are needed to generate a flexural wave field : a wave absorbing element which *acts* in the y-direction and a wave absorbing element

which *acts* about the z-axis. Therefore, in the case of simple beam sections, 6 damping elements are needed to absorb the energy of all waves (figure 6.7). If a force is applied on the beam then a linear varying phase and a constant amplitude regarding the local displacement of a section is obtained.

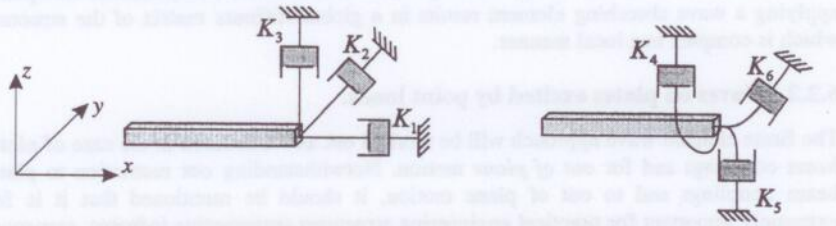

Figure 6.7 : Wave absorbing elements for simple beam sections (left side : translational DOF's; right side rotational DOF's).

The latter only holds for simple beam sections for which torsion, bending and longitudinal motion are decoupled. If not so, a 6×6 fully occupied semi-infinite stiffness should be used at the end of the beams.

It can be noted that in the case of a more complex beam section, the linear and constant behavior with respect to phase respectively amplitude in a local beam coordinate system vanishes because of the coupling between the different types of motion. A torsional wave can incorporate some bending and a bending wave can embody some torsion. However, it is likely that torsional waves and bending waves exhibit a different wavenumber. Hence, the sum of the basic displacements associated with these two wave types will be such that the phase and amplitude are respectively non linear nor constant along the local x-axis. The phase and amplitude of the generalized coordinates (obtained by applying the wave decomposition of section *5.4.3.3*) on the other hand, will vary in a respectively linear and constant way along the beam.

Suppose the global stiffness matrix of a beam (not incorporating the wave absorbing element) is given by equation (6.3)

$$[K]_{global} = \left[\begin{array}{c|c} K_{aa} & K_{an} \\ \hline K_{na} & K_{nn} \end{array}\right] \qquad (6.3)$$

Where n denotes the DOF's at the wave absorbing boundary of the model. a stands for the complementary DOF's.

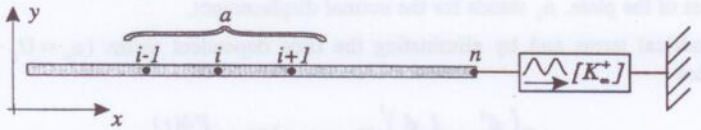

Figure 6.8 : A general wave absorbing beam end.

By applying the wave absorbing element at the end of the beam, the global stiffness matrix becomes :

$$[K]_{global} = \left[\begin{array}{c|c} K_{aa} & K_{an} \\ \hline K_{na} & K_{nn} + K_{\infty}^{+} \end{array}\right] \tag{6.4}$$

The submatrices $[K_{aa}]$, $[K_{an}]$, $[K_{na}]$ and $[K_{nn}]$ are all real (if no damping is present in the beam), the submatrix $[K_{\infty}^{+}]$ is complex. Hence, from the mathematical viewpoint, applying a wave absorbing element results in a global stiffness matrix of the structure which is complex in a local manner.

6.2.2 Waves on plates excited by point loads.

The finite element wave approach will be worked out and illustrated in the case of *plate-beam* couplings and for *out of plane* motion. Notwithstanding our restriction to plate-beam couplings and to out of plane motion, it should be mentioned that it is felt extremely important for practical engineering structures (automotive industry, aerospace industry, building construction) to extend the finite element wave approach toward *plate-plate* couplings, toward a fully combined out of plane and in-plane motion and to include other relevant phenomena such as thick bending. The latter items require further development. Only plate-beam couplings are considered exclusively including flexural motion of the plate.

Below is described a method to calculate the relevant dynamic stiffness (relation between internal plate forces and corresponding displacements corresponding to absorbing boundary conditions) of an infinite plate which is excited by external forces and moments at the origin. Two types of excitations are retained : force perpendicular to the plate and a moment excitation.

6.2.2.1 External force perpendicular to plate.

The aim of this paragraph is to establish the relation between the relevant[•] internal plate forces and the associated displacements at a certain point of the plate in cases for which the excitation takes place at the origin and consists of a point force perpendicular to the plate (figure *6.9*).

The equation of motion for a thin, transversely vibrating plate excited by a point force is given by :

$$D \cdot \nabla^4 u_z + \rho t \cdot \frac{\partial^2 u_z}{\partial t^2} = F \cdot \delta(r) \cdot e^{j\omega t} \tag{6.5}$$

Where D represents the bending rigidity. ρ stands for the material density. t denotes the thickness of the plate. u_z stands for the normal displacement.

In cylindrical terms and by eliminating the time dependent terms ($u_z = U_z \cdot e^{j\omega t}$), it holds that :

$$D\left(\frac{d^2}{dr^2} + \frac{1}{r}\frac{d}{dr}\right)^2 U_z - \rho t \omega^2 U_z = \frac{F\delta(r)}{2\pi} \tag{6.6}$$

• with respect to energy flow.

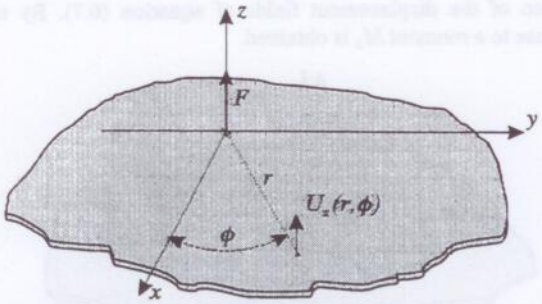

Figure 6.9 : Infinite plate excited at the origin by a point force.

The general harmonic solution of equation (6.6) is a linear combination of Hankel functions (CREMER et al. [79]):

$$U_z(r,\phi) = \frac{-jF}{8Dk^2}\cdot\left(H_o^{(2)}(kr) - H_o^{(2)}(-jkr)\right) \tag{6.7}$$

k denotes the bending wave number, defined by :

$$k = \sqrt[4]{\frac{\omega^2\rho t}{D}} \tag{6.8}$$

$H_o^{(2)}(kr)$ represents the propagating wave term. $H_o^{(2)}(-jkr)$ represents the exponential decaying wave term.

For this investigation, the asymptotic expansion of equation (6.7) is taken in order to obtain the farfield solution. In the farfield, the Hankel functions can be approximated according to :

$$H_o^{(2)}(x) \cong \sqrt{\frac{2}{\pi x}}\cdot e^{j(x-\pi/4)} \tag{6.9}$$

As a rule of thumb, the farfield is considered to be $\lambda/2$ away from any boundary, discontinuity or excitation. λ stands for the wavelength.

Substituting (6.9) into (6.7) results in :

$$U_z(r,\phi) = \frac{e^{-3j\pi/4}\sqrt{2}}{8Dk^2\sqrt{k\pi}}\cdot\frac{e^{jkr}}{\sqrt{r}}\cdot F = C\cdot\frac{e^{jkr}}{\sqrt{r}}\cdot F \tag{6.10}$$

Where C is defined by $-(1+j)/8Dk^2\sqrt{k\pi}$.

6.2.2.2 External moment.

The response due to a moment M_x applied at the origin (figure 6.10) is established. The approach adopted in here consists of considering the plate to be excited by two oppositely directed point forces : F and -F at the points $y=a$ respectively $y=-a$. The equivalent moment equals $M_x = 2aF$ and the resultant force vanishes. The displacement field corresponding to this system of excitation forces is given through a

linear combination of the displacement fields of equation (6.7). By taking the limit $a \to 0$, the response to a moment M_x is obtained.

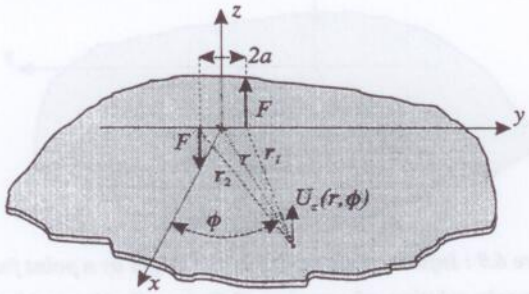

Figure 6.10 : Infinite plate excited at the origin by a moment M_x

$$U_z(r,\phi) = \lim_{a\to 0} \frac{C}{2a} \cdot \left(\frac{e^{jkr_1}}{\sqrt{r_1}} - \frac{e^{jkr_2}}{\sqrt{r_2}} \right) \cdot M_x \qquad (6.11)$$

Where r_1 and r_2 are approximated by :

$$\begin{cases} r_1 \approx r - a \cdot \sin\phi \\ r_2 \approx r + a \cdot \sin\phi \end{cases} \qquad (6.12)$$

By substituting equation (6.12) into equation (6.11), equation (6.11) becomes :

$$U_z(r,\phi) = \lim_{a\to 0} \frac{C}{2a} \cdot \left(\frac{e^{jk(r-a\cdot\sin\phi)}}{\sqrt{r - a\cdot\sin\phi}} - \frac{e^{jk(r+a\cdot\sin\phi)}}{\sqrt{r + a\cdot\sin\phi}} \right) \cdot M_x \qquad (6.13)$$

Using l'Hôpitals rule :

$$U_z(r,\phi) = \lim_{a\to 0} \frac{C}{2} \cdot \left(\begin{array}{l} -\dfrac{e^{jk(r-a\cdot\sin\phi)}}{\sqrt{r - a\cdot\sin\phi}} \cdot jk\sin\phi + \dfrac{1}{2} \cdot \dfrac{e^{jk(r-a\cdot\sin\phi)}}{\sqrt{(r - a\cdot\sin\phi)^3}} \cdot \sin\phi - \\ \dfrac{e^{jk(r+a\cdot\sin\phi)}}{\sqrt{r + a\cdot\sin\phi}} \cdot jk\sin\phi + \dfrac{1}{2} \cdot \dfrac{e^{jk(r+a\cdot\sin\phi)}}{\sqrt{(r + a\cdot\sin\phi)^3}} \cdot \sin\phi \end{array} \right) \cdot M_x \qquad (6.14)$$

Or finally :

$$U_z(r,\phi) = C \cdot \frac{e^{jkr}\sin\phi}{\sqrt{r}} \cdot \left(-jk + \frac{1}{2r} \right) \cdot M_x \qquad (6.15)$$

Similarly, the response in terms of displacements $U_z(r,\phi)$ caused by an external moment M_y is given by :

$$U_z(r,\phi) = -C \cdot \frac{e^{jkr}\cos\phi}{\sqrt{r}} \cdot \left(-jk + \frac{1}{2r} \right) \cdot M_y \qquad (6.16)$$

In conclusion, it holds that by combining the displacement fields associated with the external point loads applied at the origin :

$$U_z(r,\phi) = C \cdot \frac{e^{jkr}}{\sqrt{r}} \cdot F + C \cdot \frac{e^{jkr}\sin\phi}{\sqrt{r}} \cdot \left(-jk + \frac{1}{2r}\right) \cdot M_x - C \cdot \frac{e^{jkr}\cos\phi}{\sqrt{r}} \cdot \left(-jk + \frac{1}{2r}\right) \cdot M_y \tag{6.17}$$

Or in a simplified form :

$$U_z(r,\phi) = f_1(r,\phi) \cdot F + f_2(r,\phi) \cdot M_x + f_3(r,\phi) \cdot M_y \tag{6.18}$$

6.2.2.3 *Establishing the corresponding infinite stiffness matrix.*

The next step is to express the internal forces of the plate as a function of the corresponding displacements. The primary[1] variables (figure *6.11*) which will be taken into account are :

$$\begin{Bmatrix} U_z \\ \Theta_r \\ \Theta_\phi \end{Bmatrix} and \begin{Bmatrix} F_z \\ M_r \\ M_\phi \end{Bmatrix} \tag{6.19}$$

for displacements respectively internal forces.

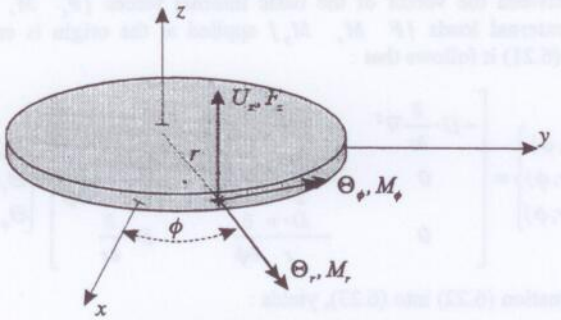

Figure 6.11 : Basic variables.

In the case of *thin* bending, the primary variables as a function of $U_z(r,\phi)$ are given by :

$$\begin{cases} U_z(r,\phi) \\ \Theta_r(r,\phi) = \dfrac{1}{r}\dfrac{\partial U_z(r,\phi)}{\partial \phi} \\ \Theta_\phi(r,\phi) = -\dfrac{\partial U_z(r,\phi)}{\partial r} \end{cases} \tag{6.20}$$

In case of the relevant internal forces it holds that :

---

[1] Primary : in the sense of essential for the out of plane energy flow within the plate.

$$\begin{cases} F_z(r,\phi) = -D\cdot\dfrac{\partial}{\partial r}\nabla^2 U_z(r,\phi) \\ M_r(r,\phi) = \dfrac{D\cdot(1-\nu)}{2}\cdot\left(\dfrac{1}{r}\dfrac{\partial\Theta_\phi}{\partial\phi}+\dfrac{\partial\Theta_r}{\partial r}\right) \\ M_\phi(r,\phi) = D\cdot\left(\dfrac{\partial\Theta_\phi}{\partial r}-\dfrac{\nu}{r}\dfrac{\partial\Theta_r}{\partial\phi}\right) \end{cases} \qquad (6.21)$$

First, the relation between the basic displacement variables $\{U_z \quad \Theta_r \quad \Theta_\phi\}$ at any point of the plate (polar coordinates (r,ϕ)) and the external load $\{F \quad M_x \quad M_y\}$ (applied at the origin) is established.

From equation (6.17) and (6.20), it follows that :

$$\begin{Bmatrix} U_z(r,\phi) \\ \Theta_r(r,\phi) \\ \Theta_\phi(r,\phi) \end{Bmatrix} = \begin{bmatrix} f_1 & f_2 & f_3 \\ 0 & \dfrac{1}{r}\dfrac{\partial f_2}{\partial\phi} & \dfrac{1}{r}\dfrac{\partial f_3}{\partial\phi} \\ -\dfrac{\partial f_1}{\partial r} & -\dfrac{\partial f_2}{\partial r} & -\dfrac{\partial f_3}{\partial r} \end{bmatrix}\cdot\begin{Bmatrix} F \\ M_x \\ M_y \end{Bmatrix} \qquad (6.22)$$

The relation between the vector of the basic internal forces $\{F_z \quad M_r \quad M_\varphi\}$ and the vector of the external loads $\{F \quad M_x \quad M_y\}$ applied at the origin is established next. From equation (6.21) it follows that :

$$\begin{Bmatrix} F_z(r,\phi) \\ M_r(r,\phi) \\ M_\varphi(r,\phi) \end{Bmatrix} = \begin{bmatrix} -D\cdot\dfrac{\partial}{\partial r}\nabla^2 & 0 & 0 \\ 0 & \dfrac{D\cdot(1-\nu)}{2}\cdot\dfrac{\partial}{\partial r} & \dfrac{D\cdot(1-\nu)}{2r}\dfrac{\partial}{\partial\phi} \\ 0 & -\dfrac{D\cdot\nu}{r}\dfrac{\partial}{\partial\phi} & D\cdot\dfrac{\partial}{\partial r} \end{bmatrix}\cdot\begin{Bmatrix} U_z(r,\phi) \\ \Theta_r(r,\phi) \\ \Theta_\phi(r,\phi) \end{Bmatrix} \qquad (6.23)$$

Substituting equation (6.22) into (6.23), yields :

$$\begin{Bmatrix} F_z(r,\phi) \\ M_r(r,\phi) \\ M_\varphi(r,\phi) \end{Bmatrix} = \begin{bmatrix} -D\cdot\dfrac{\partial}{\partial r}\nabla^2 & 0 & 0 \\ 0 & \dfrac{D\cdot(1-\nu)}{2}\cdot\dfrac{\partial}{\partial r} & \dfrac{D\cdot(1-\nu)}{2r}\dfrac{\partial}{\partial\phi} \\ 0 & -\dfrac{D\cdot\nu}{r}\dfrac{\partial}{\partial\phi} & D\cdot\dfrac{\partial}{\partial r} \end{bmatrix}\cdot\begin{bmatrix} f_1 & f_2 & f_3 \\ 0 & \dfrac{1}{r}\dfrac{\partial f_2}{\partial\phi} & \dfrac{1}{r}\dfrac{\partial f_3}{\partial\phi} \\ -\dfrac{\partial f_1}{\partial r} & -\dfrac{\partial f_2}{\partial r} & -\dfrac{\partial f_3}{\partial r} \end{bmatrix}\cdot\begin{Bmatrix} F \\ M_x \\ M_y \end{Bmatrix} \qquad (6.24)$$

By combining equations (6.24) and (6.22), the relation between the basic displacement vector and the basic internal force vector at any point (r,ϕ), excited by an external loads $\{F \quad M_x \quad M_y\}$ at the origin readily follows :

$$\begin{Bmatrix} F_z(r,\phi) \\ M_r(r,\phi) \\ M_\varphi(r,\phi) \end{Bmatrix} = \begin{bmatrix} -D\cdot\frac{\partial}{\partial r}\nabla^2 & 0 & 0 \\ 0 & D\cdot(1-\nu)\cdot\frac{\partial}{\partial r} & \frac{D\cdot(1-\nu)}{r}\frac{\partial}{\partial\phi} \\ 0 & -\frac{D\cdot\nu}{r}\frac{\partial}{\partial\phi} & D\cdot\frac{\partial}{\partial r} \end{bmatrix} \cdot \begin{bmatrix} f_1 & f_2 & f_3 \\ 0 & \frac{1}{r}\frac{\partial f_2}{\partial\phi} & \frac{1}{r}\frac{\partial f_3}{\partial\phi} \\ -\frac{\partial f_1}{\partial r} & -\frac{\partial f_2}{\partial r} & -\frac{\partial f_3}{\partial r} \end{bmatrix} \cdot$$

$$\begin{bmatrix} f_1 & f_2 & f_3 \\ 0 & \frac{1}{r}\frac{\partial f_2}{\partial\phi} & \frac{1}{r}\frac{\partial f_3}{\partial\phi} \\ -\frac{\partial f_1}{\partial r} & -\frac{\partial f_2}{\partial r} & -\frac{\partial f_3}{\partial r} \end{bmatrix}^{-1} \cdot \begin{Bmatrix} U_z(r,\phi) \\ \Theta_r(r,\phi) \\ \Theta_\phi(r,\phi) \end{Bmatrix} \tag{6.25}$$

Note that the matrix containing the differential operators (matrix on the left) only acts on the matrix just right of it.

Or in a more classical form, equation (6.25) can be written as :

$$\begin{Bmatrix} F_z(r,\phi) \\ M_r(r,\phi) \\ M_\varphi(r,\phi) \end{Bmatrix} = \left[K_\infty^+(r,\phi)\right] \cdot \begin{Bmatrix} U_z(r,\phi) \\ \Theta_r(r,\phi) \\ \Theta_\phi(r,\phi) \end{Bmatrix} \tag{6.26}$$

The matrix $[K_\infty^+(r,\phi)]$ constitutes the dynamic (complex) stiffness matrix of the wave absorbing elements which are applied at the circular boundary of the plate. An example dealing with waves on plates is given in section 6.5.2.

As a final point, it is worthwhile to mention that the stiffness matrix of the wave absorbing element derived in here only holds for *point loads* at the origin and for *flexural motion*.

6.3 The evaluation of the transmission matrix of beam junctions : the more explicit approach.

The approach highlighted in this paragraph to calculate the transmission matrix of beam junctions based on the finite element wave approach, is not the one which should preferably be used from the *practical* viewpoint. Despite, the procedures outlined in here offer a comprehensible, physical insight into the problem of evaluating transmission coefficients through finite element models, being the main reason why the explicit approach is explained in here.

The procedure is illustrated for a two-beam junction (figure *6.13*) and for a bending input wave with displacements in the *y*-direction (in a local coordinate system).

First, the semi-infinite stiffness matrix of the beams should be calculated based on the techniques explained in chapter *5* and should be applied at the end of all beams. Next, the energy flow within the beam associated with an input wave should be evaluated. For reasons of clarifying the wave absorbing principle, the latter can be done through a finite

element calculation on the input beam (beam 1 of figure *6.13*)✎ . Two wave absorbing elements should be attached at either end of the beams, as depicted in figure *6.12*.

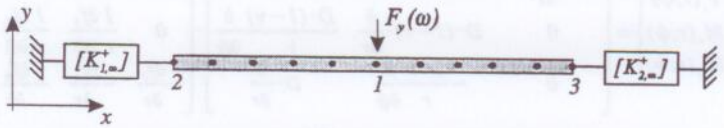

Figure 6.12 : Beam incorporating wave absorbing elements at both ends.

A unit force $F_y(\omega) = 1$ is applied at node *1* and the *y*-displacement at node *1* is calculated by means of a direct frequency response analysis. The energy input into the beam equals :

$$P_\infty = \frac{1}{2} Re\left(F_y \cdot V_y^*\right) \qquad (6.27)$$

Two propagating waves are generated and are absorbed by the dampers. Both waves carry an energy flow $P_\infty / 2$.

Next, the entire junction is modeled and wave absorbing elements are applied at the boundaries (figure *6.13*). Again, a unit force is applied at node *1* of the input beam. Two propagating bending waves (one in the negative direction and one in the positive direction) and two near field waves are generated. Each propagating wave carries an energy flow : $P_\infty / 2$.

Where P_∞ is obtained by means of equation (6.27).

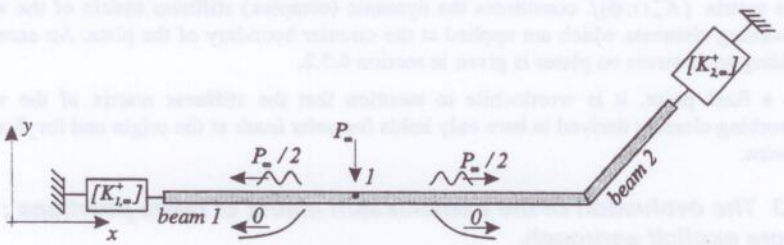

Figure 6.13 : Waves generated in beam 1.

The wave traveling in the negative *x*-direction (global *x*-direction) is absorbed by the wave absorbing element $[K^+_{1,\infty}]$ The positive going wave impinges upon the junction, thereby transmitting energy into beam *2* and reflecting energy back into beam *1*. For reasons of comprehensibility, only *bending* waves are considered in beam *2*, notwithstanding the fact that all types of waves are actually generated at the junction. The relevant transmission coefficient is given by *T* and the transmitted energy in beam *2* is given by $T \cdot P_\infty / 2$ (figure *6.14*). The reflection coefficient is denoted *R*.

✎ It is also possible to calculate the input impedance of a beam excited by a point force. The energy flow associated with an input wave equals 0.5 times the energy input into the beam.

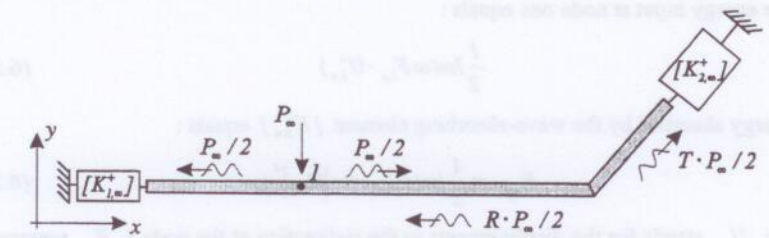

Figure 6.14 : Reflected and transmitted waves.

The wave which is reflected at the junction will propagate towards point *1* where part of its energy is lost via the point of excitation (point *1*). The remaining part of the reflected wave travels towards the end of beam *1*, where it is absorbed by the wave-absorbing element $[K^+_{1,\infty}]$.

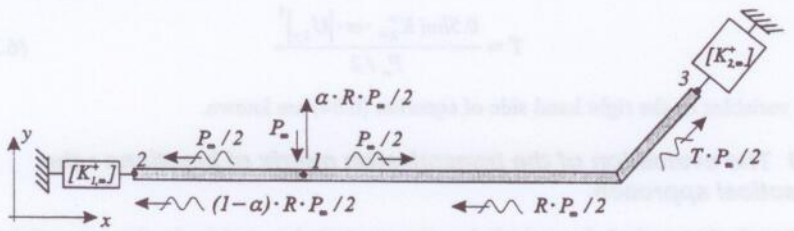

Figure 6.15 : Energy flow within the two beams in case of steady state conditions.

Summary :

- The energy which is absorbed by the wave-absorbing element $[K^+_{1,\infty}]$ equals :

$$E_{1,K^+_{1,\infty}} = P_\infty/2 + (1-\alpha) \cdot R \cdot P_\infty/2 \qquad (6.28)$$

- The energy input at node *1* is given by :

$$P_\infty - \alpha \cdot R \cdot P_\infty/2 \qquad (6.29)$$

- The energy absorbed by the wave-absorbing element $[K^+_{2,\infty}]$ equals :

$$T \cdot P_\infty/2 \qquad (6.30)$$

Where R and T represent respectively the unknown reflection and transmission coefficients. α is an unknown coefficient and P_∞ represents the energy input into an infinite beam (obtained via equation (6.27)).

All three energy flows (equations (6.28), (6.29) and (6.30)) can also be calculated based on the appropriate complex product of forces and particle velocities (or displacements) at the appropriate nodes obtained from the finite element analysis. Hence, it holds that :

- Energy which is absorbed by the wave-absorbing element $[K^+_{1,\infty}]$ equals :

$$E_{K^+_{1,\infty}} = \frac{1}{2} Im(K^+_{1,\infty} \cdot \omega \cdot |U_{2,y}|^2) \qquad (6.31)$$

- The energy input at node one equals :

$$\frac{1}{2} Im(\omega F_{1,y} \cdot U_{1,y}^{*}) \tag{6.32}$$

- Energy absorbed by the wave-absorbing element $[K_{2,\infty}^{+}]$ equals :

$$E_{K_{2,\infty}^{+}} = \frac{1}{2} Im(K_{2,\infty}^{+} \cdot \omega \cdot |U_{3,y}|^{2}) \tag{6.33}$$

Where $U_{i,y}$ stands for the displacements in the y-direction at the node i. $F_{1,y}$ represents the external force applied at node *1*, all calculated via the direct frequency response analysis of the finite element model.

By combining equations (6.28) -(6.33), it is possible to calculate the reflection coefficient R and the transmission coefficients T. For example, the transmission coefficient T is given by :

$$T = \frac{0.5 Im(K_{2,\infty}^{+} \cdot \omega \cdot |U_{3,y}|^{2}}{P_{\infty} / 2} \tag{6.34}$$

All variables on the right hand side of equation (6.34) are known.

6.4 The evaluation of the transmission matrix of junctions : the practical approach.

Although the method for calculating the transmission matrix in the case of beam junctions as explained in the previous section has the advantage that one obtains a comprehensible, physical insight into the problem, it does not represent the most suitable efficient way to implement the evaluation of transmission coefficients. Especially if the *entire* transmission matrix of the junction needs to be evaluated at several frequencies, practical problems can arise. If only one or few transmission coefficients of the junction are needed, then the method previously explained can definitely be applied. If on the other hand, *all* elements of the transmission matrix are needed, then it is more appropriate to streamline the procedure as described below. Use is made of an external program which reads in the dynamic stiffness matrix of the junction and which performs a set of calculations in order to obtain the transmission matrix. The procedure will be outlined in the case of a beam-beam and in case of a beam-plate junction.

6.4.1 Beam-beam junction.

For reasons of simplicity, attention will be focused on a beam-beam junction comprising *three* beams. The junction is modeled based on finite elements and is schematically pictured in figure *6.16*.

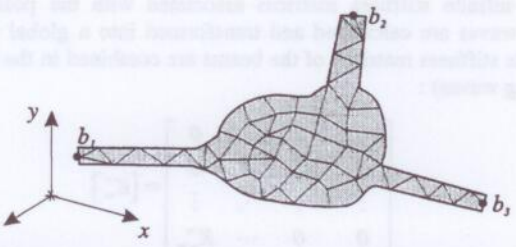

Figure 6.16 : Schematic representation of a finite element model of a beam-beam junction.

Let *[K]* be the global finite element stiffness matrix of the junction. *[M]* denotes the global mass matrix of the junction. Without taking into account damping phenomena, it holds that :

$$\left([K]-\omega^2[M]\right)\cdot\{U\}=\{F\} \tag{6.35}$$

The matrix $[K]-\omega^2[M]$ is denoted $[K^d]$ further on (the superscript d stands for dynamic).

The dynamic stiffness matrix of the junction $[K^d]$ is reduced to the nodes lying at the ends of the beams. (Node b_1, b_2 and b_3). A classical, static condensation of the internal degrees of freedom is carried out. Let subscript b denote the degrees of freedom at the boundaries of the beams. Subscript i denotes the internal degrees of freedom. No internal forces are acting upon the internal nodes of the finite element model of the junction (why should there be external forces on the internal nodes if only the transmission of energy from each end of the beams to the other ends is considered ?).

Therefore, equation (6.35) can be partitioned to yield :

$$\left[\begin{array}{c|c} K^d_{bb} & K^d_{bi} \\ \hline K^d_{ib} & K^d_{ii} \end{array}\right]\cdot\left\{\begin{array}{c} U_b \\ \hline U_i \end{array}\right\}=\left\{\begin{array}{c} F_b \\ \hline 0 \end{array}\right\} \tag{6.36}$$

From the second row of equation (6.36), it follows that :

$$\{U_i\}=-\left[K^d_{ii}\right]^{-1}\cdot\left[K^d_{ib}\right]\cdot\{U_b\} \tag{6.37}$$

Combining equation (6.36) and (6.37) yields :

$$\left[K^d_{bb}\right]\cdot\{U_b\}-\left[K^d_{bi}\right]\cdot\left[K^d_{ii}\right]^{-1}\cdot\left[K^d_{ib}\right]\cdot\{U_b\}=\{F_b\} \tag{6.38}$$

Hence, the dynamic stiffness matrix of the junction, reduced to its boundaries b, is given by :

$$\left[K^d_{reduced}\right]=\left[K^d_{bb}\right]-\left[K^d_{bi}\right]\cdot\left[K^d_{ii}\right]^{-1}\cdot\left[K^d_{ib}\right] \tag{6.39}$$

Consequently, the relation between the external forces acting upon the junction at the boundaries and the displacements at the boundaries is given by :

$$\{F_b\}=\left[K^d_{reduced}\right]\cdot\{U_b\} \tag{6.40}$$

Next, the semi-infinite stiffness matrices associated with the positive and with the negative going waves are calculated and transformed into a global coordinate system. The semi-infinite stiffness matrices of the beams are combined in the following way (for positive outgoing waves) :

$$\begin{bmatrix} K^+_{1,\infty} & 0 & \cdots & 0 \\ 0 & K^+_{2,\infty} & \cdots & 0 \\ \vdots & \vdots & \ddots & \vdots \\ 0 & 0 & \cdots & K^+_{n,\infty} \end{bmatrix} = [K^+_\infty] \qquad (6.41)$$

Subscript n represents the number of beams.

The forces and displacements of the beams, acting at the boundaries of the beam can be partitioned into forces and displacements associated with positive and associated with negative going waves. Therefore, equation (6.40) becomes :

$$\{F^+_b\} + \{F^-_b\} = [K^d_{reduced}] \cdot \{U^+_b\} + [K^d_{reduced}] \cdot \{U^-_b\} \qquad (6.42)$$

Where $\{F^+_b\}$ represents the vector of beam forces at the end-nodes associated with the positive going waves. $\{U^+\}$ represents the vector of displacements associated with positive going waves. A similar notation holds for negative going waves.

The internal forces of the beams which are assumed to be associated with a specific wave field (positive or negative) can be replaced by the corresponding product of the appropriate semi-infinite stiffness and displacement. Hence, equation (6.42) becomes :

$$[K^+_\infty] \cdot \{U^+_b\} + [K^-_\infty] \cdot \{U^-_b\} = [K^d_{reduced}] \cdot \{U^+_b\} + [K^d_{reduced}] \cdot \{U^-_b\} \qquad (6.43)$$

by rearranging the terms of equation (6.43), one obtains the following equation :

$$\{U^+_b\} = \left([K^+_\infty] - [K^d_{reduced}]\right)^{-1} \cdot \left([K^d_{reduced}] - [K^-_\infty]\right) \cdot \{U^-_b\} \qquad (6.44)$$

Or in simplified form :

$$\{U^+_b\} = [A] \cdot \{U^-_b\} \qquad (6.45)$$

Thus, equation (6.45) expresses the relation between the displacements of the incidence waves and the displacements of the outgoing waves at the boundaries of the junction. From here on, the same procedure as explained in chapter *5* to calculate the transmission matrix can be followed.

In summary :

- The dynamic stiffness matrix of the junction based on a finite element model is reduced to the nodes at the boundaries.
- The semi-infinite stiffness matrix of each beam is evaluated using the procedure outlined in chapter *6*.
- The relation between displacements associated with positive going waves and displacements associated with negative going waves is established.
- From here on, the equations (5.55-5.64) can be applied to calculate the transmission matrix.

6.4.2 Beam-plate junction.

This paragraph will focus on the identification of the transmission coefficients of junctions as pictured schematically in figure 6.17

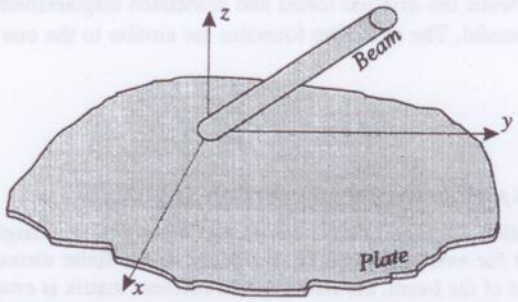

Figure 6.17 : Schematic representation of a beam-plate junction.

The procedure to calculate the transmission matrix is explained below :

- First, a finite element model of the junction is built. The extent of the model should be such that at the boundary of the plate, a farfield vibration condition is obtained similar to the one considered in section 6.2.2. In practical situations, the dimension of the structural connection between the beam and the plate is *finite*. Therefore, it is not possible to *perfectly* satisfy this condition. Nevertheless, satisfactory results are obtained if the plate is made large enough to diminish the effect of the finite dimension of the connection. Figure *6.18* shows schematically two models of a beam-plate coupling. On the right side, the (finite element) model is quite small (and perhaps too small) and therefore the vibration field which will be noticed at the boundary of the plate does not correspond to the vibration field observed when dealing with point loads applied at the origin. Therefore, one should try to make the finite element model large enough in order to eliminate local effects. The extent of the finite element model will be of the order of a few wavelength (left side of figure *6.18*).

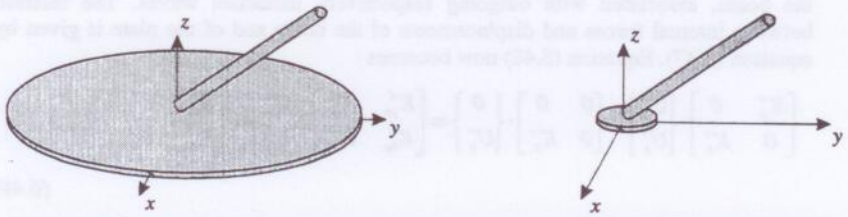

Figure 6.18 : Schematic representation of the extension of a finite element model of a beam-plate coupling.

- Subsequent to the construction of the finite element model, the global dynamic stiffness matrix is reduced to include only degrees of freedom situated at the

boundary of the plate and situated at the end of the beam. Hence, if the boundary of the plate comprises n nodes, then the size of the reduced dynamic stiffness matrix of the junction equals $5\times n+6$, corresponding to 5 DOF's per node on the boundary of the plate and 6 DOF's per node associated with the beam. Equation (6.46) expresses the relation between the external forces and associated displacements of the reduced finite element model. The reduction formulas are similar to the one stated in section 6.4.1.

$$\begin{Bmatrix} F_p \\ F_b \end{Bmatrix} = \begin{bmatrix} K^d_{pp} & K^d_{pb} \\ K^d_{bp} & K^d_{bb} \end{bmatrix} \cdot \begin{Bmatrix} U_p \\ U_b \end{Bmatrix} \qquad (6.46)$$

The subscripts p and b stand for plate respectively beam.

- Next, the relation between internal forces and corresponding displacements should be established for every node on the boundary of the finite element model. In the case of the end of the beam, the semi-infinite stiffness matrix is established using the procedures as explained in chapter 5. In the case of the plate, the procedure to calculate the relation between the internal forces and displacements is explained in detail in section 6.2.2. The following relations can now be established :

$$\{F_b^+\} = [K_b^+] \cdot \{U_b^+\} \quad \{F_b^-\} = [K_b^-] \cdot \{U_b^-\} \text{ and } \{F_p^+\} = [K_p^+] \cdot \{U_p^+\} \qquad (6.47)$$

For reasons of clarity and without loss of generality, only *outgoing waves* with respect to the plate are considered. Negative going waves (incidence waves) are applied on the beam only. In order to calculate the transmission of energy from the plate to the beam, it is sufficient to consider *reciprocity* of the transmission matrix.

- Equation (6.47) can be written in terms of the positive (outgoing) waves and the incidence waves :

$$\begin{Bmatrix} F_p^+ \\ F_b^+ + F_b^- \end{Bmatrix} = \begin{bmatrix} K^d_{pp} & K^d_{pb} \\ K^d_{bp} & K^d_{bb} \end{bmatrix} \cdot \begin{Bmatrix} U_p^+ \\ U_b^+ + U_b^- \end{Bmatrix} \qquad (6.48)$$

Where $\{F_p^+\}$ represents the $5\times n$ nodal force vector (in a global coordinate system) incorporating all nodes at the boundary of the plate, associated with outgoing waves. $\{F_b^+\}$ and $\{F_b^-\}$ represent the nodal force vector (in a global coordinate system) of the beam, associated with outgoing respectively incidence waves. The relation between internal forces and displacements of the beam and of the plate is given by equation (6.47). Equation (6.48) now becomes :

$$\begin{bmatrix} K_p^+ & 0 \\ 0 & K_b^+ \end{bmatrix} \cdot \begin{Bmatrix} U_p^+ \\ U_b^+ \end{Bmatrix} + \begin{bmatrix} 0 & 0 \\ 0 & K_b^- \end{bmatrix} \cdot \begin{Bmatrix} 0 \\ U_b^- \end{Bmatrix} = \begin{bmatrix} K^d_{pp} & K^d_{pb} \\ K^d_{bp} & K^d_{bb} \end{bmatrix} \cdot \begin{Bmatrix} U_p^+ \\ U_b^+ \end{Bmatrix} + \begin{bmatrix} K^d_{pp} & K^d_{pb} \\ K^d_{bp} & K^d_{bb} \end{bmatrix} \cdot \begin{Bmatrix} 0 \\ U_b^- \end{Bmatrix} \qquad (6.49)$$

Or in simplified form :

$$\begin{Bmatrix} U_p^+ \\ U_b^+ \end{Bmatrix} = [A] \cdot \begin{Bmatrix} 0 \\ U_b^- \end{Bmatrix} \qquad (6.50)$$

Hence, a relation between displacements associated with positive going waves (in the plate as well as in the beam) and the displacements associated with negative going waves (in the beam only) is established.

- *Calculation of transmission matrix.* From equation (6.50), it is possible to calculate for each incidence wave into the beam (given vector $\{U_b^-\}$) the corresponding displacements of the outgoing waves. The calculation of the associated energy flow is straightforward, the transmission matrix readily follows.
- Because the transmission matrix is symmetric, the transmission coefficients related to energy flow from the plate to the beam readily follows.

6.5 Examples.

6.5.1 Wave simulation : mesh density aspect.

The influence of the density of the finite element mesh regarding wave transmission and wave simulation is established for the structure pictured in figure *6.19*. The junction which connects two semi-infinite beams is constructed using NASTRAN bar elements. The semi-infinite stiffnesses which are applied at both ends of the finite element model and which model the semi-infinite beams are calculated utilizing identical properties of the NASTRAN bar elements of the finite element model. The global specifications are stated in table *6.1*.

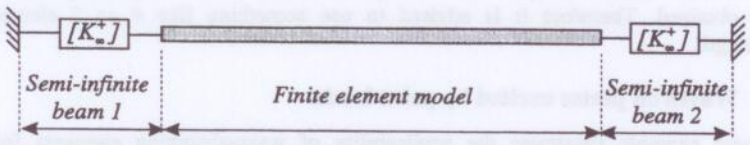

Figure 6.19 : Junction composed of two collinear semi-infinite beams.

Property	*Value*
Beam section	$10 \times 10\ mm^2$
Length finite element model	*100 mm*
Material	*Rigid PVC*
Frequency	*5000 Hz*

Table 6.1 : Properties of the analysis.

In the case of beams exhibiting the properties of table *6.1*, it holds that the bending wavelength equals *70 mm* for flexural waves. By making use of the procedure as described in paragraph *6.4.1*, it is possible to establish the transmission coefficient of the junction. Because the properties of the two semi-infinite beams and of the NASTRAN bar elements are similar and because the two semi-infinite beams and the finite element model are colinear, it should hold that no reflections may occur or in other words, a wave in beam *1* which is impinging upon the junction should theoretically completely be transmitted into beam 2. If however only few finite elements are taken or in other words if the mesh is too rough then reflections are likely to occur.

The reflection coefficient is calculated in the case of flexural waves and is plotted against the corresponding number of *elements / wavelength* which is used for the finite element model of the junction.

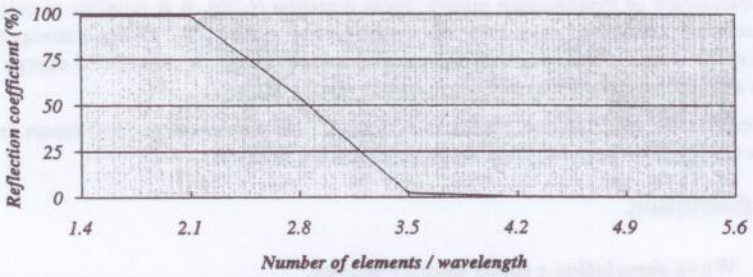

Figure 6.20 : The reflection coefficient of a junction composed of two collinear semi-infinite beams.

Clearly, above more or less *4* elements / wavelength, no reflections occur any longer and all energy is transferred from the semi-infinite beam *1* into the semi-infinite beam *2*.

In general, it can be stated that the mesh density which is needed to obtain reliable results regarding wave transmission is similar to the mesh density which is taken in the case of classical finite element analyses for which *global* results (such as eigenfrequencies) are to be obtained. Therefore it is advised to use something like *4* or *5* elements / wavelength.

6.5.2 Waves on plates excited by point loads.

The next example illustrates the applicability of wave-absorbing elements for the simulation of wave fields in the case of an isotropic flat plate. The properties of the wave-absorbing elements which are applied at the boundary of the plate are calculated via the formulas developed in section *6.2.2*.

The entire procedure (from the building of the finite element model to the visualization of the waves) the way it is implemented in the framework of this dissertation is illustrated in figure *6.21*.

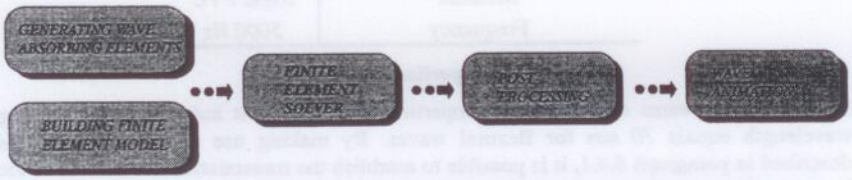

Figure 6.21 : Application of wave absorbing elements : configuration of the implemented procedures.

The software which is developed and which is illustrated below in the case of waves on plates does also apply for waves on beams or other structures.

The properties of the plate which is examined in here are stated in table *6.2*.

Property	*Value*
Thickness plate	*10 mm*
Radius finite element model	*400 mm*
Number of QUAD elements	*3650*
Material	*Rigid PVC*
Frequency	*3000 Hz*

Table 6.2 : Properties of the analysis.

Figure *6.22* depicts the finite element model of the plate.

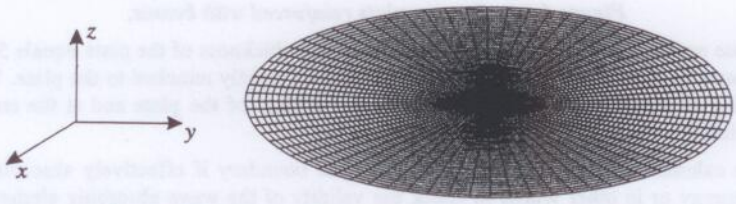

Figure 6.22 : Finite element model of the circular plate.

Figure *6.23* shows the wave pattern for two load cases :

- Load case *1* : external point force perpendicular to the plate applied at the origin (upper side of figure *6.23*).
- Load case *2* : external moment M_x applied at the origin (lower side of figure *6.23*).

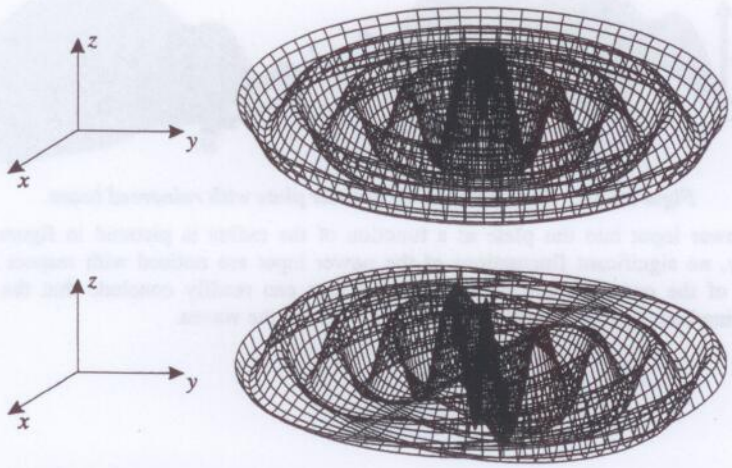

Figure 6.23 : Wave pattern of a circular plate excited by point loads at the origin.

The following example deals with the application of reinforcing beams at both sides of a quarter plate. The structure is pictured in figure *6.24*.

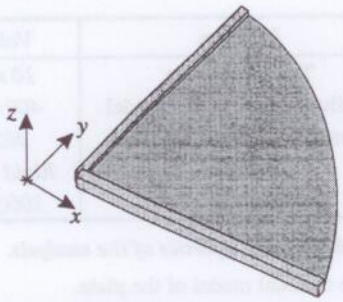

Figure 6.24 : Quarter plate reinforced with beams.

The plate and beams are made up of Aluminum. The thickness of the plate equals *5* mm. The beams have a *15×15* mm^2 square section and are rigidly attached to the plate. Wave absorbing elements are applied at the circular boundary of the plate and at the ends of both reinforcing beams.

First, a calculation is made to check whether the boundary if effectively absorbing all wave energy or in other words to check the validity of the wave absorbing elements in the presence of the *reinforcing* beams. A direct frequency response analysis is performed for several values of the radius of the plate. The excitation consists of a unit harmonic force perpendicular to the plate applied at the origin respectively of a unit harmonic moment M_x applied at the origin at *1000 Hz*. The wave patterns for both load cases are pictured in figure 6.25.

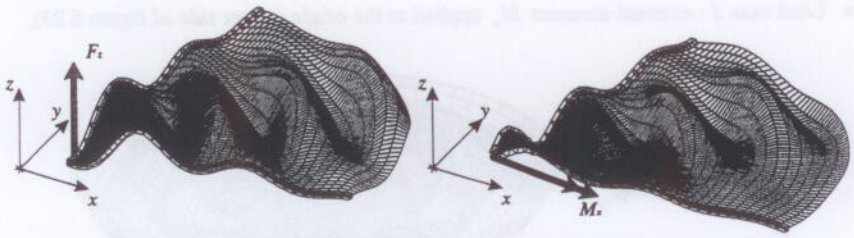

Figure 6.25 : Wave patterns of quarter plate with reinorced beam.

The power input into the plate as a function of the radius is pictured in figure *6.26*. Clearly, no significant fluctuations of the power input are noticed with respect to the radius of the quarter plate. Because of this, one can readily conclude that the wave absorbing boundary does work effectively, i.e. aborbs the waves.

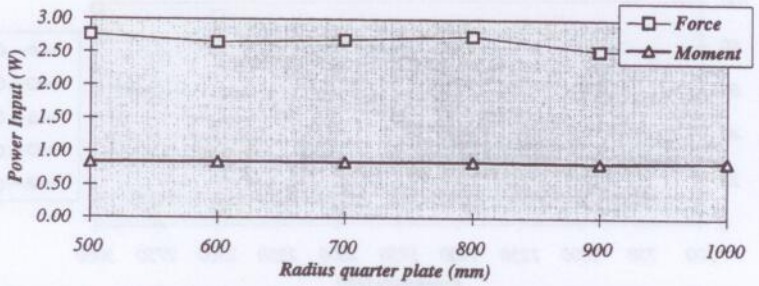

Figure 6.26 : Power input into the quarter plate as a function of the radius.

Next, the influence of the reinforcing beams regarding the transmission properties of the quarter plate is illustrated. Only the DOF in the z-direction is retained. At the origin, an additional beam (section $15 \times 15\ mm^2$) is attached, perpendicular to the plate. The transmission coefficient relating the longitudinal energy in the latter beam (displacements in the global z-direction) to the out of plane energy in the beam-plate subsystem is evaluated for five cases :

Case 1 : only the reinforcing beams are retained and the calculation is based on the *finite element* wave approach.

Case 2 : beam-plate structure with reinforcing beams; calculation based on a *finite element* model.

Case 3 : quarter plate without reinforcing beams; calculation based on *finite elements*.

Case 4 : only the reinforcing beams are retained and the calculation is based on *analytical formulas*.

Case 5 : only the quarter plate is retained and the calculation is based on *analytical formulas*.

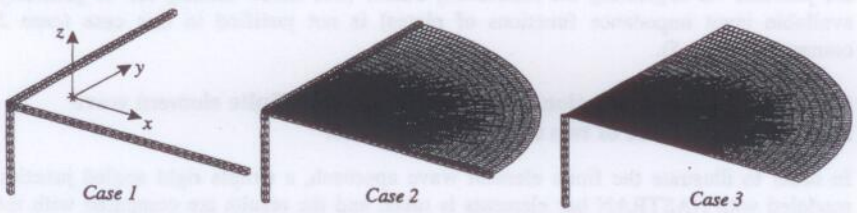

Figure 6.27 : Finite element models associated with cases 1 - 2 and 3.

The corresponding transmission coefficients for all five cases are presented in figure *6.28* in the *500-3000 Hz* frequency range.

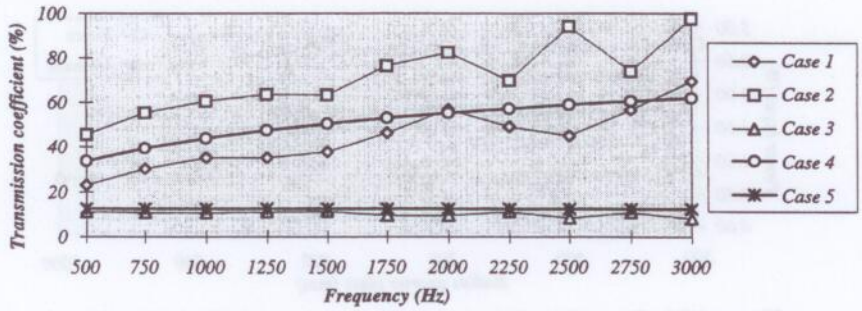

Figure 6.28 : Transmission coefficient of beam-plate connection.

Discussion of the results. Clearly, the correspondance between the finite element wave approach and the classical analytical approach is fairly good : case *3* compared to case *5* and case *4* compared to case *1*. Hence, if one is dealing with simple subsystems for which the input impedance is known (such as for two coupled right angled beams and such as for a quarter plate *without* reinforcements), then the finite element wave approach and the classical analytical approach do agree well. However, when it comes to modelling the connection between subsystems for which it is hard to evaluate the transmission properties by means of simple analytical formulas because accurate values of input impedances are not generally available (e.g. in the case of quarter plate *with* reinforcing beams), then the finite element wave approach explained above effectively contributes to the accurate evaluation of the transmission properties.

- For the structure presented in figure *6.24*, it is shown by means of the finite element wave approach (see figure *6.28*) that the presence of reinforcing beams is critical with respect to the transmission characteristics of a beam-plate junction. The idealisation of the junction via neglecting the reinforcing beams (and hence making use of generally available input impedance functions of plates) is not justified in this case (case *2* compared to case *5*).

6.5.3 Classical computational approach versus the finite element wave approach in the case of two right angled beams.

In order to illustrate the finite element wave approach, a simple right angled junction modeled with NASTRAN bar elements is taken and the results are compared with the classical approach of chapter *5*. The structure is schematically pictured in figure *6.29*.

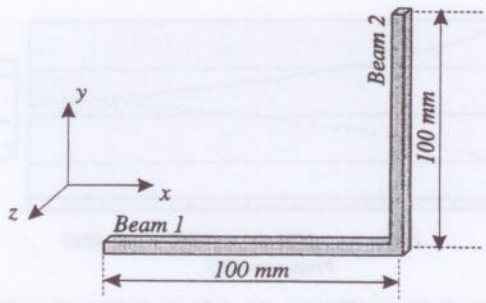

Figure 6.29 : Junction composed of two right angled beams.

The structure is composed of two right angled beams with the following specifications :

Property	*Value*
Section	*10x10 mm²*
Number of elements	*200*
Material	*Rigid PVC*

Table 6.3 : Properties of the analysis.

As an example, the characteristic stiffness matrix at *5000* Hz equals :

$$[K_e]=\begin{bmatrix} -5.68e6\cdot j & 0 & 0 & 0 & 0 & 0 \\ 0 & 1.24e6+1.65e6\cdot j & 0 & 0 & 0 & -3.36e6-1.58e7\cdot j \\ 0 & 0 & 1.24e6-1.65e6\cdot j & 0 & 3.36e6-+.58e7\cdot j & 0 \\ 0 & 0 & 0 & -3.52e7\cdot j & 0 & 0 \\ 0 & 0 & 3.36e6+1.58e7\cdot j & 0 & -2.01e8-1.51e8\cdot j & 0 \\ 0 & -3.36e6-1.58e7\cdot j & 0 & 0 & 0 & -2.01e8-1.51e8\cdot j \end{bmatrix} \qquad (6.51)$$

Figure *6.30* shows some representative transmission coefficients based on the finite element wave approach. Figure *6.31* shows the corresponding values obtained by the classical computational approach.

The notation concerning the transmission coefficients is explained below and will further on be used for all examples in this respect. All transmission coefficients are indicated $\tau_{i,j,}$ or *tau i k j l*. The indices *i* and *j* stand for the wave type, i.e. longitudinal, flexural or torsional. *k* and *l* stand for the beam number. For example, the coefficient τ_{l,b_2} represents the transmission coefficient relating longitudinal energy in beam *1* and flexural energy in beam *2*.

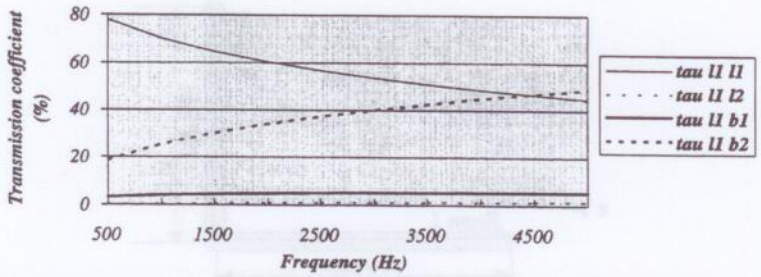

Figure 6.30 : Transmission coefficient of a right angled junction obtained by the finite element wave approach.

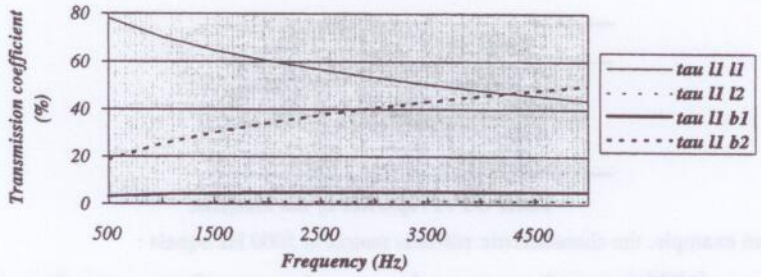

Figure 6.31 : Transmission coefficient of a right angled junction obtained by the classical computational approach.

As a supplementary check, it is interesting to point out that the sum of the transmission and reflection coefficients is *100%*. As can be noticed from figure *6.30* and *6.31*, there are no significant differences between the two approaches (finite element - classical), thereby confirming the validity of the finite element wave approach.

6.5.4 Right angle incorporating a round off.

The following example has been chosen to demonstrate the superiority of the finite element wave approach compared to the classical computational approach in the case of a simple round off contained in the junction. Within the framework of the classical approach, based on the standard work to-date, it is not possible to take into account round offs at the junction as the classical approach models the round off as a right angle assuming a *rigid point connection*, eventually taking into account an additional off-set or eventually taking into account a finite predefined stiffness at the connection of the beams. The finite element wave approach encompasses this problem because the round off can be modeled in detail by finite elements.

The example described in here consists of two right angled semi-infinite beams, incorporating a round off at the connection between both beams. The section of the beam at the round off is similar to the one used for the two semi-infinite beams. The structure which is analyzed is schematically pictured in figure *6.32* (left side). The finite element

model is pictured on the right hand side of figure *6.32*. Additional properties of the beams are stated in table *6.1*. Note that for the finite element model, only the curved part is modeled as it is redundant to incorporate the straight parts into the finite element model. The semi-infinite stiffnesses are directly applied at the ends of the curved parts of the junction.

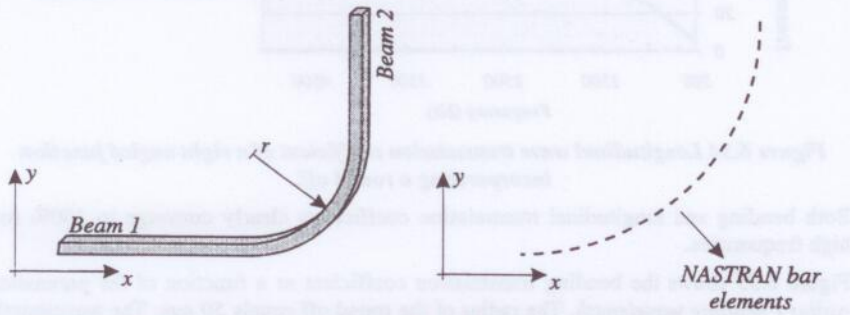

Figure 6.32 : Two right angled semi-infinite beams incorporating a round off : schematic representation of the problem (left side); finite element model (right side).

The graph of figure *6.33* shows the bending transmission coefficient in the case of a flexural wave into beam *1* and a flexural wave out of beam 2. Figure *6.34* displays the longitudinal transmission coefficient for a longitudinal wave into beam *1* and flexural wave out of beam *2* as a function of frequency. Three cases are considered : a radius of *0 mm (no radius, classical approach)*, *50 mm* and *100 mm*.

From the physical viewpoint, it can be expected that the transmission coefficients converge to *100%* for high frequencies, i.e. for frequencies for which the wavelength tends to equal or becomes smaller than the radius *r* of the round off. In other words and in a metaphoric phraseology, a wave with a small wavelength compared to the radius of the round off of the junction does not *see* the round off and passes the junction without reflecting energy back into the input beam. Clearly, the finite element wave approach is capable of modeling this behavior, the classical computational approach is not.

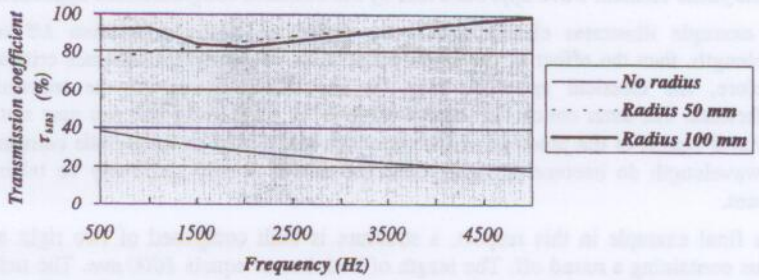

Figure 6.33 : Flexural wave transmission coefficient of a right angled junction incorporating a round off.

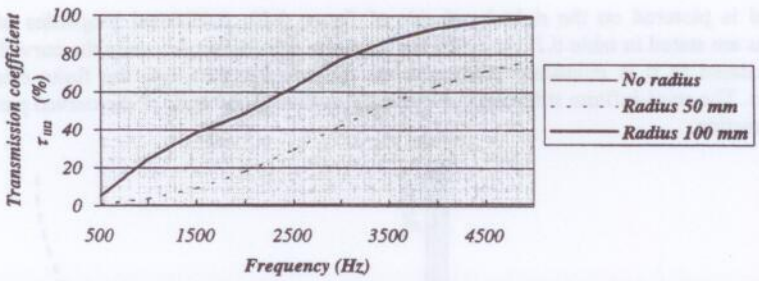

Figure 6.34 Longitudinal wave transmission coefficient of a right angled junction incorporating a round off.

Both bending and longitudinal transmission coefficients clearly converge to *100%* for high frequencies.

Figure *6.35* shows the bending transmission coefficient as a function of the parameter *radius / bending wavelength*. The radius of the round off equals *50 mm*. The wavelength is calculated through the wavenumber obtained by the equation (5.29).

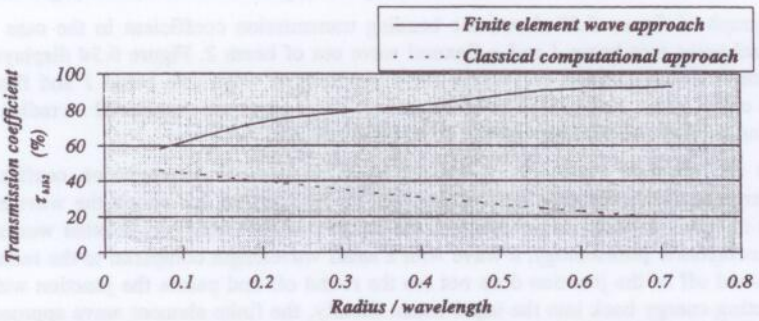

Figure 6.35 : Comparison between bending wave transmission coefficients obtained by the finite element wave approach and by the classical computational approach.

The example illustrates clearly that if the radius becomes larger than *1/5* of the wavelength, then the effect of the finite dimensions of the radius becomes critical and therefore, the classical approach fails for the determination of the transmission coefficients. The latter conclusion can be extended in such a way that one may state that structural details of the junction which are of the same order of magnitude compared to the wavelength do become important and the effects should definitely be taken into account.

As a final example in this respect, a structure is built composed of two right angled beams containing a round off. The length of both beams equals *1000 mm*. The radius of the round off is taken *100 mm*. The properties of the beams are stated in table *6.3*. The application of PIM yields the coupling loss factors and internal loss factors of both subsystems. For verification purposes, energy is injected into subsystem 1, the energy

level of subsystem 2 is assessed based on the experiments and based on the predictive theory of this chapter. Figure *6.36* displays the results.

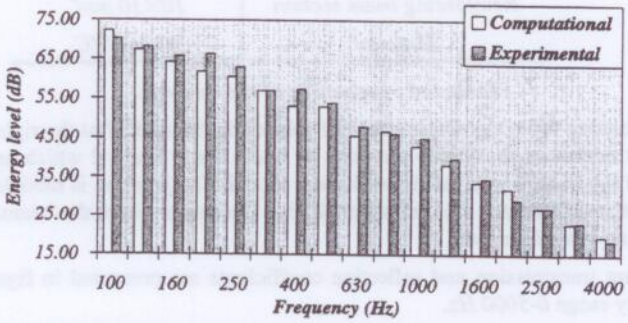

Figure 6.36 : Comparison between computationally and experimentally identified energy levels.

Clearly, SEA, based on the theory developed in this chapter predicts fairly well the energy level in the second beam.

As an interesting industrial application, the transmission of energy through pipeline structures which often contain round offs can be analyzed in an accurate way using the finite element wave approach.

6.5.5 Angle with reinforcement

The following example aims at illustrating the applicability of the finite element wave approach in the presence of local resonances. In this case the transmission coefficient will not exhibit a smooth behavior as a function of frequency, because of the presence of local resonances.

A structure consisting of two right angled beams, reinforced with a third beam (*45°* angle) is considered and is schematically displayed in figure *6.37* (left side).

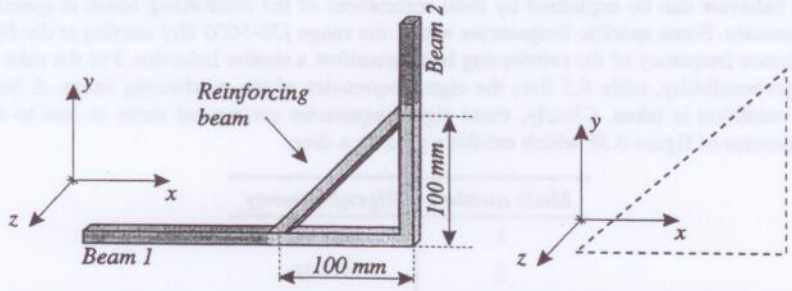

Figure 6.37 : Two right angled beams, reinforced with a third beam : schematic representation of the problem (left side); finite element model (right side).

Additional properties of the analysis are stated in table *6.4*.

Property	*Value*
Main beam section	$10 \times 10\ mm^2$
Reinforcing beam section	$10 \times 10\ mm^2$
Material	*Rigid PVC*

Table 6.4 : Properties of the analysis.

The corresponding finite element model is displayed in figure *6.37* at the right side. Note that it is not necessary to include the parts of beam *1* and beam *2* which are indicated dark gray on figure *6.36* into the finite element model. The junction is modeled such that the semi-infinite stiffnesses are directly applied at the points where the beams *1* & *2* and the reinforcing beam intersect.

Some relevant transmission and reflection coefficients are presented in figure *6.38* for the frequency range *0-5000 Hz*.

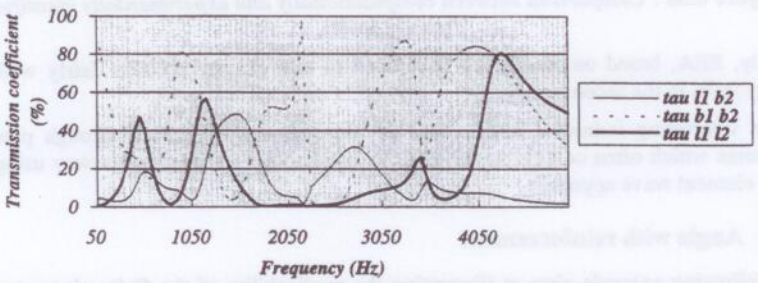

Figure 6.38 : Some relevant transmission coefficients of a junction with a reinforcing beam.

Presumably, the transmission coefficient does not show a smooth continuous curve as a function of frequency such as the one obtained in the previous examples. At some frequencies the transmission coefficients exhibit an abrupt drop or increase.

This behavior can be explained by local resonances of the reinforcing beam at specific frequencies. Some specific frequencies within the range *[50-5000 Hz]* starting at the first resonance frequency of the reinforcing beam manifest a similar behavior. For the sake of comprehensibility, table *6.5* lists the eigenfrequencies of the reinforcing beam. A free-free condition is taken. Clearly, these eigenfrequencies correspond more or less to the frequencies of figure *6.38* which exhibit a peak or a drop.

Mode number	*Eigenfrequency*
1	*600 Hz*
2	*676 Hz*
3	*851 Hz*
4	*1045 Hz*

Table 6.5 : Eigenfrequencies of the reinforcing beam.

6.5.6 Application of solid elements.

The finite element models which are examined in the previous examples consist of beam elements (NASTRAN bar elements) exclusively. This section focuses on the employment of other types of elements for the determination of the transmission coefficients of beam-beam junctions.

If for a particular application, geometrical details of the junction are important, then the exclusive use of beam elements may in some occasions not be satisfactory to calculate the transmission coefficients in a sufficiently adequate way. Eventually solid, plate or other types of elements should be employed. The next example in this respect concentrates on the application of *solid* elements.

As a foregoing point of interest, the compatibility of solid elements and beam elements regarding wave transmission is examined. The latter is done by studying the transmission of waves at the interface of solid and beam elements. In other words, a wave traveling in a beam may not be reflected at the interface between solid elements and beam elements as long as the beam section is similar to the section composed by the solid elements.

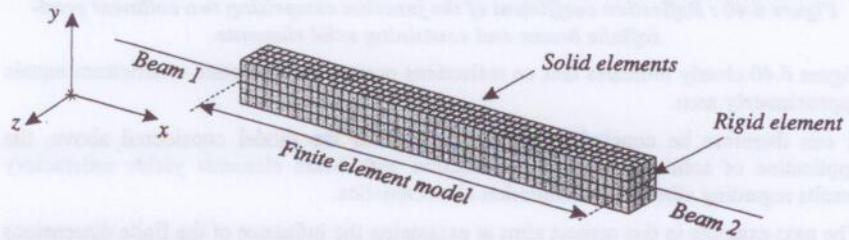

Figure 6.39 : Two collinear semi-infinite beams constructed via solid elements.

The model consists of two beams and a joint (finite element model) composed of solid elements (NASTRAN HEXA elements). The beams and solid elements are connected to each other by means of rigid elements (NASTRAN RBE2 elements). Additional properties of the problem are stated in table *6.6*.

Property	*Value*
Beam section	$10 \times 10\ mm^2$
Length finite element model	*100 mm*
Total number of beam elements	*2*
Total number of solid elements	*808*
Material	*Rigid PVC*
Frequency	*5000 Hz*

Table 6.6 : Properties of the analysis.

To include shear deformation effects, a shear coefficient of *0.833* is used for the bar elements. Each rigid element (left and right side) is connected to a NASTRAN bar element. The NASTRAN bar element is connected to the characteristic stiffness of the semi-infinite beams (wave absorbing elements).

Figure *6.39* displays the longitudinal and flexural wave reflection coefficients as a function of frequency, based on the finite element wave approach. Theoretically, the reflection coefficients should be zero because the section of the bar elements is taken similar to section of the part containing the solid elements.

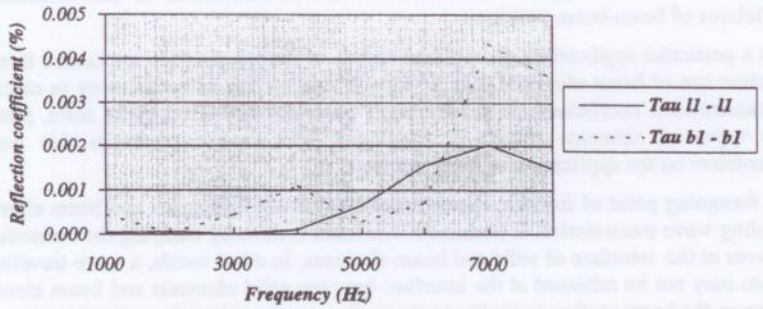

Figure 6.40 : Reflection coefficient of the junction comprising two collinear semi-infinite beams and containing solid elements.

Figure *6.40* clearly indicates that no reflections occur : the reflection coefficients equals approximately zero.

It can therefore be concluded that in the case of the model considered above, the application of solid elements in conjunction with beam elements yields satisfactory results regarding vibration transmission characteristics.

The next example in this respect aims at examining the influence of the finite dimensions of the beam section (10×10 mm^2) on the vibration transmission behavior of a right angled junction in order to assess the importance of geometrical details of the junction at high frequencies with respect to the identification of the transmission coefficients. A junction composed of two right angled beams is analyzed using a combination of beam and solid elements (figure *6.41*). Additional properties are listed in table *6.1*.

For the sake of simplicity, only flexural waves about the z-axis and longitudinal waves are retained. Several influences including frequency, mesh density of the solid elements and off-sets are examined.

Before presenting the results of the right angled junction, a reduction of the finite element model is carried out. Because only transmission coefficients between longitudinal and flexural waves about the local z-axis are retained (particle velocity in the local y-direction), it has been found favorable not to use solid elements (NASTRAN HEXA elements) but rather to employ membrane elements (NASTRAN QUAD4 elements). Both models are schematically pictured in figure *6.41*. The reason for applying shell elements is that it reduces the model quite drastically because of the elimination of the DOF's in the z-direction. Because no transmission coefficients are evaluated with respect to torsional waves nor with respect to bending waves about the y-axis, the elimination of the z-coordinate is justified.

The reduction is shown to be justified in the example which is presented below. Figure *6.41* pictures two finite element models of a right angled junction. The model on the left side employs shell elements. The model on the right side incorporates solid elements.

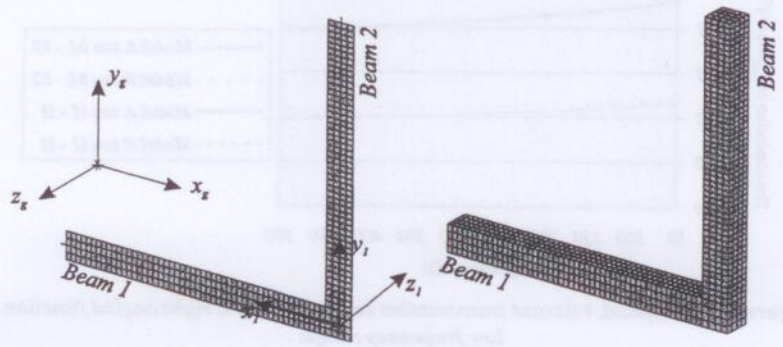

Figure 6.41 : Two finite element models of a right angled junction : on the left side modeled with shell elements; on the right side modeled with solid elements.

Figure *6.42* displays typical, relevant transmission coefficients of both models. The curves of the graph represent the transmission coefficients associated with longitudinal energy in beam *1* in case of the input and flexural energy (bending about *z*-axis) in beam *2* in case of the output. Clearly, no significant differences between both models (shell and solid) is noticed. For this reason, only shell elements are further on applied to study the right angled junction, keeping in mind that the results obtained by the utilization of shell elements also apply for solid elements.

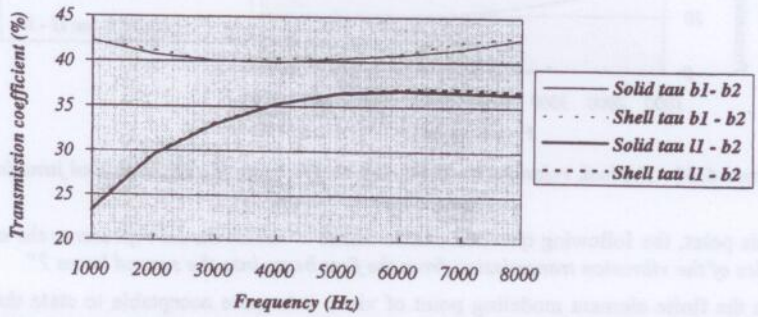

Figure 6.42 : Solid elements and shell elements : a comparison of some relevant transmission coefficients.

For the next example, the influence of local geometrical details at the point where the beams intersect with respect to the transmission characteristics is addressed. First, the lower frequency range (*50-500 Hz* - exhibiting large wavelength) is considered. A comparison between the application of shell elements (or indeed solid elements) referred to as model *B* and bar elements referred to as model *A* is carried out. Both models are pictured in figure *6.47*. The model composed of shell elements contains *680* CQUAD4

elements. The bar model contains *20* elements. Some characteristic transmission coefficients are shown below.

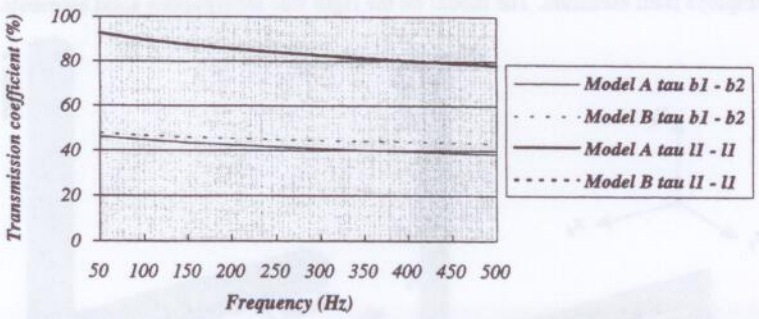

Figure 6.43 : Typical, relevant transmission coefficients of a right angled junction : low frequency range.

At low frequencies (figure *6.43*), the results of both models agree acceptably well. In the higher frequency range (*1000-8000 Hz*) on the other hand, a substantial disagreement between both models can be noticed (figure *6.44*).

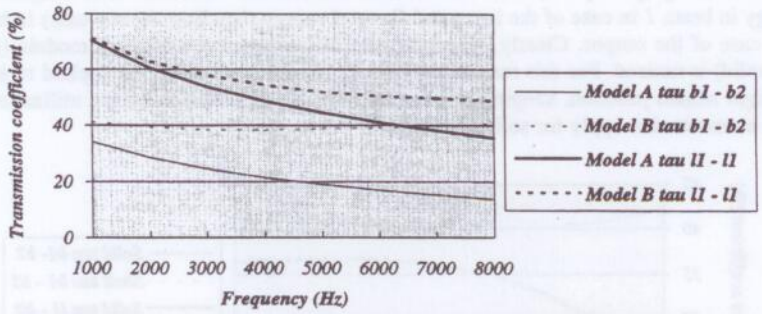

Figure 6.44 : Typical, relevant transmission coefficients of a right angled junction : high frequency range.

At this point, the following question can be raised : *"which model represents the actual physics of the vibration transmission from the first beam into the second beam ?"*

From the finite element modeling point of view, it is quite acceptable to state that the solid (or indeed shell) models tend closer toward the actual physics of vibration transmission in general and in particular at higher frequencies. This is because in the case of the beam model, the Timoshenko (or eventually the Bernouilli-Euler) beam theory is applied, meaning that plane section remain plane when a wave travels along the beam. If a wave impinges upon the junction, then the sections still remain plane at the point where the beams intersect. No local stress concentrations are noticed at this point. Physically however, it is quite amenable that if a wave exhibiting a short wavelength impinges upon

a junction then local stress concentrations which influences the energy transfer from the first beam into the second are likely to occur.

The latter corresponds to the local stress concentrations which are also observed in case of a static calculation performed on the right angled beam of figure *6.45*.

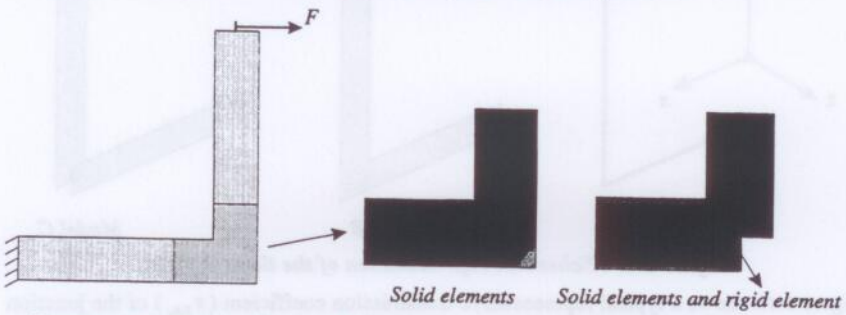

Figure 6.45 : Stress contour at the point where two right angled beams intersect.

The previous statement (namely the fact that the application of solid elements is advised in the higher frequency range) is verified by means of a calculation performed on a model containing shell elements and rigid elements at the point where the beams intersect. The results of the latter model are compared to the results of the model incorporating solid elements only.

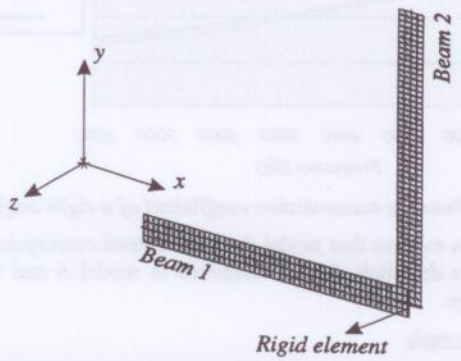

Figure 6.46 : The application of a rigid element in combination with shell elements to enforce Timoshenko's beam theory.

The model displayed in figure *6.46* is expected to represent the Timoshenko beam conditions. Therefore, plane sections are expected to remain plane after deformation at the point where the beams intersect due to the presence of the rigid elements.

Three models (figure *6.47*) are examined :

- **Model A** : based on bar elements.
- **Model B** : based on solid elements.

- **Model C** : based on solid elements and including rigid elements at the point of intersection to enforce Timoshenko's beam theory.

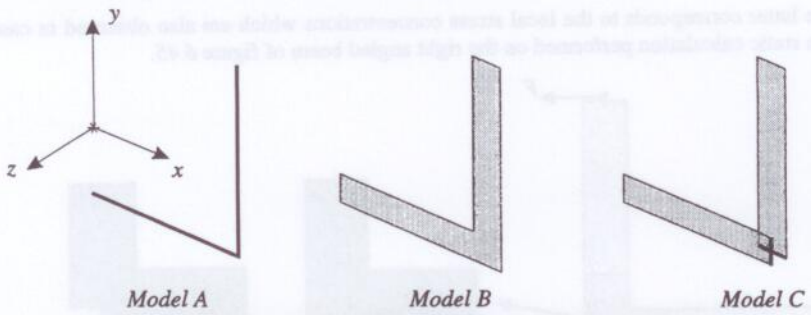

Figure 6.47 : Schematic representation of the three models.

Figure *6.48* shows a typical representative transmission coefficient ($\tau_{b_1 b_2}$) of the junction in the case of the three models.

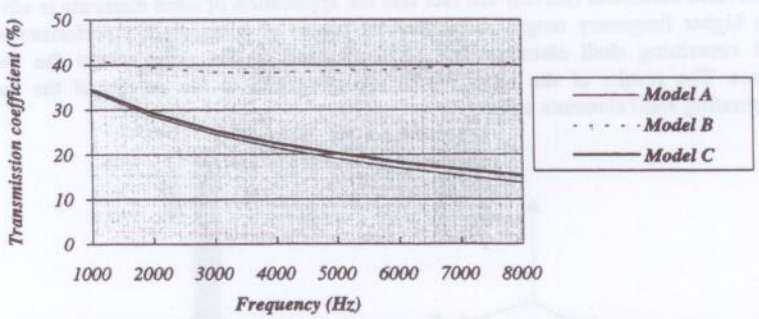

Figure 6.48 : Bending transmission coefficient of a right angled junction.

From figure *6.48*, it is evident that model *A* and *C* indeed correspond well (as could be expected). Model *B* is definitely far off compared to model *A* and *C*, especially in the higher frequency range.

Conclusion of the example

It is clear that model *B* includes all geometrical details, i.e. the model is built up of solid element without any additional constraints at the point where the beams intersect. Model *C* on the other hand is derived from *B* by including an additional constraint at the junction (rigid element) to enforce plane sections remaining plane at the point where the beams intersect. Because of this additional constraint, model *C* is definitely further off the actual, physical situation for which there is no such "*constraining condition*" in terms of plane sections remaining plane at the point where the beams intersect. Besides, it is shown that the finite element model based on the bar elements (model *A*) corresponds to model *C*.

Consequently, it can be concluded that the bar model is not suitable to be used for the determination of vibration transmission characteristics at high frequencies, i.e. in case of frequencies for which the influence of the beam section becomes important.

As a final example, figure *6.50* shows a typical, relevant transmission coefficient of the junction pictured in figure *6.49* (model *D*). The difference between model *D* and model *C* is enclosed in the off-set of the beams at the point of intersection.

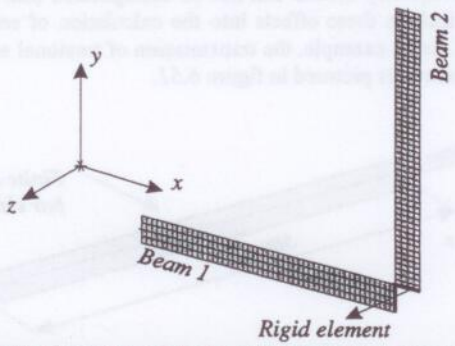

Figure 6.49 : Finite element model of a right angled junction incorporating an additional off-set at the points where the beams intersect.

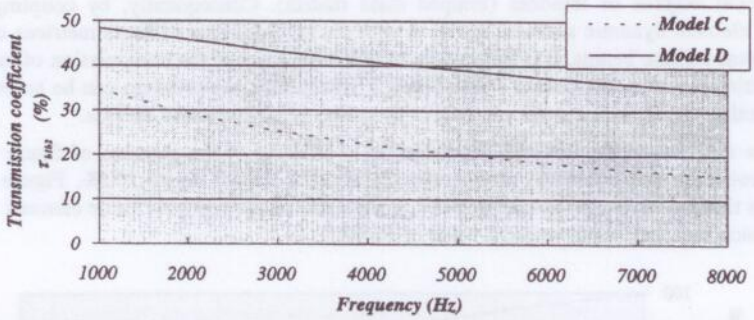

Figure 6.49 : Flexural transmission coefficient of a right angled junction : influence of the off-set.

According to the remarkable disagreement between the model of figure *6.49* (model *D*) and model *C*, it can be stated that a detailed modeling of the off-set of the junction is essential in the high frequency range (somewhere around *500 Hz* in case of the example considered above). At *500 Hz*, the bending wavelength equals *250 mm* which is still much larger that a typical dimension of the section of the beam, i.e. *10 mm*. The latter implies that high frequency effects already become critical and should be taken into consideration at seemingly low frequencies. For example, *500 Hz* is expected to be in the low frequency range because the bending wavelength equals *250 mm* and the height of the beam equals only *10 mm*.

6.5.7 Restrictions of the finite element wave approach due to properties of the finite elements.

A final paragraph of chapter 6 deals with a topic which is of noteworthy importance when applying the finite element wave approach to calculate transmission coefficients. It is essential that the semi-infinite stiffnesses which are calculated according to the procedure of chapter 6 should be adjusted to the characteristics of the finite elements. In other words, if high frequency effects can not be incorporated into the finite elements, then it is fruitless to include these effects into the calculation of semi-infinite stiffness matrices of the beam. As an example, the transmission of torsional energy along a beam is considered. The structure is pictured in figure *6.51*.

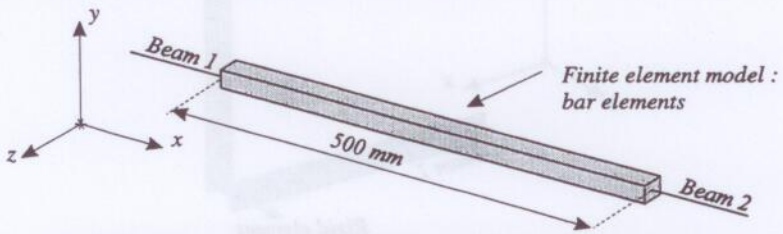

Figure 6.51 : Junction connecting two collinear semi-infinite beams.

The properties of the NASTRAN bar elements are such that no inertia is attributed to the rotational degrees of freedom (lumped mass matrix). Consequently, by coupling the finite element dynamic stiffness matrices with the semi-infinite stiffness matrices of the two semi-infinite beams, it is impossible to take into account the transmission of energy of torsional waves from beam *1* into beam 2. Eventually, the problem can be solved by attributing inertia to the rotational DOF's by means of concentrated masses.

Figure *6.52* shows the torsional transmission coefficient of the junction of figure *6.51*. Theoretically, the torsional transmission coefficient should equal *100%*. Figure *6.52* shows that the transmission coefficient $\tau_{11'2}$ obtained by applying the finite element wave approach is far off the theoretical value of *100%*.

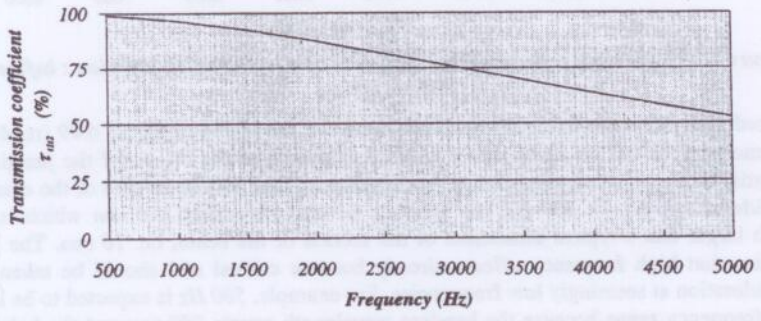

Figure 6.52 : Torsional transmission coefficient of a junction comprising two collinear semi-infinite beams.

A final example in this respect shows the influence of the shear factor on the transmission coefficient of the junction pictured in figure *6.51*. The technique explained in chapter 6 to calculate semi-infinite stiffnesses takes into account thick bending effects (shear correction coefficients and rotatory inertia of the sections). However, if the finite element program does not allow to incorporate the thick bending terms, then the coupling between the semi-infinite stiffnesses (calculated based on the procedures of chapter 6 and including thick bending terms) with the finite element stiffnesses is not justified. The incorporation of thick bending terms into the calculation of semi-infinite stiffnesses does not give rise to a refinement of the model.

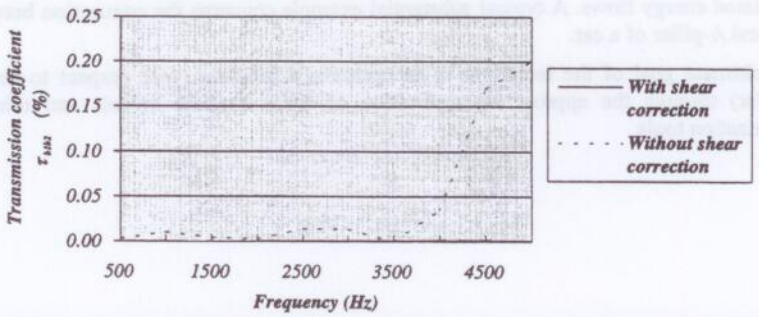

Figure 6.53 : Influence of the shear correction on the transmission properties.

As a final conclusion, it can be stated that the adaptation of the semi-infinite stiffnesses to the finite element models should always be pursued in such a way that the effects (such as thick bending) which are included in the calculation of the semi-infinite stiffnesses are also included in the finite element models. Hence, a thorough knowledge of the characteristics of the finite elements is definitely essential.

6.6 Conclusion.

When applying SEA to complex structures in an accurate way, it is necessary to obtain good values of the transmission coefficients of the structural junctions. Because in the high frequency range, the transmission of vibrational energy from one subsystem to another subsystem is unquestionably dependent upon the local structural details of the junction, it is advised to apply finite elements in order to model the junction in an accurate way.

The transformation of the finite element stiffness and mass matrix into the matrix of transmission coefficients of the junction is described in chapter *6*. The utilization of wave absorbing elements is fundamental in this respect. The complex dynamic stiffness matrix of the wave absorbing elements corresponds to the wave stiffness of the subsystem. The evaluation of the wave stiffness is addressed in chapter *5*.

The so-called "finite element wave approach" is developed, implemented and worked out extensively in the case of beam-beam junctions. The technique makes it possible to take into account whatever geometrical complexity within the beam-beam junction. A typical example manifestating the significance of the technique concerns the incorporation of round-offs at the junction. The theory developed in chapter *6* is shown to work properly

for this example. Other examples, highlighting the importance of the finite element wave approach, are dealing with the application of solid elements and the influence of a reinforcing beam at the junction on the transmission coefficient.

The extension of the theory to incorporate plates has been addressed briefly. Some relevant equations (with respect to the formulations of the wave absorbing elements) were derived, an example exhibiting the wave pattern of a plate is given. The excitation consisted of a point force and moment applied at the origin. Only bending behavior of the plate is taken into account. Later on, the finite element wave approach in the case of plates should be extended to include a combined in-plane - out of plane motion and hence to make it possible to analyze very accurately the plate-beam connections and its associated energy flows. A typical substantial example concerns the connection between roof and *A*-pillar of a car.

The ultimate goal of the technique is to optimize a junction (with respect to energy transfer) through the appropriate application of finite element models and relevant optimization tools.

7. GENERAL CONCLUSIONS.

In order to perform dynamic analyses in the high frequency range, it is beneficial to adopt statistical energy approaches to bypass the problems which arise when applying classical "deterministic" methods.

This thesis provides a general description of Statistical Energy Analysis (SEA), a method which constitutes the primary high frequency modeling method at present. In particular, the computational and experimental identification procedures of the SEA parameters are addressed. Most often the computational approach aims at analyzing high frequency vibrations in the early design stage of vibro-acoustic systems. The experimental approach aims at evaluating the model parameters of existing structures. The latter technique offers a tool for trouble-shooting and structural modification analysis based on energy flow paths within the structure.

Experimental identification of the SEA parameters.

The experimental part of SEA is based on the Power Injection Method which consists basically of a set of input-output measurements : every subsystem is excited in turn; the response of all subsystems is measured. By applying inverse SEA (inverting the responses, i.e. the normalized energy matrix), one can obtain the model parameters : the internal loss factor and the coupling loss factor. The normalized energy matrix consists of elements being the relevant ratio of measured energy levels and power input levels into the subsystems. The measured energies and power inputs can be obtained through FRF data in which case an equivalent energy and power input is obtained or via power spectral data.

PIM is a "novel" and even an "atypical" method for identifying the SEA parameters. In the beginning of the *80's*, very simple two-subsystem models were examined. The research on applying PIM to complex structures (such as cars) was initiated at the end of the *80's*. Nonetheless, the equations which are involved have not been optimized since then and PIM still faces some shortcomings.

The first contribution of this thesis to experimental SEA therefore deals with an in-depth investigation of the fundamentals of PIM. The equations involved are critically reviewed

and reformulated in a comprehensive way (resulting in a reduction of the dimension of the energy matrix). Secondly, the problem of energy measurements and of power input measurements is tackled. The equivalent mass principle is generally applied within the PIM framework to ameliorate the energy measurements. In here, the concept of equivalent mass is substituted by the concept of "correction coefficient" because it is believed that this quantity does describe (let's call it) "make-up" procedure in a more correct way. One of the items which has been developed in here and which can be considered as a generalization of the equivalent mass theory is the so-called "updating of the parameters", allowing one to apply prior knowledge concerning the SEA parameters in such a way that measurement errors can be decreased. The example which is given in chapter *3* indicates that even very substantial measurement errors can be corrected through the updating procedure. Measured quantities which are amenable to be updated consist of the acoustic power input, the structural power input or the energy correction coefficient. In addition, chapter *3* also presents important thoughts on the measurement sequence which can become critical for very large systems (for a car the number of subsystem equals more or less *50*). Several measurement procedures are thought over and are illustrated by means of an example.

Sensitivity and statistical related items are covered in chapter *4*. Although the statistical procedures have been worked out in the past by researchers and engineers in the case of predictive SEA, this has not been done so far for experimental SEA, in particular PIM. The basis of the statistical procedures originally worked out in chapter *4* deals with the variance of the measured quantities, basically the indirect and direct FRF's. Formulations are developed to assess the confidence levels of the SEA parameters based on the confidence levels of the measured quantities. In addition, a complete statistical analysis scheme is worked out and exemplified for the SEA predictions (energy input, source localization etc.).

It is worth a note that chapter *4* also provides a novel and clear insight into some sensitivity aspects of PIM. The equations the way they are worked out in chapter *4*, allow to perform a simple optimization of the energy level of a subsystem with respect to an SEA parameter. The influence of measurement errors (energy and power input errors) on the model parameters and on the predicted vibration levels is also briefly addressed and some important conclusions are drawn.

Although chapter *3* contributes to the minimization of the measurement effort, still and all, PIM measurements on large structures (even *50* subsystems can be considered as large) are very expensive and therefore every substantial reduction of measurement effort (without affecting the SEA parameters) should be welcomed. Some novel contributions in this respect are discussed in chapter *4*. Neglecting response measurements during PIM constitutes one of the appealing applications of the sensitivity formulations when it comes to minimizing the measurement effort. The influences of this type of measurement reduction on the SEA parameters and on the SEA predictions is extensively addressed in chapter *4*. The appearance of decoupling between subsystems of the SEA model when neglecting response measurements during PIM is also worth a note.

Another interesting unique application of the sensitivity procedures worked out in chapter *4* deals with the measurement of specific coupling loss factors between two subsystems. It is shown that it is not necessary to perform a complete set of measurements, i.e. to excite *every* subsystem and to measure the response of *all*

subsystems. One can restrict the number of measurements and concentrate on a small number of subsystems which are substantially contributing to a specific coupling loss factor. Chapter *4* addresses the mathematics involved and presents an example in this respect.

As a general conclusion of the experimental identification technique, it can be mentioned that chapter *3* and *4* aimed at clarifying and optimizing in a general, comprehensive and original way the main aspects of PIM.

Still and all, additional work has to be done on the subject of experimental SEA, such as with respect to the contribution of in-plane motion, a further optimization of the power input measurements, non-uniformly distributed subsystems, choice of subsystems etc.

Computational identification of SEA parameters.

The second main part of the dissertation covers the application of computational techniques. A general description of the evaluation of the basic SEA parameters based on the state of the art knowledge is given in a general and comprehensible way. Chapter *5* partially covers existing techniques which are used at present in commercially available software's and which are dealt with in literature, in particular with respect to modal densities and internal loss factors. The main part of chapter 5 synthesizes and extends the classical formulations with respect to predictive coupling loss factor evaluation. More specifically, in the case of beam-beam couplings, the procedures allow to analyze the transmission characteristics of junctions for which an arbitrary number of general Timoshenko beams join. For plate-plate couplings, formulations are developed and implemented allowing one to take into account an arbitrary number of thick plates, joining at an arbitrary angle and including additional off-sets of the junction line. The transmission coefficients of the plate-plate junctions are calculated for incidence angles of the incidence waves ranging from *0°* to *90°*. For the plates, shear, longitudinal and bending motion is coupled and integrated into one coupled analysis. The *fully coupled* analysis is shown to be essential when performing structural vibration analyses in the *high* frequency range. Due to the generality of the formulations which are implemented in the framework of this dissertation, a wider variety of couplings can be evaluated compared to the techniques which are used today by industry.

A novel, further extension of the coupling formulations is given in chapter *6*. In this chapter, the coupling loss factors are calculated based on a detailed finite element analysis of the junction. By applying wave absorbing boundary conditions, it is possible to transform the dynamic stiffness matrix into the transmission matrix of the junction and hence into coupling loss factors. The technique allows to take into account beam-beam junctions of arbitrary geometrical complexity. The beam-beam junctions are extensively addressed and examples are given showing that this new approach is valid and is contributing substantially to predictive SEA.

In addition, formulations are developed to evaluate the wave absorbing boundary condition for plates excited by point loads. An example showing the wave pattern of a circular plate, excited by a point load is presented. No spurious reflections occur. The technique to calculate the transmission coefficients of plate-beam junctions is analogous to the procedure for beam-beam junctions. A second example illustrates the capabilities of this new approach in the case of a quarter plate reinforced with beams. One typical, industrial relevant application of the technique constitutes the assessment of the energy

flow from the *A*-pillar to the roof of the car. The techniques developed in chapter *6* should lead to accurate models in this respect. Further research on this topic is however imperative, possibly leading to an accurate evaluation of energy transmission through generic types of complex junctions.

To conclude, it can be emphasized that the foremost contribution to the computational SEA research performed in the framework of this thesis deals with the extension of the library of coupling loss factors (eventually based on finite element models) towards a wide variety of junctions. Although chapter *6* contributes to this field by applying finite element models, accurate formulations of wave absorbing boundary conditions are not yet *generally* available and additional research is definitely required.

REFERENCES.

[1] **"Statistical energy analysis of dynamical systems"**; LYON, R.H.; *M.I.T. Press;1975.*

[2] **"The experimental determination of vibrational energy balance in complex structures"**; LALOR, N.; *Conference on Stress and Vibration : Recent developments in industrial measurement and analysis; Paper No 1084 - 29; 1990.*

[3] **"The Measurement of SEA loss factors on a fully assembled structure"**; LALOR, N.; *ISVR Technical Memorandum; No 150; 1987.*

[4] **"An introduction to statistical energy analysis of structural vibration"**; WOODHOUSE, J.; *Applied Acoustics; 14, pp. 455-469; 1981.*

[5] **"Statistical Energy Analysis"**; FAHY, F.J.; *Noise and Vibration; Ellis Horwood Limited; Chapter 7; pp.165-186; 1982.*

[6] **"SEA for the time integrated transient response of vibrating systems"**; LAI, M.L.; SOOM, A.; *Transactions of the ASME Journal of Vibration and Acoustics; 112, pp. 206-213; 1990.*

[7] **"On the estimation of loss factors in lightly damped pipeline systems : some measurement techniques and their limitations"**; NORTON, M.P.; GREENHALGH, R.; *Journal of Sound and Vibration; 105, pp. 397-423; 1986.*

[8] **"Experimental determination of modal densities and loss factors of flat plates and cylinders"**; CLARKSON, B.L.; POPE, R.J.; *Journal of Sound and Vibration; 77, pp. 535-549; 1981.*

[9] **"A computer system to predict internal noise in motor cars using SEA"**; WALSH, S.J.; STIMPSON, G.; LALOR, N.; *Proceedings Internoise; pp. 969-972; 1990.*

[10] **"The use of energy techniques for the prediction of machinery noise - application to the diesel engine"**; STIMPSON, G.J.; *Proceedings Internoise; pp. 315-318; 1990.*

[11] **"Statistical energy analysis of a gearbox with emphasis on the bearing path"**; LIM, T.C.; SINGH, R.; *Noise control engineering journal; 37(2), pp. 63-69; 1991.*

[12] **"A comparison of modal density measurements techniques"**; KESWICK, P.R.; NORTON, M.P.; *Journal of Applied Acoustics; 20, pp. 137-153; 1987.*

[13] **"Measurement of modal density : an improved technique for use on lightly damped structures"**; BROWN, K.T.; *Journal of Sound and Vibration; 96(1), pp. 127-132; 1984.*

[14] **"In situ determination of loss and coupling loss factors by the power injection method"**; BIES, D.A.; HAMID, S.; *Journal of Sound and Vibration; 70(2), pp. 187-204; 1980.*

[15] **"Practical noise modelling of car body structures using energy flow analysis"**; STIMPSON, G.; LALOR, N.; *Proceedings Internoise; pp. 1233-1236; 1991.*

[16] **"Can statistical energy analysis be used in transient conditions ?"**; LEDNIK,D.; PINNINGTON, R.J.; *Proceedings Internoise; pp. 949-952; 1990.*

[17] **"The derivation of modal densities from point impedances"**; CLARKSON, B.L.; *Journal of Sound and Vibration; 77(4), pp. 583-584; 1981.*

[18] **"The role of inplane vibrations on structure borne sound"**; LYON, R.H.; TRATCH, J. JR.; *Proceedings Internoise; pp. 697-699; 1985.*

[19] **"A study of high frequency vibrations due to pyrotechnic shocks in coupled systems"**; LEDNIK, D.; PINNINGTON, R.J.; *Proceedings international conference on : "Spacecraft structures and mechanical testing", Noordwijk, the Netherlands; pp. 625-630; 1991.*

[20] **"Asymptotic modal analysis of a rectangular acoustic cavity excited by wall vibration"**; PERETTI, L.F.; DOWELL, E.H.; *AIAA Journal; 30(5), pp. 1191-1198; 1992.*

[21] **"Energy and structural intensity formulations of beam and plate vibrations"**; BOUTHIER, O.; BERNHARD, R.; WOHLEVER, C.; *Proceedings of the international congress on Intensity Techniques, Senlis, France; pp. 37-44; 1990.*

[22] **"Power flow finite element analysis of dynamic systems : basic theory and application to beams"**; NEFSKE, D.J.; SUNG, S.H.; *Transactions of ASME Journal of Vibration and acoustics; 111, pp. 94-100; 1989.*

[23] **"Elastic wave transmission through plate/beam junctions"**; LANGLEY, R.S.; HERON, K.H.; *Journal of Sound and Vibration; 143(2), pp. 241-253; 1990.*

[24] **"Experimental investigation of asymptotic modal analysis for a rectangular plate"**; KUBOTA, Y.; DOWELL, E.H.; *Journal of Sound and Vibration; 106(2), pp. 203-216; 1986.*

[25] **"Asymptotic modal analysis and statistical energy analysis of an acoustic cavity"**; KUBOTA, Y.; DIONNE, H.D.; DOWELL; E.H.; *Journal of Vibration, Acoustics, Stress and Reliability in Design; 110(3), pp. 371-376; 1988.*

[26] **"Sound transmission and mode coupling at junctions of thin plates, part II : parametric survey"**; CRAVEN, P.G.; GIBBS, B.M.; *Journal of Sound and Vibration; 77(3), pp. 429-435; 1981.*

[27] **"Experimental verification of the asymptotic modal analysis method as applied to a rectangular acoustic cavity excited by structural vibration"**; PERETTI, L.F.; DOWELL, E.H.; *Transactions of the ASME Journal of vibration and acoustics; 114, pp. 546-554; 1992.*

[28] **"Neue Werkzeuge fur die schwingungstechnik; A new NVH toolkit"**; HANISH, W.; *VDI Berichte; NR 791, pp. 455-472; 1990.*

[29] **"A review of sound transmission through buildings using statistical energy analysis"**; CRAIK, R.J.M.; *Proceedings NOISE-93, St. Petersburg, Russia; pp. 215-220; 1993.*

[30] **"Identification of internal loss factors during statistical energy analysis of automotive vehicles"**; RADCLIFFE, C.J.; HUANG, X.L.; *Proceedings of the 1993 SAE Noise and Vibration Conference; Traverse City, Michigan, US; pp. 311 - 318; 1993.*

[31] **"Wave propagation theory in anisotropic periodically layered fluid-saturated porous media"**; SUN, F.; BANKS-LEE, P.; PENG, H.; *Journal of the Acoustical Society of America; 93(4), pp. 1277-1285; 1993.*

[32] **"Methods for predicting noise levels in ships; experiences from empirical and SEA calculations methods"**; PLUNT, J.; *Department of building acoustics, Chalmers University, Gothenburg, Sweden; Report 80-07; 1980.*

[33] **"Derivation of energy flow with a finite element model"**; FREDÖ, C.L.; *Thesis for the degree of Licentiate of Engineering.; Chalmers University, Gothenburg, Sweden; Report F 93 - 01 ISSN 0283 - 832X; 1993.*

[34] **"Power flow between non-conservatively coupled oscillators"**; FAHY, F.J.; YUAN, Y.D.; *Journal of Sound and Vibration; 114(1), pp. 1-11; 1987.*

[35] **"Power flow and energy balance of non-conservatively coupled structures I : theory"**; SUN, J.C.; LALOR, N.; RICHARDS, E.J.; *Journal of Sound and Vibration; 112(1), pp. 321-330; 1987.*

[36] **"Bending and in-plane wave transmission in thick connected plates using statistical energy analysis"**; MCCOLLUM, M.D.; CUSHIERI, J.M.; *Journal of the Acoustical Society of America; 88(3), pp. 1480-1485; 1990.*

[37] **"Thick plate bending wave transmission using a mobility power flow approach"**; MCCOLLUM, M.D.; CUSHIERI, J.M.; *Journal of the Acoustical Society of America; 88(3),pp. 1472-1479; 1990.*

[38] **"Structure-borne sound transmission at elastically connected plates."**; MEES, P.; VERMEIR, G.; *Journal of Sound and Vibration; 166(1), pp. 55-74; 1993.*

[39] **"Energy flow in an L-shaped plate"**; FREDÖ, C.R.; SANDERSON, M.A.; *Proceedings internoise; pp. 1193-1196; 1993.*

[40] **"Power flow investigation in dynamic continuous systems"**; CARCATERRA, A.; SESTIERI, A.; *Proceedings of the 4th international congress on intensity techniques, Senlis, France; pp. 355-362; 1993.*

[41] **"An approximate power flow solution for one-dimensional dynamic structures"**; CARCATERRA, A.; SESTIERI, A.; *Proceedings of the 4th international congress on intensity techniques, Senlis, France; pp. 363-370; 1993.*

[42] **"Definition and calculation of transmission paths within an SEA framework"**; MAGRANS, F.X.; *Journal of Sound and Vibration; 165(2), pp. 277-283; 1993.*

[43] **"Mode coupling and energy partition of sound in a system of plate junctions"**; GIBBS, B.M.; *Journal of Sound and Vibration; 104, pp. 127-136; 1986.*

[44] **"Interior noise scatter in four-cylinder sedans and wagons"**; WOOD, .A.; JOACHIM, C.A.; *International Journal of Vehicle Design; 8 (4/5/6), pp. 428-438; 1987.*

[45] **"Propagation of vibrational energy in absorbing structures"**; BELOV, V.D.; RYBAK, S.A.; TARTAKOVSKII, B.D.; *Journal of Sovjet Physics Acoustics; 23(2), pp. 115-119; 1977.*

[46] **"Energetics of vibrating systems."**; BOUTHIER, O.M.; *PhD dissertation Purdue University, Herrick Laboratories, Indiana, Michigan, US; 1992.*

[47] **"Energy formulation for one dimensional problems"**; LEBOT, A.; JEZEQUEL, L.; *Paper presented at the Institute of Acoustics Meeting, Southampton England; ; 1993.*

[48] **"Energy flow analysis of coupled structures."**; CHO, P.E.; *PhD dissertation Purdue University, Herrick Laboratories, Indiana, Michigan, US;1993.*

[49] **"Power flow as a complement to statistical energy analysis and finite element analysis"**; CUSHIERI, J.M.; *ASME Publication, NCA 3 (G00403);1987.*

[50] **"Power flow through machine isolators to resonant and non-resonant beams"**; PINNINGTON, R.J.; WHITE, R.G.; *Journal of Sound and Vibration; 75(4), pp. 179-197; 1981.*

[51] **"Analyse energetique de quelques problemes vibratoires"**; LEBOT, A.; *Report Number HP-62/93017, département acoustique et mécanique vibratoire, direction des études et récherches, électricité de France; 1993.*

[52] **"Analysis of a dynamic system based on a new energetics formulation"**; LASE, Y.; JEZEQUEL, L.; *Proceedings of the 3rd International Congress on Intensity Techiques, Senlis, France; pp. 145-150; 1990.*

[53] **"Mechanical energy flow models of rods and beams"**; WOHLEVER, J.; BERNHARD, R.J.; *Journal of Sound and Vibration; 153(1), pp. 1-19; 1992.*

[54] **"Influence of rotary inertia and shear on flexural motion of isotropic elastic plates"**; MINDLIN, R.D.; *Journal of Applied Mechanics; 18, pp. 31-38; 1951.*

[55] **"Determination of loss factors for statistical energy analysis of a diesel engine with geometric averaging approach"**; WU, L.; AGREN, A.; SUNDBACK, U.; *Acta Acustica; 2, pp. 127-142; 1994.*

[56] **"Frequency averaging effects in SEA."**; MACE, B.R.; *Proceedings Third International Congress on air-and structure-borne sound and vibration, Montréal, Canada; pp. 177-184; 1994.*

[57] **"Vibration intensity methods : 20 years after."**; PAVIC, G.; *Proceedings Internoise; pp. 1657-1662; 1994.*

[58] **"Response and radiation of structural modes excited by sound"**; SMITH, P.W.JR.; *Journal of the Acoustical Society of America; Vol. 34, pp. 640-647; 1962.*

[59] **"Power flow between linearly coupled oscillators"**; LYON, R.H.; MAIDANIK, G.; *Journal of the Acoustical Society of America; 34, pp. 623-639; 1962.*

[60] **"Thermal circuit approach to vibrations in coupled systems and the noise reduction of a rectangular box"**; EICHLER, E.; *Journal of the Acoustical Society of America; 34, pp. 995-1007; 1963.*

[61] **"Random vibration of connected structures"**; LYON, R.H.; EICHLER, E.; *Journal of the Acoustical Society of America; 36, pp. 1344-1354; 1964.*

[62] **"Stress and strain limits on the attainable velocity in mechanical vibrations"**; HUNT, F.V.; *Journal of the Acoustical Society of America; 32, pp. 1123-1128; 1960.*

[63] **"Maximum stresses in beams and plates vibrating at resonance"**; UNGAR, E.E.; *Journal of Engineering for Industry; 84, pp. 149-155; 1962.*

[64] **"Statistics of acoustically induced vibration"**; FAHY, F.; *7th International congress on acoustics, Budapest, Hungary; pp. 561-564; 1971.*

[65] **"Spatial variation of stress, strain and acceleration in structures subject to broad frequency band excitation"**; STEARN, S.M.; *Journal of Sound and Vibration; 12, pp. 85-97; 1970.*

[66] **"Experiments on the correlation of dynamic stress and strain with pipe wall vibrations for SEA applications"**; NORTON, M.P.; FAHY, F.J.; *Noise control engineering; 30(3), pp. 101-111; 1988.*

[67] **"Prediction mechanical shock transmission"**; MANNING, J.E.; LEE, K.; *Shock and Vibration Bulletin.; 37(4), pp. 65-70.; 1968.*

[68] **"Statistical energy analysis of transient vibration"**; POWELL, R.E.; QUARTARARO, L.R.; *ASME winter meeting Boston MA, USA; Book no 4; pp. 535-547; 1987.*

[69] **"Research on thick plate vibration : a literature survey"**; LIEW, K.M.; XIANG, Y.; KITIPORNCHAI, S.; *Journal of Sound and Vibration; 180(1), pp. 163-176; 1995.*

[70] **"Characteristics of wave propagation and energy distributions in cylindrical elastic shells filled with fluid"**; FULLER, C.R.; Fahy, F.J.; *Journal of Sound and Vibration; Vol. 81(1), pp. 501-518; 1982.*

[71] **"Vibrational energy flow in elastic circular cylindrical shells"**; PAVIC, G.; *Journal of Sound and Vibration; Vol. 142(2), pp. 293-310; 1990.*

[72] **"Application of vibrational power measurement to the piping system in an air-conditioner"**; SATO, K.; *Proceedings Internoise; pp. 591-594; 1988.*

[73] **"Model size requirements for finite element prediction of low frequency cabin noise and vibration"**; LANDMANN, A.; TILLEMA, H.; *Proceedings of the 12th aeroacoustics conference, San Antonio, Texas, US; Paper AIAA-89-1076; 1989.*

[74] **"Measurement of the statistical variation of structural-acoustic characteristics of automotive vehicles"**; KOMPELLA, M.S.; BERNHARD, R.J.; *Proceedings of the SAE Noise and Vibration conference, Traverse City, Michigan, US; SAE paper 931272; 1993.*

[75] **"Measurement of power flow in uniform beams and plates"**; NOISEUX, D.U.; *Journal of the Acoustical Society of America; 47, pp. 238-247; 1970.*

[76] **"Nearfield acoustic holography : I. Theory of generalized holography and the development of NAH"**; MAYNARD, J.D., WILLIAMS, E.G.; LEE, Y.; *Journal of the Acoustical Society of America; 78, pp. 1395-; 1985.*

[77] CARNIEL, X.; *Proceedings OPTO 93; pp. 468-; 1993.*

[78] **"Transfer function method of measuring in-duct acoustic properties. I. theory"**; CHUNG, J.Y.; BLASER, D.A.; *Journal of the Acoustical Society of America; 68(3), pp. 907-913; 1980.*

[79] **"Structure-borne sound"**; CREMER, L.; HECKL, M.; UNGAR, E.E.; *Springer-Verlag;1973.*

[80] **"Fundamentals of noise and vibration analysis for engineers."**; NORTON, M.P.; *Chapter 6 : Statistical energy analysis of noise and vibration; Cambridge University Press; 1989.*

[81] **"An acoustic power injection device with built-in calibration"**; YANG-SUB, O; *Msc. thesis Institute of Sound and Vibration Research;Southampton, U.K. ; 1991.*

[82] **"Sound Intensity"**; FAHY, F.J.; *Elsevier Applied Science;1989.*

[83] **"On the modal density and damping of cylindrical pipes"**; RENNISON, D.C.; BULL, M.K.; *Journal of Sound and Vibration; 54(1); pp. 39-53; 1977.*

[84] **"The acoustic radiation efficiency of rectangular plates"**; LEPPINGTON, F.G.; BROADBENT, E.G.; HERON, K.H.; *Proc. R. Soc. Lond. A; 382, pp. 245-271; 1982.*

[85] **"Vibration damping"**; NASHIF, A.D.; JONES, D.I.G.; HENDERSON, J.P.; *A Wiley-Interscience Publication; 1985.*

[86] **"Acoustic radiation damping"**; CLARKSON, B.L.; BROWN, K.T.; *Journal of Vibration, Acoustics, Stress and Reliability in Design; 170, pp. 357-360; 1985.*

[87] **"Interaction of sound waves with solid structures"**; VER, I.L.; HOLMER, C.I.; *Noise and Vibration Control, Chapter 11; Mc Graw-Hill; 1971.*

[88] **"Titan IV payload vibro-acoustics WIS, LOIS and wind tunnel comparisons"**; TANNER, C.S.; *Presentation of the Environmental Criteria and Tests Department of the Aerospace Corporation.;1990.*

[89] **"PAM-S acoustic test results and VAPEPS comparisons"**; THINCH, D; *Presentation of the Environmental Criteria and Tests Department of the Aerospace Corporation.; 1990.*

[90] **"Response of ribbed panels to reverberant acoustic fields"**; MAIDANIK, G.; *Journal of the Acoustical Society of America; 34, pp. 809-826; 1962.*

[91] **"Radiation properties of cylindrical shells"**; MANNING, J.E.; MAIDANIK, G.; *Journal of the Acoustical Society of America; 36. pp. 1691-1698; 1964.*

[92] **"The propagation of structure borne sound"**; CREMER, L.; *Department of Scientific and Industrial Research Report; No. 1, Series B.; 1948.*

[93] **"Transmission of structure-borne sound in buildings"**; KIHLMAN, T.; *National Swedish Institute for building Research; Report 9 UDC 699-844; 1967.*

[94] **"Variable direction dependent transmission coefficients in the transmission of flexural waves at a rectangular corner of a wall"**; REICHARDT, W.; RICHTER, U.; *Acustica; 23, pp. 16-20; 1970.*

[95] **"Investigation of vibrational energy transfer in connected structures"**; HWANG, C.; PI, W.S.; *Nothrop corporation NASA; contract NAS8-28171; 1973.*

[96] **"The effect of transverse shear deformation on the bending of elastic plate"**; REISSNER, E.; *Transactions of the ASME Journal of Applied Mechanics; 12, pp. 69-77; 1945.*

[97] **"Quadrilateral plate bending elements with shear deformations"**; BERGAN, P.G.; WANG, X.; *Journal of Computers and Structures; 19, pp. 25-34; 1984.*

[98] **"A refined theory for laminated orthotropic plates"**; Nelson, R.B.; LORCH, D.R.; *American Society of Mechanical Engineers Journal of Applied Mechanics; 41, pp. 177-183; 1974.*

[99] **"Vibration of annular plates including the effects of rotatory inertia and transverse shear deformation"**; RAO, S.S.; PRASAD, A.S.; *Journal of Sound and Vibration; 42, pp. 305-324; 1975.*

[100] **"Das eulersche knickproblem unter berucksichtigung der querkrafte."**; NANNI, J.; *Zeitschrift fur angewandte Mathematic und Physik; 22, pp. 156-185; 1971.*

[101] **"Resonant and non-resonant acoustic properties of elastic panels. II. The transmission problem."**; LEPPINGTON, F.G.; HERON, K.H.; BROADBENT, E.G.; MEAD, S.M.; *Proc. R. Soc. Lond. A; 412, pp. 309-337; 1987.*

[102] MAA; *Journal of the Acoustical Society of America; 10. pp. 235; 1939.*

[103] **"Sound transmission between columns and floors in framed buildings."**; STEEL, J.A.; CRAIK, R.J.M.; *Applied Acoustics; 39, pp. 191-208; 1993.*

[104] **"Calculation of power flow between coupled oscillators."**; NEWLAND, D.E.; *Journal of Sound and Vibration; 3, pp. 262-276; 1966.*

[105] **"Power flow between a class of coupled oscillators."**; NEWLAND, D.E.; *Journal of the Acoustical Society of America; 43, pp. 553-559; 1968.*

[106] **"An Introduction to Statistical Energy Analysis."**; FAHY, F.J.; *Seminar notes ISAAC5 Advanced techniques in applied and numerical acoustics; Part III; 1994.*

[107] **"Statistical models of coupled dynamical systems and the transition from weak to strong coupling."**; SMITH, P.W. JR.; *Journal of the Acoustical Society of America; 65, pp. 695-698; 1979.*

[108] **"Recent progress in Statistical Energy Analysis Modeling of Noise and vibration."**; CIMERMAN, B.P.; *Proceedings NVH Solution symposium Japan; pp. 157-170; 1995.*

APPENDIX A.

The general form of a $n^2 \times n^2$ normalized energy matrix is given by :

$$\begin{bmatrix}
E_{11} & E_{11} & \cdots & E_{11} & -E_{21} & 0 & \cdots & 0 & \cdots & -E_{n1} & 0 & \cdots & 0 \\
0 & -E_{11} & \cdots & 0 & E_{21} & E_{21} & \cdots & E_{21} & \cdots & 0 & -E_{n1} & \cdots & 0 \\
\vdots & \vdots & \ddots & \vdots & \vdots & \vdots & \ddots & \vdots & \cdots & \vdots & \vdots & \ddots & \vdots \\
0 & 0 & \cdots & -E_{11} & 0 & 0 & \cdots & -E_{21} & \cdots & E_{n1} & E_{n1} & \cdots & E_{n1} \\
E_{12} & E_{12} & \cdots & E_{12} & -E_{22} & 0 & \cdots & 0 & \cdots & -E_{n2} & 0 & \cdots & 0 \\
0 & -E_{12} & \cdots & 0 & E_{22} & E_{22} & \cdots & E_{22} & \cdots & 0 & -E_{n2} & \cdots & 0 \\
\vdots & \vdots & \ddots & \vdots & \vdots & \vdots & \ddots & \vdots & \cdots & \vdots & \vdots & \ddots & \vdots \\
0 & 0 & \cdots & -E_{12} & 0 & 0 & \cdots & -E_{22} & \cdots & E_{n2} & E_{n2} & \cdots & E_{n2} \\
\vdots & \vdots & \vdots & \vdots & \vdots & \vdots & \vdots & \vdots & \ddots & \vdots & \vdots & \vdots & \vdots \\
E_{1n} & E_{1n} & \cdots & E_{1n} & -E_{2n} & 0 & \cdots & 0 & \cdots & -E_{nn} & 0 & \cdots & 0 \\
0 & -E_{1n} & \cdots & 0 & E_{2n} & E_{2n} & \cdots & E_{2n} & \cdots & 0 & -E_{nn} & \cdots & 0 \\
\vdots & \vdots & \vdots & \vdots & \vdots & \vdots & \vdots & \vdots & \cdots & \vdots & \vdots & \ddots & \vdots \\
0 & 0 & \cdots & -E_{1n} & 0 & 0 & \cdots & -E_{2n} & \cdots & E_{nn} & E_{nn} & \cdots & E_{nn}
\end{bmatrix}$$

APPENDIX B.

In general, it holds that :

$$\frac{\partial[A]^{-1}}{\partial x} = -[A]^{-1} \cdot \frac{\partial[A]}{\partial x} \cdot [A]^{-1}$$

Where *[A]* represents a $n \times n$ matrix. x stands for a dependant variable.

Hence, by replacing *[A]* by $[E^n]$ and by replacing x by E^n_{lm}, it follows that :

$$\frac{\partial[E^n]^{-1}}{\partial E^n_{lm}} = -[E^n]^{-1} \cdot \frac{\partial[E^n]}{\partial E^n_{lm}} \cdot [E^n]^{-1}$$

or for a specific element *ij*, it holds that :

$$\frac{\partial[E^n]^{-1}_{ij}}{\partial E^n_{lm}} = -\sum_{p,q}[E^n]^{-1}_{ip} \cdot \frac{\partial[E^n]_{pq}}{\partial E^n_{lm}} \cdot [E^n]^{-1}_{qj}$$

After replacing the inverse of the normalized energy matrix by the total loss factor matrix, it follows that :

$$\frac{\partial \eta^o_{ij}}{\partial E^n_{lm}} = -\sum_{p,q} \eta^o_{ip} \cdot \delta_{l,p} \cdot \delta_{m,q} \cdot \eta^o_{qj}$$

Or finally, it holds that :

$$\frac{\partial \eta^o_{ij}}{\partial E^n_{lm}} = -\eta^o_{il} \cdot \eta^o_{mj}$$

APPENDIX C.

Sensitivity with respect to SEA predictions.

C.1 Influence on vibration level prediction.

For vibration level prediction, the SEA model and the power inputs are given. The energy levels of the different subsystems are predicted by :

$$E_j = \frac{1}{\omega} \cdot \sum_{k=1}^{n} \eta_{jk}^{\circ\,-1} P_k = \frac{1}{\omega} \cdot \sum_{k=1}^{n} E_{jk}^{n} \cdot P_k \qquad (C.1)$$

C.1.1 Energy measurement errors.

Suppose that during the PIM measurements, the energy of subsystem i is incorrectly measured such that a bias factor α can be introduced to quantify the error. The influence of α on the predicted energy levels is given by :

$$\frac{\partial E_j}{\partial \alpha} \qquad (C.2)$$

by making use of equations (C.1), it follows that :

$$\frac{\partial E_j}{\partial \alpha} = \frac{1}{\omega} \cdot \delta_{j,i} \cdot \sum_{k=1}^{n} E_{jk}^{n,exact} \cdot P_k = \frac{\delta_{j,i}}{\alpha \cdot \omega} \cdot \sum_{k=1}^{n} E_{jk}^{n,meas} \cdot P_k \qquad (C.3)$$

Or finally :

$$\frac{\partial E_j}{\partial \alpha} = \frac{\delta_{j,i}}{\alpha} \cdot E_j \qquad (C.4)$$

Conclusion :

$$\Delta P_i = -\frac{\Delta\alpha}{\alpha}\cdot\omega\cdot\eta_{ii}^{\circ}\cdot E_i \qquad (C.10)$$

C.2.2 Power input measurement errors.

In this case, the measured power input during PIM into subsystem i is off by a factor α. The predicted source levels are given by equation (C.6).

The influence of α on the sources is :

$$\frac{\partial P_j}{\partial\alpha} = \omega\cdot\sum_{k=1}^{n}\frac{\partial\eta_{jk}^{\circ}}{\partial\alpha}\cdot E_k = \frac{1}{\alpha}\cdot\delta_{j,i}\cdot\omega\cdot\sum_{k=1}^{n}\eta_{ik}^{\circ}\cdot E_k \qquad (C.11)$$

Or finally :

$$\frac{\partial P_j}{\partial\alpha} = \frac{\delta_{j,i}}{\alpha}\cdot P_i \qquad (C.12)$$

Conclusion :

In the case of the prediction of source levels, an error on a measured power input during PIM will only affect the predicted power input level into subsystem i.

On the same basis, the effect of measurement errors on other SEA predictions can be assessed. Because of the similarity with the previous equations, the derivation will not be outlined in here.

If during PIM measurements, the energy of subsystem i is wrongly measured then this fault will only influence the predicted energy level of subsystem i in the postprocessing phase. The predicted energy level will also be off by a factor α.

C.1.2 Power input measurement errors,

Suppose the power input into subsystem i is wrongly measured during the PIM measurements and is off by a factor α. The influence of α on the predicted energy levels is given by equation (C.2) :

By making use of equation (C.1), it holds that :

$$\frac{\partial E_j}{\partial \alpha} = -\frac{1}{\omega \cdot \alpha^2} \cdot E_{ji}^{n,exact} \cdot P_i = -\frac{E_{ji}^{n,meas} \cdot P_i}{\alpha \cdot \omega} \qquad (C.5)$$

Conclusion :

There is an influence of power input measurement errors on *all* predicted vibration levels. The influence will be maximal for $j=i$, i.e. in case of the subsystems for which the power input is biased.

C.2 Influence on source prediction.

The SEA application concerning source prediction assumes known energy levels during operating conditions and a given, experimentally identified SEA model. The power input values into the different subsystems are predicted by :

$$P_j = \omega \cdot \sum_{k=1}^{n} \eta_{jk}^{\circ} \cdot E_k \qquad (C.6)$$

C.2.1 Energy measurement errors.

Assume that the measured energy levels of subsystem i obtained during PIM, are off by factor α. The influence of α on the predicted source levels is given by :

$$\frac{\partial P_j}{\partial \alpha} \qquad (C.7)$$

By making use of equation (C.6) :

$$\frac{\partial P_j}{\partial \alpha} = \omega \cdot \sum_{k=1}^{n} \frac{\partial \eta_{jk}^{\circ}}{\partial \alpha} \cdot E_k = -\omega \cdot \sum_{k=1}^{n} \frac{\eta_{ji}^{\circ}}{\alpha} \cdot \delta_{i,k} \cdot E_k \qquad (C.8)$$

Or finally :

$$\frac{\partial P_j}{\partial \alpha} = -\frac{\omega}{\alpha} \cdot \eta_{ji}^{\circ} \cdot E_i \qquad (C.9)$$

Conclusion :

Errors on measured vibration levels will affect *all* predicted sources. Mainly the predicted source of subsystem i will be affected. In that case it holds that :

APPENDIX D.

The algebraic form of matrix [A] (see equation (5.29)) is given by :

$$[A]=\begin{bmatrix}
0 & 0 & 0 & 0 & 0 & 0 & \frac{j}{EA} & 0 & 0 & 0 & 0 & 0 \\
0 & 0 & 0 & 0 & 0 & j & 0 & \frac{j}{K_y GA}+\frac{jz_t^2}{GJ} & \frac{-jz_t y_t}{GJ} & \frac{jz_t}{GJ} & 0 & 0 \\
0 & 0 & 0 & 0 & j & 0 & 0 & \frac{-jz_t y_t}{GJ} & \frac{-j}{K_z GA}+\frac{jy_t^2}{GJ} & \frac{-jy_t}{GJ} & 0 & 0 \\
0 & 0 & 0 & 0 & 0 & 0 & 0 & \frac{jz_t}{GJ} & \frac{-jy_t}{GJ} & \frac{j}{GJ} & 0 & 0 \\
0 & 0 & 0 & 0 & 0 & 0 & 0 & 0 & 0 & 0 & \frac{j}{EI_y} & 0 \\
0 & 0 & 0 & 0 & 0 & 0 & 0 & 0 & 0 & 0 & 0 & \frac{j}{EI_z} \\
-j\omega^2\rho A & 0 & 0 & 0 & 0 & 0 & 0 & 0 & 0 & 0 & 0 & 0 \\
0 & -j\omega^2\rho A & 0 & 0 & 0 & 0 & 0 & 0 & 0 & 0 & 0 & 0 \\
0 & 0 & -j\omega^2\rho A & 0 & 0 & 0 & 0 & 0 & 0 & 0 & 0 & 0 \\
0 & 0 & 0 & -j\omega^2\rho I_x & 0 & 0 & 0 & 0 & 0 & 0 & 0 & 0 \\
0 & 0 & 0 & 0 & -j\omega^2\rho I_y & 0 & 0 & 0 & -j & 0 & 0 & 0 \\
0 & 0 & 0 & 0 & 0 & -j\omega^2\rho I_z & 0 & -j & 0 & 0 & 0 & 0
\end{bmatrix}$$